RECYCLING HIGH PERFORMANCE CARBON FIBRE REINFORCED POLYMERS USING SUB- AND SUPERCRITICAL FLUIDS

By

MATTHEW JAMES KEITH

A thesis submitted to the University of Birmingham
for the degree of
DOCTOR OF PHILOSOPHY

School of Chemical Engineering
College of Engineering and Physical Sciences
University of Birmingham
August 2019

ABSTRACT

The research presented in this thesis considers the solvolytic recycling of high performance composite materials using an acetone / water solvent mixture, supplied both neat and in conjunction with alkaline and weak-Lewis acids. The neat solvent was capable of recovering clean fibres within 120 and 90 min when heated to 320 and 330˚C respectively. The alkaline catalysts did not accelerate the decomposition of the matrix due to a reaction with acetone thus eliminating one of the solvents from the system. $ZnCl_2$, $MgCl_2$ and $AlCl_3$ all facilitated a reduction in the process temperature necessary for the complete elimination of the resin of 40˚C.

A kinetic study of all solvent systems was carried out using two different approaches: a conventional, first order rate equation and a shrinking core model (SCM). Both models were successfully fitted to the experimental data and were able to predict the decomposition of the resin to within ± 10% of the measured value. $ZnCl_2$ appears to be the most effective catalyst, reducing the activation energy, E_A (kJ mol^{-1}), of the degradation reaction by up to 29% compared to the neat solvent mixture.

Characterisation of carbon fibres demonstrated that at temperatures of less than 330˚C, there was no statistically significant change in the tensile strength or modulus. Higher process temperatures, and the presence of $AlCl_3$, caused a reduction in strength of up to 12.4%. $ZnCl_2$, however, caused an increase in both the tensile strength and modulus of up to 22%. Analysis of the fibre surface showed a reduction in the relative

abundance of oxygen for all conditions investigated which may correspond to the loss of the sizing.

Fourier transform infrared spectroscopy (FTIR) of the dried organic products demonstrated that both the neat solvent at temperatures in excess of 320˚C and the metal chloride systems successfully cleaved the C-N bonds within the epoxy resin. These products were further analysed with gas chromatography-mass spectrometry (GC-MS) which demonstrated that the resin was predominantly decomposed to benzene and phenolic derivatives.

The findings discussed throughout this work describe and analyse a novel CFRP recycling process. The use of chloride catalysts facilitated a significant reduction in the operating temperature required while characterisation of the recovered fibres demonstrated that, under certain conditions, there is no change in the mechanical properties. Furthermore, analysis of the organic resinous products revealed the presence of a mixture of potentially useful compounds, which may have further use in a new polymer matrix. It is hoped, therefore, that this research contributes towards the circular economy through the effective recycling of CFRPs.

To Eleanor Anne Keiller,

Love always

ACKNOWLEDGMENTS

This thesis represents the culmination of eight years of my time at the University of Birmingham. It is with great pleasure that I have reached this stage in my life, but it certainly would not have been possible without the people I have met along the way. I have had the enormous good fortune of having two brilliant supervisors, without whom this project would never have been completed. To Prof. Gary Leeke and Dr. Andrew Ingram, thank you for your guidance, patience and encouragement over the past four years. I am eternally grateful to the both of you for the support you have provided.

To Dr. Phillip Robbins, thank you for making my time in Chemical Engineering indescribably rewarding. Thanks also to David Boylin, Lynn Draper, Iain Kings and all the staff, postgraduate and undergraduate students within the School who I have had the utmost pleasure to work with.

To my family, friends and housemates I would like to express my immense gratitude for your love, friendship and support throughout the completion of this project. Thanks also to Carnival RAG for always providing a very welcome distraction to the endless hours spent in the lab.

Finally, to Ellie, my editor-in-chief and partner-in-life, thank you. Without you this thesis would never have become a reality.

PEER-REVIEWED PUBLICATIONS

i. Recycling a carbon fibre reinforced polymer with a supercritical acetone / water solvent mixture: Comprehensive analysis of reaction kinetics
Polymer Degradation and Stability, Impact Factor = 3.780
Published
doi.org/10.1016/j.polymerdegradstab.2019.01.015

ii. Catalytic degradation of a carbon fibre reinforced polymer for recycling applications
Polymer Degradation and Stability, Impact Factor = 3.780
Published
doi.org/10.1016/ j.polymerdegradstab.2019.05.020

iii. Characterisation of carbon fibres recycled using an acetone / water solvent and metal chloride catalysts.
Composites Part B: Applied Science and Manufacturing, Impact Factor = 6.864
Under Review

CONFERENCE PROCEEDINGS

i. Optimisation of solvolysis for recycling carbon fibre reinforced composites,
17th European Conference on Composite Materials, Munich, Germany, 2016

ii. Chemical recycling of carbon fibre composites with a super-critical acetone / water solvent,
21st International Conference on Composite Materials, Xi'an, China, 2017

iii. Catalytic degradation of a carbon fibre reinforced epoxy resin with an acetone / water solvent
18th European Conference on Composite Materials, Athens, Greece, 2018

iv. Recycling carbon fibre with an acetone / water solvent and zinc chloride catalyst: Resin degradation and fibre characterisation
Society for the Advancement of Materials and Process Engineering (SAMPE) European Conference 2018, Southampton, UK, 2018

CONTENTS

LIST OF FIGURES

LIST OF TABLES

ABBREVIATIONS

ABS	Acrylonitrile butadiene styrene
AFM	Atomic force microscopy
$Al_2(SO_4)_3$	Aluminium sulphate
$AlCl_3$	Aluminium chloride
$CaCl_2$	Calcium chloride
CFRP	Carbon fibre reinforced polymer
CH_4	Methane
CO	Carbon monoxide
CO_2	Carbon dioxide
Cs_2CO_3	Caesium carbonate
$CsCl_2$	Caesium chloride
CsOH	Caesium hydroxide
$CuCl_2$	Copper chloride
DDS	4,4'-Diamino-diphenyl sulphone
DGEBA	Diglycidyl ether of bisphenol A
EoL	End of life
EoS	Equation of state
FRC	Fibre reinforced composite
FRP	Fibre reinforced polymer
FTIR	Fourier transform infrared spectroscopy
GC-MS	Gas chromatography - mass spectrometry
GFRP	Glass fibre reinforced polymer
GRAS	Generally recognised as safe

H_2	Hydrogen
H_2O_2	Hydrogen peroxide
HTP	High temperature and pressure
IFSS	Interfacial shear strength
IR	Infra-red
K_3PO_4	Tripotassium phosphate
KOH	Potassium hydroxide
LCA	Life cycle assessment
LCM	Liquid composites moulding
LTP	Low temperature and pressure
$MgCl_2$	Magnesium chloride
$MgSO_4$	Magnesium sulphate
NaOH	Sodium hydroxide
OLP	Organic liquid products
PAN	Polyacrylonitrile
PC-SAFT	Perturbed chain - statistical associating fluid theory
PE	Polyethylene
PEEK	Poly(ether ether ketone)
PEG	Polyethylene glycol
PRC	Particle reinforced composite
PP	Polypropylene
PPS	Poly(phenylene sulphide)
PS	Polystyrene
PVC	Polyvinyl chloride
RA	Relative abundance
RDS	Rate determining step

RTM	Resin transfer moulding
SCM	Shrinking core model
SCRIMP	Seaman composite resin infusion moulding process
SEM	Scanning electron microscopy
SFTT	Single fibre tensile testing
SMC	Sheet moulded compond
SRIM	Structural resin infusion moulding
TEM	Transmission electron microscopy
VARFIM	Vacuum assisted resin film infusion moulding
VARTM	Vacuum assisted resin transfer moulding
XPS	X-ray photoemission spectroscopy
XRCT	X-ray computed tomography
XRD	X-ray diffraction
$ZnCl_2$	Zinc chloride
$ZnSO_4$	Zinc sulphate

NOMENCLATURE

A_f	Cross sectional area of fibre (m^2)
d_f	Fibre diameter (m)
E_A	Activation energy (kJ mol^{-1})
E_f	Single fibre tensile modulus (GPa)
F_{max}	Maximum tensile force applied to single carbon fibre (N)
i	Rank number in Weibull distribution
k	Rate constant (min^{-1})
K	System compliance for tensile testing machine
k_0	Frequency factor (min^{-1})
$k_{A,H}$	Arrhenius rate constant during the heating phase (min^{-1})
$k_{A,R}$	Arrhenius rate constant during the reaction phase (min^{-1})
k_{SCM}	Rate constant for shrinking core model (min^{-1})
L	Fibre length (m)
M	Mass fraction of resin remaining within the CFRP (dimensionless)
$m(t)$	Mass of resin remaining at time, t (g)
mf	Final mass of CFRP (g)
M_H	Mass fraction of resin remaining within the CFRP after heating time (dimensionless)
m_i	Initial mass of CFRP (g)
M_R	Mass fraction of resin remaining within the CFRP after reaction (dimensionless)
n	Order of reaction (dimensionless)
P	Probability of fibre failure
p_c	Critical pressure (MPa)

R	Ideal gas constant (kJ $mol^{-1}°C^{-1}$)
RD	Resin decomposition (wt. %)
R_i	Initial resin content in CFRP (wt. %)
R_P	% resin remaining after processing (wt. %)
T	Temperature (˚C)
T_c	Critical temperature (˚C)
T_g	Glass transition temperature (˚C)
T_R	Reactor temperature (˚C)
t_H	Heating time (min)
t_R	Reaction time (min)
X	Conversion (in shrinking core model - dimensionless)
α	Extent of conversion (dimensionless)
ΔL	Difference in fibre length (m)
σ_0	Single fibre tensile strength (GPa)
w	Weibull shape factor (dimensionless)

CHAPTER 1.
INTRODUCTION

Carbon fibre reinforced polymers (CFRPs) exhibit exceptional mechanical properties including high specific strength, excellent stiffness and resistance to fatigue. These characteristics have made CFRPs a material of choice in applications where high performance must be combined with light weight; most notably in the aerospace, automotive and wind energy industries. Within the transport sector, the use of CFRPs can lead to improved environmental performance and large increases in efficiency: the lighter the vehicle, the less fuel is needed. Due to their exceptional stiffness, wind turbine blades made from a CFRP rather than metals or glass fibre reinforced polymers (GFRPs) can be longer, resulting in increased power output and thereby contributing towards a zero-carbon economy. However, the growth in global annual production of CFRPs from 51 kt in 2010 to 114 kt in 2017 [1] has also contributed to a wider environmental problem; the generation of waste from both manufacturing off-cuts and end-of-life equipment. The quantity of material to be disposed of within the next 20 years has been predicted to reach 115 kt [2] and, at present, the majority of this waste is sent to landfill.

In order to improve resource efficiency, multiple studies have been conducted into the mechanical, pyrolytic and solvolytic recycling of CFRPs. When applied to the recovery of carbon fibre, mechanical technologies such as grinding or milling are not considered economical due to greatly down-grading a previously high-value material [3].

Pyrolysis, where the resinous matrix of the composite is thermally degraded, has reached commercial maturity with ELG Carbon Fibre Ltd. in the UK, CFK Recycling in Germany and Carbon Conversions in the US capitalising on this technology [4]. However, it is a resource inefficient process due to the loss of the polymer and environmentally harmful due to the generation of greenhouse gasses. Solvolytic techniques have the potential to address these disadvantages: by dissolving the resin, fewer emissions are produced during the recycling process and a mixture of organic products are generated which may have further use elsewhere in the chemical industry. Although Adherent Technologies have developed a commercial wet-chemical method, solvolysis of CFRPs for recycling applications is not widespread and remains an active area of research. Recent work has focussed on the reduction of process time and temperature, either through the inclusion of catalysts or semi-continuous operation. A mixture of acetone and water has been shown to be a promising solvent system, however, there has been little investigation into the recycling of a commercial CFRP using this technique. The research presented in this thesis therefore aims to develop and analyse a novel solvolytic CFRP recycling process using this solvent mixture by fulfilling the following objectives:

1. Establish the reaction conditions necessary to decompose a commercially available CFRP thus facilitating the recovery of carbon fibres.

2. Assess the performance of a range of catalysts through the analysis of the reaction kinetics of the decomposition reaction.

3. Characterise fibres recovered from the developed recycling process in order to determine the influence of the reaction conditions on their mechanical and surface properties.

4. Identify the organic products obtained from the reaction and develop an understanding of the action of the solvent and the catalysts.

In order to meet these objectives, this thesis is structured into seven chapters, the first of which introduces the project and defines the objectives of this research. Chapter 2 presents a review of the literature and includes an overview of composite materials before focussing on the manufacture and disposal routes of high performance CFRPs. Chapters 3 to 6 are all similarly structured. Each aims to meet one of the objectives listed above and begins with a methodology specific to the results presented in that chapter only. A summary of the content of each chapter is provided below.

Chapter 3: Resin Decomposition

This chapter specifies the solvent systems used, the potential catalysts investigated and the reaction conditions selected. The methods implemented to quantify the resin decomposition are described and the CFRP that was used in the majority of experiments is also characterised. The results of the decomposition reactions at various conditions are also presented in this chapter.

Chapter 4: Reaction Kinetics

In order to verify the assumptions made when applying two different kinetic models for the degradation reaction of the CFRP, this chapter includes an investigation into changing the reactor loading and images partially degraded CFRP samples using X-ray computed tomography (XRCT). A first order rate equation and shrinking core model (SCM) are fitted to the decomposition data presented in Chapter 3. Both approaches are used to evaluate E_A and k_0 and an evaluation of how well both models fit the data is conducted.

Chapter 5: Fibre Characterisation

As a result of the findings presented in Chapter 3, a set of 11 conditions were identified which are capable of recovering fibres from the polymer matrix. Samples of the CFRP were imaged with scanning electron microscopy (SEM) in order to confirm that the resin was fully solubilised. Virgin carbon fibre was also processed at these conditions and then characterised through single fibre tensile testing (SFTT) and X-ray photoemission spectroscopy (XPS).

Chapter 6: Organic Product Analysis

This chapter describes the analysis of the organic liquid products (OLPs) remaining at the end of the solvolytic process using gas chromatography with mass spectrometry (GC-MS) and Fourier Transform Infrared Spectrometry (FTIR). As the initial formulation of the CFRP is held in commercial confidence, a model thermoset epoxy resin was also synthesised, decomposed at the same conditions and analysed.

Finally, this thesis concludes with Chapter 7 which summarises the key findings of this project and outlines possible future directions that research within this field could take.

Significant parts of the research presented in Chapters 3, 4 and 6 are published across two articles, both in the peer-reviewed journal *Polymer Degradation and Stability*. Aspects of this work have also been presented at national and international conferences, a full list of which is provided as part of the front matter of this thesis.

CHAPTER 2.
LITERATURE REVIEW

2.1 Introduction

This literature review includes six key areas of research, the first two of which consider the two components of a CFRP: the carbon fibre reinforcement and the polymer matrix. As it is desirable to produce a secondary composite material using recovered carbon fibre, it is necessary to consider common CFRP manufacturing techniques before developing an understanding of how these materials may be recycled. The second half of this chapter critically evaluates recent research into a broad range of recycling processes which can be grouped into mechanical, thermal and chemical technologies. This chapter concludes by summarising the findings of the literature review and using the information gathered to direct the research presented in Chapters 3 to 6.

2.2 Background to Composite Materials

Although often considered a modern technology, humans have been creating composite materials for millennia. One of the very earliest examples, dating to 1500 BC, is the manufacture of bricks by blending natural materials such as straw and mud together. In medieval times, two types of wood, one strong in tension, the other strong in compression, were combined with animal glue to form a longbow capable of firing arrows further and faster than a bow made of a single material [5]. Wood in its own right is also a composite material consisting of spiral cellulose fibres bound together with

lignin. Another instance of a commonly-occurring, natural composite is bone where the protein collagen is reinforced with small, rod-like hydroxyapatite crystals [6]. All of these examples have two traits in common: the first is that the constituent materials have different properties and, when combined together, the properties of the composite formed are also noticeably different. Secondly, both materials are present in significant proportions. Typically, the minimum quantity of any one constituent must be approximately 5% for a material to be considered a composite [7]. Modern synthetic composites must also meet a third criterion: the different phases must be intimately combined during manufacture, yet still be separated by a distinct interface. For this reason, metal alloys which are produced by the solidification of a homogenous melt, are not normally thought of as composite materials [5].

Within a composite material, the continuous phase, called the matrix, is usually present in a greater quantity and may be polymeric, metallic or ceramic [5]. Generally, polymers are inexpensive, have good corrosion resistance and a tensile strength and stiffness of 10 to 100 MPa and 0.3 to 30 GPa respectively. They are also relatively easy to process with a variety of manufacturing techniques for polymer matrix composites reaching commercial maturity as described in Section 2.5 [8]. Metals are ductile with mechanical properties in between those of polymers and ceramics and are used in heavy duty electrical contacts or components of internal combustion engines [9]. Ceramics are the strongest category of matrix material and also exhibit very high Young's moduli in the range of 86 to 340 GPa. However, they are also very brittle and typically have much

higher density which makes them less suited to applications, such as transport, where it is desirable to minimise weight [10].

The second constituent of a composite is the reinforcement agent which enhances the mechanical properties of the matrix. The volume fraction of this reinforcement within a composite is a key parameter in determining the final properties of the material: the reinforcement is generally stronger and stiffer than the matrix and it is, therefore, desirable to maximise its content. However, beyond a certain volume fraction, adhesion between the two phases is reduced and the bulk mechanical properties of the composite are diminished. The geometry of the reinforcement also influences the final properties of the composite and is, therefore, carefully controlled during its manufacture. At least one of its dimensions is small and may be anywhere between 1 to 500 μm [11]. The geometry also defines whether the reinforcement can be described as particulate or fibrous. The former may be spherical, cubic or have no regular shape but, as they are particles, all three dimensions (length, width and depth) are approximately equal. Concrete is the most widely used particulate reinforced composite (PRC) material consisting of a cement matrix and stone or sand particles [5]. As the subject of this thesis is recycling a fibre reinforced composite (FRC), a detailed discussion of PRCs is beyond the scope of this review.

Unlike particles, fibrous reinforcements have a cross sectional diameter which is much smaller than its length. The aspect ratio of these two dimensions can, however, vary significantly depending on the fibre type and the desired properties of the final

product. Short or discontinuous fibres have a low aspect ratio with a typical length of 5 to 50 mm and may be orientated randomly or aligned in a preferred direction within a mat [12]. When used in a composite, short fibres do not provide the same degree of reinforcement as long, continuous fibres. Long fibres may be unidirectional or woven together to form a ply which provides greater strength and stiffness in two directions rather than only along the axis following the fibre length [5]. Different fibre types may also be mixed together either in the same ply or in distinct, separate layers in order to produce a material which benefits from the properties of both reinforcement agents. For example, a relatively inexpensive, yet high performance, composite can be manufactured from glass and carbon fibres bound by a polymer matrix due to the low cost of glass fibre and the exceptional mechanical properties of carbon [8]. Similarly, particulate and fibrous reinforcements may also be used within the same composite material [5].

2.3 Matrix Materials

Of the 154.7 kt of carbon fibre reinforced composites manufactured in 2018, 82.7 wt.% used a polymer matrix [1] and it is, therefore, CFRPs which are likely to contribute to the majority of waste material. Polymers can be classified as either a thermoplastic or a thermoset resin depending on their thermal behaviour [13]. Due to their long polymer chains, thermoplastics soften and eventually melt in the presence of heat, meaning they can be reshaped and easily recycled [14]. Thermosets, however, contain shorter monomers between the polymer chains meaning they are cross-linked together during the curing process. This is generally irreversible which leads to a material with

high chemical and thermal stability, but also one which is difficult to recycle [15]. The following section focusses on these two classes of matrix material, describing their different formulations, properties, processing methods and applications.

2.3.1 Thermoplastic Polymers

Thermoplastic resins consist of long polymer chains usually based on an aliphatic carbon skeleton with functional groups such as carbonyls, amines or organic cyclic compounds bonded to the network. The chemical bonds within and between each monomer are exceptionally strong: the strength of a C-C bond has been reported as between 353.3 and 377.4 kJ mol^{-1} depending on the chain length and surrounding environment [16]. For example, average bond strengths within polypropylene (PP) and polyvinyl chloride (PVC) are 357.1 and 373.8 kJ mol^{-1} respectively [17]. The result of this is, in theory, polymers should be able to support very high loads with specific strengths of the order of 10^{10} Pa m^3 kg^{-1} [16]. However, only weak van der Waals forces exist between each molecule and, therefore, the strength and stiffness of the polymer are derived not just from the properties of the monomer, but also the orientation of the chains [18]. Thermoplastic polymers may be amorphous where there is a high degree of molecular entanglement, or semi-crystalline where the chains at local points are aligned in the same direction. Due to the complexity of the polymer chains, it is very difficult to form a purely crystal structure. As an amorphous polymer is heated, molecules become less entangled which leads to it changing phase to a viscous liquid, while semi-crystalline thermoplastics form an amorphous viscous liquid [18]. This enables relatively easy

recycling of thermoplastic materials as they can be melted and remoulded into the shape of a new product with little degradation of the polymer [19].

Thermoplastics can be classified according to their various applications. Traditional plastics tend to be amorphous and, in addition to PP and PVC, include polyethylene (PE), polystyrene (PS) and acrylonitrile butadiene styrene (ABS). These are inexpensive and more typically contain a short, rather than long, fibre reinforcement [7] meaning they are only suited for low performance applications, for example, as car panels [20]. Since the 1980s, engineering thermoplastics such as polycarbonates, polyketones, polyimides and polysulphones, have also been developed for high-performance applications [21]. Compared to traditional plastics which use an aliphatic carbon skeleton, these resins are typically based on a network of benzene rings; a highly stable monomer which tends to give rise to a high degree of crystallinity. As such, high glass transition and melt temperatures are characteristic of these engineering thermoplastics [7]. Specific examples include poly(ether ether ketone) (PEEK) which is manufactured by Victrex, polyamide made by the Dupont Chemical Company and poly(phenylene sulphide) (PPS) which is produced by Phillips 66 [22]. Despite being first developed in 1936 [23], novel acrylic polymers have also been recently reintroduced to the market due to their ability to polymerise at room temperature, their low density and their good mechanical performance [24].

Compared to thermoset polymers, thermoplastics benefit from a much longer shelf life as, over a timescale of days or weeks, thermosets can self-cure resulting in a

hard, unworkable material [25]. Thermoplastic CFRPs also tends to have a higher ductility and fracture toughness compared to thermoset composites [25]. As the polymer chains are not cross-linked together, they are also relatively mobile upon heating. This not only leads to a more recyclable material, but also one where any fractures or defects can be healed using heat treatment [26]. There are, however, some significant challenges in the manufacturing of thermoplastic composites. Carbon fibre tapes bound by a thermoplastic tend to be stiff and more difficult to align within a mould [27]. The liquid melts are also highly viscous and are of the order of 10^3 to 10^5 Pa s [28], [29] compared to 10^2 Pa s for uncured, thermoset epoxy resins [30]. This means that high temperatures are needed during the manufacturing of thermoplastics and may be anywhere from 325˚C for PPS to 390˚C for PEEK [7]. There is an additional complexity due to the potential for thermal decomposition of the polymer before sufficiently low viscosities are obtained. Due to the viscosity, it may also be difficult to incorporate the fibrous reinforcement into a thermoplastic matrix [25] and there is a risk of creating voids within the material [31].

Although the use of thermoplastic matrix materials is rising, thermoset polymers remain the most widely used accounting for 76.2% of all CFRPs manufactured in 2017 [32]. As the majority of CFRP waste is likely to be composed of these materials, the research presented in this thesis considers the recycling of high performance thermoset carbon fibre composites. For this reason, the remainder of this literature review focusses on the properties, manufacturing and recycling of thermoset resins and its composites. However, the recycling of thermoplastics is also considered where novel

techniques described in the literature have only been applied to this class of polymer and not thermosets.

2.3.2 Thermoset Polymers

While thermoplastic polymer chains may contain hundreds or thousands of carbon atoms, typical thermoset prepolymers may only contain twenty to thirty. These much shorter molecules mean the majority of thermosets are liquid at temperatures below 80˚C [7]. In order to solidify the resin, a cross-linking or curing agent must be mixed in to the liquid. This may also be referred to as a hardener. Heat, pressure, a catalyst and / or ultraviolet light is normally applied in order to accelerate the cross-linking reaction [33]. When the resin is fully cured, solid, three dimensional networks are created, and the polymer chains are no longer held together by weak van der Waals forces alone, but also strong covalent bonds. As this reduces molecular mobility, thermoset polymers tend to be stiffer, of equivalent strength and more brittle than thermoplastics [34]. They also tend to have higher thermal and chemical stability meaning they can be used in high temperature applications [7]. The most common types of thermoset resins can be divided into three classifications: phenolics, polyesters and epoxies, the chemical structure of each is shown in Figure 1.

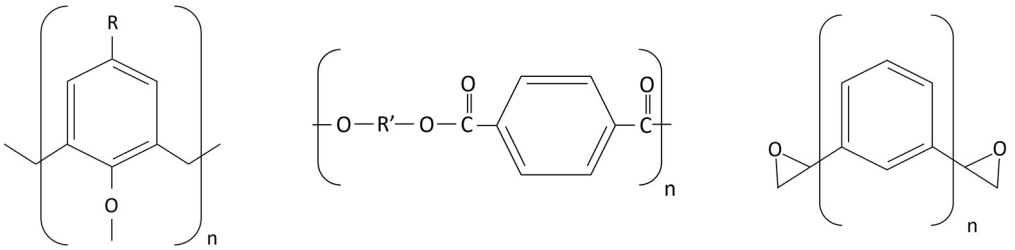

a) **b)** **c)**

Figure 1*. Molecular structure of common resins a) phenolic; b) polyester and; c) epoxy.*

Phenolic resins are amongst the oldest variety and were the first to reach commercial success in the early 20th century under the trade name Bakelite [35] . Since then, multiple varieties have been brought to the market and are classified as either one-stage or two-stage resins, termed resoles and novalacs respectively [5]. Resoles are supplied as a mixture of phenol, formaldehyde, occasionally water, and a basic catalyst and are cured in a single stage through heating above approximately 120˚C [36]. Novalacs are a mixture of phenol and formaldehyde only which means only a partially cross-linked network is created and the resultant material maintains some thermoplastic properties. These can be impregnated across carbon fibre tapes or weaves to form a prepreg which are laid directly in to a mould as described in Section 2.5. A hardener, such as hexamethylenetetramine, is added in order to create a fully cross-linked thermoset matrix at temperatures of above 90˚C [36].

Compared to phenolics and epoxies, polyesters have a much simpler bonding network and are generally less costly, but their lower strength, stiffness and fracture toughness means they are more suited to less safety-critical applications such as pipes, boat hulls and car parts [34]. The hardeners used to cross-link the polyester chains often

do not readily react with the ester bonds and so may be mixed into the polymer prior to fabricating a composite material [37]. Once the fibres are incorporated into the polymer, an initiator, usually an organic peroxide, is added. This attacks the C=C double bond in either the polyester chain or cross linking agent, reducing it to a single bond and creating a free radical [38], [39]. Due to the lone pair of electrons, these are highly reactive groups which bond together when they come into contact. This results in linking the polyester chains together to form a large, three dimensional matrix [40].

The third class of thermoset polymers are epoxies. These are the most commonly used matrix in advanced composite materials due to their high strength, resistance to corrosion and ease of processing [7]. An epoxy group is a three membered, cyclic structure consisting of two carbon atoms both bound to an oxygen atom. This is often modified such that one of the carbon atoms within the epoxy is also bonded to another carbon, a group known as a glycidyl [34] and it is this which acts as the reactive site [41]. To cure an epoxy polymer, a hardener is mixed into the liquid epoxy, which is often heated to above ambient conditions in order to reduce its viscosity [42]. The cross-linking agents are typically either amines, anhydrides or a tertiary amine / accelerator mixture. The cure is completed by raising the temperature to, typically, between 100 and 250˚C [42]. The maximum service temperature of the final material is usually approximately that of the cure temperature [34]. The ratio of epoxy polymer to cross linking agent also has a significant influence on the final properties of the material. If there is an excess of epoxy, the resultant product is only partially cross-linked and will, therefore, have a lower strength and reduced glass transition temperature, T_g,

compared to a thermoset manufactured using a stoichiometric ratio of 1 : 1. In this instance, the polymer is fully cross-linked creating a three dimensional matrix with maximum mechanical properties. If the curing agent is in excess, the material exhibits the properties of a low molecular weight thermoplastic which are generally inferior to those of a stoichiometrically cured resin system [42].

There are a wide variety of epoxy resin systems which are commercially available, and two types have been selected for initial investigation within this work. The first is HexFlow RTM6 manufactured by Hexcel Corporation. RTM, an acronym for "resin transfer moulding", is a common manufacturing technique described in detail in Section 2.5. Although the exact formulation is held in commercial confidence, this mono-component resin system has been developed for the aerospace industry and is, therefore, suitable for safety critical applications. T_g was measured by dynamic mechanical analysis (DMA) and was found to be 210 ± 5˚C [43]. It also has a high thermal stability with a service temperature range of -60 to 120˚C and a high tensile strength and modulus of 75 and 2890 MPa respectively [43]. Furthermore, upon immersing this material in water at 70˚C for 14 days, the moisture uptake was less than 2.5 wt.% [43] suggesting it is resistant to solvent penetration. High moisture uptake of more than 3.5 wt.% rapidly increases the leaching of molecules from the matrix and subsequently degrades the polymer [44], [45]. As these properties demonstrate that HexFlow RTM6 is a durable thermoset polymer, it is expected that the conditions identified as capable of decomposing this material can be applied to the recycling of a wide range of CFRPs. Also considered within Chapter 6 of this thesis is the decomposition of 2,2-Bis[4-

(glycidyloxy)phenyl]propane (also referred to as diglycidyl ether of bisphenol A or DGEBA) cured with 4,4'-diaminodiphenyl sulphone (DDS). The structure of each compound and that of the cured resin is shown in Figure 2.

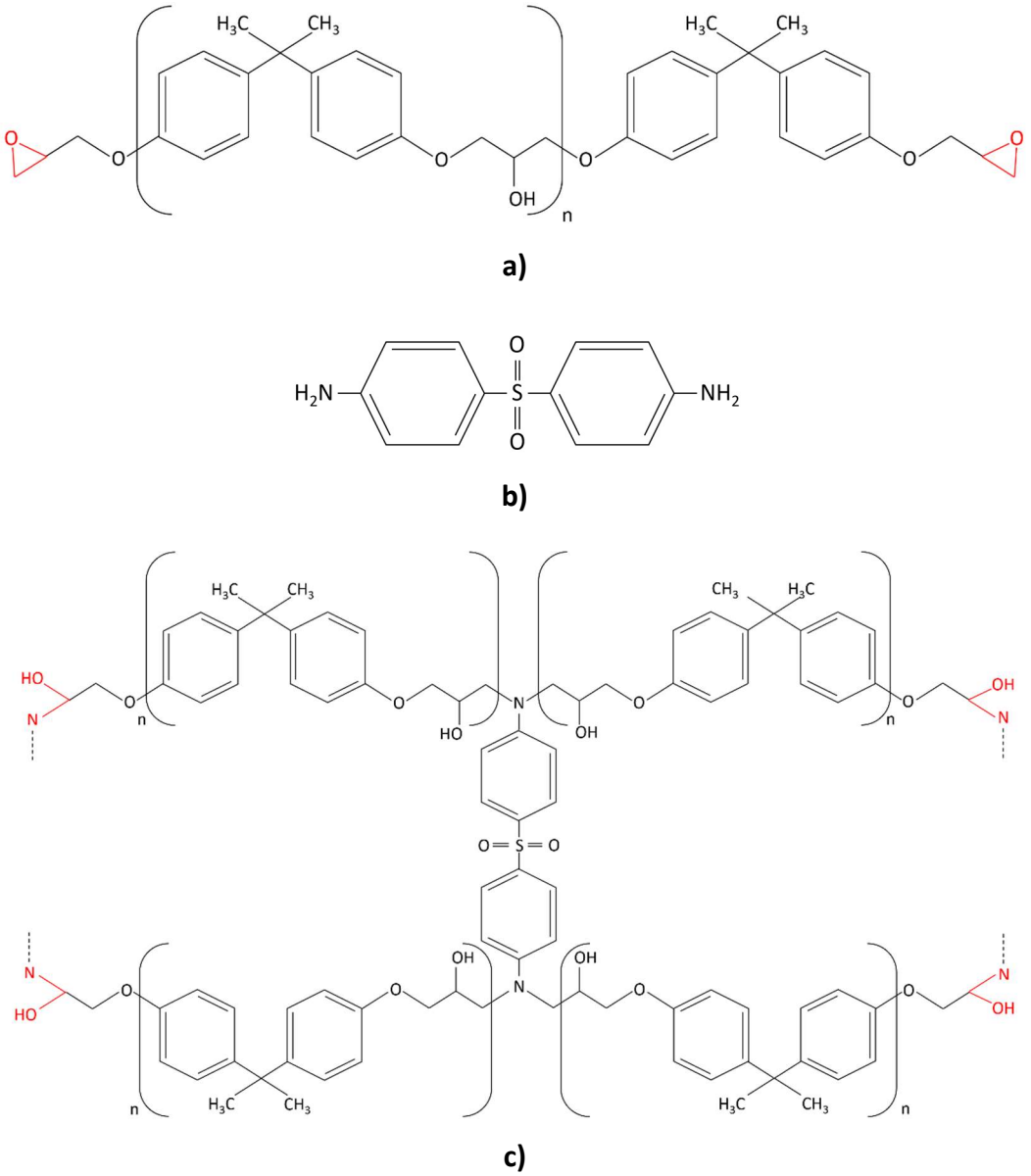

***Figure 2**. Molecular structure of a) DGEBA prepolymer; b) DDS curing agent and; c) cured DGEBA / DDS resin*

This commercially available formulation was selected as the DGEBA prepolymer accounts for an estimated 75 to 90% of all epoxy resins manufactured [46]. DDS was used as the hardener due to the presence of two benzene rings which increases thermal and chemical stability of the resin [47] and its ability to achieve a high degree of cure [48]. This resin system also exhibits desirable mechanical and physical properties [49], although it has been shown that these properties are strongly dependent on the curing cycles implemented. Consequently, the influence of cure time and temperature on T_g, flexural and tensile strength, impact toughness and electrical conductivity have been subject to a number of investigations [50]–[55]. Relevant to the recycling of these materials, however, is the thermal degradation temperature of a cured DGEBA epoxy resin with research demonstrating that this is dependent on the cross-linking agent used [56]. In addition to this, the three dimensional matrix formed contributes to the chemical resilience of the cured product [57], [58] and, although this is an essential feature of high performance thermoset polymers, it also creates a significant challenge for the recycling of these materials.

Multiple studies have explored the uptake of moisture into, and ageing of, DGEBA epoxy polymers, the findings of which may be applicable to the solvolytic recycling of thermoset resins. The results of various studies suggest that water absorption is not temperature dependent [59]–[61], possibly due to the medium to high polarity of DGEBA resins [62]. However, the maximum temperature investigated of 70˚C is well below that necessary to fully decompose the polymer as would be necessary for recycling applications. In addition to hydrothermal ageing, radiochemical ageing has also

been a subject of interest due to the application of amine cured epoxy resins in the nuclear industry [63]–[65]. Previous work has demonstrated that, in the absence of moisture, the properties of the polymer are degraded due to the formation of carbonyl and amide radicals when aged using thermo-oxidative techniques [66], [67]. Radical formation may be accelerated by exposure to ϒ-radiation which results in a small increase in water absorption [65]. However, this does not appear to cause a significant change in the properties of DGEBA polymers with hydrothermal and thermo-oxidative effects leading to more substantial degradation [68].

For high performance applications, both thermoplastic and thermoset resins can be reinforced with various types of fibres such as carbon, glass and aramid, in addition to natural fibres such as hemp [5]. However, it is carbon fibres which are the most durable, most valuable and have the highest manufacturing energy cost [69]. For these reasons, it is this fibre which is the most desirable to recover and is, therefore, the subject of this research project. Consequently, the remainder of this chapter reviews the literature surrounding their production, characterisation and recycling.

2.4 Carbon Fibre Reinforcement

2.4.1 Overview

The market demand for carbon fibre has rapidly expanded in the preceding decade from a global production of 33.0 kt in 2010, to 70.5 kt in 2017 and a projection of 120.5 kt by 2022 [1]. Almost all carbon fibre manufactured is used as a reinforcement agent within a composite material [1]: the manufacture, properties and applications of

which are discussed in Section 2.5. Each individual filament is typically 5 to 10 μm in diameter and may be supplied in a continuous tow tens of metres long which results in a material with an exceptionally high aspect ratio [70]. Carbon fibres themselves consist of highly ordered carbon atoms arranged hexagonally into graphene rings which gives rise to an electrical conductivity of the order of 10^4 to 10^5 S cm^{-1} [71]. This is a particularly useful property when considering applications such as lightning strike protection in exterior aircraft components [72]. The graphene rings are aligned in the direction of the fibre length meaning the inherently high tensile strength of, typically, 1.4 [7] to 7.0 [73] GPa is derived from the strength of the C-C bonds. Under maximum loading, low and high modulus fibres have an elongation of 0.9 to 1.4% and 0.4 to 0.6% [7] respectively resulting in a high stiffness material with a tensile modulus of up to 935 GPa [73]. With such a high stiffness, carbon fibres (and their composites) are typically brittle materials, although there has been some research into different matrices aiming to improve elasticity [74]. The variation in mechanical properties across different varieties of carbon fibre are largely due to the different precursors and manufacturing processes employed which are described in the following section.

2.4.2 Manufacturing Processes

Approximately 96% of the carbon fibre manufactured globally is based on the carbonisation of the precursor poly-acrylonitrile (PAN) [71]. Ammonia and propylene react to form acrylonitrile which subsequently undergoes a solution, suspension or emulsion polymerisation reaction to produce PAN [71]. Other techniques such as free-radical polymerisation have been reported but appear to be less frequently employed

[75]. Fibres are formed by drawing the liquid polymer mixture through a spinneret using a range of techniques such as wet-spinning, dry-spinning, gel-spinning, electro-spinning or dry-jet wet spinning [76]. Research has also demonstrated that PAN can be melt processed into carbon fibres [77], however, this technology has not yet reached commercialisation: it begins to degrade at the temperatures which are often required [73]. During spinning, the PAN fibres are drawn out which begins to align the polymer chains and, by increasing the tension, minimises any variation in fibre diameter [78]. Prior to stabilising the PAN filaments, it is necessary to coat the material with an oil in order to protect them and prevent the fibres from sticking together. This oil is usually silicon based [79], however, the exact formulations are commercially sensitive and details are, therefore, unpublished. For exceptionally high performance applications, it has been shown that gel-spinning is capable of producing carbon fibres with a tensile strength and modulus of up to 12.1 and 375 GPa respectively [80].

Stabilisation is induced by heating the PAN fibres to between 200 and 300˚C which forces the PAN molecules to move from a linear polymer phase to a rigid, ladder structure [81]. Recent research has focussed on the development of techniques to accelerate this process through electron beam [82], [83] and UV irradiation [84]. The second heating stage, known as carbonisation, takes place in an inert atmosphere and removes most of the remaining hydrogen and nitrogen from the PAN fibre to form filaments with a carbon content of between 93 and 99% [85]. The temperature and draw weight have a significant influence on the mechanical properties of the final product. At 1500˚C, low modulus fibres with a distorted, columnar structure are formed [86].

Research has demonstrated that the tensile modulus increases linearly with process temperature [71] and commercially, temperatures in excess of 3000˚C may be used in order to generate high stiffness fibres [87]. However, it should be noted that when the process temperature exceeds 2800˚C, there is a greater risk of forming voids within the fibre which subsequently results in a loss of strength [88]. Following carbonisation, fibres may also be graphitised in order to increase crystallinity and hence further increase the modulus. This must be carried out using an argon atmosphere as carbon reacts with nitrogen to form nitrides at temperatures above 3000˚C [87], [89]. The structure of these graphitised fibres is heterogeneous: the outer layers form highly ordered graphitic sheets with a relatively high modulus and low tensile strength compared to the fibre core [90].

Following the heat treatment processes, the carbon fibre surface is etched, either by plasma-etching [91], [92] or electrochemical-etching [93], [94], in preparation for the application of a polymeric coating known as sizing. The composition of this is held in commercial confidence but it is known to often be silica based. Carbon fibres are sized in order to facilitate good adhesion to the polymer matrix and to protect the fibre during the final stages of its production [95]. This sizing is critical in preventing fibre pull-out from the matrix and has, therefore, been the subject of a number of different studies [96]–[101]. Recently, research has focused on graphene oxide complexes incorporated into the sizing [102], [103] or modifying the fibre surface directly through the chemical bonding of various nano-species [104]. As CFRP recycling technologies act to eliminate the polymer matrix, it is possible that the sizing is also removed and hence must be

reapplied before incorporating the recovered fibres into a new matrix. During winding, fibres are grouped together to form tapes or tows. The latter consists of bundles typically containing between 3000 and 12000 individual fibres [87]. The tows are gathered on a yarn and may be subsequently woven into mats which are used in the manufacture of CFRPs as described in Section 2.5.

2.4.3 Characterisation Techniques

When considering the recovery of carbon fibres from polymer matrices, it is desirable to minimise the influence of the recycling process on the quality of the fibres: damaging this high-value material results in downgrading the product, thus limiting its future applications. To this end, carbon fibres may be characterised separately to the composite material using a number of different methods; those employed as part of this research project are detailed in Chapter 5 while a range of characterisation techniques which are available are summarised as part of this literature review. The mechanical properties most commonly considered are the tensile strength and modulus. Both are typically measured through either single fibre [105]–[109], or bundle testing [110], [111]. It has been demonstrated in previous research that electrical impedance spectroscopy (EIS) is able to exploit the conductivity of carbon fibre and allow the number of fibres within a bundle to be determined to a high degree of accuracy [112].

The modulus is determined by considering the strain (or elongation) of the filament; ductile materials will stretch and undergo plastic deformation whereas carbon fibres, as brittle materials, will elastically deform and usually fail at elongations of less

than 1.4% [7]. The tensile strength of the fibres is limited due to the presence of surface defects and internal flaws: it is at these points that failure occurs due to the magnification of stress upon the application of a load [108]. Some work has been completed on calculating what the critical flaw size is for a variety of different fibre types [113]. As failure points are randomly distributed along a fibre, the gauge length of the test specimen has a large impact on the measured strength and stiffness. Long filaments will appear weaker but have a smaller spread of data while the inverse is true for short fibres [109] with tensile strengths of up to 13 GPa being recorded when the gauge length is of the order of a few microns [105]. For this reason, a gauge length of 25 mm is defined as part of the standard test protocol described by ISO 11566:1996 [114]. In addition, a minimum of 30 fibres must be characterised in single filament testing for the sample size to be representative of all fibres within a single batch [114]. This is likely to give a large spread of data, an average of which may be skewed by particularly strong or weak fibres and thus not give a good indication of the true strength. To overcome this limitation, the data set may be characterised using a Weibull, rather than a normal, distribution which enables the calculation of a scale and shape factor instead of a mean and standard deviation [105], [108], [109], [115]–[117]. The scale factor may then be used to quantify the likely strength of an individual fibre, while the shape parameter may be quoted to indicate the shape of the distribution: when this is approximately equal to 1, the failure rate is constant across the data set [105].

As the load applied to a composite is transferred to the fibre through the matrix / fibre interface, the interfacial shear strength (IFSS) between the fibre and the matrix is

critical to developing a high performance composite material [118]. This property is derived from the adhesion between the two materials and the geometry of the reinforcement. Below a critical fibre length, less than the maximum possible load is transferred to the reinforcement and thus the strength of the composite is less than what may be achieved. The critical length depends on the fibre and matrix material but is typically approximately 30 to 50 mm within CFRPs. Provided this critical length is exceeded, composites manufactured from discontinuous fibres may therefore demonstrate similar mechanical properties to equivalent CFRPs made using long, continues carbon fibre tapes [118].

Due to the lack of chemical reactivity of carbon fibre, there is generally poor adhesion between the fibre surface and a polymer which may lead to fibre pull-out [95] and a subsequent reduction in the mechanical performance. There has, therefore, been extensive research into enhancing the interfacial properties through both wet chemical methods such as the application of sizing [119], [120], acidic modification [121] and electrochemical modification [122]. Dry techniques, for example, plasma modification [123] and high energy irradiation [124] have also been investigated, although it is the application of sizing which appears to be most widely used in industry [7]. To this end, the wettability of the fibre surface has also been investigated using contact angle measurements [125], [126]. The IFSS is typically measured using fibre pull out tests whereby a polymer droplet is deposited on a fibre surface and the force required to remove it is measured [97], [127]–[130]. Compared to unsized carbon fibre, previous work has shown that it is possible to increase IFSS by 14% when using a polyacrylate

emulsion [130]. When solutions containing epoxies and amines are applied, IFSS can be increased by up to 60 [127] and 80% [129] respectively thus demonstrating that this property is highly dependent on the sizing agent used.

The presence of functional groups on the fibre surface has also been shown to influence adhesion to the matrix and, therefore, analysis of the surface chemistry has also been conducted. Techniques include X-ray diffraction (XRD) [131], infrared (IR) spectroscopy [130], [132] or Raman spectroscopy [133], although the most common appears to be X-ray photoemission spectroscopy (XPS) [97], [127], [132], [134]. This is capable of identifying, and quantifying the ratio of, various different species bonded to the carbon surface. Desirable functional groups include hydroxyls, carbonyls and nitriles, although research has shown fluorinated compounds also facilitate excellent adhesion due to the polarity of the C-F bond [131].

The surface of the fibres may also be inspected through different imaging techniques in order to identify any of the defects which lead to a reduction in tensile strength. Chief among these is scanning electron microscopy (SEM) which has been used in the characterisation of both individual fibres [95], [105], [132], [135], [136] and fibre-polymer composites [137], [138]. Transmission electron microscopy (TEM) appears to be more commonly employed in the characterisation of nano–carbon fibres which typically have diameters of less than 0.5 μm [139]–[141], although there are some reports on the application of this technique to conventional carbon fibres [142]. Surface characteristics such as roughness have also been quantified through atomic force

microscopy (AFM) [99], [101], [132], [143], [144] with this technique in particular also used to characterise recycled carbon fibre with the aim of identifying cracks and / or any polymeric residue [145], [146]. Although not applied to individual fibres, it has also been demonstrated that alternative imaging techniques such as X-ray computed tomography (XRCT) are capable of identifying voids within composite materials [137], [147]–[149] and hence may be useful when considering the degradation mechanisms taking place within a CFRP.

With the advancement of smart, multifunctional materials, carbon fibres have also found applications in sensors, resistive heating, electromagnetic shielding and energy storage [150]. Success in these markets rely primarily on the electrical properties of carbon fibre and as such, some recent work has characterised fibres in terms of their conductivity in addition to their mechanical performance [151]–[153]. In these experiments, a potential difference is normally applied across a sample of known dimensions and the resultant current measured. Using this data, the resistance and hence conductivity can be calculated. As recycled carbon fibres may also find applications in these multifunctional materials [154], quantifying any changes in electrical, as well as mechanical and surface, properties due to the developed recycling process will be of interest in future research. As it is likely that recycled carbon fibres will be incorporated into a polymer matrix, it is it is necessary to consider the various manufacturing techniques employed in the production of CFRPs. This will also provide some insight into the processing of carbon fibres prior to reaching their end-of-life (EoL).

2.5 Manufacturing CFRPs

2.5.1 Lamination

Following the manufacturing process described in Section 2.4.2, carbon fibres may be supplied on a yarn as a continuous tow, as a unidirectional tape, or woven together into a variety of structures. Several different processes exist to incorporate these fibres into a polymer matrix; the process selected depends on the final application of the product. As it is likely that existing methods will be used to produce CFRPs from recycled fibres, it is necessary to consider the requirements of the main manufacturing technologies. One of the simplest is lamination, or hand lay-up, whereby a resin is coated onto the inside of a mould before draping a carbon fibre fabric into it. By pressing the fabric into the mould, the resin penetrates into the fibres. An additional coating of resin is applied onto the fabric and, if required, further layers of carbon fibre can also be pressed into the mould until the desired thickness is reached [33]. At this point, the resin is cured using one of the techniques described in Section 2.3.2. Although this is a simple technology with good versatility in terms of the final product, the quality of the composite is usually low due to the entrapment of air and lack of compaction. This process relies on the use of continuous fibres [33] and may, therefore, be unsuitable for manufacturing a secondary composite material as CFRPs are usually shredded prior to being recycled.

2.5.2 Compression Moulding

To overcome the concerns regarding product quality, compression moulding may be considered a viable alternative manufacturing process. This is similar to

lamination, however, rather than manually coating the fibre weave with a liquid resin, pre-impregnated (pre-preg) fabrics are used. Anywhere from two or three, to twenty layers may be stacked within a mould, the second half of which is then hydraulically pressed on top and heated. This activates the cross-linking agent within the polymeric mixture and so cures the resin. The composite material is then removed and the edges are trimmed to remove any excess material. This technique can be used to produce parts with complex shapes for specific applications [155]. The carbon fibre pre-preg may also be combined with sheet moulding compound (SMC) which consists of glass-fibre reinforced polyester which allows the final product to benefit from the superior properties of carbon fibre while minimising manufacturing costs [156].

2.5.3 Liquid Composite Moulding

Unfortunately, the pre-pregs used in compression moulding have a finite shelf life, are often expensive and the fibre orientation can only be in-plane thereby limiting the composite toughness and shear strength [33]. To overcome these issues, liquid composite moulding (LCM) is used to manufacture parts for a number of applications as a cost effective alternative with a relatively high production rate [157]. A dry, continuous carbon fibre weave or random mat is assembled into a pre-form which has a similar geometry of the final component. This is then placed into one half of a stiff, normally metal, mould which is closed and sealed prior to injecting a mixture of resin and cross-linking agent [158]. Effectively wetting all fibres is essential to forming a high quality composite part without any voids in the matrix. Consequently, a number of different studies have been conducted investigating various techniques which facilitate good

permeability of the resin through the fibres [159]. Resin transfer moulding (RTM) pumps the monomer mixture into the mould typically at a pressure of between 600 and 700 kPa [159], [160]. The application of a vacuum (vacuum-assisted resin transfer moulding, VARTM) can selectively draw the resin through the fibre layers to less accessible parts of the mould and thereby reduce the likelihood of forming voids. This may give a high fibre volume content of up to 60 vol.%. The infusion time for these techniques is usually of the order of minutes, occasionally hours [161]. To accelerate the process and reduce this to seconds, higher pressures of up to 7 MPa may be used, such as in structural reaction injection moulding (SRIM) [162]. Alternatively, the Seaman composite resin infusion moulding process (SCRIMP) has also been developed where one half of the mould is metal and the other is a membrane. Here, only a vacuum is used to draw the resin in between the preform and the membrane. As the polymer only needs to flow through a small thickness of the tortuous preform, infusion is fast despite the small pressure differential of less than 100 kPa [163]. Once the resin is fully infused, it is cured at a specific heating rate, temperature and time before the mould is opened and the composite removed. As the heating stage is costly both in terms of initial capital and operation, some research has been conducted with the aim of producing CFRPs by a resin transfer process without the need for an autoclave. Samples manufactured with this technique demonstrated good mechanical performance but, with a relatively low T_g of approximately 119˚C [160], this production technique is less suited to high temperature applications.

2.5.4 Vacuum Assisted Resin Film Infusion Moulding

Vacuum assisted resin film infusion moulding (VARFIM) aims to combine the advantages of LCM technologies with the versatility of lamination. Preparation of the material and mould is similar to the latter technique; however, the resin is not just cured. A vacuum bag is placed over the open mould and the pressure reduced in order to degas the polymer minimising the presence of voids in the composite product. The pressure differential may be used to draw additional resin into the mould and forces it to infuse through the fibres [164]. Once the vacuum infusion is complete, the resin is allowed to cross-link following a specified curing cycle. Although rapid cure resins may be used [165], VARFIM is a relatively slow process. It does, however, facilitate the incorporation of a wide variety of fibre orientations into a polymer matrix. This enables the manufacture of high quality CFRPs with complex geometries which are suitable for use in aerospace and structural applications [166].

2.5.5 Filament Winding and Fibre Placement

Automated manufacturing processes have the potential to lower the production costs of CFRPs and hence enable their continued entry into additional markets, such as the automotive industry, where the weight saving brought by CFRPs is seen as an environmental benefit. One of the most established automated processes is filament winding where, as the name suggests, fibres in a tow or tape are drawn from a yarn, pulled through a resin bath and wound around a rotating mandrel under tension. This means the composite product must have axial symmetry and this technique is, therefore, used in the manufacture of pressure vessels, pipes and some aircraft

components [167]. Mandrels are typically cylindrical, but rotationally symmetrical geometries such as cones [168], arches [169] and disks [170] are also discussed in the literature.

Fibre placement is similar to filament winding, except this is a dry process whereby pre-preg tows or tapes are pushed towards the surface of a mandrel. Heat is applied and rollers push the pre-preg into the shape of a mould, meaning this technique does not require the composite part to be axially symmetrical [171], [172]. Where a uni-directional (UD) tape is used, fibre placement is generally a fast production method as the relatively large tape widths allow high coverage of the mandrel surface in a single application [171], [173]. The high degree of precision and repeatability when using both tapes and pre-preg tows in filament winding and fibre placement has led to these technologies being a production method of choice for safety critical components, particularly within the aerospace industry [172].

2.5.6 End of Life Options

Although CFRPs have a large potential for improving sustainability through the weight reduction of aircraft and vehicles, manufacturing of high-capacity wind turbines, and increased service life of structural components [174], they are, at present, a resource inefficient material. The environmental burden of manufacturing may be quantified by considering the embodied energy of production. For epoxy matrices, this stands at 76 to 80 MJ kg^{-1}, while carbon fibres are even higher at 183 to 286 MJ kg^{-1} [69] with maximum estimates in the literature of up to 585 MJ kg^{-1} [175]. This compares to

13 to 32 MJ kg^{-1} and approximately 6.5 MJ kg^{-1} for glass and flax fibres respectively [69]. In addition to manufacturing offcuts and out-of-date pre-pregs, the quantity of EoL CFRP components which require disposal is also forecast to reach 115 kt by 2035 [2], [176]. Although the proportion of CFRP waste sent to landfill does not appear to be quantified in the available open literature, multiple sources agree that only a fraction is recycled [177], [178]. Within Europe in particular, growing environmental concerns have led to the introduction of legislation, the Waste Framework Directive, which severely restricts the quantity of material sent to landfill [179]. Similarly, the End of Life Vehicle Directive states 85% of a vehicle must be recycled [180]. However, until effective composite recycling techniques are commercialised, this is likely to act as a barrier to the further adoption of CFRPs in the automotive industry.

Multiple economic studies have demonstrated that the financial cost of recovering carbon fibre from CFRPs may be as low as 5 to 10% of the cost of manufacturing virgin material [181], [182]. For this reason, effective recycling is not only an environmental responsibility, but also a fiscal opportunity. At present, however, there are very few commercial recycling processes in operation [3]. Due to the inherently complex nature of CFRPs, the exploration of various technologies to recover carbon fibre and polymer matrices remains an active area of research. As illustrated by the manufacturing techniques described in this chapter, the majority of processes rely on the use of continuous fibre. This may cause some concern when considering the manufacture of CFRPs from recovered fibres: it is almost always necessary to reduce the size of the composite structure prior to separating the fibre from the resin due to the

size limitations of processing equipment. For this reason, recovered fibres tend to be relatively short and are unsuitable for use in woven architectures. Although non-aligned, short fibre mats are commercially available [183], suggesting that there is a market demand for this product, manufacturing of secondary CFRPs may be limited to an injection moulding process which consequently reduces the number of potential applications. As the focus of this research project is the recycling of carbon fibre, the literature surrounding the range of techniques which have been previously investigated is, therefore, discussed in the remainder of this review.

2.6 Mechanical Recycling Technologies

The primary objective of recycling CFRPs is to separate the fibres from the polymer matrix, with focus usually on the recovery of the former component: carbon fibres are of greater economic value than most resins. It is also important to draw the distinction between mechanical recycling and size reduction which is generally employed regardless of the recycling method considered. As composites are often used in large structures such as a aerofoils, fuselages and wind turbines, it is not feasible to develop a recovery technique which could handle the entire component. Mechanical techniques reduce a composite to a fine powder which may then be incorporated as a filler into a new composite material, low grade polymers or roads [184]. Although this has reached commercial maturity for glass fibre reinforced polymers (GFRPs) [185], it is currently considered uneconomical for CFRP recycling due to significantly downgrading a previously high value material [3]. Despite this, there is some literature studying

mechanical recycling technologies for CFRPs with numerous works considering milling and high voltage fragmentation.

2.6.1 Milling

Within a milling recycling process, a CFRP is first shredded, typically to 50 to 100 mm in length. This is followed by ball milling or fluidised bed grinding to create a fine particle mixture [186]. This may be sieved to create fibre-rich and resin-rich fractions which each have separate applications. Thermoplastics may be melt processed to recover useful, if low-grade, polymers, however, this is not possible for thermosets [172]. As the effective separation of fibre reinforced plastics (FRPs) according to matrix material is not easily achieved [187], the primary disposal route for the resin-rich fraction appears to be incineration with energy recovery.

The fibre particulates recovered from a CFRP may be incorporated into SMCs and it has been demonstrated that, at a proportion of 20 wt.%, the impact and flexural strength and flexural modulus is similar to that of standard SMC formulations containing glass fibres [188]. However, it was necessary to carefully control the distribution of recycled carbon fibre and virgin glass fibres in order to ensure sufficient product quality. This may mean changes to manufacturing stages or additional quality control measures are necessary for the widespread deployment of this technique. It has also been reported that CFRPs produced with carbon fibres that have been recovered following a grinding process showed similar mechanical properties to composite materials manufactured from virgin fibres of a similar length [189]. Although this suggests that the

mechanical properties of the recovered carbon fibres are not significantly altered, the size reduction involved in this process results in downgrading the material, thereby limiting future applications.

Additional research has demonstrated that the properties of PP are enhanced when reinforced with short fibres typical of those recovered from mechanical recycling techniques. Coarse, intermediate and fine sizes were considered with the fibre length ranging from 75 to 600 μm. Results showed that tensile strength and stiffness increased by as much as 50 and 100% respectively compared to unfilled polypropylene when fibre fraction was increased to 30 wt.% [190]. Similar findings have also been reported when using ABS [191] and an epoxy matrix [192] thus demonstrating potential uses for carbon fibre recovered from mechanical recycling methods.

Multiple life cycle assessments (LCAs) for the mechanical recycling of carbon fibre have been conducted which all demonstrate the significant environmental benefit of this disposal method when compared to landfilling waste CFRPs [193]–[195]. It has been estimated that, for a recycle rate of 10 kg h^{-1}, the energy intensity of a CFRP milling process is 2.03 MJ kg^{-1} [195] which compares to the embodied energy of carbon fibre alone of up to 585 MJ kg^{-1} [175]. Unfortunately, the market for such small carbon fibre particulates remains limited with target applications focussed on the replacement of virgin glass fibres. Despite the large potential energy saving, financial analysis has demonstrated that milling, as a CFRP recycling technology, is currently not an

economical disposal route [194] and as such, this is not, at present, a commercially exploited technology [3].

2.6.2 Electrodynamic Fragmentation

Originally developed for the extraction of metals from ore [196], electrodynamic fragmentation has also been investigated as a potential recycling technology for FRPs, with most research considering the recovery of glass fibres. This process involves immersing a composite into a dielectric liquid, such as water, and placing two electrodes either side. A high potential difference, typically between 100 and 200 kV is then applied in a series of pulses which forces separation of the fibres from the polymer [197]–[199]. Although this technique is capable of fracturing epoxies [200], initial characterisation of the fibres demonstrated that up to 40 wt.% of the resin remained adhered to the surface [197] which may limit their future application over concerns of adhesion to a new polymer. With respect to the recycling of carbon fibres, electrodynamic fragmentation has been compared to milling technologies in terms of its cost, energy consumption and scalability, amongst other criteria [201]. This study reported that, beyond a lab scale, this approach is not competitive with conventional mechanical recycling methods. As the latter technique is also not considered economically viable [194], electrodynamic fragmentation is thought to be unfeasible as a CFRP recycling process.

2.7 Thermal Recycling Technologies

Of all potential CFRP recycling techniques, only pyrolytic processes have achieved commercialisation [202]. Here, the composite waste is heated either in air or an inert

atmosphere at temperatures ranging from 450 to 750˚C which results in the cracking of the polymer to low molecular weight compounds [203]. Unlike mechanical recycling, it is possible to attain clean fibres using pyrolysis and it is consequently easier to incorporate them into a new polymer matrix. Various methods based on the pyrolysis of the resin are described in the literature and are reviewed in this section.

2.7.1 Fixed Bed Reactors

Within a fixed bed reactor, the polymer matrix is decomposed into a mixture of oils, gases and char, the composition of which depends on the type of resin and local atmosphere. The presence of oxygen results in the oxidation of oils and, therefore, favours the production of a synthetic gas mixture comprising mostly of carbon dioxide (CO_2), carbon monoxide (CO), methane (CH_4) and hydrogen (H_2) [204]. This gas may be used as a fuel for the process, thereby recovering some energy and possibly making it self-sustaining. Although this process has been investigated for the recycling GFRPs, the high temperatures necessary, particularly for the decomposition of high performance thermoplastics and thermosets, results in significantly degrading the properties of the material. Research has also shown that there may be a loss in the strength of the glass fibres by more than 50% [205]. For this reason, pyrolysis appears to be more suited for the recovery of carbon fibres; as they are frequently processed at more than 1500˚C during their manufacture (described in Section 2.4.2), carbon fibres are less susceptible to thermal degradation.

Fixed bed pyrolysis tends to be a two stage process whereby the resin is first combusted between 350 and 500˚C [206]. Due to the formation of char, the second stage involves an elevated temperature up to 750˚C, possibly in an oxygen atmosphere to facilitate the recovery of clean fibres [207]. The total process time, typically between 20 and 150 min, seems dependent on the matrix material with high performance polymers such as PEEK and epoxies requiring longer [204], [206], [208]–[212]. To ensure the mechanical properties of the fibres are maintained, reports in the literature suggest an upper temperature limit of 550˚C is necessary, although this also appears to be dependent on the variety of carbon fibre: Hexcel AS4 fibres demonstrated greater degradation than Toho-Tenax HTA fibres when processed under similar conditions [213].

On an industrial scale, CFRPs from various sources and of large geometries up to several metres in length are loaded on to a moving conveyor which is fed into a furnace. The atmosphere and operating temperature are carefully controlled, which facilitates the recovery of clean fibres. It is claimed by ELG Carbon Fibre Ltd. that the mechanical properties are 90% of those of virgin material [3]. As the fibres are blended together to ensure a consistent product, this claim is difficult to verify, although literature sources investigating similar conditions report comparable findings [207], [211].

Recent research has examined the potential for superheated steam to recover carbon fibres, both as a method for decomposing the matrix [210], [211] and to activate the fibre surface [208]. Compared to the use of an inert or air atmosphere, a similar process time of 60 min was necessary, although these works relied on the use of higher

temperatures of up to 850˚C. At less severe conditions, there is reportedly little change in the mechanical properties of the fibres [211], however, compared to virgin material, there was a reported reduction in tensile strength of up to 35% after processing at 850˚C [210]. Unless the objective is to produce activated carbon fibres, it therefore does not appear beneficial to use a steam atmosphere.

2.7.2 Fluidised Bed Reactors

Compared to a fixed bed reactor, fluidised beds offer the advantage of improved heat and mass transfer which may, therefore, facilitate greater throughputs of material and subsequently lower operating costs. This process, initially developed at the University of Nottingham, uses hot air at 450 to 550˚C to fluidise silica sand particles [214], [215]. The temperature selected depends on the matrix material with more severe conditions needed to decompose thermally stable epoxies. Decomposition of the polymer matrix takes place due to heat and attrition of the scrap CFRP by the sand. Liberated carbon fibres are collected in a cyclone and the exhaust gasses used in energy recovery. As dense contaminants such as metals drop to the bottom of the reactor, this process is particularly suited for the recycling of EoL parts, however, almost all of the polymer is converted to gasses meaning the recovery of potentially valuable oils is not possible [3].

Although some research has shown that secondary CFRPs have similar mechanical properties to the equivalent virgin fibre reinforced composites, characterisation of the individual fibres recovered from a fluidised bed process have

shown a strength reduction of approximately 25% [216]. Surface analysis, however, demonstrated little change in the oxygen content suggesting that a new polymer will adhere well to these fibres [217]. Financial assessments have estimated that the cost of the fibre product may be as low as £4 kg^{-1} [218] compared to the price of virgin carbon fibre of £27 to £54 kg^{-1} [3], [219]. Virgin glass fibre, which recycled carbon fibre may be able to displace, currently retails at approximately £1 to £10 kg^{-1} [220]. Similarly, the primary energy demand and global warming potential of manufacturing CFRPs with carbon fibres recovered from this process are estimated to be 32 to 50% and 33 to 51% lower respectively, compared to using virgin carbon fibres [214]. Despite the loss of the polymer matrix and the fact that this technology remains at the pilot stage, the significant energy and financial savings compared to the use of virgin fibres suggest that fluidised bed pyrolysis is also a viable recycling technology.

2.7.3 Microwave Induced Pyrolysis

Microwave heating may offer an advantage over the conventional heating methods used in fixed and fluidised bed reactors: as heating occurs from within the material, the temperature is rapidly increased resulting in very short process times. Lester et al. demonstrated that it is possible to obtain clean fibres from an epoxy resin within 8 s using a 3 kW microwave, although it was noted that the tensile strength and modulus of the recovered fibres had been reduced by 20 and 12% respectively [221]. Differences in the topology were also noted, possibly due to the exposure of carbon to microwaves. Although there has been some commercial interest in the microwave

processing of polymeric composites for recycling applications [222], there has been very little development of this technique over the past decade.

2.7.4 Molten Salts

Some recent research considering the thermal reclamation of carbon fibres has involved the use of molten salts; both potassium hydroxide (KOH) [223] and zinc chloride ($ZnCl_2$) [224] have been applied to carbon fibre / epoxy matrix composites. In both cases, clean fibres were recovered in reasonable reaction times of less than 120 min, although $ZnCl_2$ required a higher process temperature of 360˚C compared to 285 to 330˚C for KOH. Aside from the different salts, this difference in process temperature may also be due to different resin formulations. In both cases, the tensile strength and modulus of the individual fibres showed very little reduction after processing. Heating the fibres in air to the same temperature even resulted in a greater reduction in mechanical properties compared to when they were in contact with $ZnCl_2$ [224]. Due to the effective recovery of clean, high quality carbon fibres using a lower temperature than conventional pyrolysis, the use of molten salts represents an interesting development in the pyrolysis of CFRPs for recycling applications.

Although only thermal recycling technologies have reached commercialisation, they are resource inefficient processes due to the loss of the polymer matrix which may make up to 50 wt.% of the CFRP [161]. As a result of the resin decomposition and high temperatures used, large quantities of CO_2 are generated: an emission which developed countries have pledged to limit under the Paris Climate Agreement [225]. It is, therefore,

necessary to consider alternative methods which enable the recovery of carbon fibres and potentially useful monomers.

2.8 Chemical Recycling Technologies

Solvolysis is a chemical treatment whereby the resin is dissolved in a suitable solvent rather than pyrolysed following one of the processes discussed in Section 2.7. Depending on the chemicals involved and reaction conditions, the solvent may be in the liquid, gaseous or supercritical state, but the general decomposition process remains the same. The solvent diffuses through the polymer matrix causing the composite to swell. Specific chemical bonds are then broken and the smaller, now soluble molecules, diffuse back out of the composite into the bulk fluid [178]. Although an effective separation process is yet to be developed, the recovery and subsequent reuse of these monomers is both environmentally and economically beneficial. Solvolysis has a further advantage over pyrolytic techniques as, usually, comparatively lower temperatures are necessary to liberate the fibres which leads to a significant energy saving. Based on the manufacture of a secondary CFRP, the energy demand for fluidised bed pyrolysis and chemical recycling has been estimated at approximately 51.7 MJ kg^{-1} [214] and 38.4 MJ kg^{-1} [226] respectively.

Chemical recycling technologies can be classified according to their reaction conditions. Low temperature and pressure (LTP) processes generally consider temperatures of less than 200˚C and ambient pressure, while high temperature and pressure (HTP) systems operate anywhere between 220 to 450˚C and 0.3 to 30 MPa.

Due to these extreme conditions, HTP decomposition reactions may be considered a thermochemical process as it is the combination of both heat and the solvent which enables recovery of the fibres. Pilot scale solvolytic CFRP recycling processes have been developed by Adherent Technologies Inc. using LTP (150˚C, 1.0 MPa) and HTP (300˚C, 3.4 MPa) conditions [227], however, the technology has not been fully commercialised. Furthermore, the solvent / catalyst systems used are not detailed in the available open literature [227], [228]. This section, therefore, discusses research conducted at lab-scale only and pertains to both LTP and HTP processes with a focus on the reaction conditions, kinetics, organic products and properties of the recovered fibres.

2.8.1 Low Temperature & Pressure (LTP) Processes

As relatively mild conditions are used, LTP processes rely on the use of various additives, acids and / or strong oxidising agents to facilitate recovery of the fibres. Nitric acid was one of the first systems applied to epoxy resins [229]–[231], however, high concentrations of up to 6 M and very long reaction times of up to 100 h were necessary to achieve a decomposition of the matrix of more than 95% [229], [230]. This has been improved through the use of sulphuric [232] acid which reduced the reaction time to several hours, however, hydrogen peroxide (H_2O_2) was also used to oxidise the matrix. It was also necessary to stir the reaction system which may result in the entanglement of the carbon fibres. Although an alignment process has been developed [233], this has not yet reached commercial maturity. Stirred reactor systems may, therefore, limit future applications of the carbon fibres as CFRPs manufactured with aligned fibres generally result in improved mechanical performance [136], [234].

The use of H_2O_2 for the decomposition of epoxies is not uncommon and has also been used in combination with dimethyl formamide (DMF) [235] and acetic acid [177], [236], [237]. Although relatively short reaction times are achievable, these recycling methods all rely on some form of pre-treatment to swell the polymer prior to its decomposition. This pre-treatment not only involves additional chemicals, but is also typically 3 to 4 h [177], [236] which results in greatly increasing the overall process time.

In addition to acids, potassium hydroxide (KOH) [231], benzyl alcohol / tripotassium phosphate (K_3PO_4) [238] and zinc chloride ($ZnCl_2$) / ethanol [239] systems have also been investigated. Although it is claimed that all are able to recover clean fibres, long reaction times of between 3 and 14 h were necessary [231], [238] which is not favourable when considering the economic case for the chemical recycling CFRPs. The sole advantage of using LTP processes is the greater reaction control offered by these systems: as secondary reactions do not seem to occur, there may be greater recovery of monomeric compounds [3]. Unfortunately, this benefit may be outweighed by the level of risk in terms of human health, safety and the environment associated with the use of concentrated strong acids and oxidising agents. These chemicals are hazardous, difficult to dispose of and their use may not be considered a sustainable approach to the recycling of CFRPs. For this reason, there has been a large amount of research focussing on the use of HTP processes which enables the use of generally recognised as safe (GRAS) solvents.

2.8.2 High Temperature & Pressure (HTP) Processes

HTP processes eliminate the need for the potentially harmful chemicals discussed in Section 2.8.1, often by operating at near- or supercritical conditions. By raising the temperature and pressure, a substance moves through the normal states of matter of liquid and gas to become a supercritical fluid (SCF). These states of matter are illustrated by the phase diagram of water provided in Figure 3.

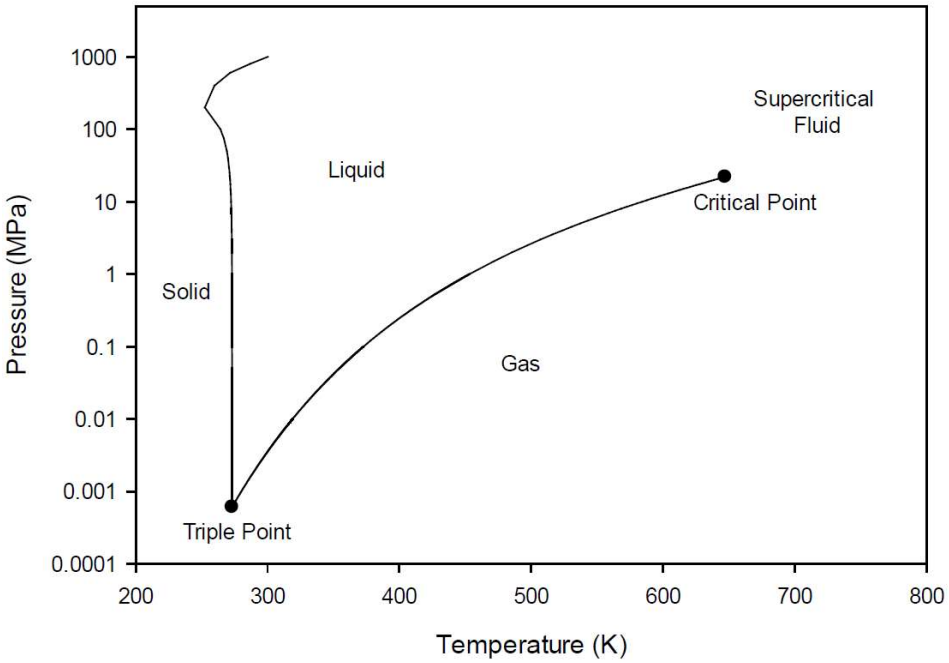

***Figure 3**. Phase diagram for water showing the triple and critical points. Solid lines represent phase transitions, taken from* [111].

In the supercritical phase, a solvent exhibits high diffusivity and mass transfer, very low viscosity and a pressure dependent solvating power. This enhanced solvating power is derived from the structure of the SCF: the density and di-electric constant is typically close to that of the liquid while the diffusivity and viscosity tend to be similar to that of the gas. Small changes in temperature and pressure lead to significant changes

in both dielectric constant and viscosity which in turn leads to SCFs acting as “tuneable” solvents [240]. These properties can be exploited in order to decompose polymer matrices thus liberating carbon fibres using GRAS solvents such as water, short chain alcohols and acetone. It is, however, difficult to compare the efficacy of these different solvents and the conditions necessary as the investigations published in the literature often also consider different types of resin. Although the polymers considered in various studies are all epoxies, an RTM6 composite required subcritical water at 360˚C while 914 epoxy was degraded at 310˚C [241]. Similarly, a BPA epoxide cross-linked with 1,2-cyclohexane dicarboxylic anhydride was also fully decomposed at 350˚C using supercritical methanol [178]. However, Cytec LTM26EL epoxy, which is cured with amines, required 450˚C to achieve a similar degree of degradation in the same reaction time [242]. It is, therefore, necessary to consider not just the solvent, additives and reaction conditions when evaluating HTP solvolysis processes, but also the polymer under investigation in order to determine which reaction systems are most effective.

Due to its widespread availability, low costs and relative lack of hazards, water seems one of the most widely studied solvents for the recycling of CFRPs [243]–[246]. However, with a critical point of 374˚C and 22 MPa [247], very high temperatures and pressures often in excess of 400˚C and 25 MPa are necessary to fully decompose an epoxy resin [243], [245]. This leads to the need for very expensive process equipment which is a barrier to the commercialisation of this technology. Although the critical points of short chain organic solvents are much lower than that of water (see Table 1), similarly high temperatures of 350 to 400˚C are often necessary to completely eliminate

the resin [178], [242], [248], although it is not apparent whether this is due to poor solvating power or slow decomposition reactions at less severe conditions. These solvents do, however, possess an advantage over water as for a similar temperature, the pressure is significantly lower resulting in a reduction in cost of the reactor systems.

***Table 1**. Critical points of common solvents (adapted from* [247]*)*

Solvent	**Critical temperature, T_C (˚C)**	**Critical pressure, p_c (MPa)**
Water	374	22.1
Methanol	240	7.95
Ethanol	241	6.30
Propan-1-ol	264	5.20
Acetone	235	4.80

Methanol [242], [249], ethanol [239], [242], [248], propanol [242], [250] and acetone [251], [252] have all been reported as suitable GRAS solvents when considering the degradation of thermoset resins. The potential for these solvents to improve resource efficiency compared to pyrolytic processing has been further demonstrated by Okajima, et al. where supercritical methanol at 320˚C was able to selectively cleave the cross-linkages which facilitated the recovery of monomeric compounds. This was subsequently recycled into a secondary material, although the mechanical properties were reduced compared to that of a virgin polymer [249].

To reduce the environmental and economic cost of recycling, recent work has focussed on minimising the necessary reaction temperature. This may be achieved through the use of a semi-continuous flow reactor whereby the solvent is continuously withdrawn while the composite remains stationary. This enhances the mass transfer of the solvent to the surface of the resin, and of the decomposition products away from the surface of the fibre, hence accelerating the decomposition reaction [117], [242], [248], [251]. Under batch conditions, solvent mixtures have also been considered with results demonstrating that the inclusion of water along with an organic solvent enhances the degradation of the polymer [145], [248], [252], [253]. For example, Oliveux, et al. showed a mixture of 80 vol% acetone and 20 vol% water heated to 350˚C achieved the highest decomposition of a DGEBA epoxy cured with DDS [252]. This data suggests that the preferred reaction pathway is hydrolysis, however the inclusion of alcohols and acetone created a mixture with a critical point lower than that of water, meaning the system benefits from the enhanced properties of supercritical fluids. The findings from this study are shown in Figure 4 [252], however, this research did not identify the minimum necessary reaction time and process temperature which enabled complete decomposition of the resin. Identification of these optimum conditions, therefore, represents an opportunity for further investigation.

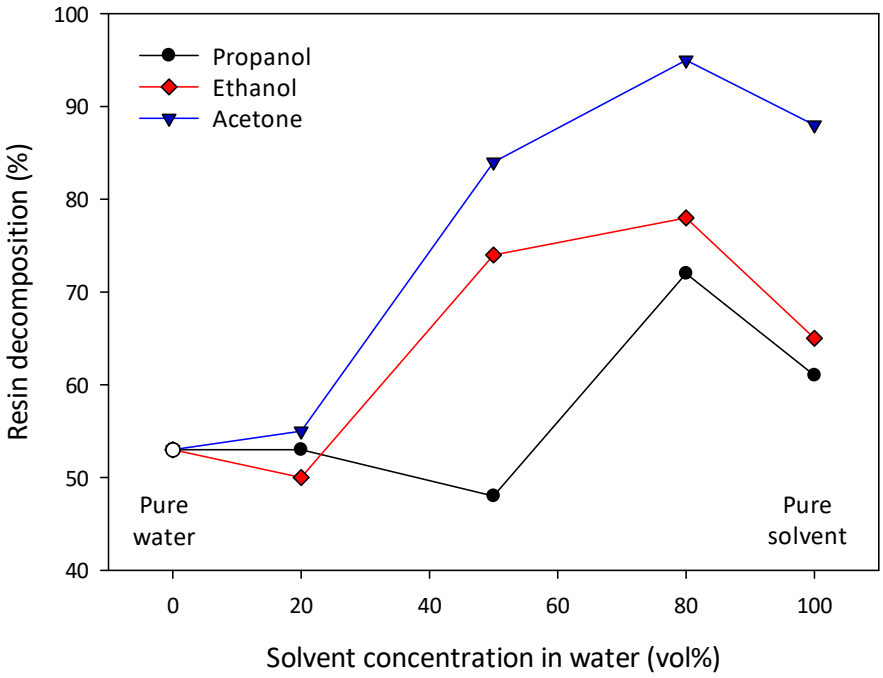

***Figure 4**. Effect of various solvent mixtures on the decomposition of DGEBA / DDS resin at 350˚C, reaction time, t_R =30 min. Data taken from* [252].

Where LTP processes have mostly considered the use of acids, alkaline salts appear more widely investigated as additives under HTP conditions. Results from numerous sources have demonstrated that the inclusion of KOH is able to significantly reduce the necessary reaction temperature from 350 to 275˚C when supplied at a concentration of 0.02 M for the same reaction conditions [250], [254]–[256]. Sodium hydroxide (NaOH) [257] and caesium hydroxide [254] (CsOH) have also been investigated, although it is KOH which appears to be the most effective. Caesium carbonate (Cs_2CO_3) has been shown to accelerate the decomposition of PEEK [111], however, as this is a thermoplastic, Cs_2CO_3 may not be suitable for catalysing the degradation of thermoset materials. More recently, weak-Lewis acids have been considered as alternative catalysts with Liu et al. demonstrating that $ZnCl_2$ dissolved in ethanol at a concentration of 1.5 M is capable of degrading aerospace composite waste

with a T_g of 210˚C at just 220˚C [239]. Furthermore, it was possible to reuse some of the decomposed matrix in a secondary CFRP up to a fraction of 15 wt.% without any deterioration in the mechanical properties [239] thus demonstrating the potential for thermochemical processes to recover useful polymeric compounds. The use of these catalysts in conjunction with an acetone / water solvent mixture, however, has not been considered in any earlier work. It would, therefore, be useful to investigate whether alkaline salts or metal chlorides are able to reduce the process time and temperature required for complete solubilisation of the polymer. If successful, this may facilitate substantial energy and economic savings.

2.8.3 Reaction Kinetics

Numerous kinetic studies concerning the decomposition of polymers have been conducted, either focussing on their degradation due to various thermal treatments [258], [259], when subjected to irradiation [260] and when solvolysed under HTP conditions, specifically for recycling applications [242], [245], [261]. Studying the kinetics of a reaction can allow the relationship between all process variables, namely temperature, time, reaction order and concentration, to be determined. This may be expressed mathematically as demonstrated by Equations (1) to (4) [262].

$$\frac{d\alpha}{dt} = k(T)\, f(\alpha) \tag{1}$$

$$k(T) = k_0\, e^{-\frac{E_A}{RT}} \tag{2}$$

$$f(\alpha) = \alpha^n \tag{3}$$

$$\alpha = \frac{m_i - m(t)}{m_i - m_f} \quad (4)$$

Where α = is the extent of conversion (dimensionless), t = time (min), T = temperature (K), k = rate constant (min^{-1}), k_0 = frequency factor (min^{-1}), E_A = activation energy (kJ mol^{-1}), R = universal gas constant (kJ mol^{-1} K^{-1}), n = reaction order (dimensionless), $m(t)$ = mass remaining after time, t (g), m_i = initial mass (g) and m_f = final mass. Note that Equation (2) is the well-known Arrhenius expression which has been used in many kinetic studies.

The reaction kinetics of the solvolysis of two polyester resins, both based on propylene glycol but one cured with phthalic anhydride, maleic anhydride and styrene, the other with isophthalic anhydride, maleic anhydride and styrene, have been investigated in detail [261]. The reactions taking place are numerous and complex, involving hydrolysis, decarboxylation and dehydration. Each were modelled individually based on the concentration of the relevant reactants. The evolution of propylene glycol was monitored and, based on the concentration of this, an apparent activation energy was calculated to be 53 to 56 kJ mol^{-1} for both resin systems [261]. A rather more simplistic approach was taken by Pinero-Hernanz, et al. where the decomposition of a thermoset epoxy was taken as proportional to the concentration of resin within the solvent [242], [245]. Assuming a reaction order of 2 for the case of sub- and supercritical water [245] and 1.5 for supercritical propan-1-ol [242], activation energies of 35.5 and 95.6 kJ mol^{-1} were determined. The differences here and with that of the work of Oliveux, et al. [261] are attributable to differences in the polymer, solvents and chosen

reaction order. Although it was shown that the developed model was within ± 1.9% of the experimental data [245], it is worth noting that only two or three reaction times for three different temperatures were investigated [242], [245] and, therefore, the Arrhenius parameters were calculated from a relatively small data set.

Alternatively, the reaction kinetics may be investigated following a shrinking core model (SCM), which is derived from a mass balance around a particle surface. The general expression for an SCM controlled by the surface reaction for a spherical particle is given by Equation (5) and the full derivation is described by Levenspiel (1999) [263].

$$1 - (1 - X)^{\frac{1}{3}} = k_{SCM}t \tag{5}$$

Where X = conversion (%) and k_{SCM} = shrinking core model rate constant (min^{-1}). This has been applied to the decomposition of an epoxy resin using an acetone solvent at temperatures in the range of 300 to 350˚C [264]. Although it was necessary to include a heating time in the model, this also showed a good fit to the experimental data and it was possible to calculate E_A and k_0 as 118.2 kJ mol^{-1} and 3.13 x10^9 min^{-1} respectively, both of which are higher than that determined in other works [242], [245], [261].

The application and evaluation of both a conventional rate equation (Equation ((1)) and a shrinking core model (Equation (5)) to the decomposition of an epoxy resin has not been described in the available open literature. Furthermore, the reaction kinetics of the degradation of a CFRP using an acetone / water solvent mixture and

various weak Lewis acids also remains poorly understood. In order to characterise the decomposition reaction and quantify the Arrhenius parameters in preparation for the design of a commercial process, it is, therefore, necessary to conduct a detailed study into the reaction kinetics.

2.8.4 Organic Liquid Products

Aside from the lower process temperature, the primary advantage of solvolysis over pyrolytic recycling techniques is the recovery of potentially useful organic compounds. This, however, represents a significant challenge with respect to the recycling of CFRPs partly because no effective separation process exists in order to sort the composite waste prior to being recycled. As it is, therefore, necessary for any recycling process to handle a mixed feedstock, the wide range of resin systems in circulation will undoubtedly generate a large and varying mixture of organic products. There has been little investigation in the literature regarding separation techniques to recover individual monomers, however, as mentioned in Section 2.8.2, the organic product mixture may be immediately reused in a secondary CFRP without further processing [239], [249].

Decomposition of both high performance thermoplastics such as PEEK and epoxy based thermosets tend to yield phenol as the major degradation product [237], [256], [265], [266]. Compounds with a high molecular weight may also be present suggesting that, although the resin was fully solubilised, it may not be fully degraded [254]. The reaction products following the hydrolysis of a DGEBA resin cross-linked with DDS have

also been analysed using gas-chromatography with mass-spectrometry (GC-MS). The results of this research confirmed the findings by other reports that phenolic compounds are the primary decomposition products. Amine derivatives were also present due to the nature of the curing agent [252]. The gaseous products were, however, not collected and it is therefore difficult to verify the claim that hydrogen sulphide was also generated. Despite this, the presence of numerous organic compounds demonstrates that, if a cost effective separation process can be developed, this waste material may represent a valuable economic resource.

2.8.5 Properties of Recycled Carbon Fibre

Carbon fibres recovered from CFRPs tend to be characterised in terms of their tensile properties and surface chemistry in order to assess their suitability for reuse within a secondary CFRP. There are some conflicting reports regarding the tensile strength of carbon fibres recycled from pyrolysis: while it seems that there is little reduction within optimised processes [267], there may be a loss of up to 83% when high temperatures are used, although this does depend on the type of fibre [268], [269]. Generally, a loss in strength of up to 10% is considered tolerable and will not result in significantly downgrading the material. Many reports in the literature characterising carbon fibres recovered from solvolysis processes claim the recovered fibre is comparable, in terms of tensile properties, to virgin material [117], [242], [248], [249], [251], [253], [270] and may even show a slight increase in strength [248], [250], [271]. It has been previously suggested that this increase may be due to the removal of weaker, graphitic planes on the surface of the fibres [116]. It is also possible that some of the

surface defects, and therefore failure initiation points, are removed as a result of solvolysis; this effect has been previously observed when subjecting fibres to a nitric acid treatment [272]. It is worth noting that after recycling, there may be a greater spread in tensile strength [251] suggesting that some individual fibres are weakened even if the overall average or Weibull scale factor is similar to virgin material. Research has also demonstrated that increasing the process temperature when using a methanol [249], ethanol [248] and propanol [242] solvent does result in a reduction in tensile properties and it is, therefore, desirable to minimise the reaction temperature.

In addition to the strength of the fibres, it is necessary to consider the surface properties to ensure that they adhere well to a new matrix. XPS has been employed in a number of investigations and the loss of surface oxygen is widely reported [116], [117], [242], [248], [249] which has subsequently led to a reduction in IFSS [116], [117], [249]. Although this may negatively influence the properties of a new CFRP, recycled carbon fibres have been successfully incorporated into a new polymer matrix which shows a tensile and flexural strength similar to an equivalent composite constructed from virgin fibres [234], [249], [255]. It therefore appears that, provided recovered fibres are resized following the recycling process, they are suitable for reuse in high performance applications.

Although some previous work has characterised carbon fibres recovered from a polymer matrix using supercritical water [245] and acetone [251], there is currently no published research investigating the properties of carbon fibres after being processed

with an acetone / water mixture. Furthermore, there is very little work on the influence of weak Lewis acids on the quality of the recyclate. It is, therefore, necessary to quantify any changes in the mechanical and surface properties as a result of exposing the carbon fibre to this solvent and various additives at the conditions required for complete decomposition of the matrix.

2.9 Summary of Literature Review Findings

Due to the development of high performance polymers since the 1950s, there are now a wide variety of both thermoplastic and thermoset materials in circulation. When reinforced with carbon fibres, these can be used in demanding, safety-critical applications and, owing to their low density, exceptional mechanical properties and chemical resilience, offer an environmental benefit through the light-weighting of aircraft and vehicles. Unfortunately, it is this chemical resilience which presents a significant challenge in terms of recycling both manufacturing off-cuts and EoL waste. Compared to pyrolytic techniques, thermochemical processing has the potential to decompose even the most thermally stable polymers, such as RTM6 epoxy resin, at a significantly reduced temperature, without the need for strong, highly concentrated acids and oxidising agents. Fibre integrity is also preserved and it may be possible to recover potentially valuable organic compounds.

The choice of the solvent used in a thermochemical process is critical when specifying the reaction conditions necessary for complete decomposition of the resin. Although research has suggested that the preferred decomposition mechanism is

hydrolysis, the use of solvent mixtures resulted in a reduction of the critical point and hence accelerated the degradation of the polymer when compared to water alone.

Although acetone / water mixtures and various additives have been considered separately, there has not yet been a comprehensive investigation into the decomposition of an RTM6 epoxy resin using this solvent system, supplied both neat and in conjunction with alkaline salts and metal chlorides. Characterisation of both the fibrous and organic liquid products recovered from this reaction system has also not been previously reported. The research presented in this thesis therefore aims to address these knowledge gaps by developing and characterising a novel process for the efficient recycling of high performance CFRPs.

CHAPTER 3.
RESIN DECOMPOSITION

3.1 Introduction

The effective recovery of carbon fibres from CFRPs relies on the successful decomposition of the polymer matrix. This decomposition can be achieved with a variety of processes through the application of mechanical, thermal and chemical technologies, all of which are discussed in Chapter 2. Compared to mechanical and thermal processes, solvolytic techniques have the potential to improve resource efficiency through the production of potentially useful organic compounds. In addition, the use of solvents facilitates a much lower operating temperature and, depending on the conditions used, minimises the risk of fibre damage. Unfortunately, low temperature and pressure (LTP) processes often require long process times and rely on strong, highly concentrated acidic solutions [229], [232], [273] or oxidising agents [235], [274], [275]. Although it is possible to recover fibres with properties similar to virgin material [232], [273], these systems are likely to produce complex and hazardous liquid product mixtures which are difficult to process and pose a safety, health and environmental risk. For these reasons, the research presented in this thesis considers only generally recognised as safe (GRAS) solvents operating under high temperature and pressure (HTP) conditions.

As discussed in Chapter 2, research has demonstrated that a combination of acetone and water supplied at a ratio of 80 : 20 v/v (mole fraction of acetone = 0.495) is one of the most effective combinations when degrading an epoxy resin [252].

Furthermore, the use of alkaline [255]–[257], [276] and weak Lewis acids [239], [277], [278] have also been investigated as potential catalysts with the aim of reducing the necessary reaction temperature. With the exception of the research published as part of this work, there have been no reports of using these additives in conjunction with an acetone / water solvent system.

The results presented in this chapter focus on the decomposition of a commercially available CFRP using a sub- and supercritical acetone / water solvent mixture, supplied both neat and in conjunction with various alkaline and weak Lewis acid solutions. The phase behaviour of the solvent was also analysed and the CFRP investigated was characterised using a variety of techniques. These findings were published across two papers: "Recycling a carbon fibre reinforced polymer with a supercritical acetone / water solvent mixture: Comprehensive analysis of reaction kinetics" and "Catalytic degradation of a carbon fibre reinforced polymer for recycling applications". Both articles are available in the journal *Polymer Degradation and Stability*.

3.2 Experimental Methodology

3.2.1 Materials

As mentioned in Chapter 2, 76.2% of all CFRPs currently manufactured use a thermoset resin as the matrix material and it is, therefore, likely that these materials constitute the majority of all CFRP waste [279]. For this reason, the material selected for investigation consisted of an RTM6 epoxy resin reinforced with 20 plies of woven Toray

T700 6k carbon fibre fabric. The thickness of the composite material was measured to be 6 ± 0.1 mm and it was cut into pieces measuring (10 x 10 ± 1) mm^2 using a diamond edged rotary saw. An example of this material, henceforth referred to as "the CFRP", is shown in Figure 5. This composite was supplied by a leading aerospace manufacturer and, according to the manufacturer's data, the fibre volume content was 53 ± 1 vol.%. Due to the commercially sensitive nature of resin systems, the formulation of the matrix material was not disclosed by the supplier, however, this composite material was characterised through calcination, thermogravimetric analysis (TGA) and differential scanning calorimetry (DSC) as detailed in Sections 3.2.2 and 3.4. This CFRP was used in all experiments except for some of those described in Chapter 6 which also considers the decomposition of a model epoxy resin.

***Figure 5**. Example of the CFRP investigated for all experiments.*

For all experiments, the solvent system consisted of analytical research grade acetone (purity > 99.0%) and water. The two solvents were mixed together in a ratio of 80 : 20 v/v which corresponds to a mole fraction of acetone of 0.495. The acetone was purchased from Sigma Aldrich (UK) and deionised (DI) water with a conductivity of 0.05 mS cm^{-1} was produced on site using an Arium Pro Type 1 Ultrapure Water System (Sartorius, Germany). In order to more closely simulate industrial conditions, some experiments were also completed using water from the mains supply. This had a conductivity of 0.16 ± 0.03 mS cm^{-1} and a pH of 7.8 ± 0.3. The expected composition is provided in Table 2 [280].

The additives listed in Table 3 were used as delivered to make up a range of solutions with the acetone / DI water solvent with the aim of reducing the necessary reaction temperature and / or process time.

***Table 2**. Expected composition of mains water at the University of Birmingham* [280]

Substance	Concentration (mg L^{-1})		
	Minimum	**Average**	**Maximum**
Aluminium	0.005	0.009	0.014
Ammonium	0.012	0.014	0.018
Boron	0.012	0.014	0.018
Bromate	0.00083	0.00131	0.00169
Chloride	12.79	15.15	18.63
Chlorine	0.15	0.42	0.72
Copper	0.0020	0.0150	0.0364
Cyanide	< 0.001	< 0.002	< 0.002
Fluoride	0.57	0.72	0.82
Iron	0.01	0.02	0.192
Manganese	0.0003	0.0012	0.0096
Nickel	0.0011	0.0014	0.0022
Nitrate	2.26	3.39	4.75
Nitrite	< 0.004	< 0.005	< 0.007
Sodium	9.7	11.2	13.0
Sulphate	16	22	28
Total organic carbon (TOC)	0.8	1.0	1.4
Total Trihalomethanes	0.01755	0.02625	0.03625

***Table 3**. Additives investigated for the decomposition of the CFRP.*

Compound	Supplier	Purity (wt.%)
Potassium hydroxide, KOH	Fisher Chemical	> 99.0
Sodium hydroxide, NaOH	Merck	> 97.0
Zinc chloride, $ZnCl_2$	Alfa Aesar	> 98.0
Magnesium chloride, $MgCl_2$	Sigma Aldrich	> 98.0
Aluminium chloride, $AlCl_3$	Merck	> 98.0
Copper chloride, $CuCl_2$	Sigma Aldrich	97.0
Calcium chloride, $CaCl_2$	Fisher Chemical	> 99.0
Caesium chloride, $CsCl_2$	Fisher Chemical	99.9
Caesium carbonate, Cs_2CO_3	Sigma Aldrich	99.0
Zinc sulphate, $ZnSO_4$	Scientific Laboratory Supplies	97.3
Magnesium sulphate, $MgSO_4$	VWR	99.0
Aluminium sulphate, $Al_2(SO_4)_3$	VWR	> 98.0

3.2.2 Characterisation of CFRP

The CFRP was characterised in order to determine the resin content and the glass transition temperature, T_g, from which the degree of cross-linking can be inferred. Using the manufacturer's data (a fibre volume fraction of 53 ± 1 vol.%) and typical densities of carbon fibre and epoxy resin of 1.80 and 1.15 kg m^{-3} respectively [281], [282], the expected resin content is 36 ± 0.9 wt.%. This was verified using both TGA and calcination. The former technique was conducted with 20 samples of the CFRP each with a mass in the range of 10 to 20 mg. Individual samples were placed into an aluminium pan which was loaded into a Seiko Exstar 6000 (Seiko Instruments Inc., Japan). An inert atmosphere was maintained by passing nitrogen (>99% purity, supplied by BOC, UK) through the

furnace at 5 mL min^{-1}. The maximum operating temperature, heating ramp and hold time were set to 500˚C, 10˚C min^{-1} and 30 min respectively. This heating profile is illustrated by Figure 6 and is hereafter referred to as TGA Method 1. At the end of each experiment, the initial and final masses (m_i and m_f (mg) respectively) were recorded and the initial resin content, R_i, was calculated using Equation (6).

$$R_i = \frac{m_i - m_f}{m_i} \times 100 \quad (6)$$

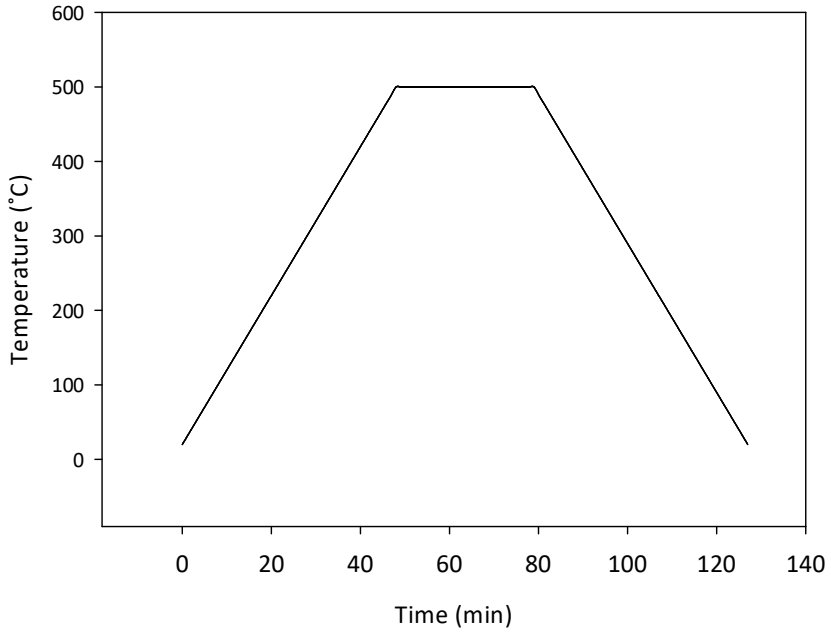

***Figure 6**. Heating profile for TGA Method 1.*

To confirm the TGA results, 10 samples with a mass in the range of 0.8 to 1.0 g were also thermally analysed using calcination. Each sample was placed into an aluminium crucible, weighed and heated to 500˚C in air using a Muffle furnace (Sanyo Gallenkamp Plc, UK). At regular time intervals, the samples were removed, cooled and weighed a minimum of 6 times. After a total heating period of 1 h, the reduction in mass

was less than 1% of the mass of the sample remaining and was, therefore, considered negligible. As the fibres also appeared clean from visual inspection, it was assumed that all resin had been pyrolysed and only fibres remained. As carbon fibres are typically processed at temperatures in excess of 1500˚C during their manufacture [86], it was also assumed that there was no mass loss from the fibres. The final mass was recorded and used in Equation (6) to calculate R_i. An average across the 10 samples was taken and compared to the results obtained from TGA.

In addition to calculating the resin content, the T_g was also determined through DSC using a Mettler Toledo DSC 1 Star System (Mettler Toledo, UK). Individual samples with a mass in the range of 25 to 30 mg were placed into a 100 µL aluminium crucible which was crimped shut before being loaded into the chamber. As the thermal history of the CFRP material is currently unknown, the sample was first heated to 250˚C, held for 30 s and then cooled to 20˚C both at a rate of 30˚C min^{-1}. The DSC curve obtained from this first run was not included in the analysis. The heating / cooling rate used can cause a shift in the resultant DSC curve leading to either over- or underestimating the T_g. To avoid this effect, each sample was thermally cycled between 20 and 250˚C five times at a heating ramp of between 10 and 50˚C min^{-1} using a constant cooling rate of 30˚C min^{-1}. The sample was held at the minimum and maximum temperature for 30 s before beginning the next cycle. This was then repeated using a constant heating ramp of 30˚C min^{-1} and changing the cooling rate at the same intervals. The heating / cooling profile described is illustrated by Figure 7 and is hereafter referred to as DSC Method 1. Extrapolating the trend line on a plot of T_g vs. heating / cooling rate then allows the T_g

for a theoretical temperature ramp of 0˚C min^{-1} to be obtained. This technique was repeated across five individual samples of the CFRP.

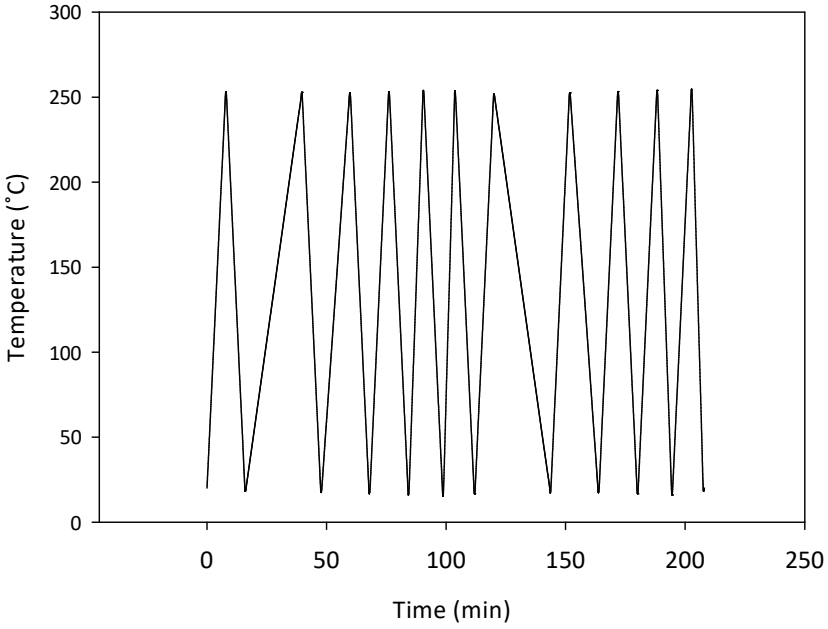

***Figure 7**. Heating profile for DSC Method 1.*

3.2.3 Fibre Recovery

All experiments were completed using a high temperature, high pressure reactor system supplied by Parr Instruments Company. This consisted of a Hastelloy stainless steel reaction vessel with a nominal volume of 100 mL and a lid assembly. As shown by Figure 8, there is some pipework due to the fittings mounted on to the reactor lid and it was therefore necessary to calculate a real reactor volume as described in Appendix 1. Using water as the working fluid, this was shown to be 107 ± 1 mL. The maximum working temperature and pressure of the system was 500˚C and 34.5 MPa respectively and was therefore fitted with a Swagelok SS-4R3A5-BU pressure relief valve. Heating was achieved with the electrical oven supplied as part of the reactor system and the

temperature was maintained at the set point using a Parr 4848 reactor controller. These units are also shown in Figure 8. The internal pressure of the reactor was monitored using an analogue pressure gauge (SPAN, USA) while a single J-type thermocouple was used to measure the temperature and provide feedback to the controller. Prior to experimentation, the thermocouple was calibrated against 2 mercury thermometers with graduations of 0.1˚C by measuring the temperature of water from its normal freezing point (0˚C) to its boiling point (100˚C) under atmospheric conditions. The maximum observed deviations between the J-type thermocouple and mercury thermometers was 0.5˚C.

a)

b)

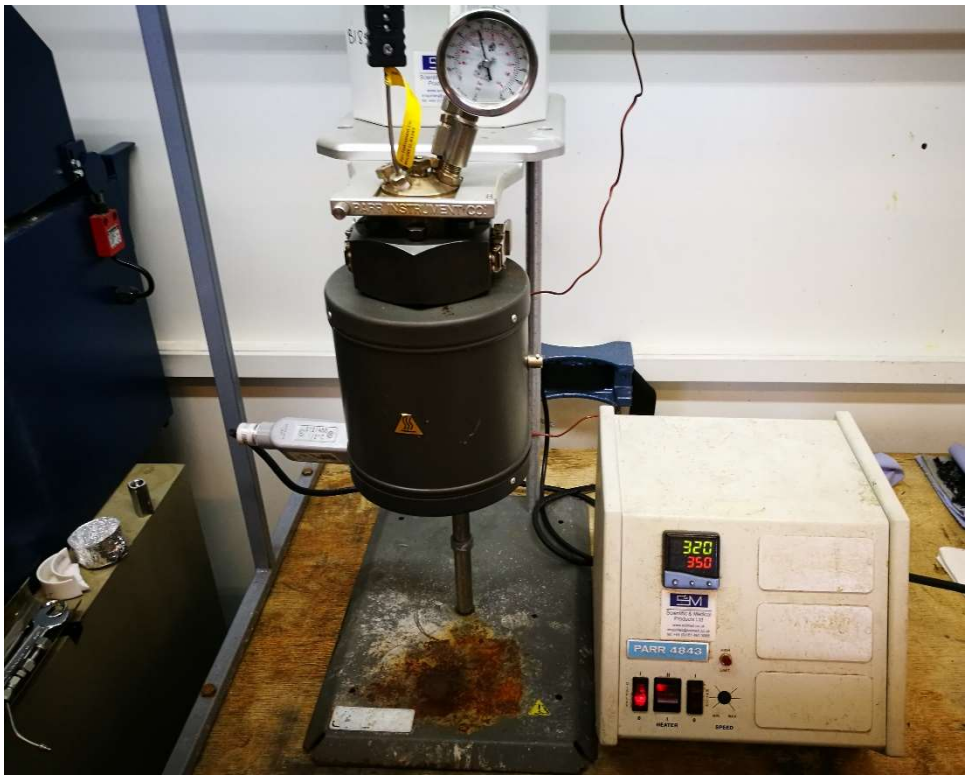

c)

***Figure 8**. High temperature, high pressure reactor system used for all experiments a) reactor loaded and sealed; b) mounted in frame; and c) operating at 320˚C.*

For all of the experiments described in this chapter, five pieces of the CFRP with a total mass of 4.17 ± 0.01 g were loaded into the reactor along with 50 ± 1 mL of the solvent mixture. This gave a reactor loading of 30 ± 1 g_{resin} $L_{solvent}^{-1}$. The mass of the samples was measured using a Sartorius R160P Semi-Microbalance (Sartorius, Germany) which had a precision of ± 0.1 mg. The solid CFRP material was placed into a stainless steel basket to prevent any contact with the reactor walls which may have led to pyrolysis of the material. This was positioned in the reactor such that the thermocouple was directly above the sample. To ensure that the system was properly sealed, a PTFE gasket was inserted into the groove of the reactor lid for operating temperatures at or below 300˚C. For conditions above 300˚C, it was necessary to replace this with a graphite gasket. Once the reactor was loaded and the lid clamped to the reaction vessel, the entire assembly was mounted into the frame (Figure 8b). Depending on the operating temperature, the total heating phase was 35 ± 5 min and the reactor was cooled by forced air convection in 25 ± 3 min. The temperature / pressure profile for the reaction system is shown in Figure 9. Initially, a neat solvent mixture consisting of acetone / mains water was used to investigate the decomposition of the CFRP at the conditions described in Table 4 in order to ensure the repeatability of the experiments. Each experiment was conducted three times and an average taken. The influence of mains and DI water within the solvent mixture was investigated at the reaction conditions listed in Table 5. Further experiments were also carried out with an acetone / mains water solvent using the parameters listed in Table 6.

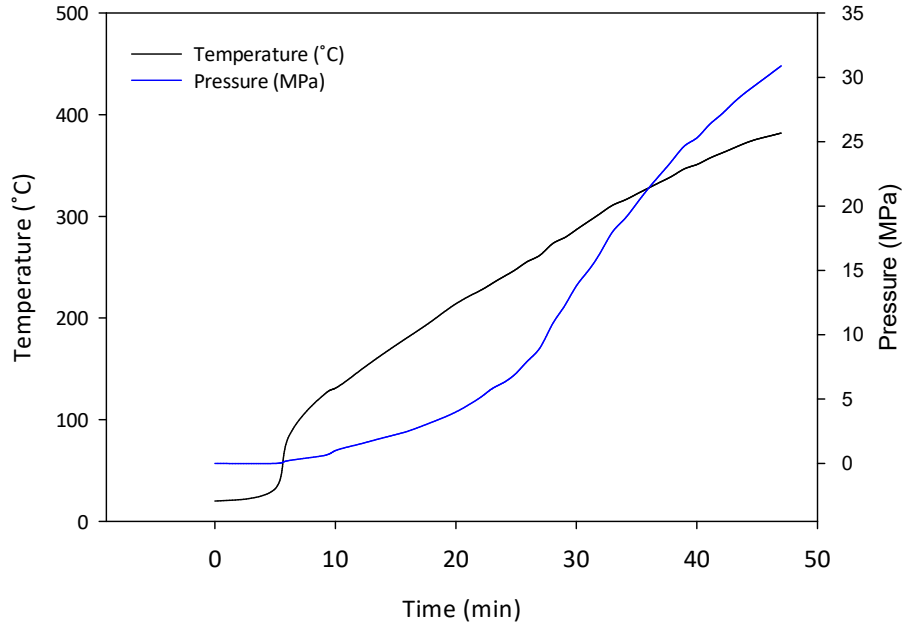

***Figure 9**. Temperature and pressure profile for the reactor heating phase*

***Table 4**. Reaction conditions used for three repeat experiments investigating the decomposition of the CFRP using acetone / mains water in the ratio of 80 : 20 v/v.*

Temperature, T_R (± 1 °C)	**Induced Pressure, p (± 0.3 MPa)**	**Reaction Time, t_R (min)**
300	15.8	
310	17.8	20, 120
320	19.7	
330	22.0	20, 90
340	23.5	20, 45
360	27.0	0, 20

***Table 5**. Reaction conditions used for the decomposition of the CFRP using acetone / DI water and acetone / mains water in the ratio of 80 : 20 v/v.*

Temperature, T_R (± 1 °C)	**Induced Pressure, p (± 0.3 MPa)**	**Reaction Time, t_R (min)**
300	15.8	30, 120
310	17.8	
320	19.7	
330	22.0	30, 90
340	23.5	15, 45
360	27.0	0, 15
380	30.0	0

***Table 6**. Reaction conditions used for the decomposition of the CFRP using acetone / mains water in the ratio of 80 : 20 v/v.*

Temperature, T_R (± 1 °C)	**Induced Pressure, p (± 0.3 MPa)**	**Reaction Time, t_R (min)**
300	15.8	0, 20, 45, 90, 120
310	17.8	
320	19.7	
330	22.0	
340	23.5	
360	27.0	

The reaction time, t_R, was measured from when the reactor temperature reached the set point. Upon completing each reaction and cooling the vessel, the solid fibrous products were removed from the basket and washed with acetone at ambient conditions to remove any organic residue which may have adhered to the fibre surface

during the cooling phase. The recovered fibres were dried overnight in a fume cupboard before being analysed as described in Section 3.2.4. The organic liquid products (OLP) were also recovered for analysis as discussed in Chapter 6.

In order to minimise both the risk of fibre damage and energy demand of the process, it is desirable to reduce the necessary reaction temperature. This was achieved through investigating the efficacy of various different additives. Based on previous research, both alkaline salts and weak Lewis acids were investigated. Initial experiments were carried out with KOH, NaOH and $ZnCl_2$ at the temperatures, pressures and concentrations given in Table 7 for a reaction time of 60 min. $MgCl_2$ and $AlCl_3$ were also investigated using an operating temperature of 300˚C, a reaction time of 60 min and the concentrations listed in Table 8. All other additives listed in Table 3 ($CuCl_2$, $CaCl_2$, $CsCl_2$, Cs_2CO_3, $ZnSO_4$, $MgSO_4$ and $Al_2(SO_4)_3$) were investigated also using a reaction time of 60 min, a temperature of 300˚C and a concentration of 0.05 M. Based on these results, $ZnCl_2$, $MgCl_2$ and $AlCl_3$ were selected for further investigation at the conditions given in

Table **9**.

***Table 7**. Reaction conditions used to investigate the decomposition of the CFRP using KOH, NaOH and $ZnCl_2$ and an acetone / DI water solvent (reaction time, t_R = 60 min).*

Temperature, T_R (± 1 °C)	**Induced Pressure, p (± 0.3 MPa)**	**Concentration, C (M)**
280	13.0	
300	15.8	0.01, 0.03, 0.05, 0.10, 0.20, 0.40
320	19.7	

***Table 8**. Concentrations used to investigate the decomposition of the CFRP using $MgCl_2$ and $AlCl_3$ (t_R = 60 min, reaction temperature, T_R = 300˚C).*

Additive	Concentration, ***C*** (M)
$MgCl_2$	0.01, 0.03, 0.05, 0.10, 0.20, 0.40
$AlCl_3$	0.001, 0.003, 0.005, 0.01, 0.03, 0.05

***Table 9**. Reaction conditions used to investigate the decomposition of the CFRP with 0.05 M $ZnCl_2$, 0.05 M $MgCl_2$ and 0.005 M $AlCl_3$ acetone / DI water solutions.*

Temperature, T_R (± 1 °C)	Induced Pressure, ***p*** (± 0.3 MPa)	Reaction Time, t_R (min)
270	12.0	
280	13.0	0, 10, 30, 60, 90
290	14.5	
300	16.0	0, 10, 20, 30, 45

3.2.4 Quantification of Resin Decomposition (*RD*)

After the reaction, the solid material remaining in the basket consisted of the carbon fibres and any resin which had not been solubilised. For all samples, the resin decomposition (*RD*) was quantified using two independent techniques. The first (RD Method 1) considered the difference in mass of the CFRP before and after processing (m_i and m_p respectively (g)) and used Equation (7)). The value of R_i was determined using the methods outlined in Section 3.2.2 and was taken as 35 wt.% as described in Section 3.4.1.

$$RD_{Method\ 1}\% = \frac{m_i - m_p}{R_i m_i} \times 100 \quad (7)$$

To confirm these results, RD Method 2 involved calcining all solid material recovered after the reaction. Samples were divided into five aluminium crucibles and heated to 500˚C in air using a muffle furnace for a total time of between 12 and 50 min depending on the degree of solubilisation. The crucibles were regularly removed, cooled and weighed a minimum of five times until the reduction in mass was negligible (i.e. less than 1%) and the recovered fibres appeared clean from a visual inspection. Upon reaching this point, it was assumed that all resin remaining after processing, R_P, had been removed. The value of R_P was determined using Equation (8) and *RD* could then also be quantified with Equation (9). An average was taken across the five samples to give the *RD* from calcination.

$$R_P\% = \frac{m_p - m_f}{m_p} \times 100 \quad (8)$$

$$RD_{Method\ 2}\% = \frac{R_i - R_p}{R_i} \times 100 \quad (9)$$

In addition to these two techniques, five samples with masses in the range of 5 to 15 mg were also taken from the solid material recovered after processing the CFRP at each of the temperatures listed in Table 4 and a reaction time of 20 min. These samples were thermally analysed following TGA Method 1 as described in Section 3.2.2 to confirm the results given from RD Methods 1 and 2. From the resultant TGA curve, the

initial and final mass of each sample was identified and used in Equation (7) to calculate the *RD*. An average *RD* value was determined from across the five samples considered.

3.3 Phase Behaviour of Solvent Mixture

As the operating conditions investigated cover a range between the critical points of acetone (235˚C, 4.8 MPa [283]) and water (374˚C, 22 MPa [247]), the phase of the solvent during the reaction is currently unknown. Supercritical fluids exhibit enhanced reactivity and improved mass transfer when compared to the same substance in a liquid or gaseous state. For this reason, determining the phase of the solvent may aid in explaining the degradation characteristics of the CFRP. The phase behaviour of the solvent was investigated both experimentally and by modelling the acetone / water mixture with the Perturbed-Chain Statistical Associating Fluid Theory (PC-SAFT) equation of state (EoS).

To characterise the phase behaviour of the solvent experimentally, 50 mL of the acetone / DI water mixture in a ratio of 80 : 20 v/v (mole fraction of acetone = 0.495) was loaded into the pressure vessel described in Section 3.2.3. The mixture was heated to 380˚C following the temperature / pressure profile provided in Figure 9. Data points for these two variables were taken every 30 s.

The PC-SAFT EoS was also used to determine the phase behaviour of the solvent. This is a modern thermodynamic model developed from statistical mechanical theories and is capable of handling association phenomena due to the hydrogen bonding present

between acetone and water molecules. Calculations were performed using Matlab R2016a macros by Luis Román-Ramírez, University of Birmingham, following the methodology which has been previously described in the literature [284]–[286]. This EoS is based on the sum of the individual contributions of the hard-chain fluid formation (*hc*), dispersive (*dis*) and associative (*assoc*) Helmholtz free energies ($\hat{a}$, J mol^{-1}) to the residual Helmholtz free energy ($\hat{a}^{res}$) and can be expressed by Equation (10).

$$\frac{\hat{a}^{res}}{RT} = \frac{\hat{a}^{hc}}{RT} + \frac{\hat{a}^{disp}}{RT} + \frac{\hat{a}^{assoc}}{RT} \quad (10)$$

Where R = Ideal gas constant (8.314 J mol^{-1} K^{-1}) and T = Temperature (K). Expressions for each of the different contributions are described in the original publications by Gross, et al. [284], [285]. Pure component parameters for the PC-SAFT model are provided in Table 10. The values for water were taken from the literature [247] while the values for acetone were obtained by fitting experimental saturated pressures and liquid densities using the procedures described by Román-Ramírez et al. [286]. This experimental data was taken from Othmer, et al. [287] which covers temperatures and pressures in the range of 57 to 230˚C and 1 to 34.5 MPa respectively. In addition to the pure component parameters, a temperature independent binary interaction parameter, k_{ij} was also calculated following the methodology described in previous work [286]; the optimum value for k_{ij} was found to be 0.015. Deviations in temperature were less than 0.65% for isobaric calculations at 34.5 bar. The phase envelope for this solvent mixture (mole fraction of acetone = 0.495) and the operating conditions for each of the experiments

are shown in Figure 10. The critical point for this solvent composition was calculated to be at 297˚C and 12 MPa. As illustrated in Figure 10, the pressure observed during each reaction is consistently 2.5 MPa above that calculated by PC-SAFT due to the presence of air in the reactor.

***Table 10**. Pure component parameters used in the PC-SAFT EoS (values for water taken from* [247]*, values for acetone were calculated using procedures described in* [286] *and data taken from* [287]*).*

Parameter	Definition	Water	Acetone
m	Segment number (dimensionless)	2.7028	2.6096
σ	Segment diameter (Å)	2.0526	3.3366
ε/κ	Segment energy (K)	218.96	262.13
κ^{AB}	Association volume of PC-SAFT (dimensionless)	0.56142	-
ε^{AB}/κ	Association energy of PC-SAFT (K)	2045.0	-

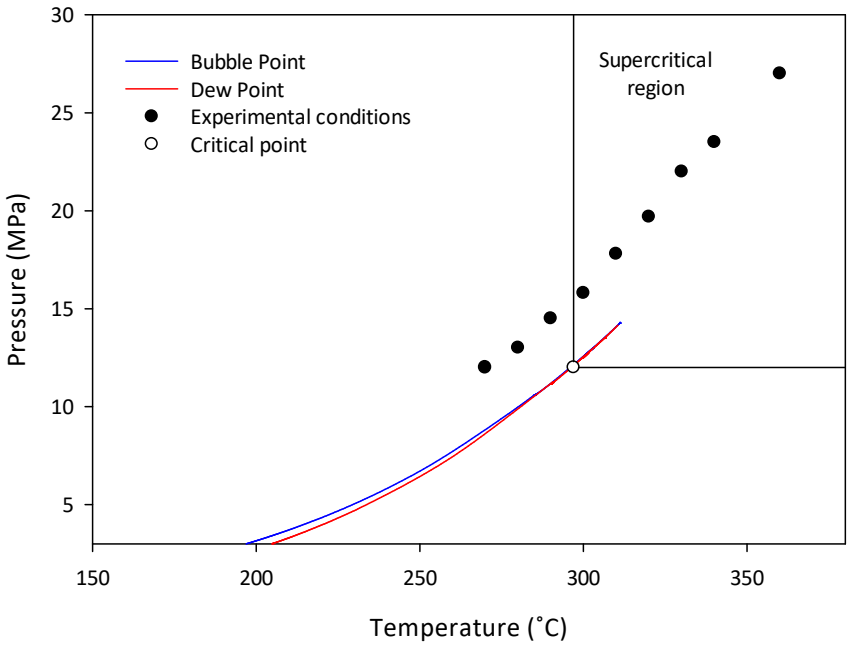

***Figure 10.** Phase diagram modelled by PC-SAFT for the acetone / water solvent system (mole fraction of acetone = 0.495) and experimental conditions investigated.*

3.4 Characterisation of CFRP

3.4.1 Resin Content

The resin content was verified using TGA and calcination and, from the manufacturers data, is expected to be 36 ± 0.9 wt.%. A typical TGA curve is shown in Figure 11 and *RD* was calculated with Equation (6). Although a temperature of 500˚C was necessary to completely pyrolyse the polymer, the greatest rate of mass loss was achieved at a temperature of 380˚C and, interestingly, there is a secondary peak at 400˚C. These two individual peaks likely correspond to the liberation of two major thermal degradation products. Across the 20 samples analysed with TGA, the average resin content was calculated to be 34.5 ± 1.4 wt.%. As a nitrogen atmosphere was used, some pyrolytic char was likely present on the surface of the fibres, which will lead to exaggerating R_i. For this reason, this result was also confirmed using calcination in air with larger samples of the CFRP.

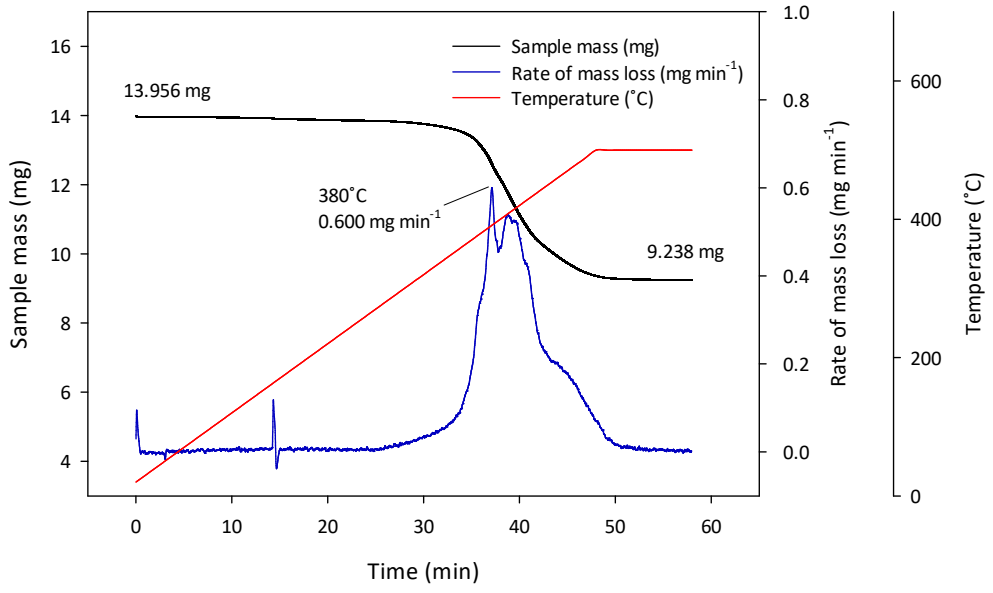

Figure 11. *Typical TGA curve for the thermal analysis of the CFRP using TGA Method 1.*

In addition to TGA, 10 samples of the CFRP were also calcined to remove the resin as shown in Figure 12. Three example curves illustrating the mass loss due to pyrolysis are also provided in Figure 13 which demonstrates that a plateau is reached within 20 min.

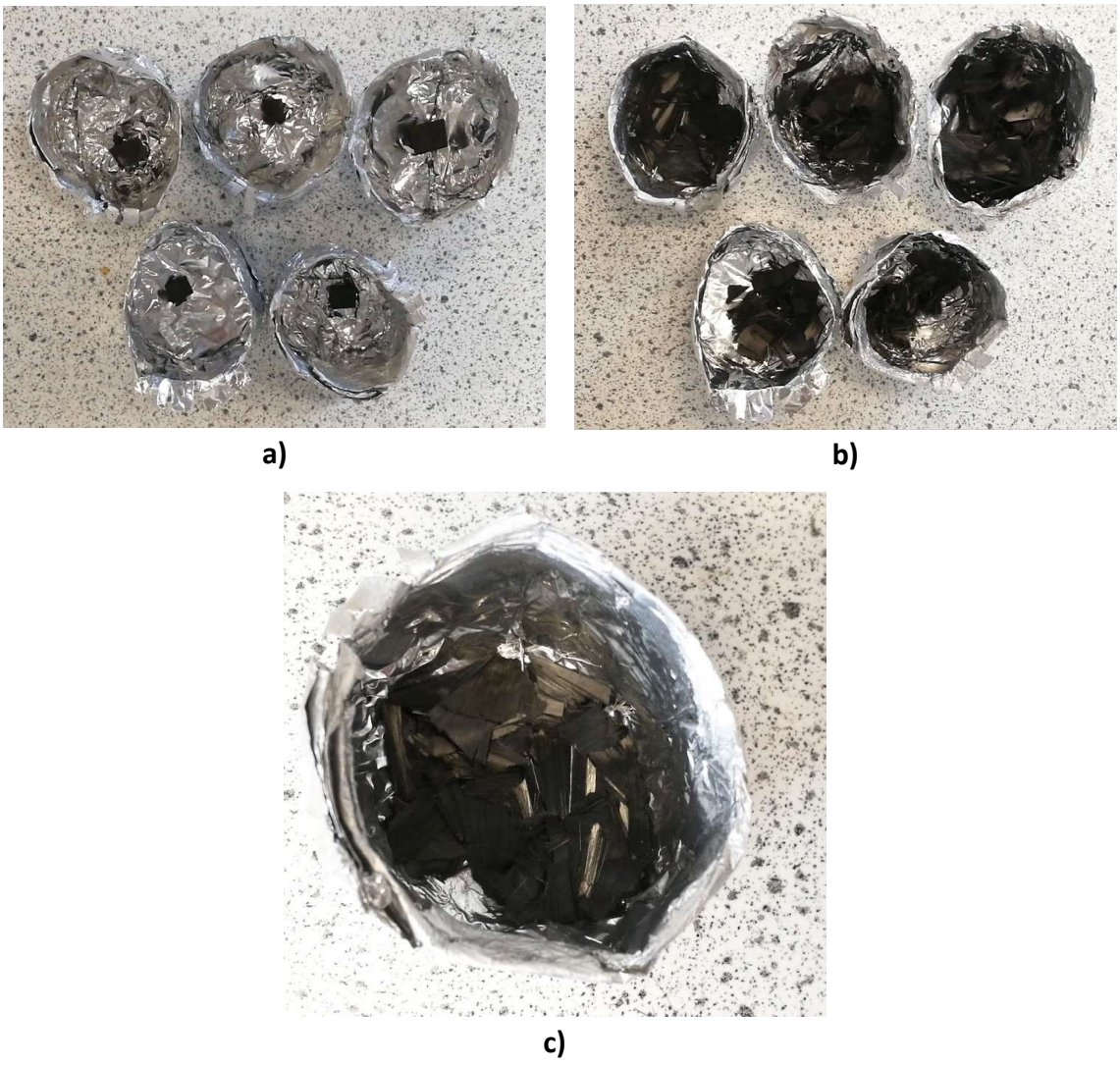

Figure 12. *Examples of the CFRP divided into 5 aluminium crucibles a) before calcination; b) and c) after calcination*

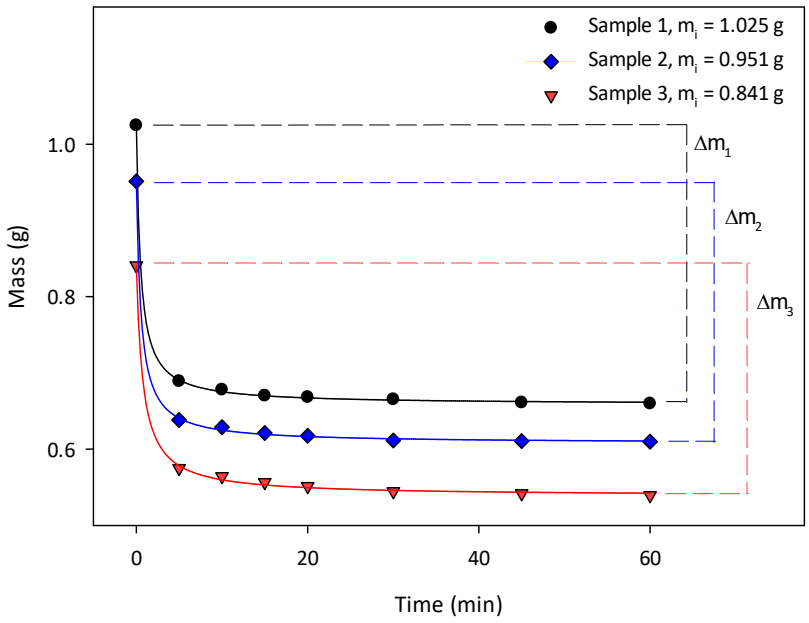

***Figure 13**. Typical calcination curves from the thermal analysis of the CFRP, m_i = initial mass (g).*

Although the change in mass between 20 and 60 min in the furnace is in the range of 1.0 to 2.5% across all samples investigated, this is equivalent to a difference in R_i of 0.66 to 1.66 wt.%. As this may equate to an error of up to 4.7%, it is necessary to consider the mass recorded at some point after 20 min. Comparing the difference in R_i calculated when using the mass of the sample at 45 min and at 60 min gives a difference of just 0.1 to 0.3 wt.% which is within the range calculated across all 10 samples. For this reason, it is appropriate to use the mass of the sample after calcining for 60 min to calculate R_i. Any difference in mass after this time (a maximum of 0.3 wt.%) amounts to an error in R_i of less than 1% which is considered negligible. Across the ten samples, the average resin content was calculated to be 35.5 ± 0.5 wt.% using this calcination technique.

There is good agreement between the values of R_i calculated from TGA Method 1 and calcination with a difference between the two averages of 1.0 wt.%. There is less variability in the latter technique, possibly due to the use of larger sample sizes. Furthermore, the Dremel cutting tool used to size the samples into the mass range of 10 to 20 mg for TGA may have removed some resin from the fibre surface resulting in an apparently lower Ri, and thus explaining why the average value is 1.0% lower than that calculated from calcination. An average value for Ri between the two techniques was taken and determined to be 35.0 ± 0.5 wt.%. This is similar to the manufacturer's data stating a fibre volume content of 53 ± 1 vol.% which is equivalent to a resin content of 36 ± 0.9 wt.% as shown in Section 3.2.2. However, as the formulation of the resin system, and therefore it's density, is unknown, the value for R_i used in all subsequent calculations was taken as 35.0 wt.%.

3.4.2 Glass Transition Temperature. T_g

To determine the T_g of the RTM6 resin used in the CFRP, samples were thermally cycled between 25 and 250˚C and a DSC curve was obtained after each heating and cooling phase. An example DSC curve showing both the heating and cooling profile is provided in Figure 14. The onset and endpoint of the glass transition period was identified at the point where the gradient of the curve was no longer constant. A straight line was drawn between these points and the middle value was taken as the T_g for that heating / cooling rate. The T_g obtained was plotted against the heating / cooling rate as shown in Figure 15 in order to eliminate the effect of shifting the T_g as described in Section 3.2.2.

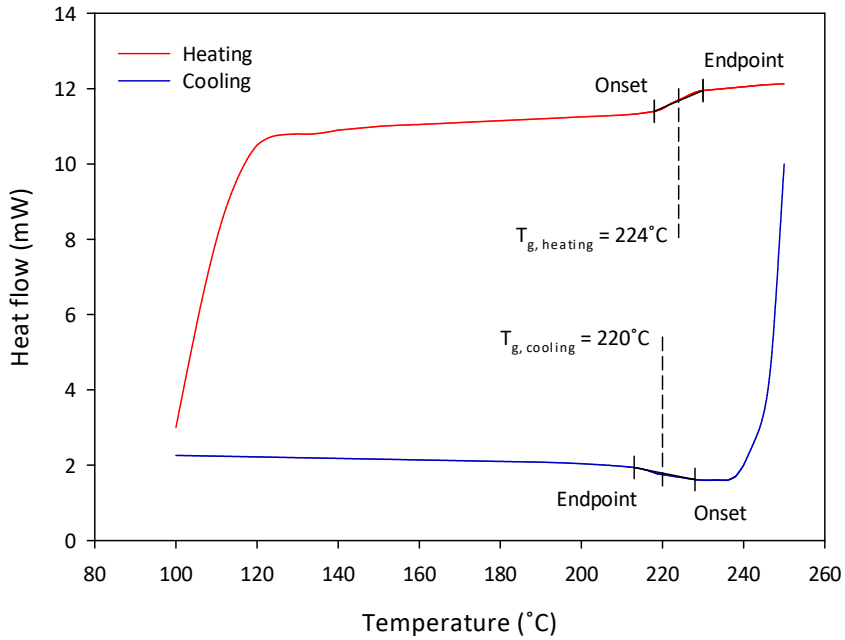

***Figure 14**. Example DSC curve for the CFRP (sample mass = 18.81 mg, heating ramp = 10˚C min^{-1}).*

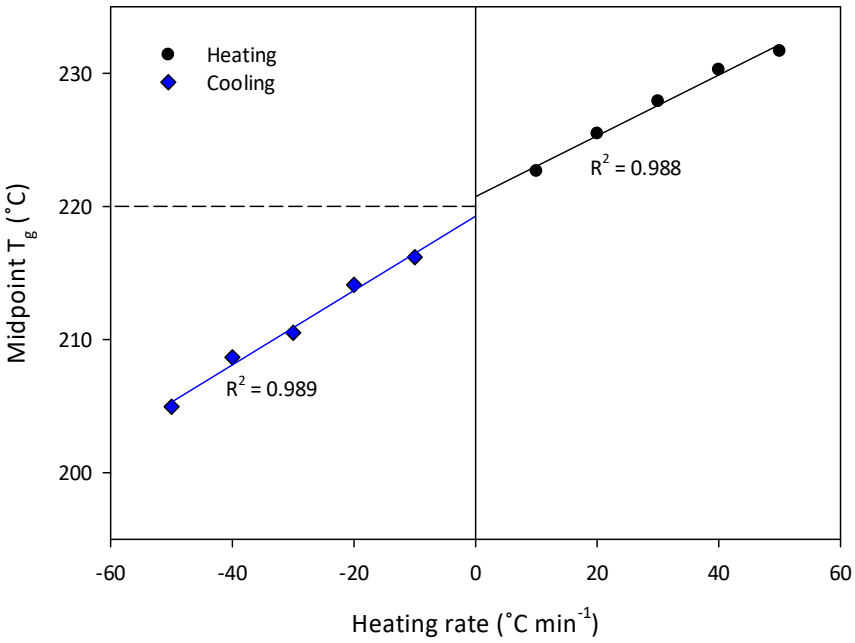

***Figure 15**. Plot of T_g vs. heating rate for the CFRP (sample mass = 24.04 mg).*

The T_g for each of the five samples was taken as the midpoint between the intersection of each of the regression lines with the y-axis. An average was then

calculated to be 221 ± 3˚C, which is similar to that quoted by the manufacturer of 210 ± 5˚C. The difference of 3 to 19˚C may be due to the measurement technique implemented; as DMA was not available, it was not possible to replicate the methodology used by the manufacturer. The high T_g, however, still indicates a high degree of cross-linking above 0.9 [288], where completely cured thermosets have a cross-linking degree of 1. For this reason, if it is possible to decompose this RTM6 epoxy resin, the conditions applied should also be capable of recovering carbon fibres from a wide range of thermoset polymers.

3.5 Resin Decomposition with Neat Solvent Mixture

The decomposition of the CFRP was investigated following the methods described in Sections 3.2.3 and 3.2.4. In order to ensure the accuracy of the experimental techniques applied, this section also compares the three different methods used to quantify *RD* and the repeatability of each experiment.

3.5.1 Verification of *RD* Quantification

The three techniques considered for the calculation of *RD* were investigated using samples recovered after processing the CFRP at the temperatures given in Table 4 and a reaction time of 20 min. All solid material which was recovered from the reactor had a mass in the range of 2.71 to 3.95 g and was calcined as described in Section 3.2.4. It is not practical to analyse this quantity of material with TGA and, therefore, five samples in the mass range 5 to 15 mg were cut from the composite using a handheld Dremel cutting tool. Each sample was thermally analysed using TGA Method 1 and an average

was taken from across all five samples. Typical calcination and TGA curves for the CFRP are provided in Figure 16 and Figure 17. In the latter technique, the first and last data points were taken as the values for m_i and m_f respectively. As the mass change is not continuously measured with calcination, both the penultimate and final data points were considered when calculating *RD*. When the two values were in close agreement with a difference of less than 1%, it was assumed that all organic residue had been removed and the penultimate value was used in all following calculations. As expected, increasing the reaction temperature resulted in a smaller observed change in mass due to a higher degree of solubilisation after processing the CFRP with the acetone / water solvent.

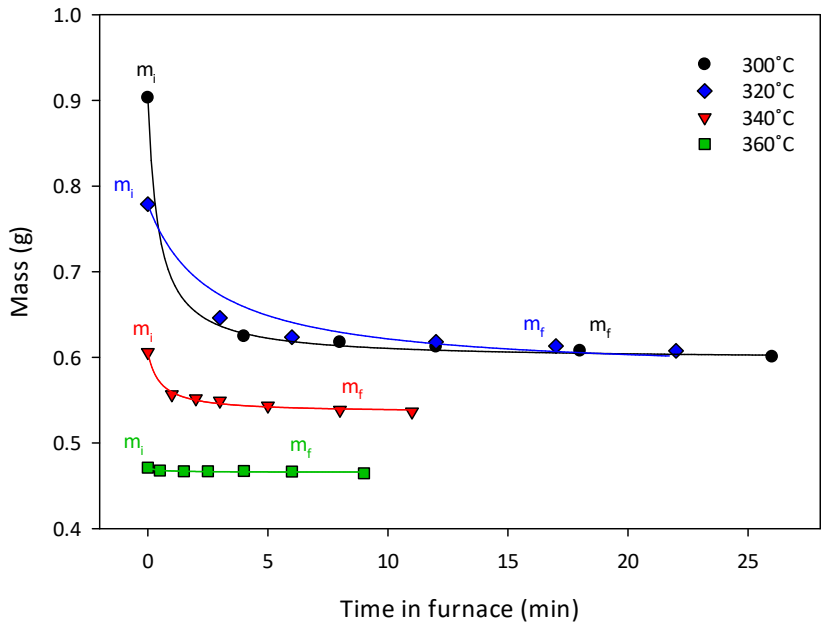

***Figure 16**. Typical calcination curves for the CFRP after processing with an acetone / mains water solvent for 20 min at a range of temperatures.*

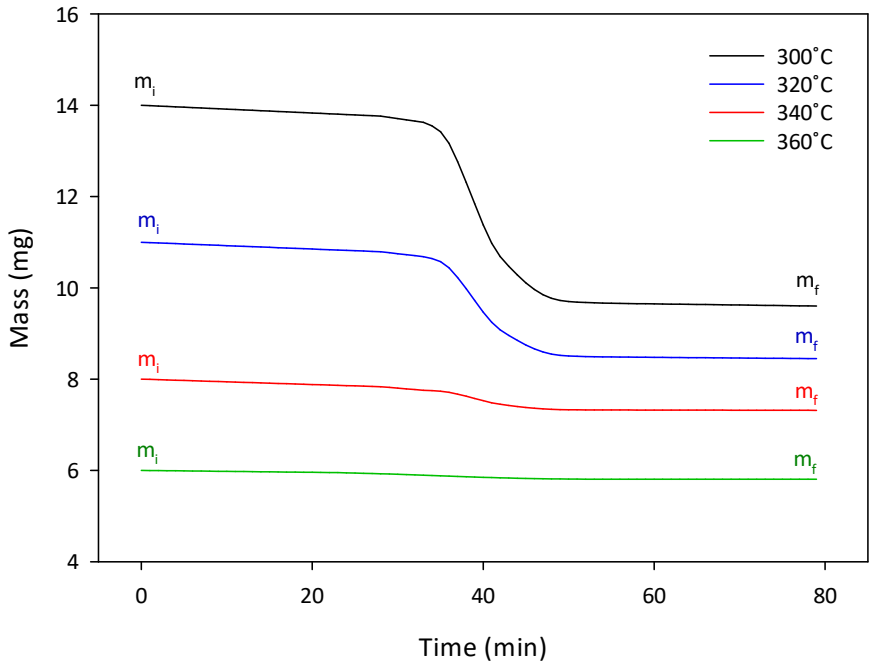

***Figure 17**. Typical TGA curves obtained from TGA Method 1 after processing the CFRP with an acetone / mains water solvent for 20 min at a range of temperatures.*

The values obtained for *RD* using all three quantification techniques after recovering samples at various reaction temperatures are shown in Figure 18. The error bars represent the range observed across the five aluminium crucibles used for calcination and across the five samples analysed with TGA Method 1. In all cases, the deviation in *RD* across the five crucibles used in calcination is less than 4.5% indicating that the reaction is uniform across the reactor with all polymer solubilised at a similar rate. The spread observed from TGA Method 1, however, is somewhat higher and reaches a maximum of 5.8% at 340˚C. Of the three techniques, *RD* calculated from TGA is also consistently higher than that determined from the other two methods. This could be due to removing some of the partially degraded polymer from the fibre surface when cutting the sample to size which explains both the wider variability and higher degree of solubilisation.

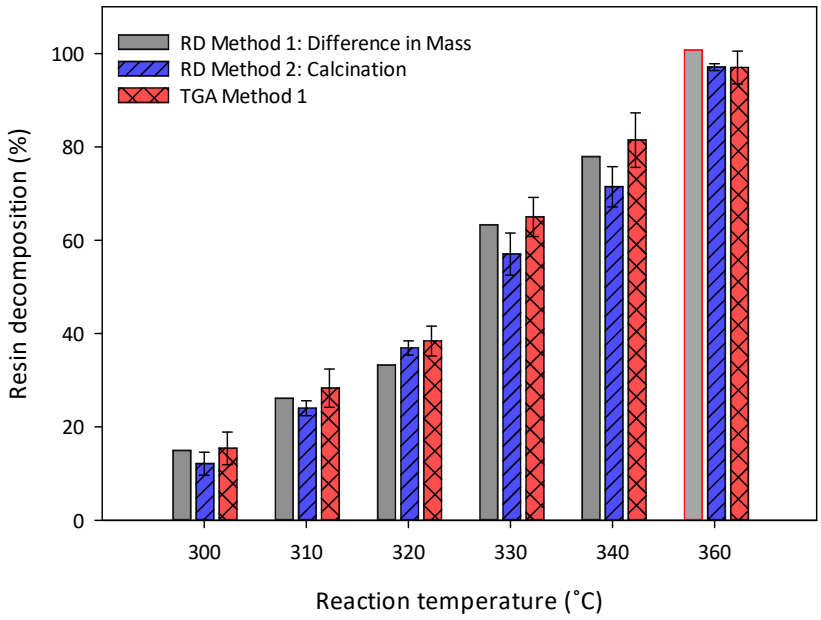

***Figure 18**. Comparison of RD Methods 1 and 2 using different reaction temperatures and an acetone / mains water solvent (t_R = 20 min). Red border indicates RD > 100%.*

There is generally good agreement between RD Methods 1 and 2 with the maximum deviation of 6.3% observed at a temperature of 330 and 340˚C. For all other conditions, the variation in *RD* was less than 3.5%. With the exception of 320˚C, RD Method 1 was slightly higher of the two results. Furthermore, at a temperature of 360˚C, an unusually high value of 100.7% was observed using this technique. This data is highlighted in red in Figure 18. This effect could be due to small fragments of the composite, or loose fibres, remaining in the basket following the reaction which will reduce the value of m_p. By inspection of Equation (7), it can be seen that this will increase the value of *RD* when calculating the degree of degradation from the difference in mass only. Higher process temperatures and longer reaction times which lead to greater decomposition are, therefore, more susceptible to this error. As it is not possible for *RD* to be in excess of 100%, the value taken from RD Method 1 was capped at a maximum

of 100%. In all other cases where this was observed, the data are similarly identified. Despite this, RD Methods 1 and 2 generally result in similar values and allow all of the composite processed in the reactor to be analysed, whereas TGA relies on a relatively small sample size. There is also a greater risk of removing some partially degraded polymer when cutting the sample following the reaction and, therefore, TGA may exaggerate the recorded value of *RD*. For these reasons, all subsequent data presented for the decomposition of the resin is an average of *RD* Methods 1 and 2 with the error bars illustrating the maximum and minimum value calculated.

3.5.2 Experimental Repeatability

To ensure the repeatability of each reaction, the experiments described by Table 4 were carried out three times with the results shown in Figure 19. Across the whole data set, the difference between each of the three repeats is 1.0 to 3.6 wt.%. The largest deviation occurs for a reaction time and temperature of 20 min and 320˚C where there is a difference in the *RD* observed of 3.6 wt.% between experiments 2 and 3. At 310˚C, 120 min and 360˚C, 0 min there is also a maximum difference between the recorded values of 2.8 wt.%. As these three largest deviations occur for differing reaction times and temperatures as well as at various levels of degradation, there does not seem to be a correlation between the deviation in the repeats and the experimental conditions. With an average difference of 2.3 ± 1.3 wt.%, the values for *RD* obtained after each experiment are within the margin of error associated with *RD* Methods 1 and 2 as described in Section 3.5.1. Furthermore, it is expected that increasing the process time and temperature will result in an increase in the decomposition of the resin and,

therefore, each data point is also verified by those adjacent to it. For this reason, and due to the high degree of repeatability, the experiments described in Section 3.2.3 were only carried out once, unless otherwise stated.

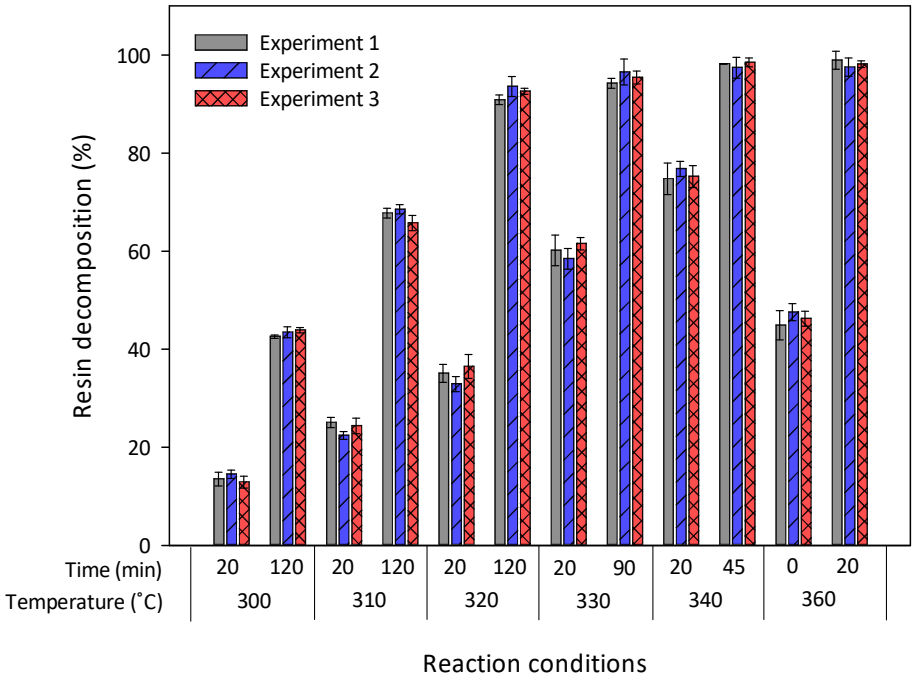

***Figure 19**. Three repeat experiments for resin decomposition after processing the CFRP with an acetone / mains water solvent at a range of conditions.*

3.5.3 Effect of Acetone / Mains Water Solvent

Due to the additional cost of deionising water for use in an industrial scale process, it is desirable to examine the difference between acetone / DI water and acetone / mains water solvent mixtures. If there is little to no influence of the ions present in the mains water (Table 2) on the degradation of the matrix, it is possible this cost can be avoided which may enhance the commercial feasibility of the developed process. The results of the experiments described in Table 5 are shown in Figure 20 and, with the possible exception of 310˚C and 320˚C after processing for 120 min, there is no

discernible difference between the use of mains and DI water. At 310 and 320˚C, the difference in *RD* for the two solvent mixtures is 3.4 and 4.2 wt.% respectively. Across all reaction conditions, however, the average difference between the two solvent systems is 2.1 wt.% which is less than that calculated from the three repeat experiments (discussed in Section 3.5.2) and is, therefore, within the margin of experimental error. For this reason, any deviation between the use of mains and DI water may be a result of slightly varying reaction temperature, rather than due to the low concentration of ions present in the mains water.

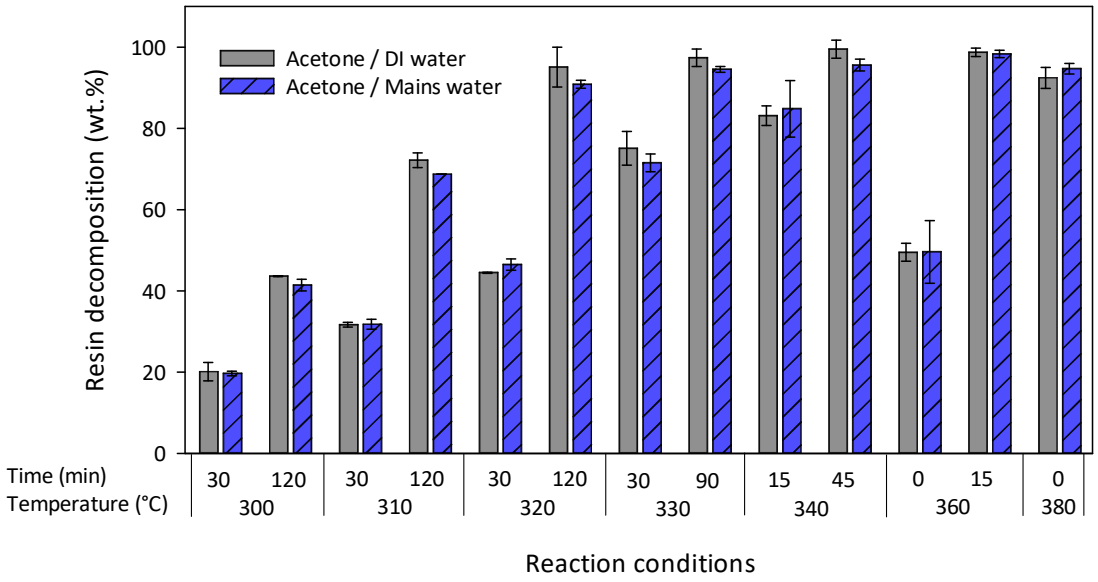

***Figure 20**. Resin decomposition for acetone / mains water and acetone / DI water at a range of process conditions.*

3.5.4 Effect of Time & Temperature

The influence of both the operating time and temperature on *RD* is presented in Figure 21 with the error bars illustrating the maximum and minimum values calculated using RD Methods 1 and 2. As alluded to in Section 3.5.2, increasing both reaction time

and temperature leads to an increase in the degradation. For t_R = 0 min, *RD* is consistently above 0 wt.% as shown by the dashed lines in Figure 21 and it is, therefore, apparent that the degradation reaction begins at some temperature below 300˚C. However, the contribution of the heating phase to *RD* is small below 340˚C; at this temperature, the degradation achieved at t_R = 0 min is only 23 wt.%.

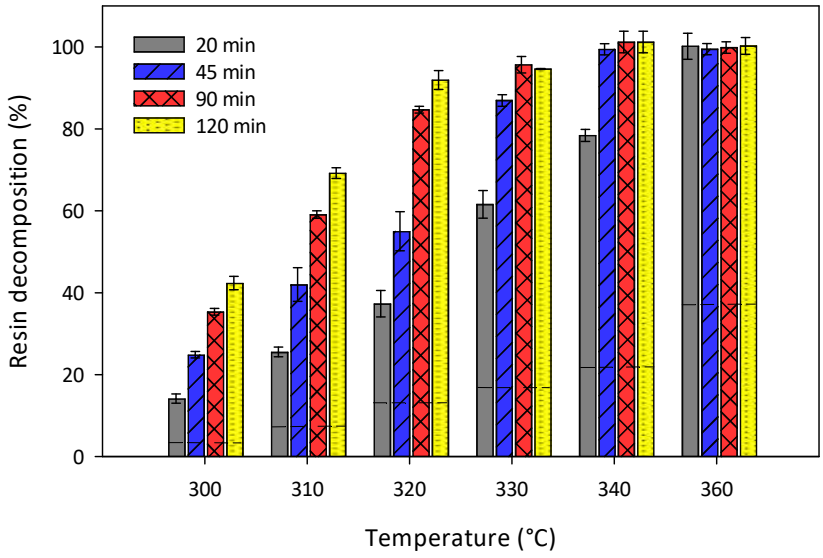

***Figure 21**. Resin decomposition after processing samples with an acetone / mains water solvent at 300 to 360˚C for 0 to 120 min (dashed line = RD at t_R = 0 min).*

Below 320˚C, the decomposition reaction appears slow; after processing for 120 min at 300˚C, the maximum *RD* observed is 42.4 ± 1.6 wt.%, while near-complete decomposition is achieved in the same reaction time at 320˚C. Under these conditions, the plies of carbon fibre fabric were completely separated as shown in Figure 22. This suggests that there is a strong dependence of *RD* on temperature and it is possible that at temperatures less than this, the RTM6 epoxy resin investigated will not be fully solubilised.

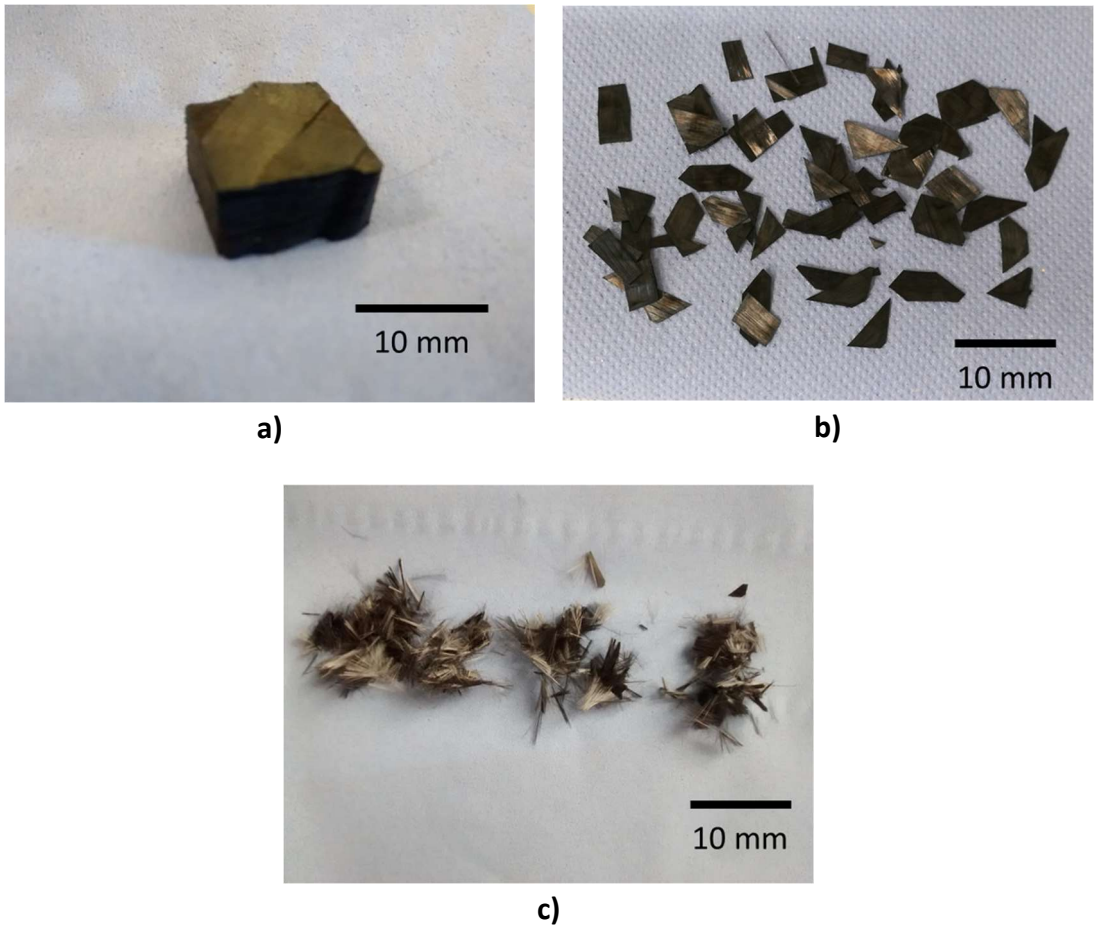

***Figure 22**. Samples of the CFRP after processing with an acetone / water solvent at a) 300˚C for 120 min; b) 320˚C, 120 min; and c) 340˚C for 45 min.*

Upon increasing the temperature to 330, 340 and 360˚C, it is possible to reduce the necessary reaction time for a similar value of *RD* to 90, 45 min and 15 min respectively; time reductions of 25, 62.5 and 87.5%. This significant temperature dependence has been previously reported [245], although it is not likely to be due to the enhanced properties of supercritical fluids; the critical point of this mixture is exceeded at 297˚C, 12 MPa. These results also suggest that, in order to effectively recover carbon fibres from this matrix, there is a minimum temperature requirement of 320˚C when operating under batch conditions. Although complete degradation of an epoxy resin with pure acetone has been achieved at this temperature in just 20 min, the authors of

this study noted a T_g of 183˚C [264]; 38 ± 3˚C lower than the polymer investigated here. This is indicative of a lower degree of cross-linking which therefore leads to differing degradation characteristics. A model epoxy resin has also been completely solubilised using this acetone / water solvent mixture and the conditions necessary of 350˚C, 30 min [252] are similar to those identified as part of this research.

Further experiments were carried out at 380˚C, however, upon just reaching the reaction temperature, the resin was completely degraded. Although the use of higher temperatures resulted in significantly faster reaction rates, these extreme conditions caused the loss of the fibre architecture. Figure 22 demonstrates that at 340˚C, the recovered material exhibited a "fluffy" quality. As an effective commercial realignment process is yet to be developed, it is unlikely that the fibres recovered after processing at these conditions are suitable for reuse in a defined structure. Despite this, it may be possible to manufacture random, non-woven mats if sufficient fibre densities can be attained in the product. As previous work has also demonstrated that increasing the reaction temperature may result in a reduction of the mechanical properties of the fibres [3], it is also necessary to characterise the recycled material. The influence of various recycling processes on the fibre quality is investigated in Chapter 5, however, at present, the conditions recommended for effective recovery of carbon fibre using a neat acetone / water solvent mixture are 320˚C for 120 min and 330˚C for 90 min.

3.6 Catalytic Resin Decomposition

As the critical point of the acetone / water solvent mixture has been calculated to be 297˚C and 12 MPa, experiments investigating the efficacy of various additives have been performed in both the sub- and supercritical regions. When the solvent is subcritical, catalysed hydrolysis is the preferred mechanism for the decomposition of polymers [248] and it should, therefore, be possible to identify which of the alkaline salts and metal chlorides listed in Table 3 are effective catalysts.

3.6.1 Alkaline Salts

Contrary to previous research which considered either water / KOH [256] or polyethylene glycol (PEG) / NaOH systems [257], [276], the results presented in Figure 23 and Figure 24 demonstrate that the presence of hydroxyl ions inhibit the decomposition of the CFRP under the conditions investigated. For KOH and NaOH solutions, the minimum degradation was observed at a concentration of either 0.03 or 0.05 M. Here, there was a reduction in *RD* of between 15.7 to 27.5 wt.% for KOH and 16.9 to 34.0 wt.% for NaOH when compared to the neat solvent mixture. In the presence of basic media, acetone readily undergoes aldol condensation to form 4-hydroxy-4-methyl-pentan-2-one (diacetone alcohol, DAA) [289]. The critical temperatures of DAA and acetone are 334 [290] and 235˚C [283] respectively and, therefore, the elimination of acetone from the solvent mixture by aldol condensation will raise the critical point of the system to beyond that of the conditions investigated. Although the preferred reaction mechanism for the degradation of epoxy resins is hydrolysis [252], [261], experiments conducted no longer benefit from the good solvating power of acetone nor

the enhanced properties of supercritical fluids. As the reaction mechanism for this solvent system is not yet fully understood, it is also possible that acetone may be a reactant in the decomposition process. If this is the case, removing acetone from the mixture will also result in a reduction in *RD* for similar reaction conditions.

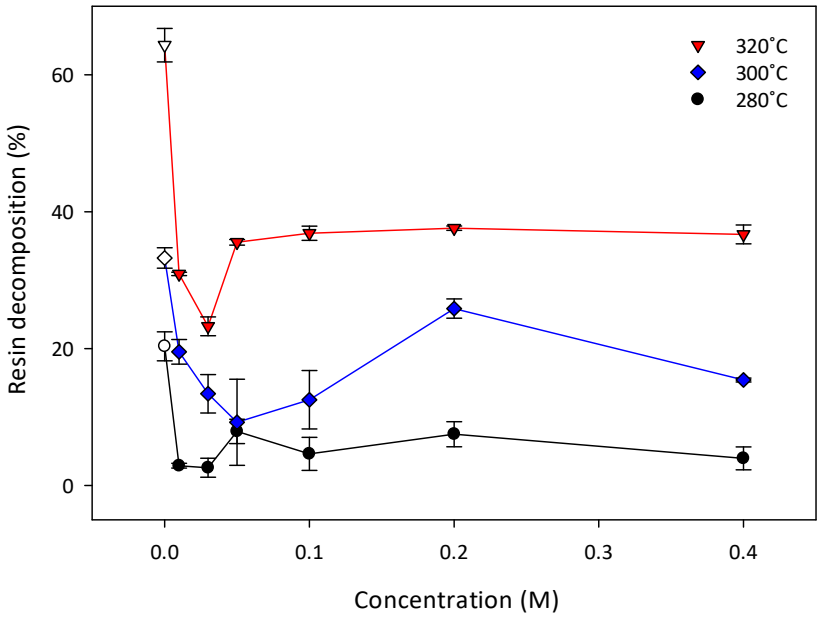

***Figure 23**. Effect of increasing concentration of KOH on resin decomposition for various reaction temperatures (t_R = 60 min). Open symbol represents neat acetone / water solvent mixture.*

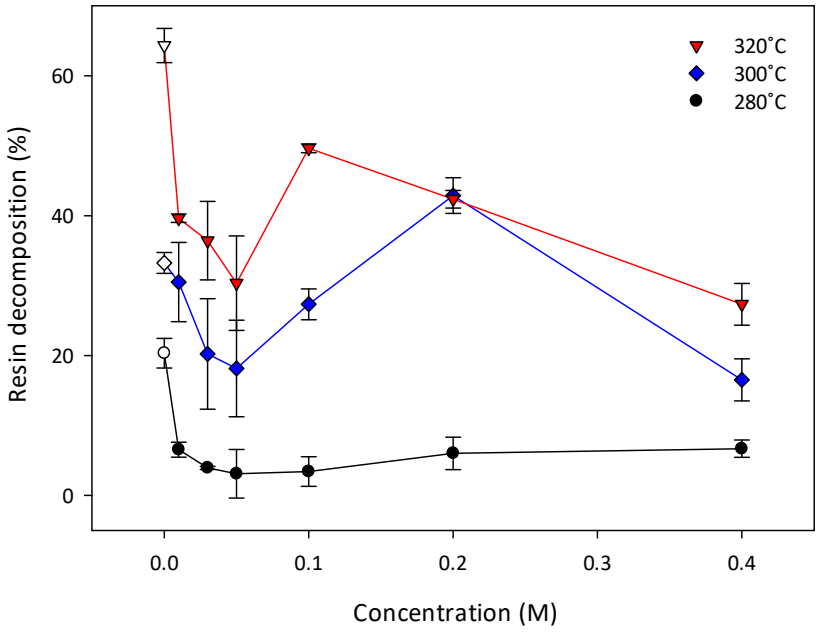

***Figure 24**. Effect of increasing concentration of NaOH on resin decomposition for various reaction temperatures (t_R = 60 min). Open symbol represents neat acetone / water solvent mixture.*

At concentrations of above 0.05 M, *RD* increases compared to more dilute systems, with a peak typically seen at 0.20 M. However, with the exception of a 0.20 M NaOH solution at 300˚C, the decomposition is still lower than that achieved with the neat solvent mixture for all temperatures investigated. As these higher concentrations are similar to those previously investigated [256], [257], it is possible that the hydroxyl ions do enhance the degradation, however, they do not compensate for the elimination of acetone. For this reason, it is apparent that additional compounds such as phenol or PEG are necessary to depolymerise the matrix and alkaline salts are not effective catalysts when used in conjunction with an acetone / water solvent mixture.

3.6.2 Weak Lewis Acids

The inclusion of the weak Lewis acids $ZnCl_2$, $MgCl_2$ and $AlCl_3$ into the solvent system are highly effective catalysts even at low concentrations as evidenced by Figure 25 and Figure 26. Metal chlorides generally have high solubility in water [291], acetone and acetone / water mixtures [292] which results in the generation of metal ions. Previous work has shown that certain solvents result in "swelling" the polymer matrix [293] facilitating the mass transfer of the metal ions which are capable of cleaving the C=N bonds present in epoxy resins [239], [293]. Figure 25 demonstrates that increasing the concentration of $ZnCl_2$ beyond 0.1 M does not enhance the decomposition of the CFRP at 280˚C with a plateau in *RD* observed at 85 wt.%. This suggests that a longer reaction time is necessary if it is possible to fully solubilise the polymer at this temperature.

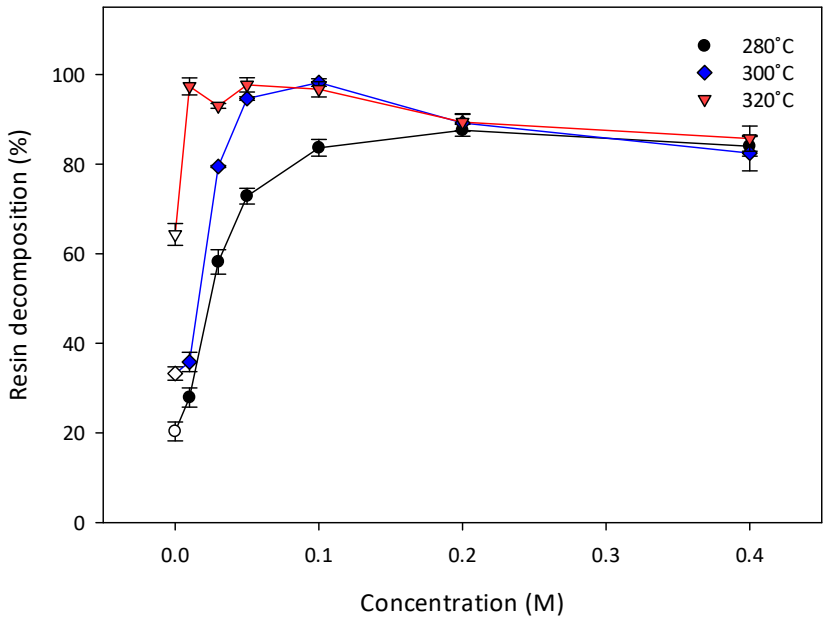

***Figure 25**. Effect of increasing concentration of $ZnCl_2$ on resin decomposition for various reaction temperatures (t_R = 60 min). Open symbol represents neat acetone / water solvent mixture.*

Earlier research investigating the decomposition of a similar epoxy resin has achieved an *RD* in excess of 90 wt.% at just 220˚C, however, much higher concentrations and longer processing times of 1.4 M and 5 h were necessary [239]. Currently, the influence of metal chlorides on the properties of the recovered fibres at these temperatures and pressures is unknown and it is, therefore, desirable to minimise the concentration of the catalyst supplied. Fibres which have been subjected to similar process conditions have been characterised as described in Chapter 5. At 320˚C, 0.01 M $ZnCl_2$ is able to completely strip the resin from the fibre surface demonstrating that for the same reaction temperature, very dilute solutions are able to halve the necessary process time. By increasing the concentration to 0.05 M, it is also possible to reduce the temperature to 300˚C; both $ZnCl_2$ and $MgCl_2$ were able to remove 95 wt.% of the resin under these conditions as illustrated by Figure 26.

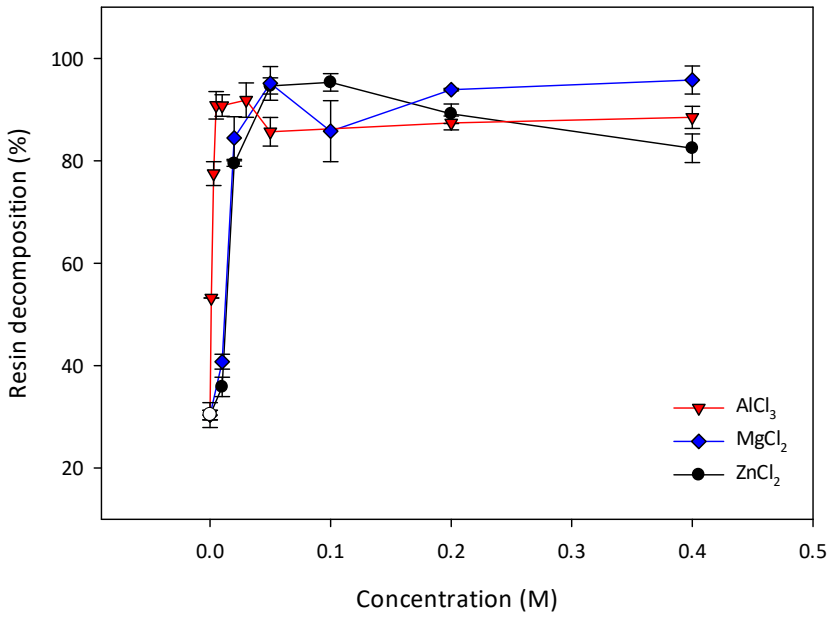

***Figure 26**. Effect of increasing concentration of chloride ions on resin decomposition (T_R = 300˚C, t_R = 60 min). Open symbol represents neat acetone / water solvent mixture.*

Of the 3 metal chlorides investigated, Figure 26 demonstrates that $AlCl_3$ is the most effective catalyst with a similar degradation achieved at a concentration of 0.005 M compared to the 0.05 M solutions of $ZnCl_2$ and $MgCl_2$. As the Al^{3+} ion carries a stronger charge, it may co-ordinate more strongly with the lone pair of electrons present on the heteroatom within the molecular structure of the epoxy resin. It may also interact less strongly with the solvent mixture than the Zn^{2+} and Mg^{2+} ions which leads to a greater availability of metal ions for the attack of the C=N bonds commonly present within epoxies. This effect has been previously reported by Wang, et al [277]. As 0.05 M solutions of $ZnCl_2$, $MgCl_2$ and $AlCl_3$ achieved near-complete degradation after processing for 60 min at 300˚C, these conditions were selected to examine the efficacy of the additional additives listed in Table 3.

3.6.3 Additional Additives

In addition to the additives described in Sections 3.6.1 and 3.6.2, the influence of 0.05 M solutions of $ZnSO_4$, $MgSO_4$, $Al_2(SO_4)_3$, Cs_2CO_3, $CsCl_2$, $CaCl_2$ and $CuCl_2$ on the degradation of the CFRP is shown in Figure 27. Under the conditions investigated, the neat solvent mixture was capable of removing 33 wt.% of the resin which was similar to the *RD* achieved with $ZnSO_4$ and $MgSO_4$. Although metal sulphates are generally insoluble in acetone [294], they are soluble in water; at 25˚C the solubility is 26.6 and 16.3 g L^{-1} respectively [295]. Solutions were made by first dissolving the salt in the latter solvent and, upon adding the acetone, no precipitation was observed. No data were available in the literature for the solubility of these salts in acetone or an acetone / water mixture at the conditions investigated, however, it is possible that $ZnSO_4$ and $MgSO_4$ do

not remain in solution. The lack of metal ions dissolved would, therefore, explain why there was no observable increase in the degradation for these systems. A slightly higher *RD* of 52.4 wt.% was observed with a 0.05 M $Al_2(SO_4)_3$ solution which may be due to a higher solubility of this salt. This result also suggests that Al^{3+} ions do enhance the decomposition, although the chloride ions may also accelerate the degradation reaction. Previous research has shown Cs_2CO_3 facilitates the depolymerisation of thermoplastics such as PEEK [265], however, there is a reduction in *RD* of approximately 50% when applying this additive to the decomposition of a thermoset epoxy resin.

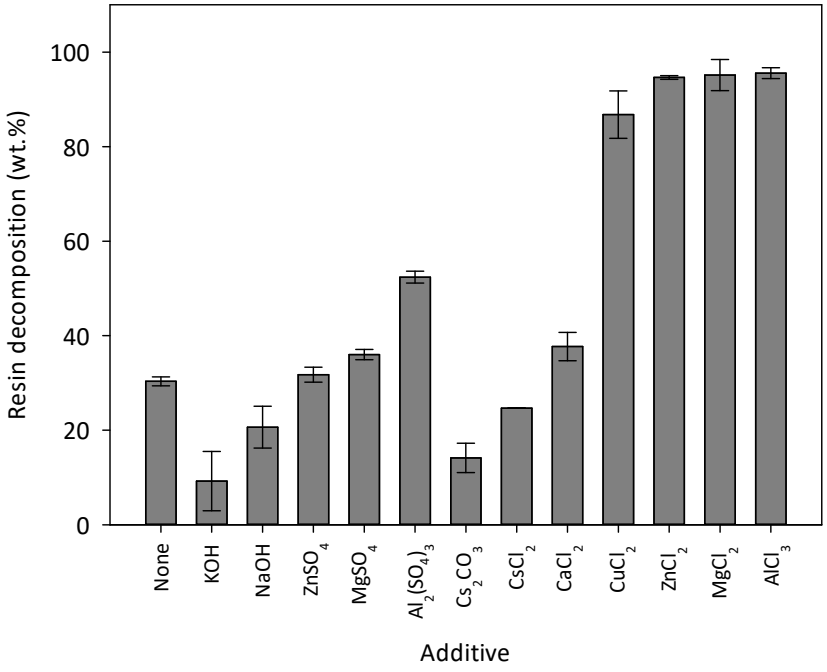

***Figure 27**. Resin decomposition for a range of additives supplied at a concentration of 0.05 M (T_R = 300˚C, t_R = 60 min).*

With the exception of $CsCl_2$ (*RD* = 25 wt.%) and $CaCl_2$ (*RD* = 38 wt.%), all metal chlorides considered are able to achieve a degradation of more than 90 wt.% at 300˚C within a reaction time of 60 min. Currently, it is not understood why these two additives

do not promote the decomposition of the matrix; there is no correlation between solubility, molecular size, bond energies or electronegativity differences which suggests that there should be a similar concentration of metal ions in solution when compared to $ZnCl_2$, $MgCl_2$, $AlCl_3$ and $CuCl_2$. Although effective, this latter catalyst is particularly hazardous with regards to human health, safety and the environment and it would, therefore, be desirable to avoid its use where possible. For this reason, only $ZnCl_2$, $MgCl_2$ and $AlCl_3$ were selected for further investigation in order to determine the minimum necessary process time and temperature to achieve complete decomposition of the resin.

3.6.4 Effect of Reaction Time & Temperature

As expected, Figure 28 to Figure 30 demonstrate that increasing both the reaction time and operating temperature leads to an increase in the degradation of the resin. At 270˚C, however, the reaction appears slow and, after processing for 90 min, the maximum *RD* observed was in the range of 36.9 to 58.5 wt.% across all three catalysts studied. Although an increase in temperature to 280˚C does give an *RD* of up to 85 wt.%, it was not possible to fully solubilise the polymer unless the temperature was raised to 290˚C under the reaction times investigated. This could be due to high molecular weight compounds which require more concentrated catalysts, or higher temperatures, to fully decompose.

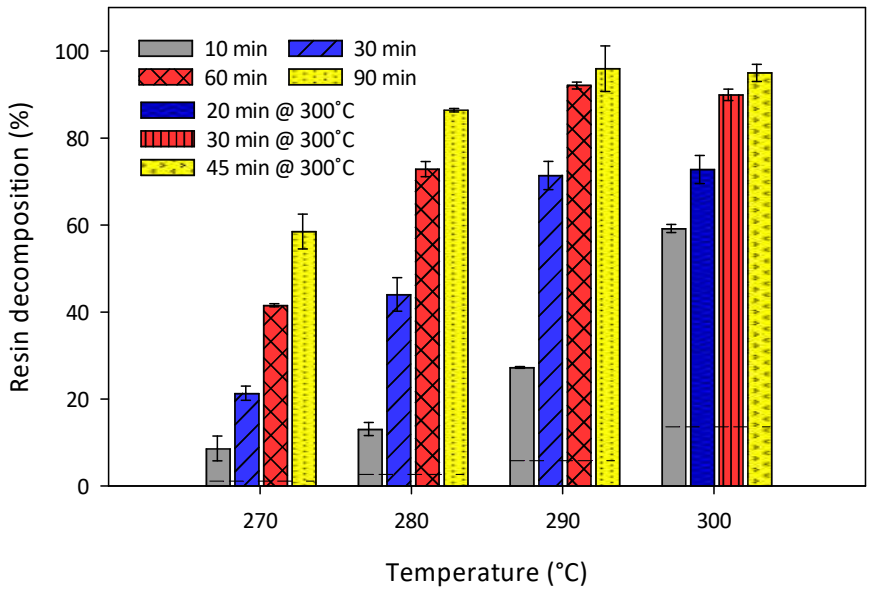

***Figure 28**. Effect of reaction time and temperature on resin decomposition using a 0.05 M $ZnCl_2$ catalyst and acetone / water solvent (dashed line indicates RD at t_R = 0 min).*

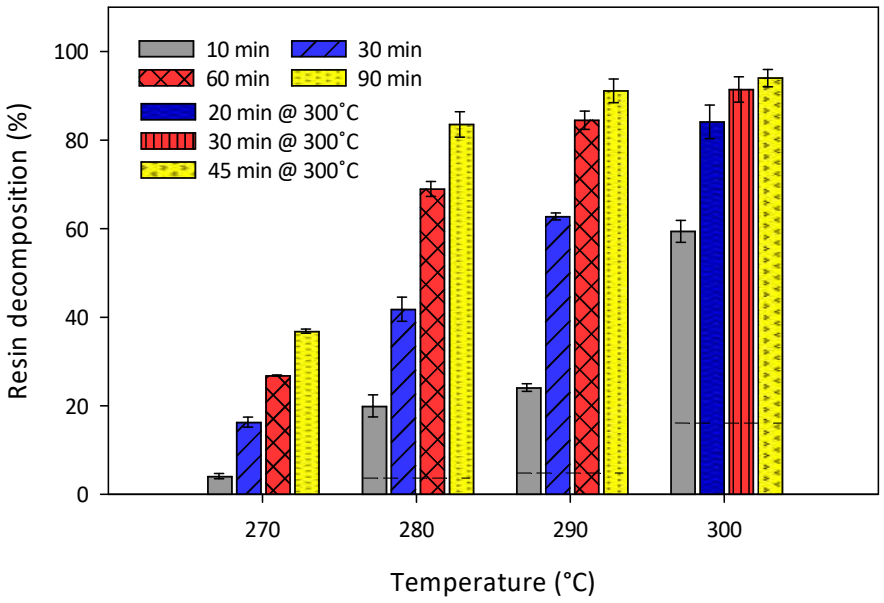

***Figure 29**. Effect of reaction time and temperature on resin decomposition using a 0.05 M $MgCl_2$ catalyst and acetone / water solvent (dashed line indicates RD at t_R = 0 min).*

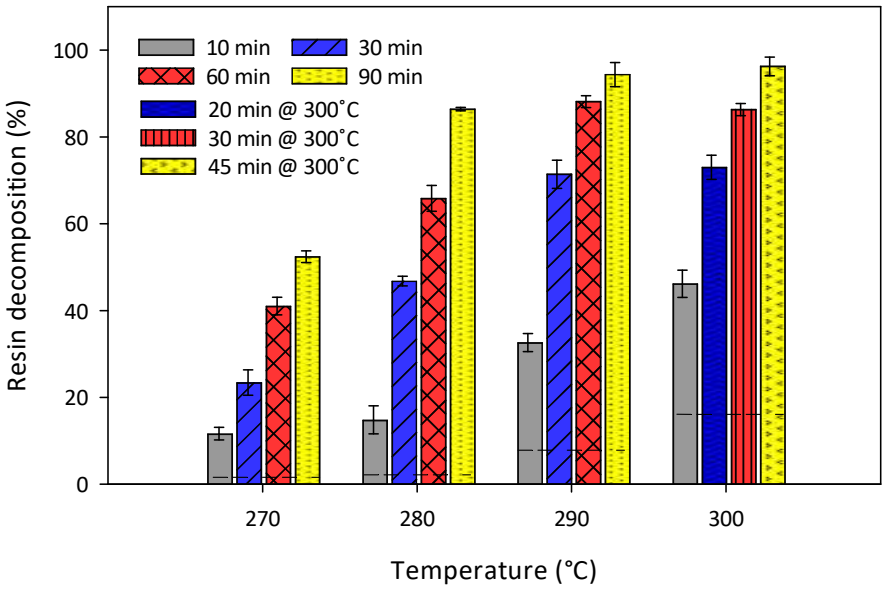

***Figure 30**. Effect of reaction time and temperature on resin decomposition using a 0.005 M $AlCl_3$ catalyst and acetone / water solvent (dashed line indicates RD at t_R = 0 min).*

At 290˚C, the resin was fully stripped from the fibre surface within 90 min while increasing the temperature to 300˚C allows a similar *RD* to be attained in half the reaction time of 45 min for all catalysts studied. Compared to the neat solvent mixture and same reaction time, the addition of 0.05 M $ZnCl_2$ and $MgCl_2$ and 0.005 M $AlCl_3$ therefore results in decreasing the required process temperature by 40˚C. In turn, this will lead to a reduction in the energy demand, environmental impact and operating cost of an industrial scale process. As relatively dilute concentrations are used, it may be possible to achieve further reductions through increasing the concentration of the catalyst.

With the possible exception of a process time and temperature of 10 min and 300˚C, 0.05 M $ZnCl_2$ and 0.005 M $AlCl_3$ solvent systems achieved similar levels of decomposition at all conditions studied. There was, however, a strong temperature

dependence of $MgCl_2$; at 270˚C, the *RD* reached just 36.9 wt.% over a 90 min reaction period compared to 52.5 and 58.5 wt.% when using $AlCl_3$ and $ZnCl_2$ respectively. At both 290 and 300˚C, $MgCl_2$ was as effective as the other two catalysts; at these temperatures, the *RD* observed across all three systems was very similar at each of the reaction times considered with the maximum difference of 11.0 wt.% occurring between $ZnCl_2$ and $AlCl_3$ (*RD* = 72.8 and 73.0 wt.% respectively) and $MgCl_2$ (*RD* = 84.0 wt.%) at 300˚C, 20 min. As this variation is outside the margin of experimental error, the results suggest that there is a slight difference in the efficacy of the catalysts. Of these three metal chlorides investigated in detail, 0.05 M $ZnCl_2$ resulted in the highest *RD* at the lowest temperature considered, although it is worth noting that $AlCl_3$ was supplied at a concentration an order of magnitude lower. There is, therefore, the potential to investigate higher concentrations of $AlCl_3$ which may facilitate complete decomposition at lower reaction temperatures. However, as the effect of metal chlorides dissolved in this acetone / water solvent mixture on the quality of the recovered fibres is not yet known, it may also be desirable to minimise the concentration of these salts. As a result of this research, the minimum necessary conditions to effectively recover carbon fibres using 0.05 M solutions of $ZnCl_2$ and $MgCl_2$ and a 0.005 M solution of $AlCl_3$ have been identified as 290˚C for 90 min and 300˚C for 45 min. To quantify the effect of these process conditions on the recycled material, fibres are characterised in Chapter 5.

3.7 Concluding Remarks

A preliminary investigation into the decomposition of a commercially available, carbon fibre reinforced RTM6 epoxy resin has been conducted. To aid understanding of

the degradation process, it was necessary to determine the phase behaviour of the solvent. Using the PC-SAFT EoS, the critical point of the mixture was identified as 297˚C and 12 MPa which demonstrates that experiments were performed in the supercritical region with the neat solvent and in both the sub- and supercritical phases when investigating the efficacy of various additives. As there is no clear step change in *RD* upon changing phase, the results presented in this chapter suggest that the temperature is of greater importance than the phase behaviour of the solvent.

In addition to the solvent, the CFRP was also characterised by quantifying the resin content and identifying the T_g. The latter property was determined using DSC and has been shown to be 221 ± 3˚C. This is indicative of a high degree of cross-linking of above 0.9 which suggests that if it is possible to solubilise this polymer, the developed conditions could be applied to the recycling of a wide range of composite materials. Two independent methods were used to measure the resin content: calcination and TGA. Both of these techniques were in close agreement and gave a value of 35.0 ± 0.5 wt.% which is similar to that calculated from the manufacturer's data and typical densities of carbon fibre and epoxy resin. For this reason, R_i = 35.0 wt.% was used in all subsequent calculations when quantifying *RD*.

Initially, three methods were considered in order to measure *RD*: TGA, calcination and the difference in mass before and after processing. The values obtained from TGA were generally higher than the other two techniques and demonstrated a higher variability across the 5 samples analysed, possibly due to the loss of resin when cutting

the samples to a suitable size. For this reason, only calcination and the difference in mass of the CFRP was used to quantify *RD* for most of the experimental conditions investigated. These two techniques generally gave a good level of agreement with a maximum variation observed across all experiments of ± 4 wt.%.

By repeating experiments at the same process conditions, it has also been possible to demonstrate that there is a high degree of repeatability across different reactions. The deviation observed across the three repeated experiments was 2.3 ± 1.3 wt.% which is within the margin of experimental error when calculating *RD* from the methods described in Section 3.2.4. As adjacent data points also verify each other, it was therefore considered sufficient to conduct most experiments only once.

The use of water from the mains supply, instead of DI water, does not appear to influence the degradation of the resin. For this reason, and in order to more closely simulate industrial conditions, the effect of varying reaction time and temperature was studied using an acetone / mains water solvent mixture. By changing these two parameters, the minimum conditions necessary for an *RD* of more than 92 wt.% were identified as 320˚C, 120 min or 330˚C, 90 min. Above this temperature, the recovered fibres exhibited a “fluffy” texture which may be more difficult to re-use in high value applications.

The inclusion of alkaline salts and metal sulphates does not accelerate the degradation reaction, however, 0.05 M $ZnCl_2$, 0.05 M $MgCl_2$ and 0.005 M $AlCl_3$ have all

been shown to be effective catalysts. At these concentrations, it is possible to reduce the necessary reaction temperature to achieve near-complete decomposition by 40˚C for the same reaction time. However, the influence of these reaction conditions on the recovered fibres is not yet known and they are therefore characterised in Chapter 5.

In order to deepen the understanding of the decomposition reaction, Chapter 4 focusses on the development of two different kinetic models with the aim of calculating the Arrhenius parameters E_A and k_0 for the neat acetone / water solvent and the $ZnCl_2$, $MgCl_2$ and $AlCl_3$ systems.

CHAPTER 4.
REACTION KINETICS

4.1 Introduction

Investigation of the kinetics of any reaction allows the relationship between temperature, time, reaction order and conversion to be mathematically determined. This facilitates a greater understanding of the processes taking place and will allow a direct comparison of the efficacy of different solvent and catalyst systems to be made. Previous research has considered a conventional rate equation with an order of 1.5 [242] and 2 [245] and a shrinking core model (SCM) [264] in order to characterise the decomposition reaction of a CFRP using either propan-1-ol, [242] water [245] or acetone [264] as the solvent. No publications currently available in the open literature have applied both kinetic models to the same data set in order to compare their ability to model the decomposition of the resin. In addition to this, the kinetics of the degradation of the CFRP using the acetone / water solvent mixture and weak Lewis acids considered in this thesis have not yet been analysed in any earlier work. For these reasons, this chapter aims to conduct a comprehensive investigation into the reaction kinetics by applying a conventional rate equation and a shrinking core model to the degradation data presented in Chapter 3. Further experiments, which were conducted to provide additional evidence for the assumptions made when

developing these models, are also discussed throughout this chapter. Following this, the Arrhenius parameters, activation energy (E_A) and frequency factor (k_0), are calculated and used to predict the decomposition at a range of conditions. This chapter concludes by evaluating which model is able to best fit the decomposition of the CFRP which may have significant applications in future research.

The models described in this chapter have been previously published in "Recycling a carbon fibre reinforced polymer with a supercritical acetone / water solvent mixture: Comprehensive analysis of reaction kinetics" [226] and "Catalytic degradation of a carbon fibre reinforced polymer for recycling applications" [296]. Both articles are available in the journal *Polymer Degradation and Stability*.

4.2 Experimental Methodology

4.2.1 Fibre Recovery

In addition to the investigation conducted in Chapter 3, further experiments were performed in order to provide supplementary data points for use in the development of the models discussed throughout this chapter. The CFRP which was characterised in Section 3.4 was used in all experiments. The equipment, solvents and additives used as part of this work are also the same as those described in Chapter 3. Five pieces of the 6 mm thick composite material measuring (10 x 10 ± 1) mm^2 with a total mass of 4.17 ± 0.01 g were placed into a basket before being loaded into the 100 mL batch reactor. 50 ± 1 mL of the solvent

mixture was also added. The vessel was sealed, heated to the desired temperature for each of the reaction times in Table 11 and Table 12 and cooled to room temperature using forced air convection. Recovered samples were then washed with acetone and dried overnight in a fume cupboard before being analysed following the procedures described in Section 3.2.4.

***Table 11**. Additional experiments performed with neat acetone / mains water solvent.*

Temperature, T_R (± 1 °C)	**Induced Pressure, p (± 0.3 MPa)**	**Reaction Time, t_R (min)**
300	15.8	10, 30, 60, 150
310	17.8	
320	19.7	
330	22.0	10, 30, 60
340	23.5	10, 30
360	27.0	5, 10, 15
380	30.0	

***Table 12**. Additional experiments performed with an acetone / water solvent and 0.05 M $ZnCl_2$ and $MgCl_2$ and 0.005 M $AlCl_3$.*

Temperature, T_R (± 1 °C)	**Induced Pressure, p (± 0.3 MPa)**	**Reaction Time, t_R (min)**
270	12.0	0, 20, 45, 120
280	13.0	
290	14.5	

4.2.2 Reactor Loading

All experiments in Chapter 3 and those described in Section 4.2.1 used a reactor loading of 30 ± 0.1 g_{resin} $L_{solvent}^{-1}$. In order to assess the capability of this system to degrade higher quantities of material and to aid in identifying the rate determining step (RDS), the experiments listed in Table 13 were completed using a loading of both 60 and 90 g_{resin} $L_{solvent}^{-1}$. These conditions were selected as they are the minimum temperature and reaction time required to fully decompose the polymer matrix of the CFRP. The increased loading was achieved by using 10 and 15 pieces of the composite which had total masses of 8.34 ± 0.01 g and 12.51 ± 0.01 g respectively. For these experiments, and those described in Section 4.2.1, the resin decomposition (*RD*) was quantified using the methods described in Chapter 3.

***Table 13**. Experimental conditions investigated for an increased reactor loading of 60 and 90 g_{resin} $L_{solvent}^{-1}$ (175 and 257 $g_{composite}$ $L_{solvent}^{-1}$).*

Catalyst	Temperature, T_R (± 1 °C)	Induced Pressure, p (± 0.3 MPa)	Reaction Time, t_R (min)
None	320	19.7	120
	330	22.0	90
	340	23.5	45
	360	27.0	20
0.05 M $ZnCl_2$	290	14.5	90
	300	15.8	45
0.05 M $MgCl_2$	290	14.5	90
	300	15.8	45
0.005 M $AlCl_3$	290	14.5	90
	300	15.8	45

4.2.3 X-ray computed Tomography (XRCT)

To study the swelling ability and mass transfer of the solvent molecules into the resin, partially degraded samples were imaged with X-ray computed Tomography (XRCT). Samples were recovered from the reactor after a process time of 30 min using a neat acetone / water solvent (T_R= 320˚C) and the 0.05 M $MgCl_2$ system (T_R = 290˚C). These temperatures were selected as they are the minimum required to achieve near-complete decomposition of the resin within the reaction times investigated. After processing, the samples were rinsed with acetone and dried overnight at ambient conditions before being loaded into the imaging chamber of a Bruker Skyscan 1172 XRCT. A camera exposure time of 500

ms and a resolution of 240 px mm^{-1} were used. The acceleration voltage and current were set to 65 kV and 80 µA respectively.

4.3 Reactor Loading

The influence of changing the reactor loading on the decomposition of the resin is illustrated by Figure 31. Similar to the data presented in Chapter 3, the *RD* plotted is an average between RD Methods 1 and 2 (described in Section 3.2.4) where the error bars illustrate the maximum and minimum values calculated. Although within the range of experimental error, experiments performed at 340˚C with the neat solvent mixture and at 290˚C with 0.05 M $ZnCl_2$ showed a slight decrease in *RD* with an increase in loading; this may be expected as the solvent becomes saturated and the mass transfer of the reactants, products and / or catalyst becomes rate limiting. However, the highest degradation is also observed at the maximum reactor loading for 320 and 330˚C and in both conditions studied with the 0.05 M $MgCl_2$ solution. In all other experiments, *RD* for 30 g L^{-1} was within ± 1.5 wt.% for the *RD* at 90 g L^{-1}. As these results are within the range of experimental error, the data presented in Figure 31**Figure** demonstrates that there is no discernible difference in the observed degradation upon increasing the reactor loading. This suggests that the loading may be further maximised in order to reduce the economic cost and environmental burden per unit weight of CFRP recycled.

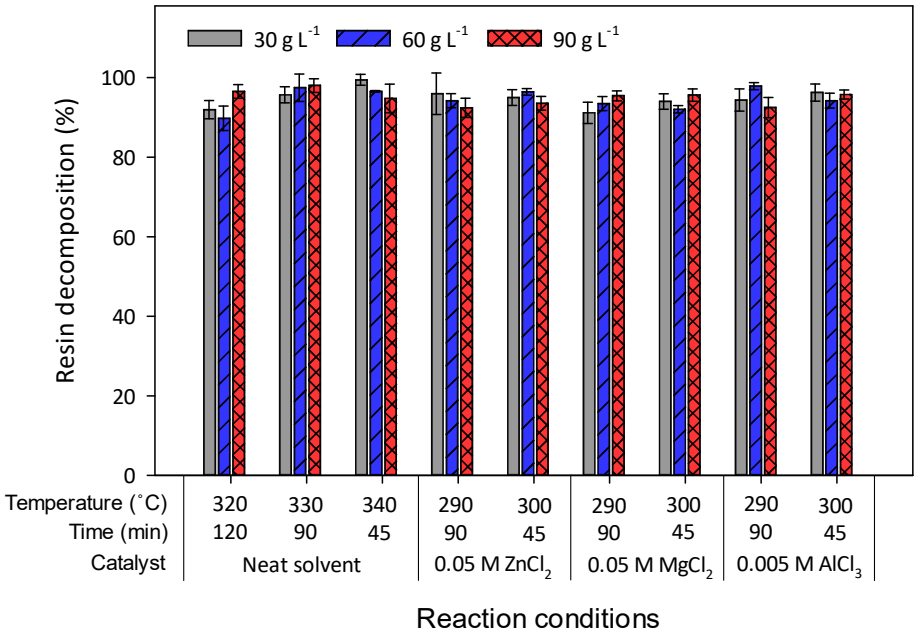

***Figure 31**. Effect of increasing the concentration of resin in the reactor from 30 to 90 g L^{-1} using various process conditions.*

As the concentration of the organic liquid products (OLP) do not appear to influence the rate of the decomposition reaction under the conditions investigated, it appears that both the solvent and the catalyst are always in excess. If the solvent was saturated with the OLP, the mass transfer of the solvent molecules and catalyst ions through the bulk fluid, penetration into the composite material and transfer of the products away from the fibre surface would slow down and become rate limiting. In turn, this would lead to a slower reaction, and thus a lower *RD* for the conditions investigated. For these reasons, the results presented suggest that the RDS of the degradation process is the decomposition reaction rather than any of the mass transfer stages.

4.4 X-ray computed Tomography (XRCT)

In order to further the understanding of the degradation process, partially degraded samples of the CFRP were imaged with XRCT. Figure 32a and Figure 33a illustrate that after processing each sample for 30 min, there is some ply separation as the solvent has moved into the polymer matrix causing it to swell. In Figure 32a, cracks are also visible on the surface of each ply thus demonstrating that even at low values of *RD*, the solvent was able to effectively penetrate to the centre of the sample. These cracks are not observed in Figure 33a where the sample was processed at 290˚C with 0.05 $MgCl_2$, however, the measured *RD* was 18 wt.% higher. The extent of the degradation appears uniform across the surface of each ply and it is, therefore, likely that at this point, the solvent had fully penetrated throughout the resin. These cracks were also visible at samples recovered from a shorter process time of 10 min as shown in Figure 34.

By removing the higher density carbon fibre from the images (Figure 32b and Figure 33b), a large volume of resin is visible at the centre of the sample. This is likely to reduce in size as the resin is degraded and it is, therefore, possible to fit the degradation data obtained to a shrinking core model as described in Section 4.6. From these images, it appears that penetration of the solvent occurs in between the plies of carbon fibre (in the *x* and *y* directions). This may be due to a lower fibre density, while the path in the *z* direction remains tortuous. Although the fibres appear to facilitate the mass transfer of the solvent into the composite,

the diffusion pathways visible in Figure 32a and Figure 34 are randomly orientated and do not follow the direction of individual fibres or tows. This suggests that the orientation of each tow does not affect the penetration and, therefore, that the solvent may migrate through the resin by following defects within the matrix.

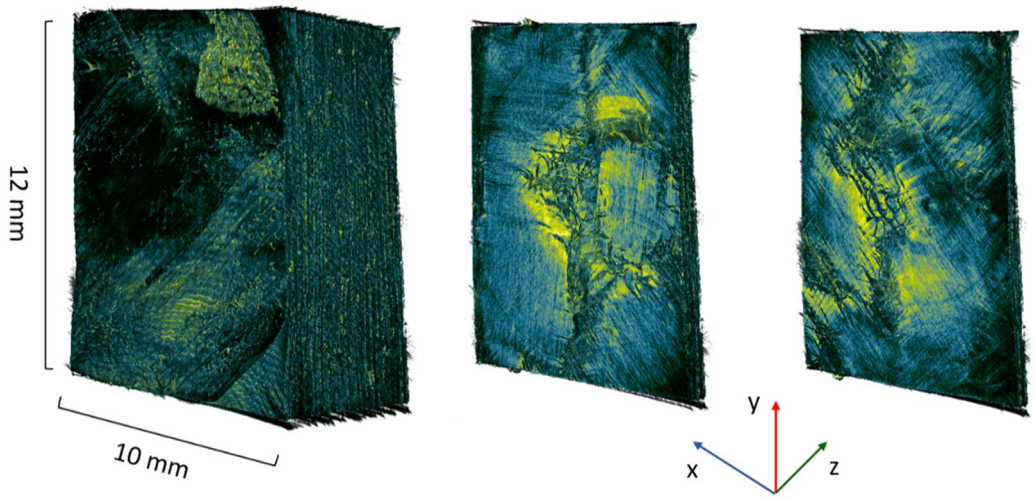

a)

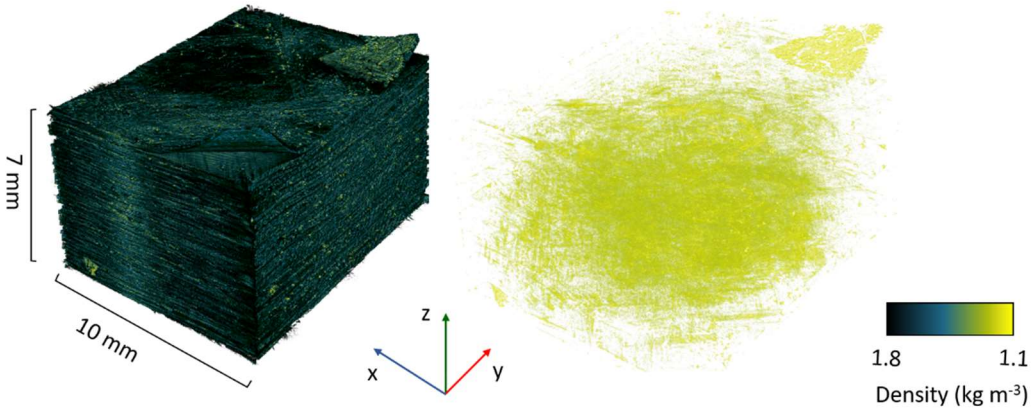

b)

***Figure 32**. XRCT image after processing a sample of the CFRP at 320˚C for 30 min with an acetone / water solvent (RD = 44 wt.%) showing a) crack propagation between plies; and b) resin concentrated at the centre of the sample with fibres removed from image.*

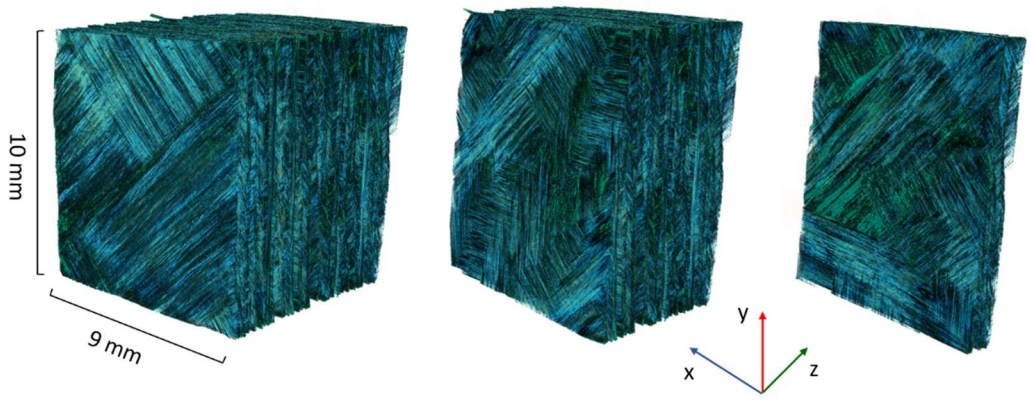

a)

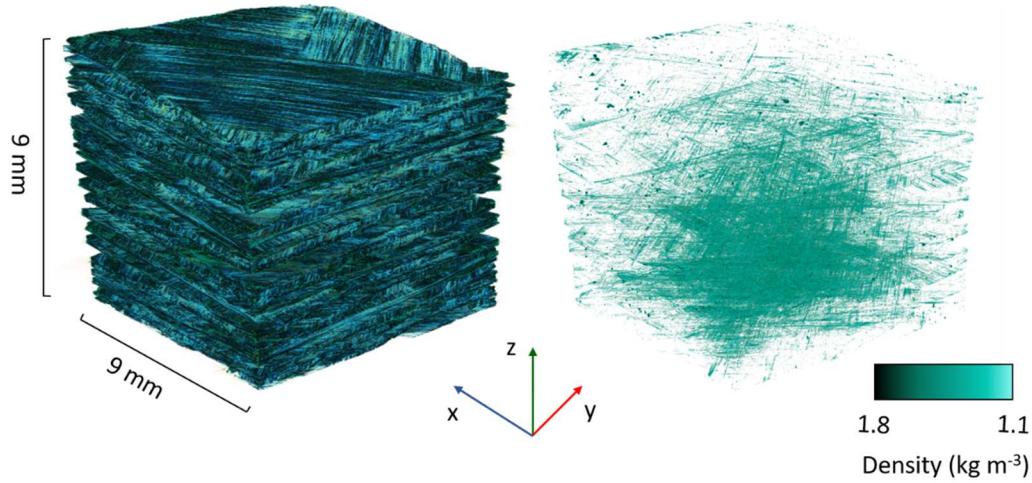

b)

Figure 33. *XRCT image after processing a sample of the CFRP at 290˚C for 30 min with an acetone / water solvent and 0.05 M $MgCl_2$ (RD = 62 wt.%) showing a) resin remaining on fibre surface; and b) resin concentrated at the centre of the sample with fibres removed from image.*

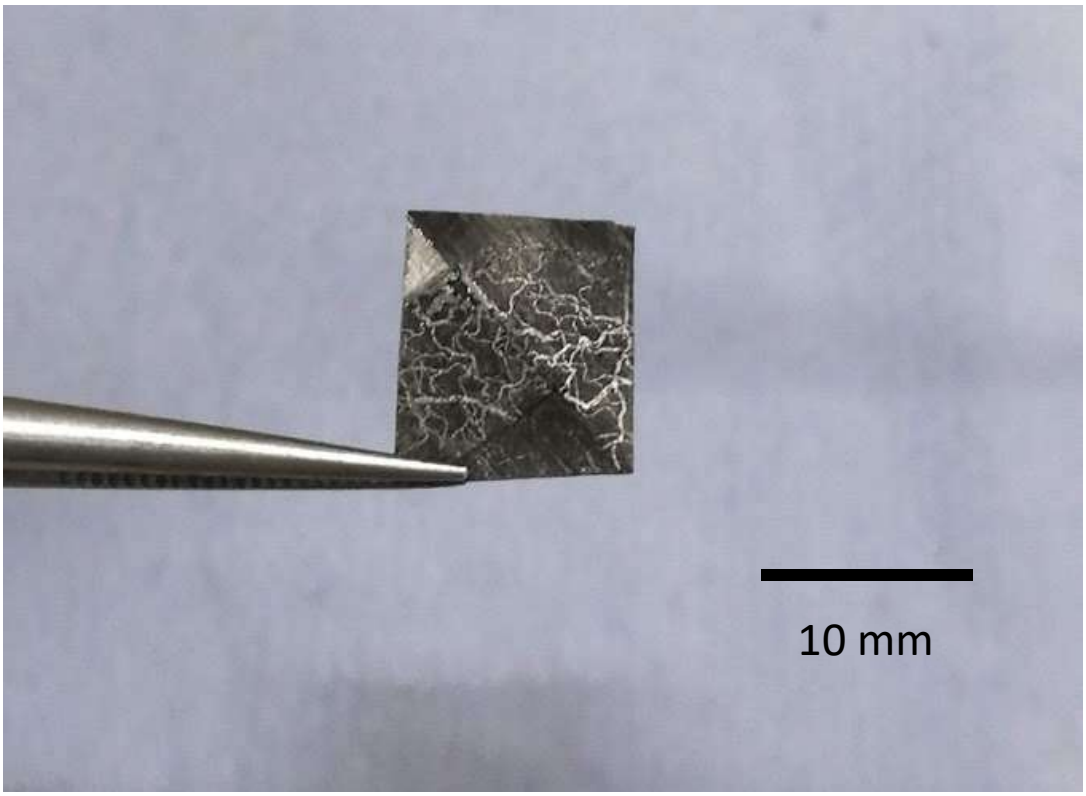

***Figure 34**. Surface of a carbon fibre ply taken from the CFRP after processing with a 0.05 M $MgCl_2$ acetone / water solvent at 290˚C for 10 min.*

Although the mass transfer of the solvent, catalyst or degradation products may influence the rate of decomposition, the results presented in Section 4.3 and the images in Figure 32 to Figure 34 suggest that the overall degradation process is reaction rate limited. Despite the fact that the solvent quickly reaches the centre of the composite within 30 min, it takes a further 90 and 60 min for the neat solvent and 0.05 M $MgCl_2$ solution respectively to achieve an *RD* of more than 90 wt.%. In addition to this, a study into the effect of scaling up the process (described in [297]) used larger samples of the same material measuring from (50 x 50) to (50 x 80) mm^2. If the rate of degradation was primarily dependent on the mass transfer

stages, the longer diffusion pathways of the larger samples would lead to an increase in the process time necessary to effectively solubilise the resin. However, the experiments conducted with these larger samples found that near-complete decomposition was observed in the same reaction time at 320˚C thereby suggesting that the process is reaction rate limited rather than controlled by any of the mass transfer stages.

4.5 First Order Rate Equation

The relationship between resin decomposition and process time has been previously investigated through the application of rate equations of the form shown in Equation (11) [242], [245]. However, these works considered either propan-1-ol [242] or water [245] as the solvent and, therefore, the kinetics of the degradation reaction with an acetone / water solvent remain poorly understood. By inspection of Equation (1) to Equation (4) described in Section 2.8.3, Equation (11) can be developed which states that the rate, $-r_A$, is proportional to the extent of conversion, α, raised to the power of the order of reaction, n. Through analysis of the degradation data presented in Chapter 3, it is possible to determine the value of n and the rate constant, k, at each of the temperatures investigated.

$$-r_A = \frac{d\alpha}{dt} = k[\alpha]^n \qquad (11)$$

Where α = is the extent of conversion (dimensionless), t = time (min), k = rate constant (min^{-1}) and n = reaction order (dimensionless).

As the decomposition reaction proceeds and the resin is solubilised, the reaction rate appears to slow down. The rate equation describing the kinetics of the reaction is, therefore, governed by the quantity of resin remaining. However, Figure 31 demonstrates that increasing the reactor loading had little to no effect on the decomposition of the resin. As the solvent always appears to be in excess, it seems that the rate is not proportional to the concentration of the resin in the reactor nor the concentration of the degradation products dissolved in the solvent. Alternatively, the extent of conversion (α, introduced in Chapter 2) can be defined as the proportion of resin remaining within the composite. This is equivalent to a mass fraction, M, and is defined by Equation (12). The reaction rate can, therefore, be modelled by Equation (13).

$$M = \frac{m(t_R)}{m_i} = 1 - RD \tag{12}$$

$$-r_A = \frac{dM}{dt} = -k_{A,R}\, M^n \tag{13}$$

Where $m(t_R)$ is the mass of resin remaining within the composite (g) after reaction time, t_R (min), m_i is the initial mass of resin (g) and $k_{A,R}$ is the rate constant during the reaction phase (min^{-1}). Although it has been previously suggested that n = 2 for a supercritical water solvent [245] and n = 1.5 when using propan-1-ol as the

solvent [242], it is not currently known what the reaction order is for this particular system. The GRG non-linear "Solver" function in MS Excel was used to find values for $k_{A,R}$ and n which minimised the error between experimental and model values for M. However, across all temperatures and catalyst systems, there were large variations in the optimum values for n of between 1 and 10. This led to no correlation between $k_{A,R}$ and temperature and any change in n was accounted for by a change in $k_{A,R}$: a major limitation of 2-parameter models such as that described by Equation (13). For this reason, a suitable value of n was determined through integrating Equation (13), as shown by Equation (14). The result of this is given by Equation (15). As this is of the form $y = mx + c$, a plot of $\frac{M^{1-n}}{1-n}$ vs. t should give a straight line with a gradient equivalent to the rate constant, $k_{A,R}$.

$$\int \frac{dM}{M^n} = -k_{A,R} \int dt \tag{14}$$

$$\frac{M^{1-n}}{1-n} = -k_{A,R}\, t + c \tag{15}$$

Based on the values from literature [242], [245], initial values for n of 2 and 1.5 were chosen. However, there was not a good correlation with the data obtained especially at higher temperatures; for n = 2 and n = 1.5 the R^2 value at 360˚C was 0.70 and 0.83 respectively. It was apparent that reducing the reaction order led to a closer fit between the data points and a linear regression line. For the case n = 1, integrating Equation (13) gives Equation (16). A plot of ln(M) vs. t_R

as shown in Figure 35 to Figure 38 demonstrates a strong linear relationship with good R^2 values in the range of 0.95 to 0.99 for the neat acetone / water solvent across the temperatures 300 to 360˚C. For the $ZnCl_2$ and $AlCl_3$ systems, values for R^2 are even higher and are in the range of 0.98 to 0.99 for all temperatures. For $MgCl_2$ at 270 and 280˚C, R^2-values are similar, however at 290 and 300˚C, this is reduced to 0.93 and 0.92 respectively, possibly due to the trend line being skewed by the data points at 290˚C, 90 min and 300˚C, 30 min. At these conditions, the resin is almost fully decomposed (M = 0.01 and M = 0.06 respectively) and, for this reason, the plotted values of ln(*M*) are more sensitive to any experimental error. It is also possible that the reaction rate is influenced by the concentration of the catalyst, however, in order to directly compare the different solvent systems, it was assumed that the decomposition rate is proportional to *M* only. Values for $k_{A,R}$ were taken as the gradient of each of the regression lines shown in Figure 35 to Figure 38 and are tabulated in Table 16 along with the R^2 values for each data set.

$$\ln(M) = -k_{A,R}t_R + c \qquad (16)$$

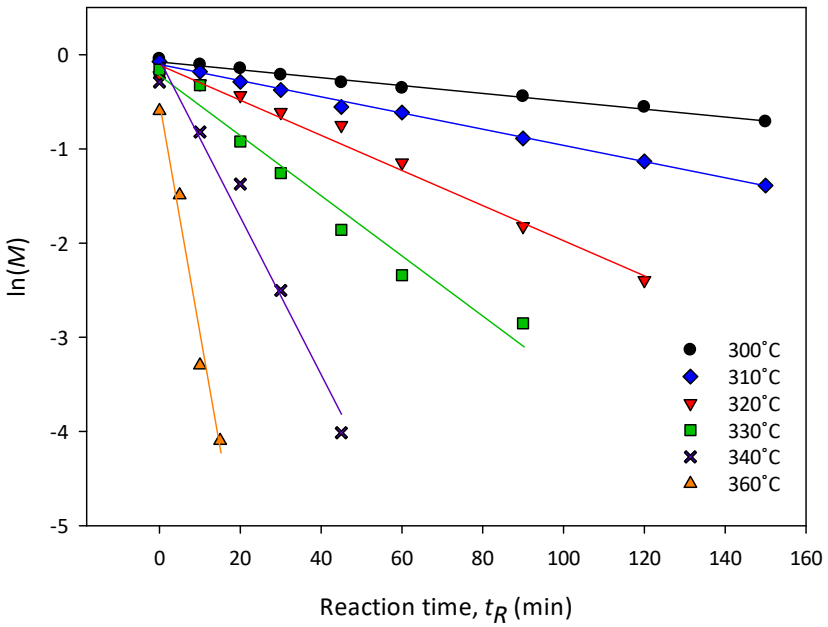

***Figure 35**. Plot of ln(M) vs. t_R for the neat acetone / water solvent in the temperature range 300 to 360˚C.*

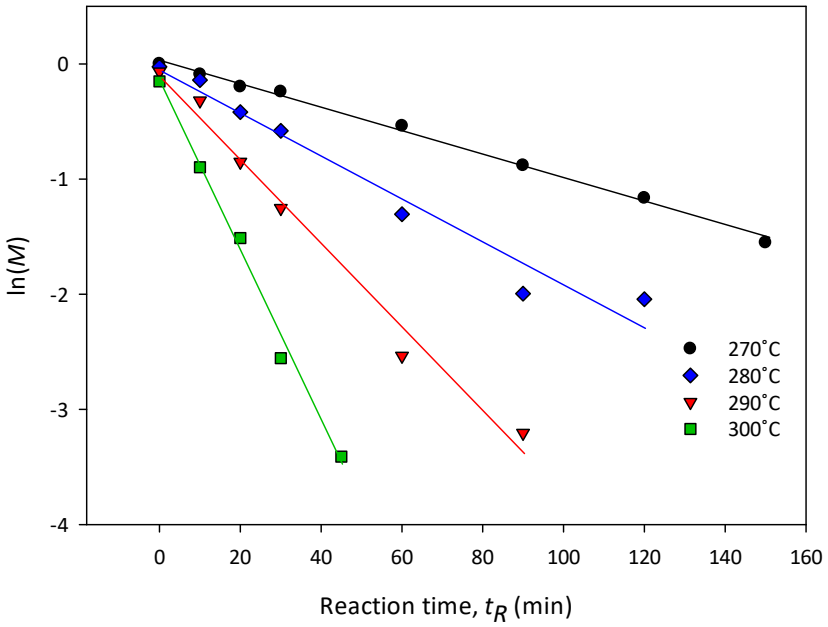

***Figure 36**. Plot of ln(M) vs. t_R for the 0.05 M $ZnCl_2$ acetone / water solvent system in the temperature range 270 to 300˚C.*

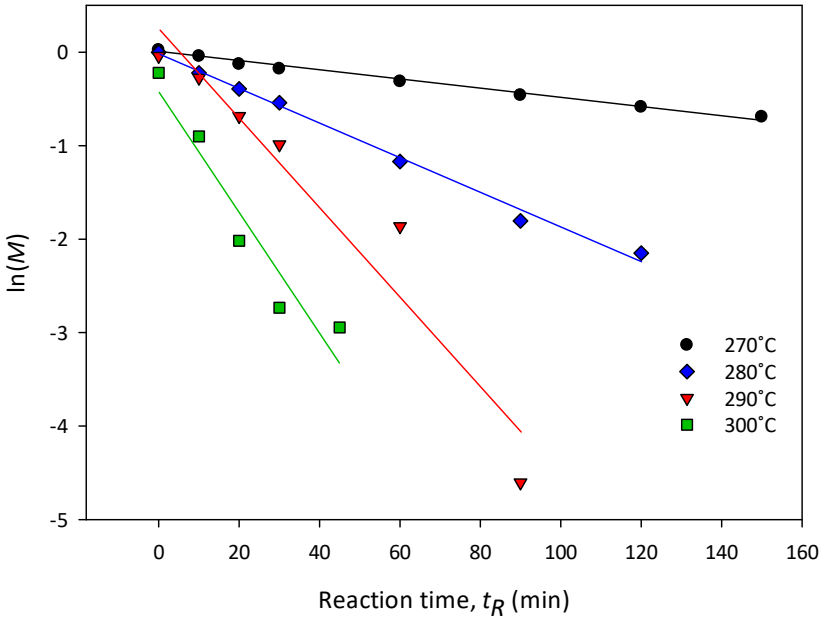

Figure 37. *Plot of ln(M) vs. t_R for the 0.05 M $MgCl_2$ acetone / water solvent system in the temperature range 270 to 300˚C.*

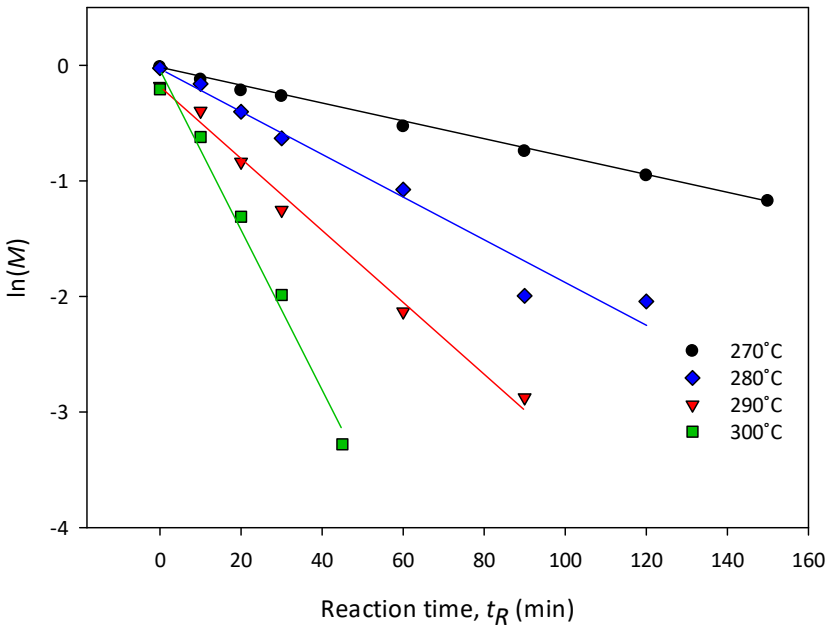

Figure 38. *Plot of ln(M) vs. t_R for the 0.005 M $AlCl_3$ acetone / water solvent system in the temperature range 270 to 300˚C.*

For all temperatures and solvent systems investigated, it was observed that there was some mass loss upon reaching the lowest process temperature considered (i.e. at t_R = 0 min). It is, therefore, apparent that the decomposition reaction begins at some temperature below 300˚C and 270˚C for the neat acetone / water solvent and metal chloride systems respectively. To account for this, the degradation of the composite can be modelled during the heating and reaction phases separately. An expression for the latter phase was derived by integrating Equation (13) with n = 1 between the limits of $M = M_H$ at t = 0 and $M = M_R$ at t = t_R. The result of this is given by Equation (17) where M_H and M_R are the mass fractions of resin remaining after the heating and reaction phases respectively. Rearranging Equation (17) to Equation (18) allows an expression for M_R to be obtained.

$$\ln\left(\frac{M_R}{M_H}\right) = -k_{A,R}t_R \tag{17}$$

$$M_R = M_H e^{-k_{A,R}t_R} \tag{18}$$

As M_H is currently unknown, an expression for this variable was developed by assuming that the decomposition reaction is also first order during the heating phase. Integrating Equation (13) with $k = k_{A,H}$ where $k_{A,H}$ is the Arrhenius rate constant during the heating phase and the limits M = 1 at t = 0 min and $M = M_H$ at

$t = t_H$ gives Equation (19). Rearranging this to Equation (20) allows values for $k_{A,H}$ to be calculated from the experimental data. These are also provided in Table 14.

$$\ln(M_H) = -k_{A,H} t_H \tag{19}$$

$$k_{A,H} = -\frac{\ln(M_H)}{t_H} \tag{20}$$

Alternatively, Equation (19) can be expressed as Equation (21) which can then be substituted into Equation (18) to model the total mass fraction of resin remaining within the composite after each reaction has taken place. This substitution and the expression used to model *RD* is shown by Equations (22) and (23).

$$M_H = e^{-k_{A,H} t_H} \tag{21}$$

$$M_R = e^{-k_{A,H} t_H - k_{A,R} t_R} \tag{22}$$

$$RD = 1 - e^{-k_{A,H} t_H - k_{A,R} t_R} \tag{23}$$

***Table 14**. Arrhenius rate constants for the heating and reaction phases for all solvent systems investigated. R^2 values demonstrate how close the linear regression lines in Figure 35 to Figure 38 fit the experimental data.*

Catalyst	Temperature, T_R (°C)	R^2	$k_{A,R}$ ($x10^{-3}$ min^{-1})	$k_{A,H}$ ($x10^{-3}$ min^{-1})
None	300	0.992	4.29	0.920
	310	0.994	9.33	1.41
	320	0.988	19.7	4.89
	330	0.986	35.0	5.75
	340	0.954	108	7.91
	360	0.983	333	27.2
0.05 M $ZnCl_2$	270	0.996	10.2	0.570
	280	0.997	22.4	0.885
	290	0.985	36.6	2.33
	300	0.992	74.0	4.70
0.05 M $MgCl_2$	270	0.991	4.71	0.907
	280	0.994	19.9	1.08
	290	0.930	30.8	1.49
	300	0.920	86.5	6.91
0.005 M $AlCl_3$	270	0.998	7.6	0.596
	280	0.983	21.3	0.885
	290	0.992	30.7	6.23
	300	0.986	69	6.45

The results of the model described by Equation (23) are shown by the continuous lines in Figure 39 to Figure 42 for the neat solvent mixture and all metal chloride systems. The model is evaluated in Section 4.8 but upon first inspection, appears to fit the data points well.

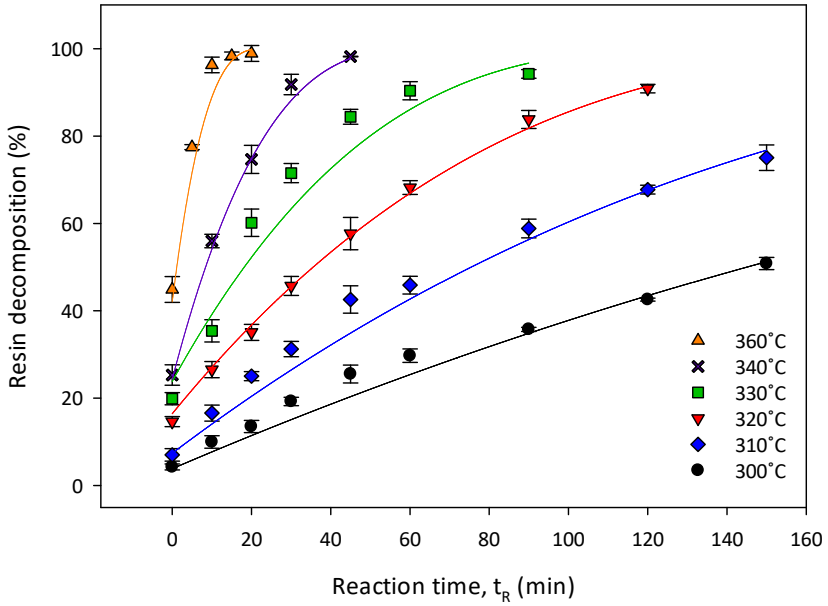

***Figure 39**. Experimental and calculated values for RD achieved with a neat acetone / water solvent system using a first order rate equation (Equation (23)). Continuous lines represent calculated values.*

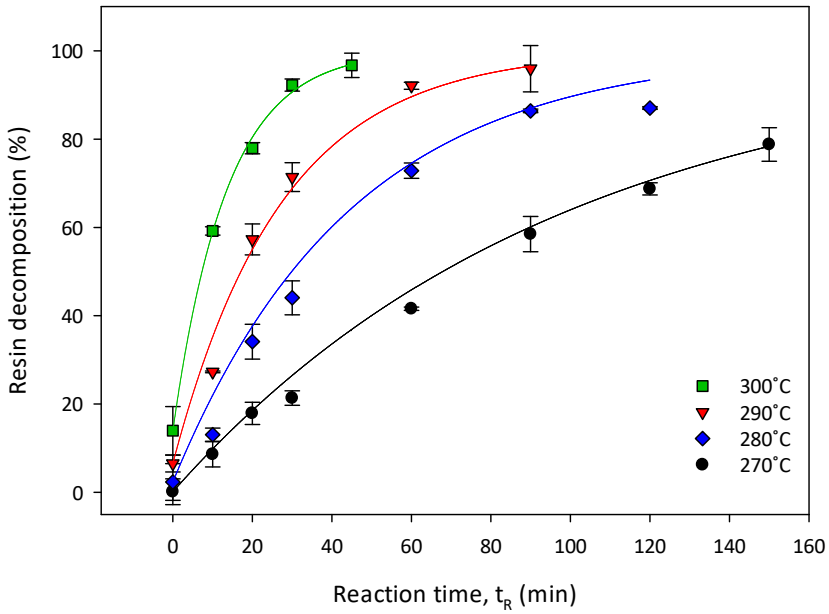

***Figure 40**. Experimental and calculated values for RD achieved with a 0.05 M $ZnCl_2$ solution and acetone / water solvent using a first order rate equation (Equation (23)). Continuous lines represent calculated values.*

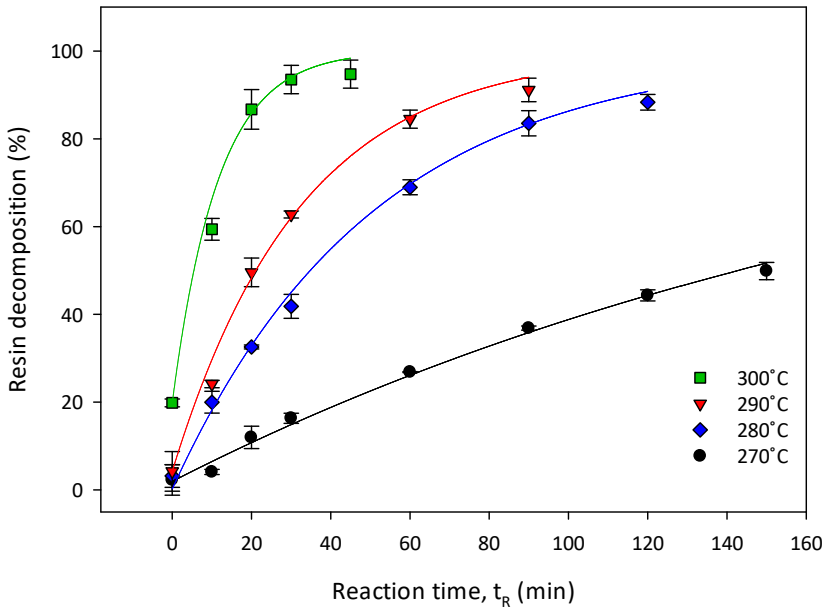

***Figure 41**. Experimental and calculated values for RD achieved with a 0.05 M $MgCl_2$ solution and acetone / water solvent using a first order rate equation (Equation (23)). Continuous lines represent calculated values.*

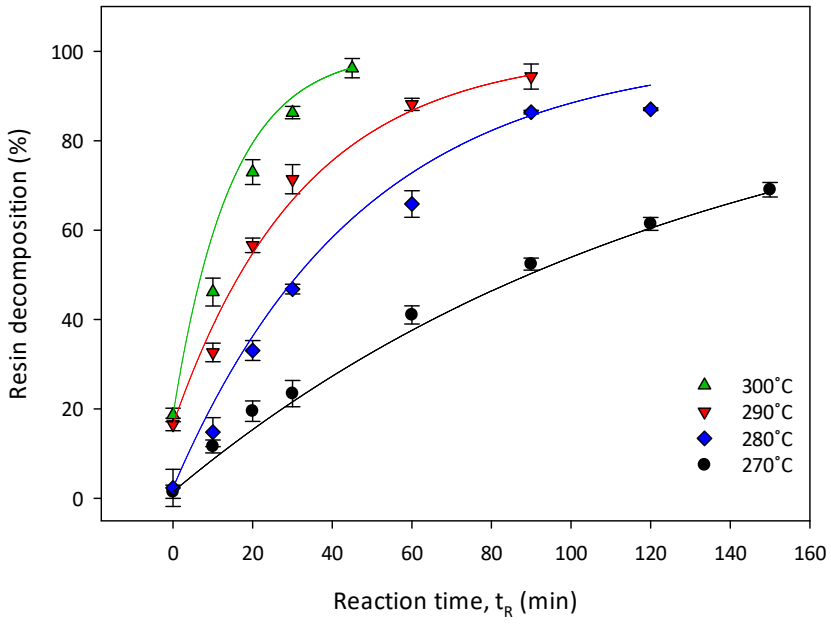

***Figure 42**. Experimental and calculated values for RD achieved with a 0.005 M $AlCl_3$ solution and acetone / water solvent using a first order rate equation (Equation (23)). Continuous lines represent calculated values.*

The Arrhenius expression (Equation (2), Chapter 2)) can also be used to calculate a value for rate constants at other process temperatures in order to model the decomposition reaction under alternative conditions. However, as there is some degradation of the resin before the target temperature is reached, Equation (23) also relies on a rate constant during the heating phase. As reaction rate constants are a function of temperature, $k_{A,H}$ can be considered an average between the process temperature and a theoretical initiation temperature, T_i, at which the reaction begins. $k_{A,H}$ can, therefore, be used to find the value of this average temperature, T_{Av}, using Equation (24). It was assumed that T_{Av} is the midpoint between the reaction temperature, T_R, and T_i and thus T_i can be determined with Equation (25).

$$k = k_0 e^{\frac{E_A}{RT}} \tag{2}$$

$$T_{Av} = -\frac{E_A}{R \ln\left(\frac{k_{A,H}}{k_0}\right)} \tag{24}$$

$$T_i = 2T_{Av} - T_R \tag{25}$$

The Arrhenius parameters activation energy, E_A (J mol^{-1}), and frequency factor, k_0 (min^{-1}), are evaluated in Section 4.7. The average values for T_i across the temperature ranges considered for each solvent system are provided in Table 15. Using this value of T_i, it is possible to calculate T_{Av} for any process temperature and subsequently $k_{A,H}$, in order to model the decomposition during the heating phase.

In the absence of a catalyst, the reaction does not appear to initiate until 273˚C, however, the inclusion of metal chlorides reduces this theoretical temperature by as much as 96˚C. As noted in Chapter 3, there appears to be a stronger temperature dependence on *RD* for the $MgCl_2$ catalysed reaction and a similar result is shown here: amongst all the weak-Lewis acids, this system has the highest calculated initiation temperature of between 198 and 234˚C. These temperatures approximately correspond with the T_g of the CFRP of 221 ± 3˚C. Earlier work in this field has suggested that the T_g of a polymer is the minimum temperature necessary to fully decompose it. Below this temperature, the polymer chains are not sufficiently mobile to allow the solvent and / or catalyst molecules to penetrate the matrix and subsequently solubilise the resin [239].

***Table 15**. Average values for the initiation temperature, T_i, calculated using Equations (24) and (25).*

Catalyst	Initiation Temperature (˚C)
None	273 ± 11
0.05 M $ZnCl_2$	201 ± 13
0.05 M $MgCl_2$	216 ± 18
0.005 M $AlCl_3$	211 ± 10

4.6 Shrinking Core Model (SCM)

In addition to fitting a first order rate equation to the degradation data obtained, a kinetic model can also be developed by applying an SCM. This has been used previously to model the degradation of an epoxy resin with pure acetone

[264] using similar process conditions to those described in this work. This model considers a reaction taking place at the surface of a particle and, as time progresses, the reactants permeate into the particle leaving behind a product, or "ash" layer. These products are then able to migrate away from the unreacted core and into the bulk solution, subsequently reducing the size of the particle causing to shrink until it disappears. This process is described in detail by Levenspiel (1999) [263] and is illustrated by Figure 43.

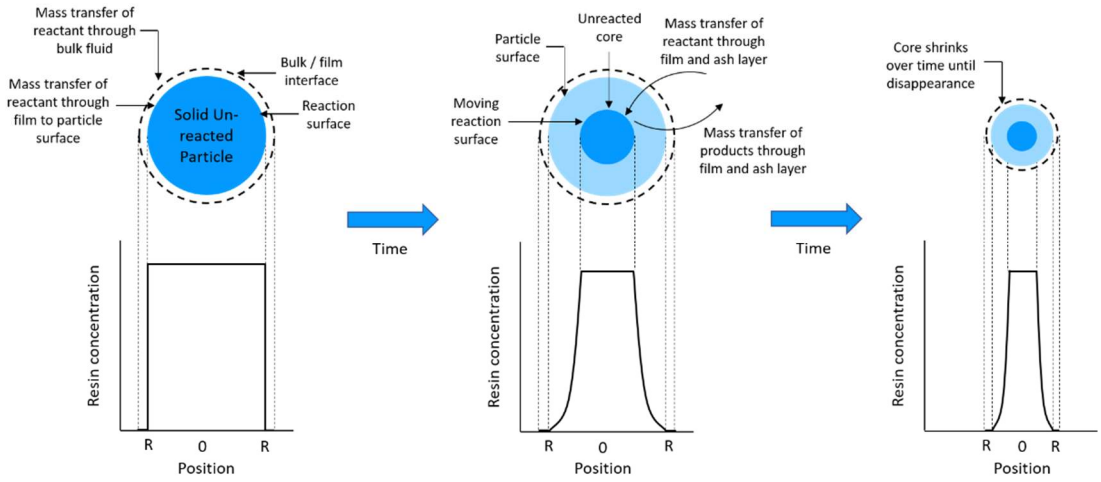

***Figure 43**. Diagram of a shrinking core model (adapted from* [263]*).*

By considering whether it is the diffusion of the solvent through the bulk fluid or film around the particle, the diffusion of the dissolved products away from the particle surface or the chemical reaction that is the rate determining step, a range of rate equations can be derived for various geometries. Although the results presented in Section 4.3 suggest that the solvent is always in excess and

Figure 32 and Figure 34 show good mass transfer of the reactants, it is not yet certain which of these stages controls the rate of the degradation process. The model also relies on the geometry of the particle and it is not immediately obvious which one, of three possible geometries, can be best applied to these CFRP samples. Firstly, as it is made up of 20 plies of carbon fibre, these samples could be thought of as a flat plate with the reaction taking place on the surface of each ply. Alternatively, by considering the resin surrounding each fibre, it could be that a cylindrical geometry is most suitable. Finally, by studying the XRCT images in Figure 32 and Figure 33, it appears that there is a large, approximately spherical, volume of resin remaining at the centre of the composite. The model which most closely agrees with the experimental values of *RD* for each set of conditions is that of a reaction rate limited SCM for a spherical particle. This equation is first introduced in Section 2.8.3 (Equation (5)) and may be described by the expression given in Equation (26) [263]. Note that this is only valid for $k_{SCM}t \leq 1$: as t approaches infinity, so will *RD* yet this variable is limited to a maximum of 1, which is equivalent to 100% decomposition of the matrix.

$$1 - (1 - RD)^{\frac{1}{3}} = k_{SCM}t \tag{26}$$

As stated in Section 4.5, the decomposition reaction begins at some temperature below the minimum process conditions investigated for each solvent system. For this reason, it is necessary to include a heating time, t_H, as shown by

Equation (27). As this is in a linear form, a plot of $1-(1-RD)^{\frac{1}{3}}$ vs. $(t_H + t_R)$ will give a straight line as illustrated by Figure 44 to Figure 47. Values for k_{SCM} were taken as the gradient of the linear regression line and are shown along with the corresponding R^2 value for each solvent system in Table 16. This rate constant is also temperature dependant and will, therefore, be an average over the heating and reaction phases. However, as the maximum *RD* observed at t_R = 0 min is < 25 wt.% for all conditions except at 360˚C, it will be dominated by the reaction phase.

$$1-(1-RD)^{\frac{1}{3}} = k_{SCM}(t_H + t_R) \tag{27}$$

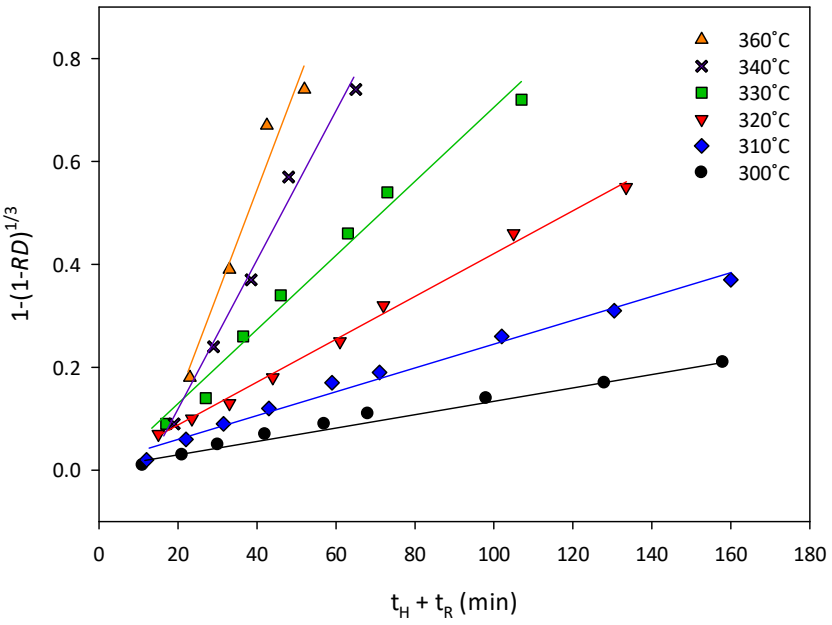

***Figure 44**. Plot of 1-(1-RD)$^{1/3}$ vs. (t_H + t_R) for the neat acetone / water solvent in the temperature range 300 to 360˚C.*

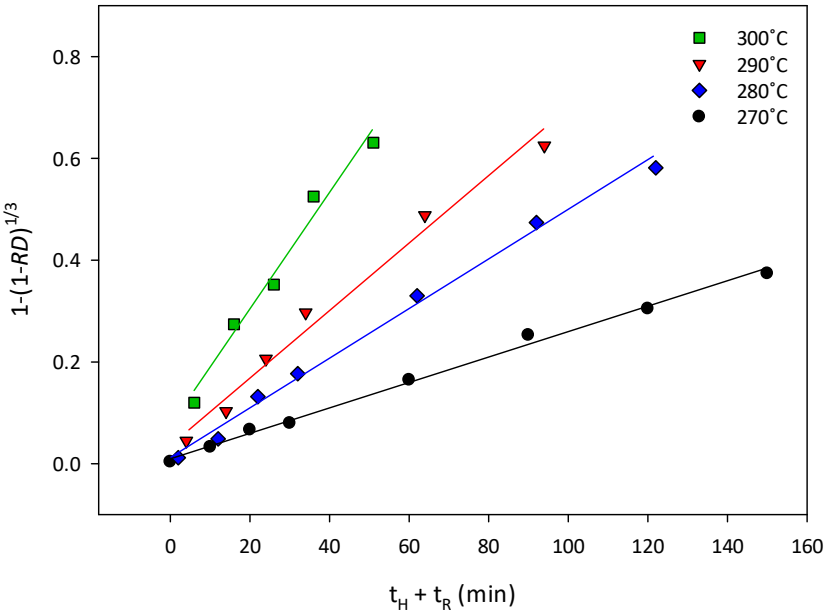

***Figure 45**. Plot of 1-(1-RD)$^{1/3}$ vs. $t_H + t_R$ for 0.05 M $ZnCl_2$ acetone / water solvent in the temperature range 270 to 300˚C.*

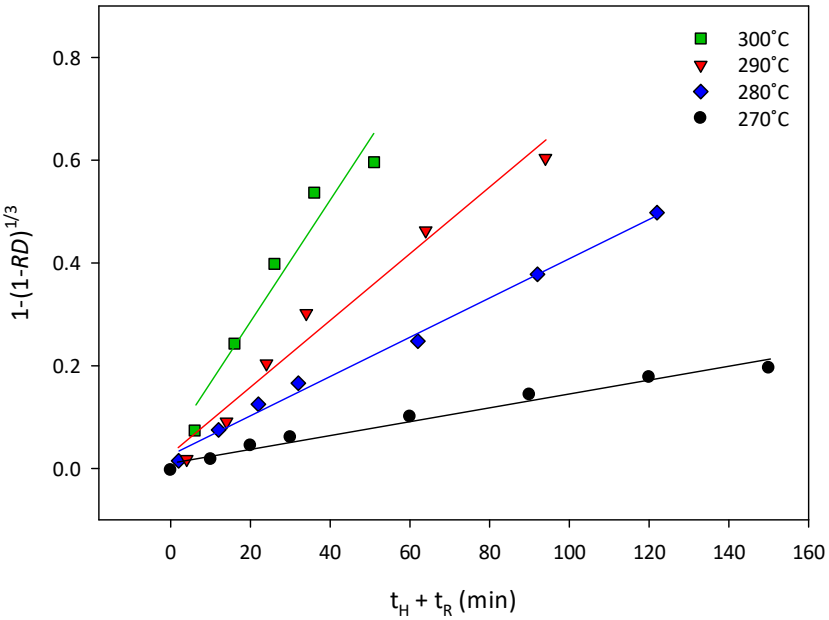

***Figure 46**. Plot of 1-(1-RD)$^{1/3}$ vs. $t_H + t_R$ for 0.05 M $MgCl_2$ acetone / water solvent in the temperature range 270 to 300˚C.*

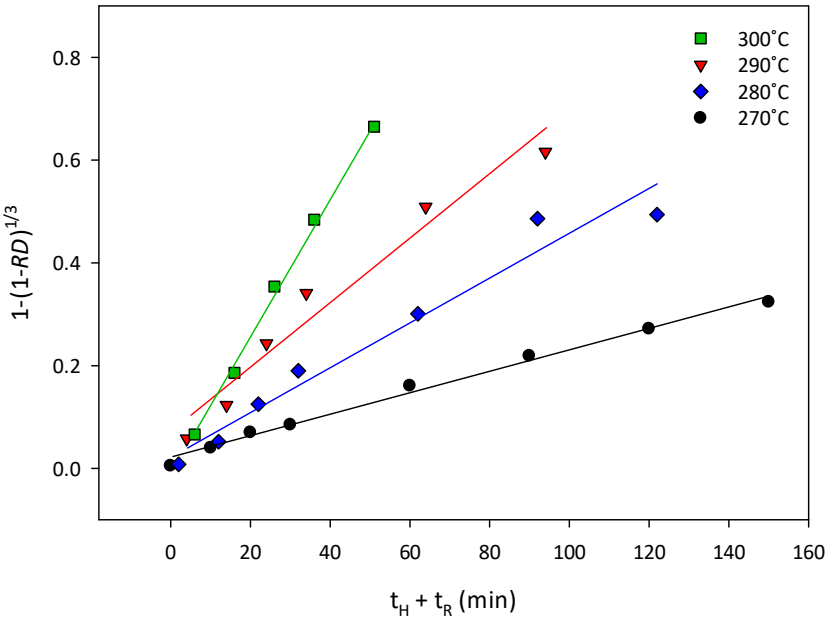

***Figure 47**. Plot of 1-(1-RD)$^{1/3}$ vs. $t_H + t_R$ for 0.005 M $AlCl_3$ acetone / water solvent in the temperature range 270 to 300˚C.*

***Table 16**. R^2 and k_{SCM} values for all solvent systems and temperatures investigated.*

Catalyst	Temperature, T_R (°C)	R^2	k_{SCM} ($x10^{-3}$ min^{-1})
None	300	0.984	1.23
	310	0.987	2.27
	320	0.991	4.17
	330	0.960	6.58
	340	0.991	14.0
	360	0.992	35.3
0.05 M $ZnCl_2$	270	0.998	2.48
	280	0.995	5.19
	290	0.988	8.78
	300	0.998	16.9
0.05 M $MgCl_2$	270	0.986	1.48
	280	0.975	5.28
	290	0.985	7.57
	300	0.99	20.4
0.005 M $AlCl_3$	270	0.992	2.09
	280	0.992	5.19
	290	0.975	7.67
	300	0.997	17.5

Once k_{SCM} is known, Equation (27) can be rearranged to Equation (28). This can then be used to predict *RD* at each of the temperatures investigated as shown by the continuous lines in Figure 48 to Figure 51. Upon an initial inspection, the SCM appears to provide a good fit to the experimental data, however, the

accuracy of this model is also evaluated alongside that of the first order rate equation (Equation (23)) in Section 4.8.

$$RD = 1 - \left(1 - k_{SCM}(t_H + t_R)\right)^3 \quad (28)$$

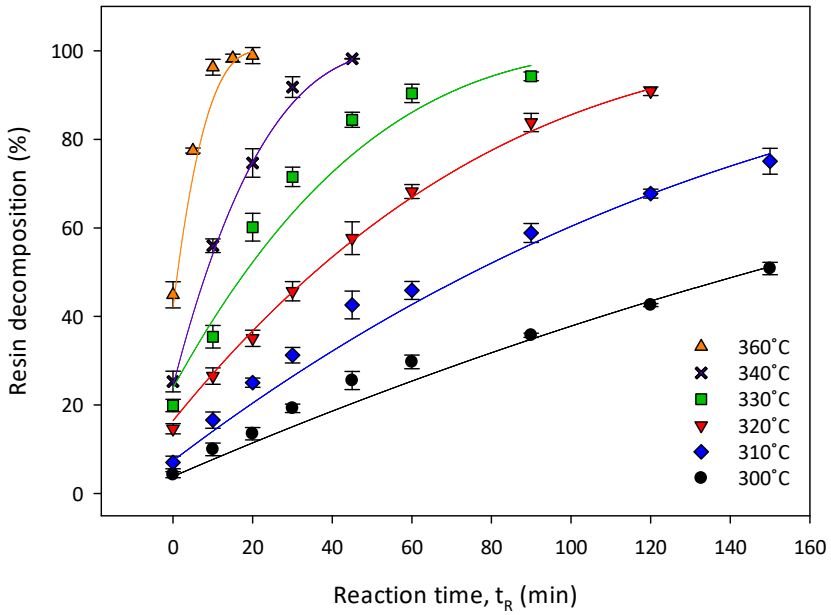

***Figure 48**. Experimental and calculated values for RD achieved with a neat acetone / water solvent system using a shrinking core model (Equation (28)). Continuous lines represent calculated values.*

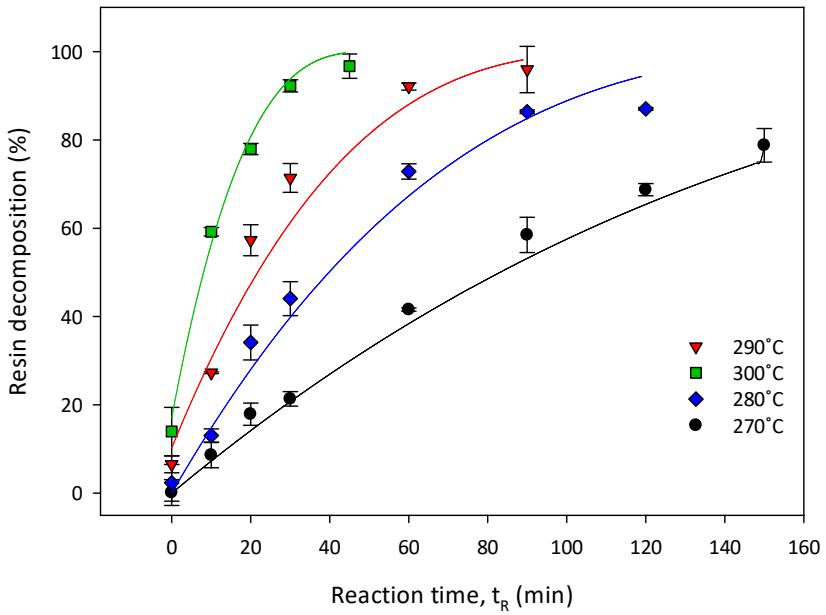

***Figure 49**. Experimental and calculated values for RD achieved with a 0.05 M $ZnCl_2$ solution and acetone / water solvent using a shrinking core model (Equation (28)). Continuous lines represent calculated values.*

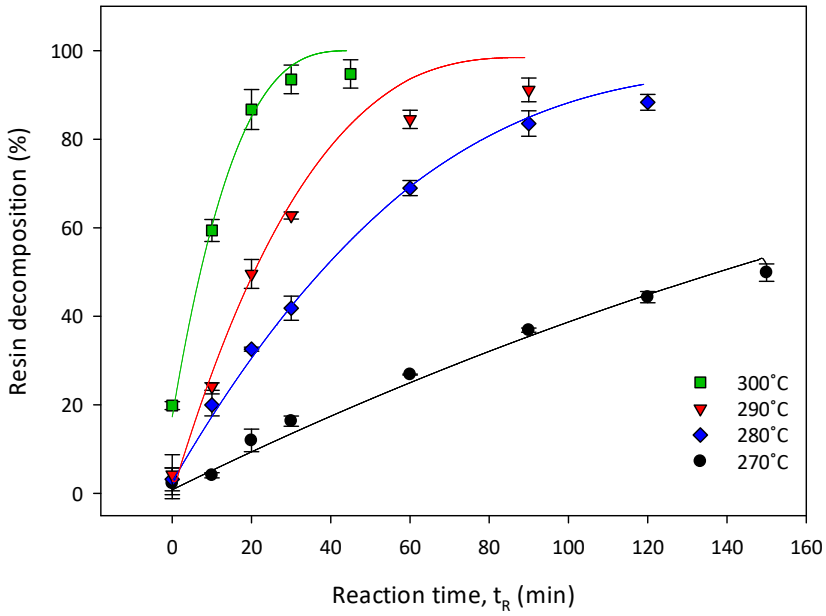

***Figure 50**. Experimental and calculated values for RD achieved with a 0.05 M $MgCl_2$ solution and acetone / water solvent using a shrinking core model (Equation (28)). Continuous lines represent calculated values.*

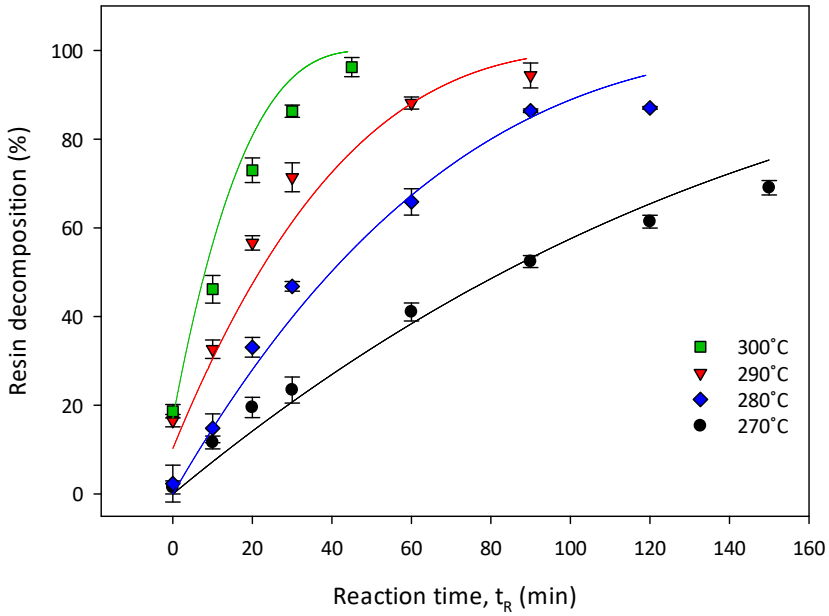

***Figure 51**. Experimental and calculated values for RD achieved with a 0.005 M $AlCl_3$ solution and acetone / water solvent using a shrinking core model (Equation (28)). Continuous lines represent calculated values.*

4.7 Analysis of Reaction Kinetics

Through the application of both a first order rate equation and a shrinking core model, rate constants have been calculated across the temperature range 300 to 360˚C for the neat acetone / water solvent and 270 to 300˚C for the catalytic systems. The relationship between the logarithm of the rate constant and the inverse of temperature is illustrated by the Arrhenius plots shown in Figure 52 and Figure 53. Both figures demonstrate that linear regression lines can be fitted to the data points with good R^2 values in the range of 0.96 to 0.99. The linearised Arrhenius expression is given by Equation (29) and it is, therefore, apparent that the frequency factor, k_0 (min^{-1}), and activation energy, E_A (kJ mol^{-1}), can be determined from the y-intercept and gradient of the regression lines respectively.

The values of each of these parameters for all solvent systems investigated are provided in Table 17.

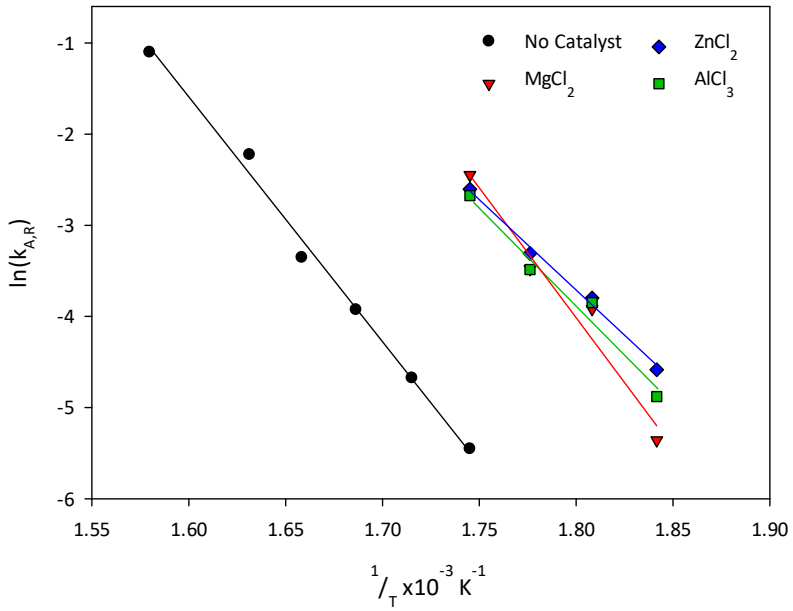

***Figure 52**. Arrhenius plot for rate constants calculated using a 1st order rate equation (Equation (16)). R^2 values are shown in Table 17.*

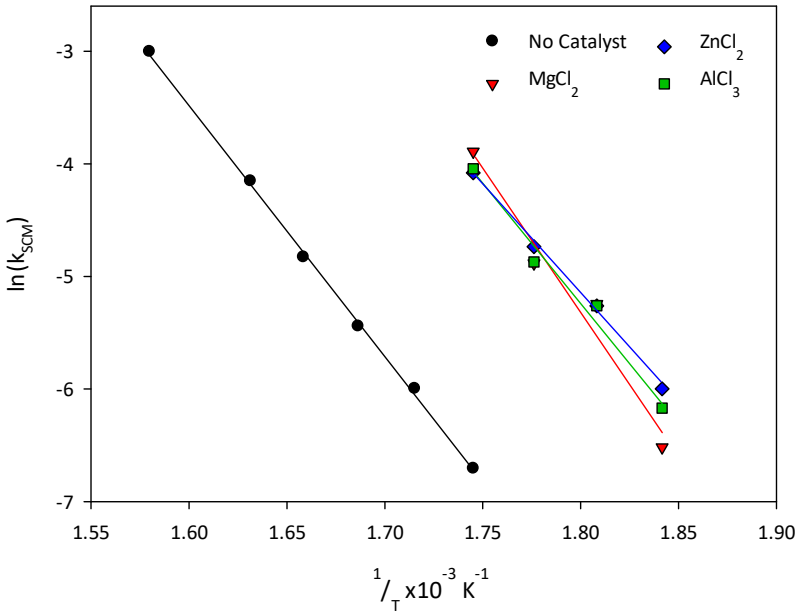

***Figure 53**. Arrhenius plot for rate constants calculated using a shrinking core model (Equation (27)). R^2 values are shown in Table 17.*

$$\ln(k) = -\frac{E_A}{RT} + \ln(k_0) \quad (29)$$

***Table 17**. R^2 values for each of the Arrhenius plots and corresponding activation energy, E_A, and frequency factor, k_0, for each of the solvent systems investigated.*

Catalyst	1st Order Rate Equation			Shrinking Core Model		
	R^2	E_A (kJ mol^{-1})	k_0 (min^{-1})	R^2	E_A (kJ mol^{-1})	k_0 (min^{-1})
None	0.99	222	7.64×10^{17}	0.99	183	6.69×10^{13}
$ZnCl_2$	0.99	157	1.34×10^{13}	0.99	151	7.87×10^{11}
$MgCl_2$	0.96	250	3.67×10^{21}	0.96	225	7.31×10^{18}
$AlCl_3$	0.97	180	2.02×10^{15}	0.98	175	1.57×10^{14}

E_A was verified by re-parameterising Equation (29) to Equation (30) and calculating a rate constant at 300˚C. This isothermal rate constant, along with the decomposition data, was used to estimate E_A using the "Solver" function in MS Excel and minimising the sum of the error squared between the calculated values of k and those obtained graphically. In all cases, E_A obtained using the "Solver" function was within 14% of that determined from the Arrhenius plots and it is this latter value which is considered in the following analysis.

$$k_{A,R} = k_0 e^{\left(\frac{E_A}{RT_0}\left(1-\frac{T_0}{T}\right)\right)} \quad (30)$$

E_A lies within the range of 157 to 250 kJ mol^{-1} for the first order rate equation and 151 to 225 kJ mol^{-1} when using values for k_{SCM}. Previous work in this field has calculated E_A to be 95.6 kJ mol^{-1} when applying a rate equation with a reaction order of 1.5 [242] and 118 kJ mol^{-1} when using an SCM [264]. Although the values determined as part of this research are up to 2.3 and 1.6 times larger for the conventional rate equation and SCM respectively, these differences are likely to be attributable to the different polymer and solvent systems used.

Within this work, two different approaches have been used to calculate the Arrhenius parameters in Table 17 from the same data sets. This allows the values for E_A calculated using the different methods to be directly compared for the first time in the open literature. Although E_A determined from the SCM is consistently lower than that calculated with the first order rate equation, the results demonstrate that there is generally close agreement between the two techniques: the largest difference is just 17% and occurs with the neat acetone / water solvent. This is reduced to a difference of 10% for the 0.05 M $MgCl_2$ system and is less than 4% when $ZnCl_2$ and $AlCl_3$ are used as the catalysts.

The change in EA relative to the neat solvent system due to the inclusion of the catalysts are shown in Table 18. It is apparent that the inclusion of 0.05 M $ZnCl_2$ and 0.005 M $AlCl_3$ act to reduce both E_A and k_0 compared to the neat solvent mixture. E_A decreases by 17 to 29% for the 0.05 M $ZnCl_2$ system and by 4 to 19%

when $AlCl_3$ is supplied at a concentration of 0.005 M. Although a 0.05 M $MgCl_2$ solution facilitated the recovery of clean fibres at lower temperatures and in shorter reaction times than the use of the neat acetone / water solvent, an increase in E_A of 13 to 23% was observed. As noted in Chapter 3, there is a strong temperature dependence of this catalyst on *RD* which results in a steeper gradient of the Arrhenius plot and subsequently a higher value of E_A.

The significant variation in E_A and k_0 between different solvent systems is indicative that the use of catalysts results in changing the preferred reaction pathways for the degradation reaction. Although the preferred oxidation state of zinc is +2, it may also exist as Zn^{2-} and Zn^{+} whereas Mg will only form Mg^{2+} ions. Similar to zinc, aluminium can also have multiple oxidation states of Al^{+}, Al^{2+} and Al^{3+} [298]. The ability of Al^{3+}, Al^{2+} and Zn^{2+} to gain a single electron may facilitate different reactions to those occurring with the $MgCl_2$ catalyst. This may, therefore, explain why both Arrhenius parameters are similar in the $ZnCl_2$ and $AlCl_3$ systems, yet significantly different to the $MgCl_2$ catalysed reaction.

***Table 18**. % change in E_A for the catalysed systems compared to the neat acetone / water solvent mixture for both the first order rate equation and SCM.*

Catalyst	1st Order Rate Equation (Equation (23))	SCM (Equation (27))
$ZnCl_2$	-29%	-17%
$MgCl_2$	+13%	+23%
$AlCl_3$	-19%	-4%

4.8 Model Evaluation

Although both a first order rate equation and an SCM have been fitted to the experimental data, it is useful to evaluate the accuracy of both of these approaches. The residual (the difference between the calculated and experimental *RD* values) can be plotted against the measured *RD* as shown in Figure 54 to Figure 57. For all solvent systems, the data points are randomly scattered about the x-axis; the lack of a clearly defined curve is indicative that there is no systematic error present and that the standard deviation across each data set is constant.

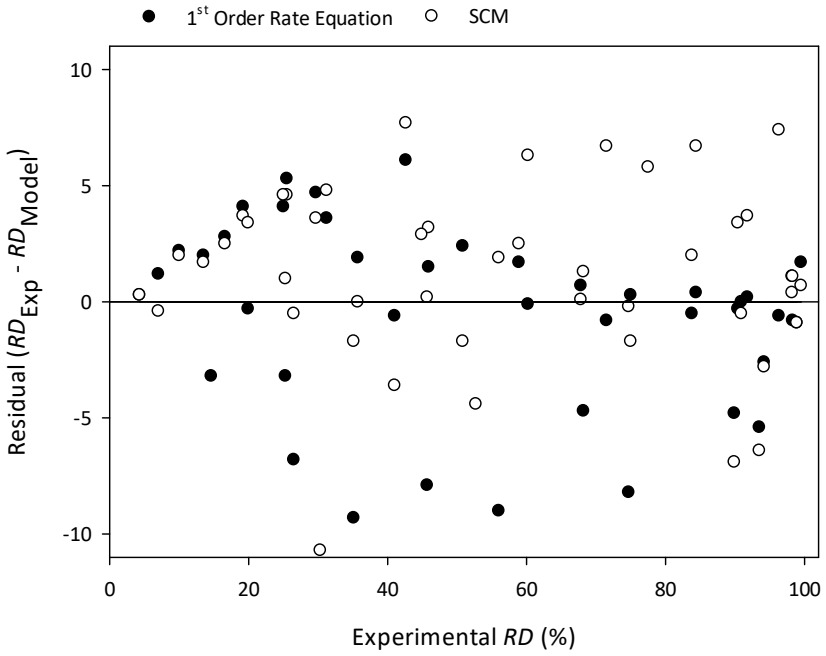

***Figure 54**. Residual plot for the Arrhenius and shrinking core models when using a neat acetone / water solvent system.*

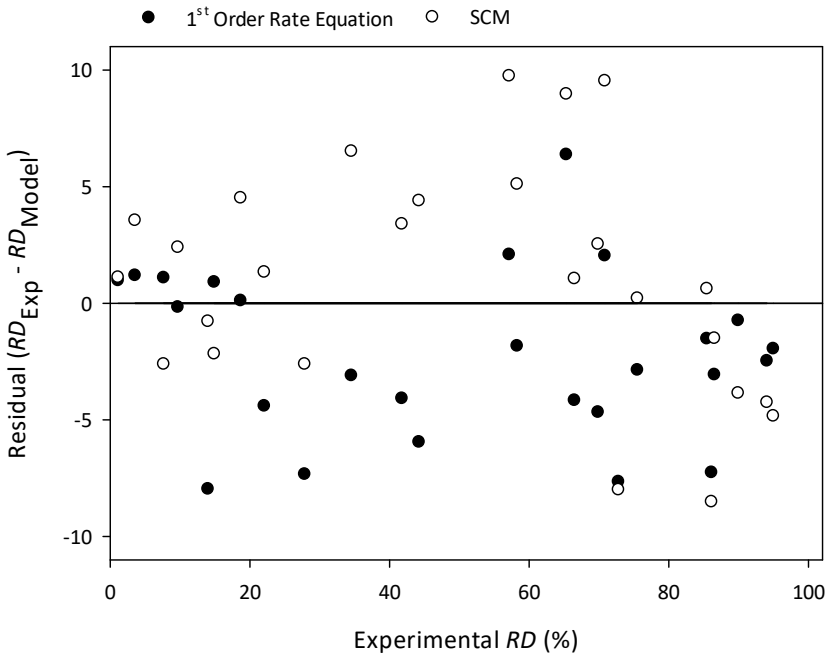

***Figure 55**. Residual plot for the Arrhenius and shrinking core models when using a 0.05 M $ZnCl_2$ and acetone / water solvent system.*

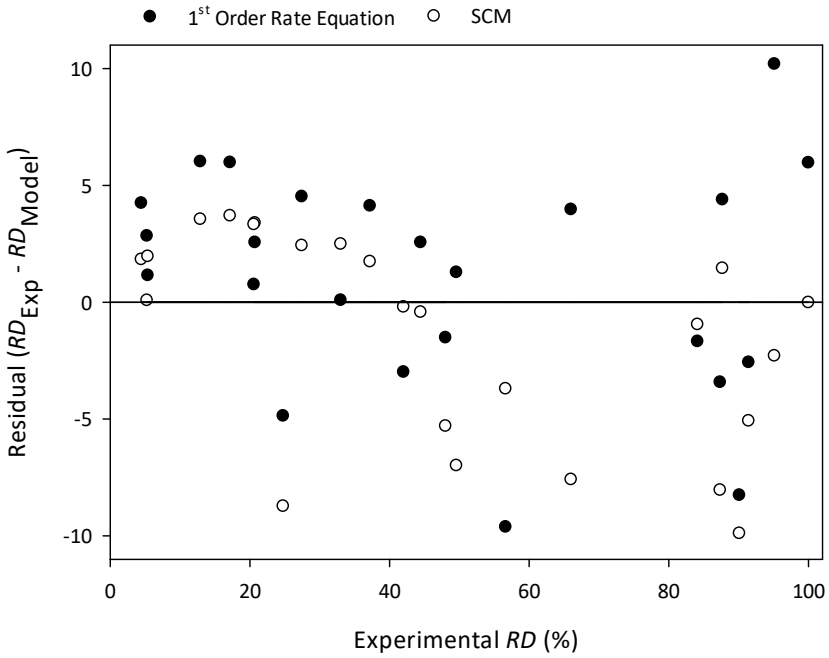

***Figure 56**. Residual plot for the Arrhenius and shrinking core models when using a 0.05 M $MgCl_2$ and acetone / water solvent system.*

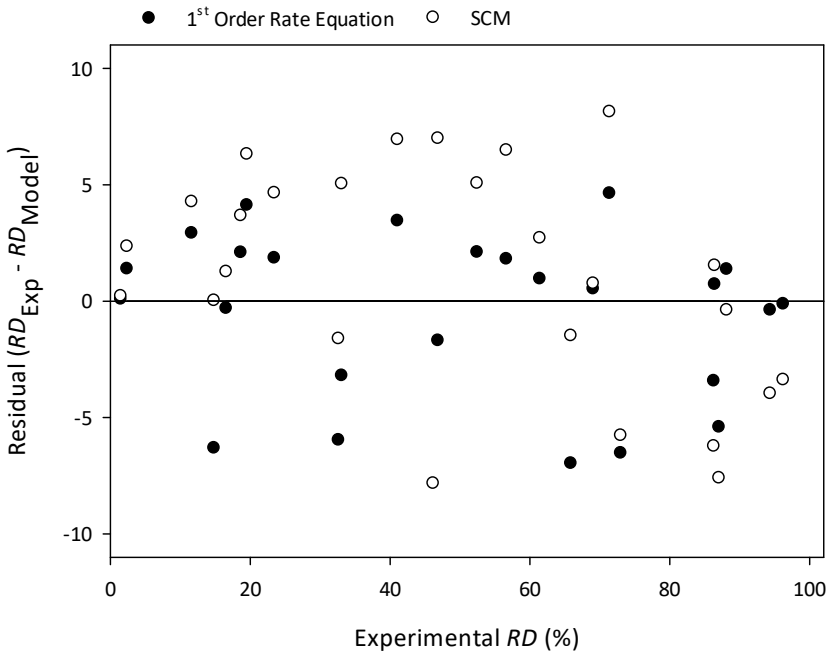

***Figure 57**. Residual plot for the Arrhenius and shrinking core models when using a 0.005 M $AlCl_3$ and acetone / water solvent system.*

Averages of the absolute value of each residual were taken across each temperature and solvent system investigated and are presented along with the standard deviation in Table 19. For both models, the average residuals are generally less than 5% which is similar to the experimental error, thus indicating that both approaches can be used to predict *RD*. For the first order rate equation, the maximum average residual of 5.3% was observed with the neat solvent mixture at a temperature of 320˚C. For the SCM, the maximum average residual is slightly higher; at 300˚C for both $ZnCl_2$ and $AlCl_3$ systems the value is 6.1% suggesting that the first order rate equation is slightly more accurate. For all conditions, the standard deviation is similar to the mean demonstrating the wide distribution of the data. This suggests that, although on average the models are

able to predict *RD* to within ± 5%, the discrepancy between the calculated and measured values may be as large as ± 10% in some cases.

***Table 19**. Values of the average absolute residual of RD and standard deviation across each temperature and solvent system investigated.*

Catalyst	Temperature (°C)	1st Order Rate Equation		SCM	
		Average residual (%)	Standard deviation (%)	Average residual (%)	Standard Deviation (%)
None	300	2.2	1.8	4.0	2.0
	310	1.8	1.6	2.4	1.7
	320	5.3	3.7	1.9	2.5
	330	3.9	5.0	5.3	5.8
	340	2.7	3.5	2.2	2.8
	360	2.3	3.9	0.5	0.6
0.05 M $ZnCl_2$	270	2.3	1.3	3.4	1.8
	280	3.7	2.4	3.6	2.7
	290	2.4	2.1	5.3	3.6
	300	5.0	4.5	6.1	3.1
0.05 M $MgCl_2$	270	3.6	1.7	2.4	1.6
	280	4.3	3.5	4.0	3.5
	290	2.4	1.6	4.2	3.3
	300	4.6	3.6	4.6	3.0
0.005 M $AlCl_3$	270	2.0	1.3	3.4	1.8
	280	3.7	2.4	3.6	2.7
	290	2.4	2.1	5.3	3.6
	300	5.0	4.5	6.1	3.1

In order to determine whether each of the models is likely to under- or overestimate *RD*, Table 20 shows the proportion of the residuals for each catalyst system which are positive (the model underestimates *RD*) and negative (the model overestimates *RD*). Assuming that any errors are random and uniformly distributed, it is expected that 50% of the data points are positive and 50% are negative. This occurs in two instances: in the $AlCl_3$ system modelled by the first order rate equation and when $MgCl_2$ is used as the catalyst and modelled with the SCM. Similar values are observed in the neat acetone / water solvent and for the first order rate equation where 53% of the residuals are positive. However, in all other cases, there is a greater likelihood that the model either under- or overestimates *RD*. The probability of this inaccuracy is greatest when the $ZnCl_2$ system is modelled with a first order rate equation: 69% of the residuals are negative demonstrating a strong tendency to overestimate *RD*. This demonstrates that the error is not uniformly distributed in this case, possibly due to an exaggeration of the Arrhenius parameters. This may be caused by the experimental error associated with long reaction times: the function ln(*M*) in Equation (16) becomes very sensitive as *M* approaches 0. As only 42% of the residuals are negative for the $MgCl_2$ system modelled with this approach, no conclusion can be drawn whether the first order rate equation is more likely to exaggerate or underestimate *RD* when considering the different catalyst systems.

***Table 20**. Proportion of residuals which are positive (model underestimates RD), negative (model overestimates RD) and within ± 5% of the measured value.*

Catalyst	1st Order Rate Equation			Shrinking Core Model		
	% positive	% negative	% within ± 5%	% positive	% negative	% within ± 5%
None	53	47	82	60	40	73
$ZnCl_2$	31	69	81	62	38	77
$MgCl_2$	58	42	77	50	50	77
$AlCl_3$	50	50	77	62	38	69
Average	48	52	79	59	41	74

With the exception of the 0.05 M $MgCl_2$ system, there is a higher proportion of positive residuals when using the SCM which indicates a tendency for this approach to underestimate *RD*. By inspection of Figure 48 to Figure 51 and Figure 54 to Figure 57, it can be seen that for short reaction periods (and therefore small experimental *RD* values) the calculated *RD* is generally lower than that measured experimentally. However, for longer reaction times this model begins to exaggerate the degradation. Equation (27) shows that *RD* is proportional to the cube of t_R and, therefore, small increases in process time will lead to a large change in the predicted decomposition. For this reason, the SCM is also only valid within the reaction times investigated: for $k_{SCM}t_R > 1$, *RD* will rapidly increase above 100%, as mentioned earlier.

Table 20 also shows that across all solvent systems, the first order rate equation predicts *RD* to within ± 5% in 79% of the cases studied. The SCM, however, only predicts *RD* to within the same margin in 74% of the conditions investigated. Analysis of the residuals presented in Table 19 also demonstrates that the first order rate equation is slightly more accurate than the SCM: the average residuals for each method are 3.31 ± 1.99 and 3.80 ± 2.31 respectively. For long reaction times, the first order rate equation will also tend towards 100%, rather than increasing proportionally to the cube of t_R as in the SCM. For these reasons, it appears that the former approach is most suited to modelling the decomposition reaction, however, this is slightly more complex due to the calculation of two rate constants, k_R and k_H.

***Table 21**. Rate constants used in predicting RD at temperatures in the range of 315 to 345˚C (t_R = 30 min) using the neat acetone / water solvent mixture. Values for k_H and k_R were calculated using Equation (2) and the parameters given in Table 17.*

Temperature (˚C)	k_H (x10^{-3} min^{-1})	k_R (x10^{-3} min^{-1})	k_{SCM} (x10^{-3} min^{-1})
315	2.70	14.5	3.71
325	4.08	31.0	6.93
335	6.11	64.7	12.7
345	9.10	131.7	22.8

The models developed in this chapter were further evaluated by conducting additional experiments with the neat acetone / water solvent at 315, 325, 335 and 345˚C. This also assesses the ability of the Arrhenius expression (Equation (2)) to

determine reliable values for k_R and k_{SCM} and whether Equations (24) and (25) can be used to calculate a suitable value for k_H. Values for the rate constants used at each of these temperatures are provided in Table 21. The reaction time, t_R, for all experiments was 30 min and the initiation temperature, T_i, was taken as 273˚C. Under these conditions, the experimental *RD* observed was in the range of 36.3 to 36.4%. The values predicted using both the first order rate equation and SCM are shown alongside the measured *RD* in Figure 58.

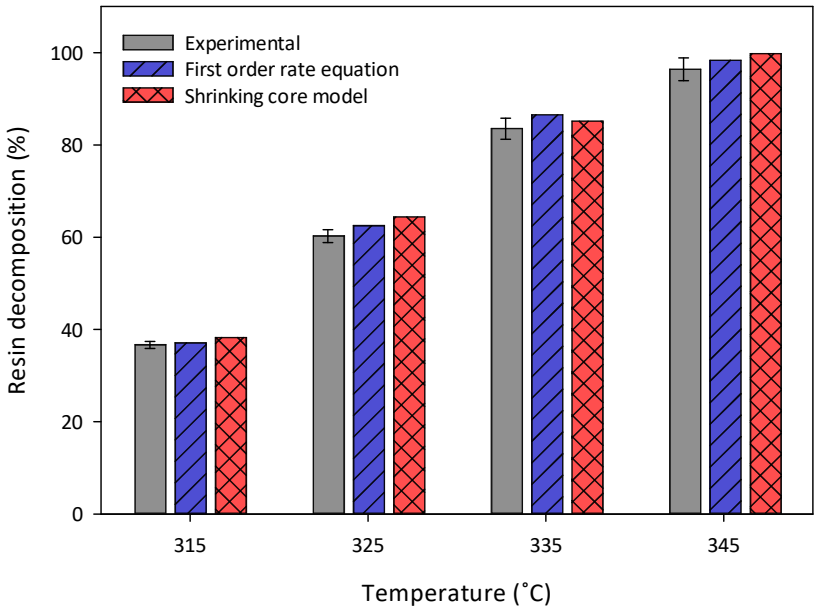

***Figure 58**. Comparison of experimental and calculated RD using the first order rate equation (Equation (23)) and the SCM (Equation (28)) in the temperature range of 315 to 345˚C (t_R = 30 min). Decomposition conducted with neat acetone / water solvent system.*

In all cases, both models overestimate *RD*, however, the difference between the experimental and calculated value is within 5% for all temperatures; similar to the margin of experimental error and the same as the majority of the data points

shown in Figure 54. The average discrepancy between the measured and calculated *RD* for the first order rate equation and SCM is 1.89 ± 1.00% and 2.66 ± 1.47% respectively. The largest discrepancy between the experimental and predicted values of 4.1% also occurs when using the SCM. Although the first order rate equation relies on the use of a theoretical initiation temperature, it appears that this is the most accurate of the two methods when considering alternative temperatures.

4.9 Concluding Remarks

The reaction kinetics of the decomposition of a carbon fibre reinforced epoxy resin have been investigated. Additional experiments were conducted in order to identify the rate determining step and, by increasing the concentration of resin within the reactor, it is apparent that the solvent and metal chlorides are always in excess under the conditions investigated. Imaging partially degraded samples using XRCT also highlighted the existence of randomly orientated diffusion pathways. As the cracks observed are random, it appears that the solvent molecules exploit defects within the polymer rather than moving into the composite in the same direction as the fibres. The solvent penetrates in between the plies of fibre as the pathway through each carbon fibre tow is tortuous. Although samples were imaged after a relatively short reaction time of 30 min, cracks in the resin were visible at the centre of the composite suggesting that the mass transfer of the solvent and catalyst is fast relative to the rate of the reaction.

For the neat acetone / water solvent and $ZnCl_2$, $MgCl_2$ and $AlCl_3$ systems, a first order rate equation was fitted to the decomposition data obtained. Although the inclusion of metal chlorides may alter the reaction mechanism and, therefore, influence the order of reaction, it was still possible to fit a first order equation to each of the catalysts considered which enabled direct comparison to the neat solvent mixture. As the reaction began at some temperature below the minimum conditions investigated, it was necessary to model the decomposition during the heating phase separately to the reaction phase. This was also assumed to be first order and a rate constant over the heating time, k_H, was calculated in order to characterise this stage of the process. This value of k_H was also used to calculate a theoretical initiation temperature, which is necessary when predicting *RD* at alternative reaction temperatures.

In addition to a first order rate equation, a shrinking core model was also fitted to the data. Although multiple expressions can be derived depending on the geometry and rate determining step, the only equation which could be successfully implemented was that for a reaction rate limited spherical particle. To account for the mass loss of the resin during the heating phase, a heating time, t_H, was included in the rate equation. The value of the rate constant in this model, k_{SCM}, is therefore, an average over the heating and reaction phases.

The rate constants calculated were used to draw Arrhenius plots for each solvent system and subsequently calculate the parameters E_A and k_0. For the neat acetone / water mixture, E_A calculated from the first order rate equation and SCM was 222 and 183 kJ mol^{-1} respectively. The inclusion of 0.05 M $ZnCl_2$ and 0.005 M $AlCl_3$ reduced this by up to 29%. 0.05 M $MgCl_2$, however, increased E_A by 13 to 23% due to the strong temperature dependence of this catalyst.

Upon comparing the first order rate equation and SCM to the data obtained, it is apparent that both approaches can be used to model *RD* to within a reasonable degree of accuracy. All calculated values are within ± 10% of the measured degradation and the majority of the data points (79% for the first order rate equation and 74% for the SCM) are within ± 5% which is similar to the margin of experimental error. Both models are also able to predict *RD* at alternative reaction temperatures to a similar accuracy.

Although novel solvent / catalyst systems and the conditions necessary to recover carbon fibres have been identified, it is necessary to evaluate the quality of the recovered fibres. Chapter 5, therefore, aims to characterise the fibres and thereby assess the impact of the process conditions on the surface and mechanical properties.

CHAPTER 5.
FIBRE CHARACTERISATION

5.1 Introduction

As part of the research presented in Chapter 3, a set of eleven process conditions have been identified as capable of decomposing the RTM6 epoxy resin within the CFRP investigated. Previous work, as described in Section 2.8.5, has characterised fibres which have been subjected to similar temperatures, pressures and reaction times, with results demonstrating that the mechanical properties can be retained, although there is usually a loss in the concentration of oxygen at the fibre surface [117], [242], [248], [249]. However, the influence of the conditions investigated as part of this work on the quality of the recovered fibres is not yet known. For this reason, this chapter aims to characterise fibres processed at the minimum conditions necessary to fully decompose the resin in order to limit their degradation and assess their suitability for re-use in a new composite material.

In this chapter, the materials used and characterisation techniques employed are first described, following which the data obtained is presented and discussed. Scanning electron microscopy (SEM) is used as the primary imaging tool in order to inspect the fibre surface. Within the same analyses, it was possible to perform elemental analysis using energy dispersive X-ray spectroscopy (EDX). The fibre surface was further analysed by X-ray photoemission spectroscopy (XPS) in order to assess any changes in the surface functional groups which may influence adhesion to a new polymer matrix. The

mechanical integrity of the recovered fibres was also investigated with single fibre tensile testing (SFTT). Similar to previous work, each of these data sets were analysed through the application of a Weibull distribution in order to calculate a scale factor, rather than relying on an average; the reasons for this are discussed in Section 5.5. This chapter concludes by identifying which of the eleven suggested process conditions have the least impact on the virgin carbon fibre and thus are recommended as most suitable for recovering carbon fibre from composite materials.

5.2 Experimental Methodology

5.2.1 Materials

All reagents used to process the fibres for analysis are the same as those described in Chapter 3. After each reaction was completed, fibre samples recovered from the CFRP were rinsed with acetone at ambient conditions and the organic residue remaining on the fibre surface was qualitatively assessed using scanning electron microscopy (SEM). In order to decouple the influences of manufacturing the CFRP, the lifetime wear of the composite and the recycling process on the fibre properties, virgin Toray T700S fibres were processed at each of the conditions described in Table 22. Although the CFRP was reinforced with T700S fibres, this approach also allows a direct comparison of the mechanical and surface properties to be made between the processed fibres with virgin material from the same batch, rather than relying solely on the manufacturer's data sheets. The virgin Toray T700S fibre was supplied on a continuous yarn and was cut into lengths measuring 50 ± 5 mm. A single length was included in the reactor alongside samples of the CFRP in order to expose the fibre

surface to the degradation products in addition to the solvents and additives. According to the manufacturer's data sheet, the fibre diameter is 7 µm, the average fibre tensile strength is 4.90 GPa and the modulus is 230 GPa [299].

In addition to the virgin material, the Toray T700S fibres recovered from the CFRP were also subjected to single fibre tensile tests in order to verify the SFTT method by comparing the data obtained to the tensile strength quoted by the manufacturer. This also examines the impact of being used in a composite and the recycling conditions. The data from these tests is provided in Appendix 3.

5.2.2 Fibre Processing

From the results presented in Chapters 3 and 4, multiple different process conditions were identified as achieving an *RD* of more than 92%. The 11 conditions which achieved this in the minimum reaction time and temperature were selected to process fibres for characterisation. These conditions are listed in Table 22.

As the virgin carbon fibre was supplied with a polymeric layer of sizing on the surface, it is desirable to also analyse the fibres with this sizing removed. Earlier work was consulted in order to develop an appropriate procedure [116]. This consisted of soaking the fibres in a 100 mL acetone bath at room temperature for 7 days before washing the fibres with fresh acetone 3 times, also at ambient conditions. These fibres were dried in a fume cupboard overnight and then refluxed for 48 h using Soxhlet extraction apparatus and 150 mL of tetrahydrofuran (THF). Fibres were placed in a paper

crucible before being loaded into the sample chamber of the Soxhlet equipment. Each 50 min cycle consisted of the sample chamber gradually filling with hot (approximately 60˚C) condensed THF before discharging to a round-bottomed flask where the solvent was reheated. After reflux, samples were removed from the crucible and dried in a fume cupboard for 3 days before being analysed. The removal of the sizing was confirmed by following TGA Method 1 (described in Chapter 3). Thermograms obtained for both the as-received carbon fibre and the fibres with the sizing removed following this method (hereafter referred to as sCF) are provided in Appendix 2.

***Table 22**. Reaction conditions used to process virgin Toray T700S carbon fibre for characterisation with X-ray photoemission spectroscopy (XPS) and single fibre tensile testing (SFTT).*

Catalyst	Sample Reference	Temperature, T_R (˚C)	Pressure, p (MPa)	Reaction time, t_R (min)
None	N-320	320	19.7	120
	N-330	330	22.0	90
	N-340	340	23.5	45
	N-360	360	27.0	15
	N-380	380	30.0	0
0.05 M $ZnCl_2$	Z-290	290	14.5	90
	Z-300	300	16.0	45
0.05 M $MgCl_2$	M-290	290	14.5	90
	M-300	300	16.0	45
0.005 M $AlCl_3$	A-290	290	14.5	90
	A-300	300	16.0	45

5.2.3 Environmental Scanning Electron Microscopy (ESEM)

Fibres recovered from the CFRP using the process conditions described in Section 5.2.2 were imaged with environmental scanning electron microscopy (ESEM) using a Philips XL30 FEG ESEM (Philips, Netherlands). A 10 ± 2 mm length was cut from a single tow and loaded onto adhesive mounting discs before being coated with gold using an EMSCOPE SC500 low-vacuum sputter coater (Quorum Technologies, UK). Although carbon fibres are electrically conductive, this metallic coating is able to improve the quality of the micrographs obtained. The samples were loaded individually into the vacuum chamber of the ESEM which was subsequently evacuated. All images were taken using an acceleration voltage of 20 kV. Depending on the surface features of interest, the working distance (WD) was varied between 9.6 and 11.7 mm and images were captured at a magnification of between 1200 and 12,000 times.

5.2.4 Energy Dispersive X-Ray Spectroscopy (EDX)

Elemental analysis of any deposits observed on the fibre surface was carried out using energy dispersive X-ray spectroscopy (EDX) using an Inca X-Sight (Oxford Instruments, UK). Analysis was conducted while samples were imaged with ESEM. Although this is a non-destructive technique, it was not possible to recover these samples for further analysis due to sputter coating the carbon fibre samples prior to imaging.

5.2.5 X-Ray Photo-emission Spectroscopy (XPS)

In order to improve adhesion between the carbon fibres and polymer matrix, the functional groups on the fibre surface are carefully controlled during the manufacturing process. However, the recycling conditions identified may alter this surface chemistry and, therefore, X-Ray photo-emission spectroscopy (XPS) was used to monitor any changes between the virgin and processed fibres. The virgin Toray T700S fibres were used as the control, however, the sizing applied to the surface is likely to alter the spectra obtained. For this reason, sCF fibres were also analysed at this stage.

The samples for analysis by XPS were prepared by applying a double-sided adhesive tape to the surface of stainless steel stub mounts. A tow of carbon fibre processed at each of the conditions in Table 22 was cut to a length of 20 ± 2 mm and placed across the tape. Analysis was conducted using a Thermo Scientific K-Alpha X-Ray photo-emission spectrometer (Thermo Fisher Scientific, USA) which was equipped with a mono-chromated aluminium kα X-ray source. The emission current and acceleration voltage was set to 3 mA and 12 kV respectively and the system was calibrated using a C-C peak at 284.8 eV. The samples were loaded into the vacuum chamber and the pressure reduced to 5×10^{-7} mbar. All spectra were measured using a take-off angle of 90˚. Survey spectra in the range of 0 – 1350 eV were recorded for each fibre sample using a pass energy of 200 eV, a step size of 1 eV and a dwell time of 10 ms. High resolution scans around the O1s and C1s peak were also performed using a pass energy of 50 eV, a step size of 0.1 eV and a dwell time of 50 ms.

The atomic composition of the fibre surface was calculated using Thermo Advantage software and Schofield sensitivity factors: the value of each of these factors is provided in Table 23. Curve fitting of the XPS spectra was also conducted using the Thermo Advantage software and a Powell fitting algorithm.

***Table 23**. Emission energy and Schofield sensitivity factors for C1s, O1s and N1s electron emission* [300].

Element and electron shell	Binding Energy (eV)	Schofield Sensitivity Factor
C1s	284.8	1.00
O1s	532.9	2.93
N1s	400.0	1.80

5.2.6 Single Fibre Tensile Testing (SFTT)

In order to quantify the impact of the recycling conditions on the tensile strength and modulus of the carbon fibres, single fibre tensile tests were conducted according to the British Standard ISO 11566 (1996) [114]. An individual filament was isolated, mounted across a paper frame and secured in place by applying a small amount of Araldite 2012 epoxy resin (Huntsman International, UK) to points 1 and 2 in Figure 59; this ensured that the gauge length of each specimen was 25 ± 1 mm. The resin was cured at room temperature overnight and the presence of a single fibre was confirmed with optical microscopy using a Zeiss Axioscope 10 (Zeiss, Germany) set to a magnification of 40 times.

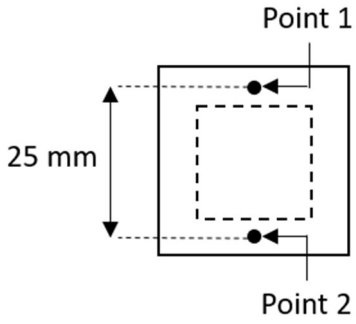

***Figure 59**. Single fibre tensile testing (SFTT) paper frame template.*

Upon completing the preparation of all samples, each specimen was aligned with the vertical axis of an Instron 5566 tensile testing machine and clamped in place with the grips. One side of the paper frame was cut away and an incision made on the opposite side to leave the fibre suspended as shown in Figure 60. Each tensile test was conducted using a 10 N load cell with a resolution of 10^{-4} N and a strain rate of 0.2 mm min^{-1}. The fibre was loaded until failure and the force-displacement curve recorded using Bluehill software. A minimum of 30 successful samples were examined for each of the reaction conditions specified in Table 22. Occasionally, the force-displacement curves showed signs of elastic deformation due to fibre pull-out and, in these instances, the data obtained was not included in the final analysis. The strength of each fibre, σ (Pa), was calculated using Equation (31).

$$\sigma = \frac{F_{max}}{A_f} = \frac{4F_{max}}{\pi d_f^2} \tag{31}$$

Where F_{max} = Maximum recorded load (N), A_f = Fibre cross-sectional area (m^2), and d_f = Fibre diameter (m).

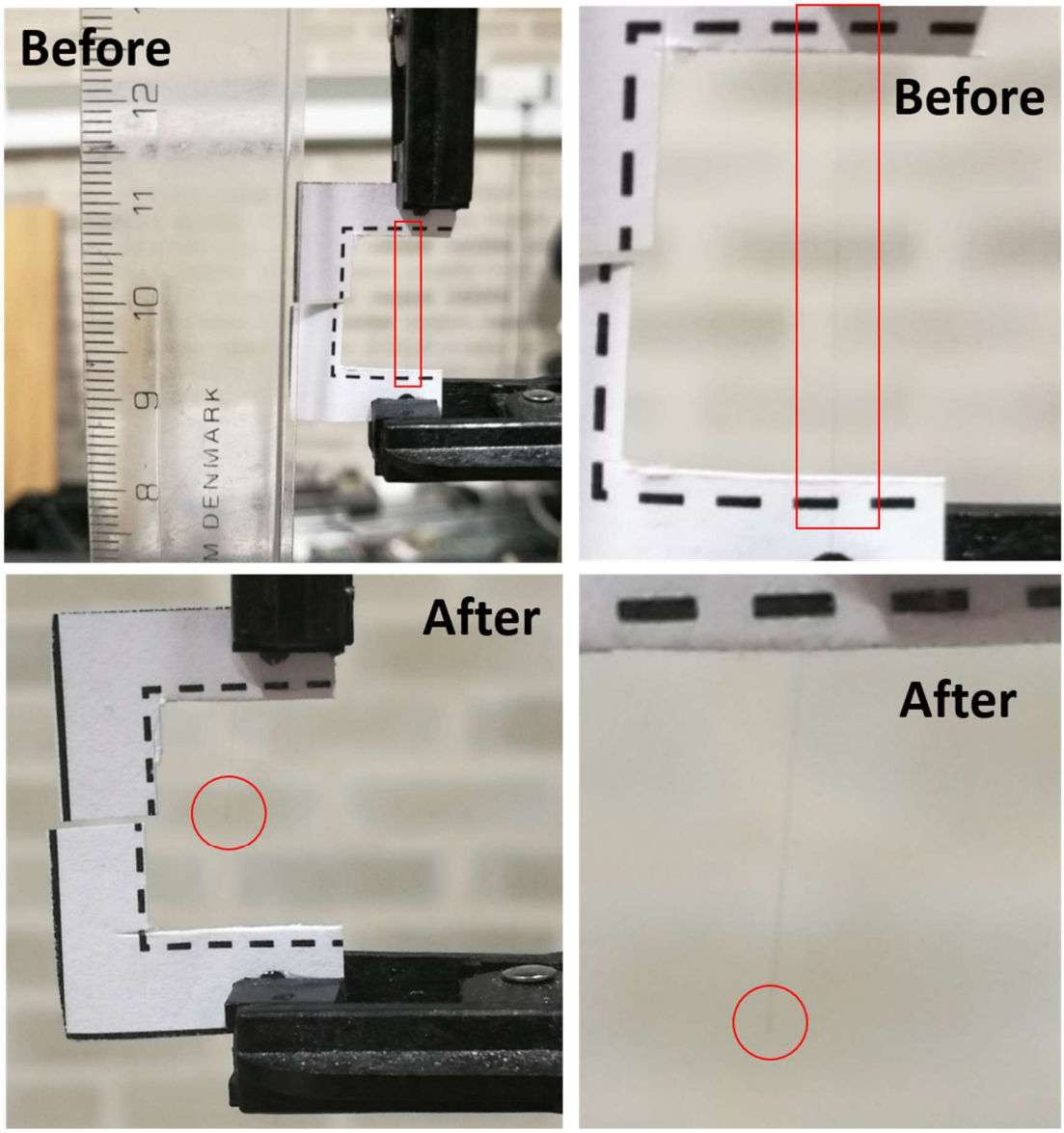

***Figure 60**. Images of before and after a single fibre tensile test (red outline shows carbon fibre).*

The diameter of the virgin carbon fibre according to the manufacturer's data was 7 µm which was confirmed through optical microscopy. 20 samples of virgin fibres, sCF fibres and fibres processed at each of the conditions specified in Table 22, were imaged with optical microscopy using a magnification of 40 times. Analysis was conducted using ImageJ software and an average was taken from across the 20 measurements to give the diameter of the fibres recovered from each set of conditions. This average was

subsequently used to calculate the fibre strength. The diameter measurements were confirmed by imaging a single fibre processed at each set of conditions using SEM, however, due to time restrictions, it was not possible to image twenty fibres for each of the eleven different process conditions, de-sized fibres and virgin fibres using this technique. Optical microscopy was also used to investigate any variation in the diameter along a length of the virgin Toray T700S fibre. five randomly selected fibres were imaged at 5 arbitrary points along a 50 mm length. For a single fibre, the greatest recorded variation along its length was 0.17 µm which is equivalent to an error of 2.45% and a standard deviation of 0.06 µm. This variation is, therefore, considered to be very small compared to the range of strengths which it is expected to be observed. Across the entire data set, the mean diameter of the virgin carbon fibre was 6.95 ± 0.1 µm which is similar to that quoted by the manufacturer [299]. The recorded diameters of the processed carbon fibres are provided in Section 5.5.

As the failure of each specimen is likely to initiate at one of the randomly distributed internal or external surface flaws along its gauge length, it is expected that there is a large variation in failure load. Due to the random nature of the distribution of these flaws, characterising the data set using a normal distribution and calculating a mean is considered insufficient. Alternatively, Weibull analysis may be used to determine the scale factor, σ_0 (GPa), for each batch of processed fibres. This is the maximum tensile strength that 63% of the weakest fibres in each population can achieve. The 3-parameter method has been previously shown to lead to unrealistic results [115] and, therefore, the 2-parameter model (Equation (32)) has been more

commonly applied to the analysis of brittle materials [116], [117], [301]. In addition, to ensure that a Weibull distribution fits each data set, MINITAB™ (version 18) statistical software was used to calculate the Anderson-Darling statistic and subsequent p-value. This test relies on the property that, if a data set follows a given distribution, the cumulative distribution function of the data set can be assumed to follow a uniform distribution. The Anderson-Darling statistic then tests the distance between each data point and the expected value based on the distribution [302]. The significance level chosen for the carbon fibre tensile strengths was 0.05 and all p-values were in the range of 0.288 to 0.432. As all p-values were much higher than the significance level, it was assumed that a Weibull distribution can be used to characterise each population; this is also described in earlier work [116], [117].

Fibres were sorted by order of magnitude and assigned a rank value from 1 to *n* where *n* is the total number of fibres investigated. The probability of fibre failure, *P*, is calculated with Equation (33). A complete description of this statistical distribution is provided by Weibull (1951) [303].

$$P(\sigma) = \frac{w\sigma^{(w-1)}}{\sigma_0^w} e^{-\left(\frac{\sigma}{\sigma_0}\right)^w} \tag{32}$$

$$P = \frac{i - 0.3}{n + 0.4} \tag{33}$$

Where *w* = shape parameter and *i* = rank value (1, 2, 3 … *n*). The shape parameter is used to characterise the spread; a higher value is indicative of a narrower distribution. σ_0 was

considered to be the tensile strength of the fibres recovered from each of the process conditions investigated. Two methods were used to calculate the two Weibull parameters (σ_0 and w). The first considered a graph of the linearised form of the 2-parameter Weibull distribution (described by Equation (34)). The functions $\ln\left(-\ln\left(1-P(\sigma)\right)\right)$ and $\ln(\sigma)$ were plotted on the y- and x-axes respectively. σ_0 and w were taken as the intercept with the x-axis and the gradient of the regression line respectively. The second method involved estimating these parameters using the statistical software MINITAB^{TM} (version 18).

$$\ln\left(-\ln\left(1-P(\sigma)\right)\right) = w\ln\left(\frac{\sigma}{\sigma_0}\right) \tag{34}$$

In addition to the tensile strength, it is also useful to quantify the fibre stiffness by calculating the tensile modulus, E_f (GPa) using Equation (35) [117].

$$E_f = \frac{\left(\frac{\Delta F}{A_f}\right)\left(\frac{L}{\Delta L}\right)}{1-K\left(\frac{\Delta F}{\Delta L}\right)} \tag{35}$$

Where ΔF = the difference in force (N) between a strain limit of 0.1 and 0.6%, L = gauge length (25 mm), ΔL = the difference in length between a strain limit of 0.1 and 0.6% and K = system compliance (taken as 2.5 x10^{-5} mm N^{-1} from [304]). As K is taken from the manufacturer's data, this value is for the equipment only and does not include the compliance of the grips, paper mount of adhesive holding the fibre in place. However, as a large number of samples (> 30) were tested using the same technique, it is thought

that any difference in modulus due to a difference in compliance is averaged out across the data set. Furthermore, the moduli of recycled fibres are directly compared to that of virgin and fibres de-sized using Soxhlet extraction and so changes in this mechanical property due to the recycling conditions should be identifiable.

5.3 Scanning Electron Microscopy & Energy Dispersive X-Ray Spectroscopy

In order to qualitatively assess the fibre surface and verify the diameter measurements taken from optical microscopy, SEM was used to image virgin carbon fibre and fibres recovered from the CFRP at each of the process conditions specified in Table 22. Where there were any visible features of interest, elemental analysis was performed using EDX. Micrographs of the virgin Toray T700S fibres are shown in Figure 61 and there is evidence of the sizing used to hold the individual filaments into a tow; a residue, visible as lighter patches, can be seen on the fibre surface in both images. In addition, the diameter of a single virgin fibre is shown to be 6.89 µm in Figure 61b, which is similar to the average taken over the twenty samples imaged with optical microscopy of 6.93 ± 0.15 µm. This is also close to the manufacturer's quoted diameter of 7 µm [299].

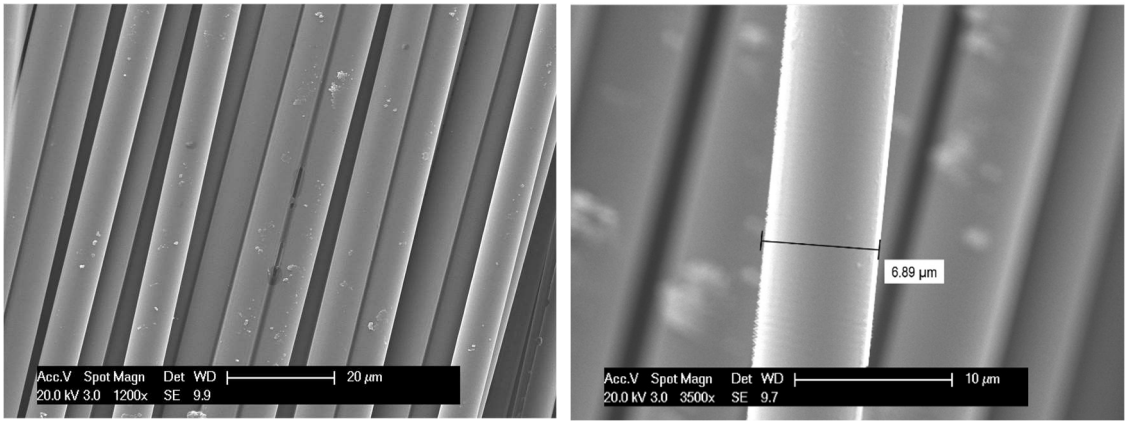

a) **b)**

***Figure 61**. Micrographs of virgin Toray T700S carbon fibre at a) magnification = 1200x, WD = 9.9; and b) magnification = 3500x, WD = 9.7.*

In addition to the virgin material, sCF fibres were also imaged using SEM. Micrographs for these fibres are shown in Figure 62 and it is apparent that, not only are these fibres free from any dust or other residue, the thin layers of sizing have been completely removed. Diameter measurements also showed a slight decrease compared to the virgin fibres. Figure 62b shows a filament with a diameter of 6.82 µm and the average across the twenty samples imaged was 6.88 ± 0.11 µm. Although this is within the margin of error, it is consistent with the approximate thickness of the sizing previously reported in the literature [305].

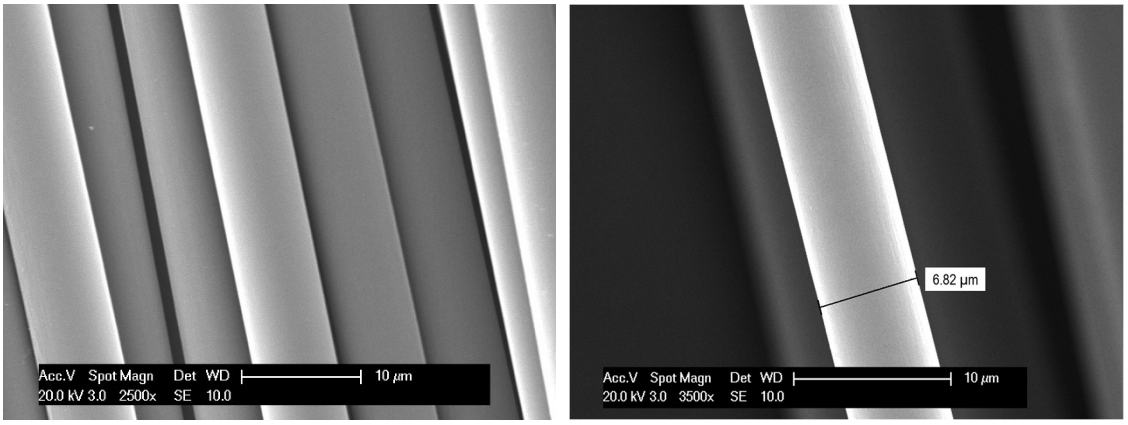

a) **b)**

Figure 62*. Micrographs of virgin Toray T700S carbon fibre with sizing removed via Soxhlet extraction at a) magnification = 2500x, WD = 10.0; and b) magnification = 3500x, WD = 10.0.*

The SEM images shown in Figure 63 have been used to qualitatively establish the relationship between temperature and resin decomposition and also give some indication of any surface defects which may have been caused by the recycling process. At 320˚C, the measured *RD* was 92% after processing the CFRP for 120 min and, despite fully extracting the fibres from the polymer matrix, it is clear from Figure 63a that there is a layer of resin surrounding the fibre surface. Although this may not impact the integrity of the fibres, it may influence the adhesion of the recovered fibres to a new layer of sizing or polymer when considering their subsequent reuse in a new composite material.

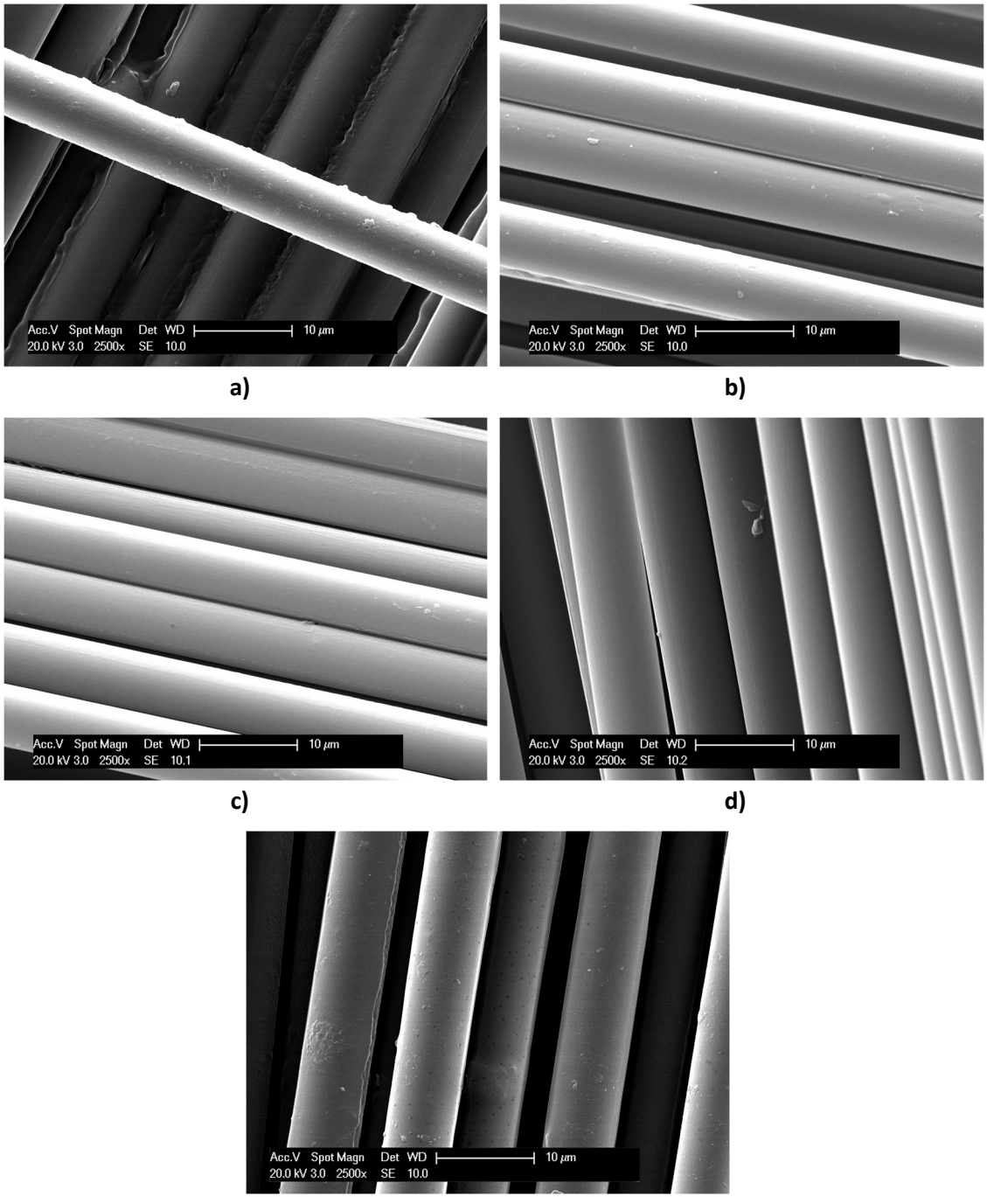

***Figure 63**. Micrographs of Toray T700S carbon fibre recovered from the CFRP at a magnification of 2500x and WD of 10.0 to 10.2 after processing with the neat acetone / water solvent mixture at a) 320˚C for 120 min; b) 330˚C for 90 min; c) 340˚C for 45 min; d) 360˚C for 15 min and e) 380˚C for 0 min.*

Upon increasing the temperature by just 10˚C to 330˚C, the surface of the recovered fibres was significantly cleaner: Figure 63b shows that only very minor fragments of residue remain on the fibre surface. Similarly, fibres recovered after processing at 340˚C (Figure 63c) and 360˚C (Figure 63d) also confirm the degradation data presented in Chapter 3 by demonstrating that the resin has been completely decomposed. At 380˚C, however, there does appear to be a light layer of residue on some fibres and there is evidence of pitting due to the appearance of small, circular shadows on the fibre surface. Higher magnification of fibres recovered after processing at 340 and 380˚C (Figure 64) shows the surface defects present in fibres which have been subjected to these higher reaction temperatures. These images suggest that under these conditions, the solvent may also begin to attack the fibre surface in addition to the polymer matrix. As fibres are likely to fail at an existing defect, it is possible that these process conditions lead to a reduction in the tensile strength: this hypothesis is explored in Section 5.5.

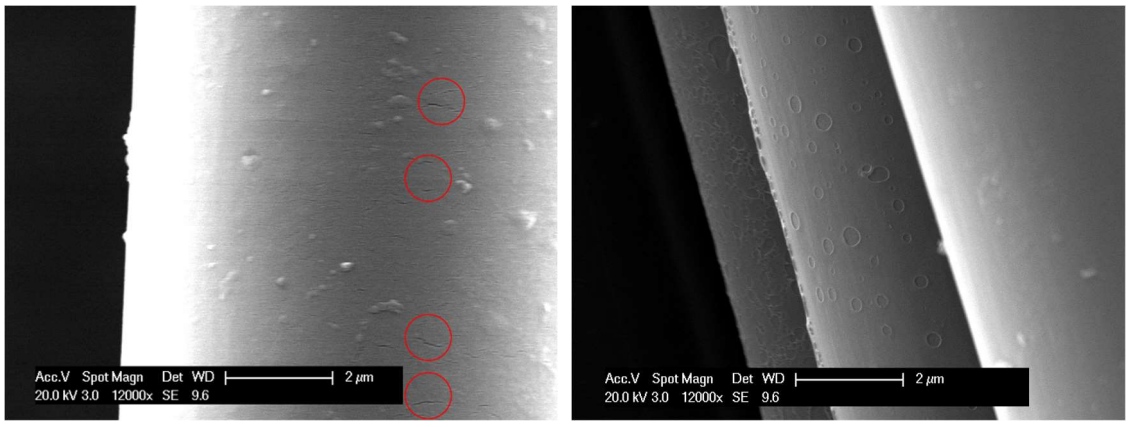

a) **b)**

Figure 64*. Micrographs of Toray T700S carbon fibre recovered from the CFRP at a magnification of 12,000x and WD of 9.6 after processing with the neat acetone / water solvent at a) 340˚C for 45 min; and b) 380˚C for 0 min.*

After processing the CFRP with a 0.05 M $ZnCl_2$ solution (samples Z-290 and Z-300), a light blue sheen was visible on the surface of the fibres recovered from the composite. Closer inspection with SEM revealed the presence of a solid deposit as shown in Figure 65. As the key difference between these fibres and those shown in Figure 63 and Figure 64 is the presence of $ZnCl_2$, it is suspected that the catalyst has deposited onto the fibre surface. The presence of $ZnCl_2$ was confirmed with EDX, the spectrum of which is also provided in Figure 65b. The relative amounts of each element identified is also shown in Table 24 and, as expected, the ratio of zinc to chlorine shows good agreement with the expected stoichiometric proportion of 1:2.

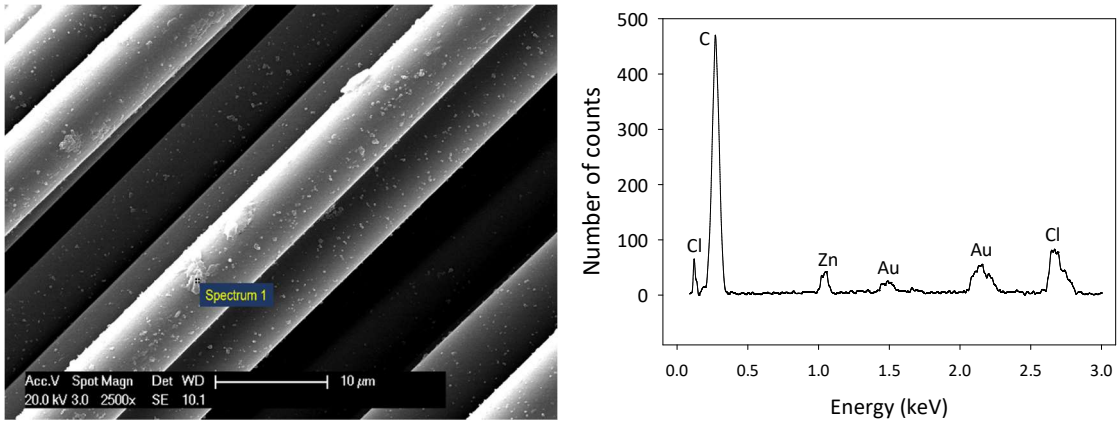

***Figure 65**. a) Micrograph of Toray T700S carbon fibre recovered from the CFRP after processing with a 0.05 M $ZnCl_2$ solution at 290˚C for 90 min (magnification = 2500x, WD = 10.1); and b) EDX spectra of the solid deposit (Au from sputter coater).*

There was no observable discolouration of the fibre surface after processing the CFRP with the 0.05 M $MgCl_2$ and 0.005 M $AlCl_3$ solvent systems, however, traces of the catalyst were still observable on the fibre surface upon inspection with SEM. Compared to $ZnCl_2$, these deposits were generally less widespread, but larger in diameter as

illustrated by Figure 66 and Figure 67. Although the use of the metal chloride catalysts resulted in contaminating the fibre surface, the images obtained demonstrate that polymer matrix had been completely solubilised, thereby confirming the decomposition data presented in Chapter 3. Table 24 also shows the relative molar quantities of Mg, Al and Cl which were determined by EDX and all are present in the expected stoichiometric quantities. Other elements which were identified primarily consisted of carbon, oxygen and gold, the presence of which can be explained by the composition of the fibres and pre-treatment process. Trace metals such as iron and nickel were also detected, both of which may be present due to contamination of the fibres by the basket they were held in within the reactor.

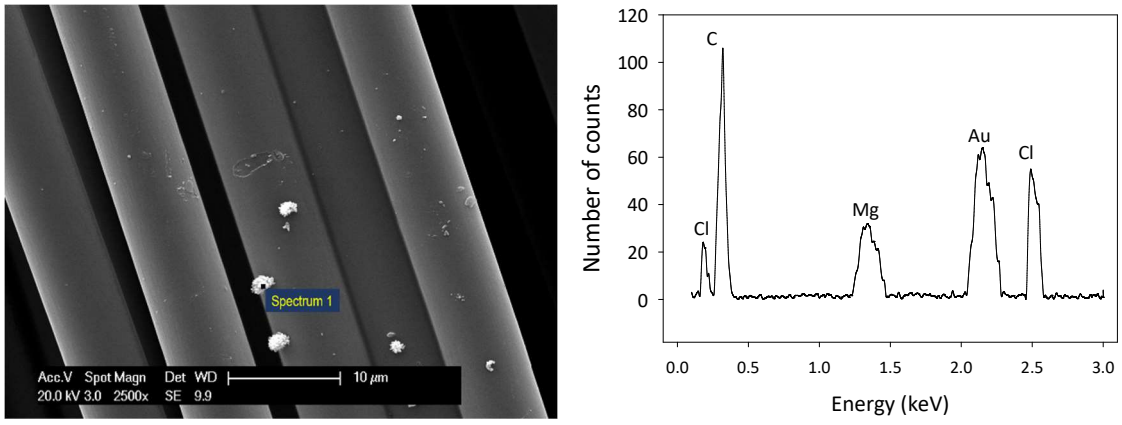

***Figure 66**. a) Micrograph of Toray T700S carbon fibre recovered from the CFRP after processing with a 0.05 M $MgCl_2$ solution at 290˚C for 90 min (magnification = 2500x, WD = 9.9); and b) EDX spectra of the solid deposit (Au from sputter coater).*

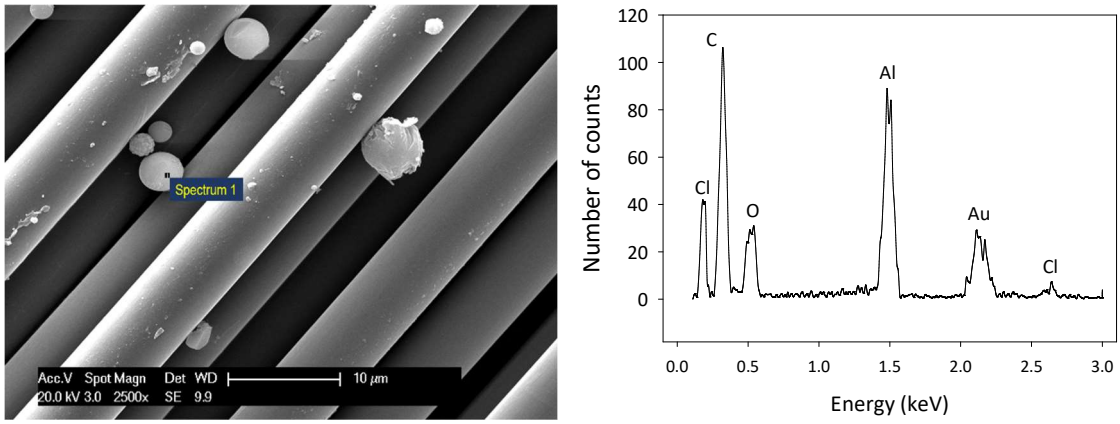

a) **b)**

Figure 67*. a) Micrograph of Toray T700S carbon fibre recovered from the CFRP after processing with a 0.005 M $AlCl_3$ solution at 290˚C for 90 min (magnification = 2500x, WD = 9.9); and b) EDX spectra of the solid deposit (Au from sputter coater).*

Table 24*. Relative quantity of each element present in the EDX spectra shown in Figure 65 to Figure 67 (M : Cl shows ratio of metal to chlorine).*

Catalyst	Figure	Proportion of element (mol%)						
		C	Cl	Zn	Mg	Al	Other	Ratio (M : Cl)
$ZnCl_2$	64	99.52	0.315	0.160	-	-	-	1: 1.97
$MgCl_2$	65	98.04	1.36	-	0.48	-	0.12	1: 1.94
$AlCl_3$	66	92.43	1.83	-	-	0.60	5.13	1: 3.03

The deposition of the catalysts on to the fibre surface gives rise to some concern as, similar to the resin residues, they may influence the adhesion of sizing and / or polymer in the manufacture of a new composite material. However, as $ZnCl_2$, $MgCl_2$ and $AlCl_3$ are all highly soluble in water, rinsing the recovered fibres at room temperature resulted in completely removing the deposits as shown by Figure 68. When compared to the neat acetone / water solvent mixture, the use of these catalysts therefore requires an additional processing step. Despite this, the catalytic solvent systems

facilitated a reduction in the minimum necessary process temperature of 40˚C and, therefore, the energy savings achieved are still likely to be beneficial when considering an industrial scale process.

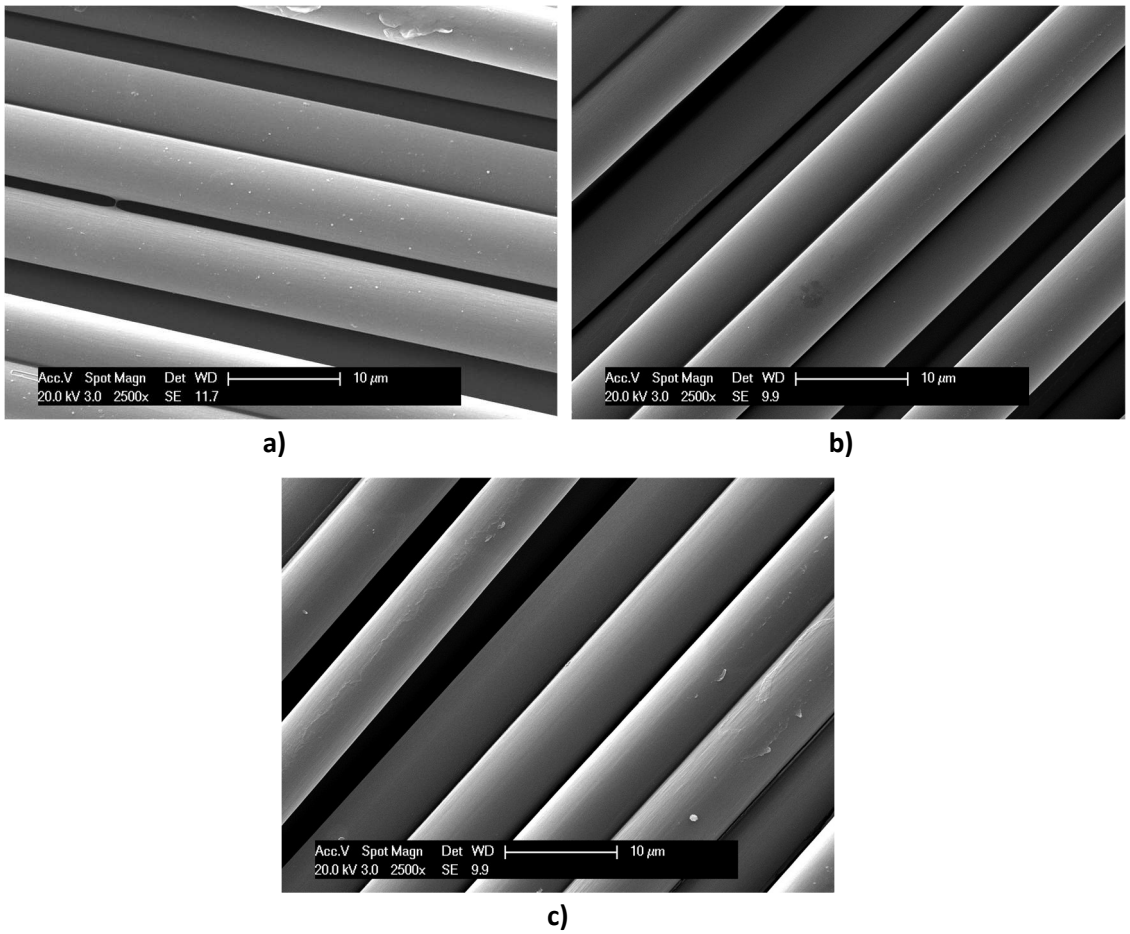

***Figure 68**. Micrographs of Toray T700S carbon fibre recovered from the CFRP at a magnification of 2500x after processing at 290˚C for 90 min with an acetone / water solvent and a) 0.05 M $ZnCl_2$ (WD = 11.7); b) 0.05 M $MgCl_2$ (WD = 9.9) and c) 0.005 M $AlCl_3$. Fibres were rinsed with water at room temperature after processing to remove the catalyst deposit.*

Micrographs similar to those shown in Figure 65 to Figure 68 were obtained for fibres recovered using the $ZnCl_2$, $MgCl_2$ and $AlCl_3$ systems and a process temperature of 300˚C: these are provided in Appendix 4. As the influence of the reaction conditions on both the surface functional groups and the mechanical properties are as yet unknown,

the remainder of this chapter is focussed on characterising processed virgin fibres using XPS and SFTT.

5.4 X-Ray Photoemission Spectroscopy (XPS)

In order to facilitate good adhesion between carbon fibres and the polymer matrix, the fibre surface is functionalised using two different techniques. During the manufacture of the fibres, the degree of surface oxidation is controlled by maintaining a specific proportion of nitrogen and oxygen within the furnace. Fibres are also coated with a polymer sizing, the chemical formulation of which is likely to differ between manufacturers and is not readily disclosed. A description of the process used to manufacture carbon fibre is provided in Chapter 2. As the developed recycling processes may change the functionality of the fibre surface, XPS was used to identify and hence assess which of the conditions in Table 22 are most able to recover fibres with surface properties similar to those of the virgin material. The survey spectra of the as-received virgin carbon fibre is shown in Figure 69; similar spectra were obtained from each of the fibres processed at the conditions listed in Table 22.

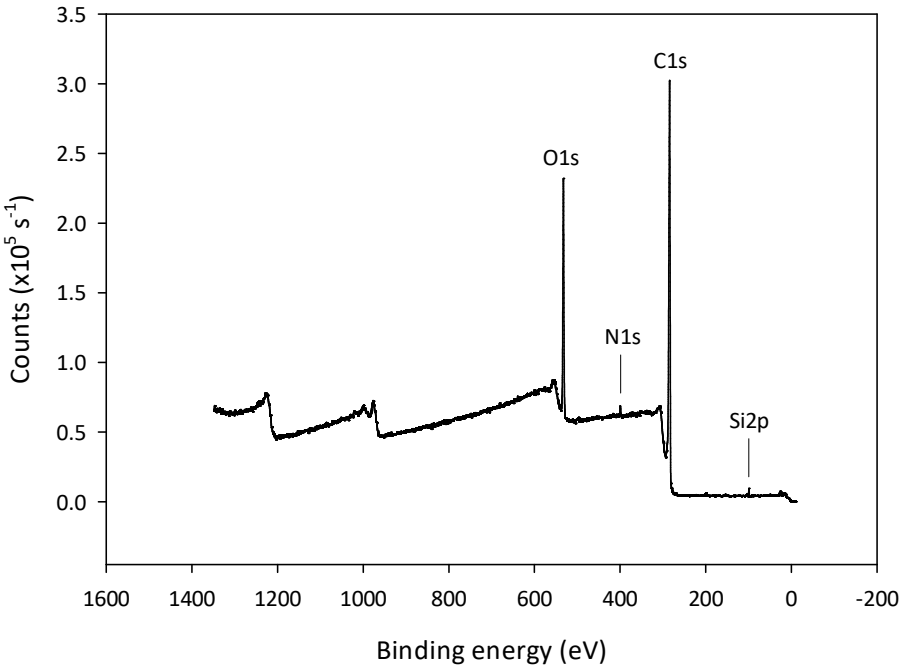

***Figure 69**. XPS survey spectra of the as-received virgin Toray T700S carbon fibre.*

As the binding energy (BE) is specific to each bond type, it is possible to identify which elements and functional groups are present on the surface of the fibres. Figure 69 demonstrates that there is a significant quantity of carbon and oxygen on the fibre surface due to peaks at 284.8 (C1s) and 532.9 (O1s) eV respectively. Small amounts of nitrogen (BE = 400.0 eV) and silicon (BE = 99.4 eV) were also detected. In order to further investigate the bond types present, high resolution spectra across the peaks of the O1s and C1s binding energies were also recorded for each fibre type. The high resolution spectra obtained from the analysis of the virgin carbon fibre are shown in Figure 70 and Figure 71. The binding energies for each element and bond type are also provided in Table 25.

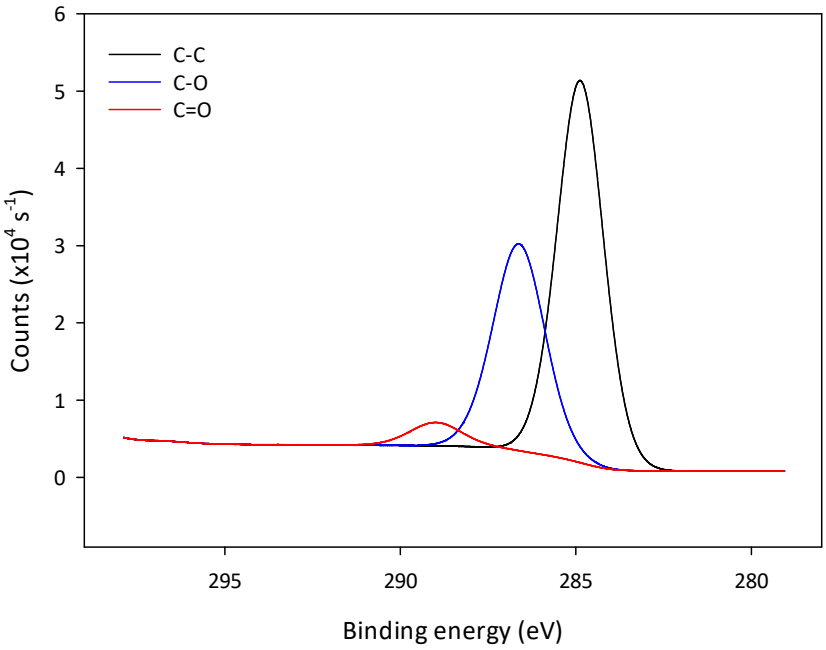

***Figure 70**. High-resolution XPS carbon spectrum of the as-received virgin Toray T700S carbon fibre.*

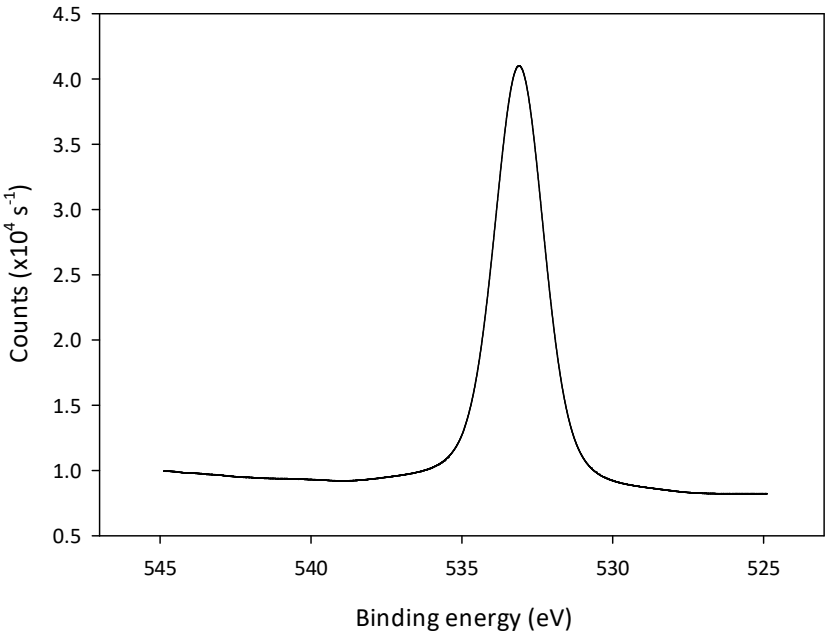

***Figure 71**. High-resolution XPS oxygen spectrum of the as-received virgin Toray T700S carbon fibre.*

***Table 25**. Binding energies of various functional groups detected on the surface of carbon fibres.*

Element	Functional group	Binding energy (eV)
C	C-C	284.8
	C-O-C	286.0
	O-C=O	288.5
O	-C-OH	532.9
N	C-NH_2	400.0
Si	Elemental Si	99.4

By inspection of Figure 70, it can be seen that there are 3 carbon species present on the surface of the virgin carbon fibre. Since the largest peak occurs at a BE of 284.8 eV, it is apparent that the majority of these constitute C-C bonds which is to be expected for carbon fibre. The two additional peaks at BE = 286.0 and 288.5 eV represent carbonyl groups which appear to occur as two distinct species of both C-O and C=O bonds. Although this may be attributable to the sizing applied, both groups were still detectable after removing the sizing following the procedure described in Section 5.2.2 and after processing the fibres after all conditions described in Table 22. The O1s bond shown in Figure 71 represents an aliphatic C-OH functional group and is, therefore, thought to be a constituent of the sizing. This was also not detected on the surface of any other fibres after processing which in turn suggests that the sizing was removed by all the conditions investigated.

By integrating the area under the curve for each peak, it is possible to determine the relative abundance (RA) of each of the elements and functional groups present on the fibre surface. Figure 72 demonstrates how the RA of oxygen changed compared to that of the virgin material.

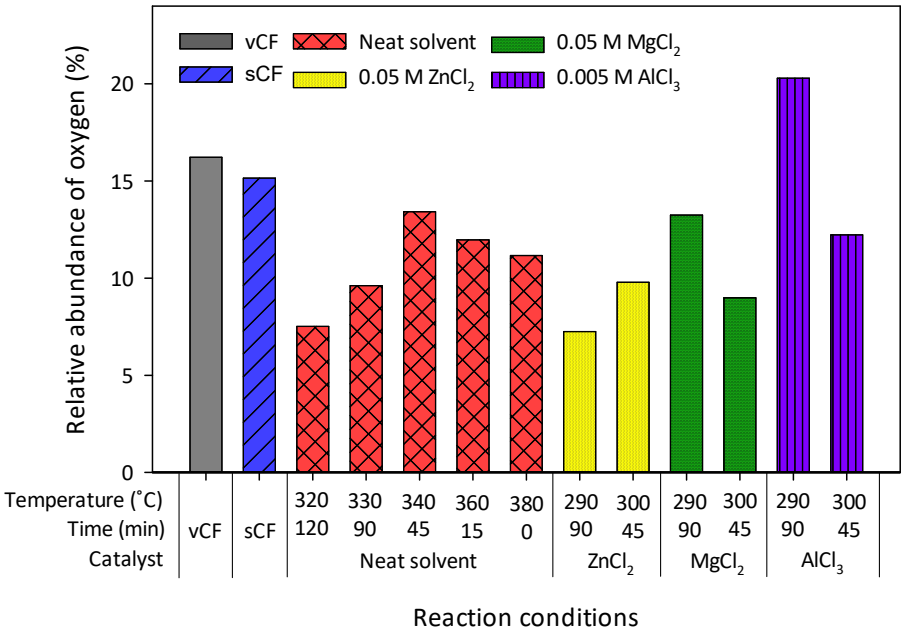

***Figure 72**. Relative abundance of oxygen present on the surface of the Toray T700S fibres after processing at each of the conditions in Table 22.*

With the exception of the 0.005 M $AlCl_3$ solvent system at 290˚C, all fibres showed a reduction in the concentration of oxygen on the fibre surface compared to the virgin and unsized (sCF) material. As oxygen is highly electronegative, the C-O-C and O-C=O moieties facilitate a strong interaction with other polar bonds, such as those present in acetone, water and metal chlorides. It has been previously suggested that this interaction may lead to hydrolysis of the carboxylic groups [248]. The loss of surface oxygen, may reduce the adhesion to a new polymer matrix; an effect which has been

noted in previous work [116], [117], [248], [249]. It is apparent from Figure 72 that, for the neat solvent mixture, both long reaction times and high temperatures lead to a reduction in the RA of oxygen. Compromise reaction conditions of 340˚C and 45 min meant the RA of oxygen was just 1.7% lower for fibres processed at this temperature than the sCF fibres. This compares to a reduction of up to 4.0% when using 380˚C, 0 min and 7.7% when using 320˚C, 120 min.

Of all solvent systems considered, a 0.005 M solution of $AlCl_3$ resulted in fibres with the highest RA of oxygen of up to 20.3%. This may be due to the very dilute concentration of the catalyst, which was supplied at an order of magnitude lower than the $ZnCl_2$ and $MgCl_2$ systems, coupled with a relatively low reaction temperature. For the $MgCl_2$ and $AlCl_3$ systems, the RA of oxygen decreased with temperature while the opposite was observed for the $ZnCl_2$ catalysed reaction. For this system, the reductions in the RA of oxygen, compared to the sCF fibres, were 7.9 and 5.4% for 290 and 300˚C respectively, meaning this had the greatest negative influence on the RA of oxygen at the fibre surface. In order to assess the impact of this change in oxygen concentration, further research may be focussed on micro-droplet shear strength tests or the manufacture and characterisation of a new composite material.

As the presence of amide and nitrate groups also support good adhesion to polymer matrices, particularly in thermoplastic resins [116], [306], it is also useful to monitor any changes in the concentration of nitrogen on the fibre surface as illustrated by Figure 73.

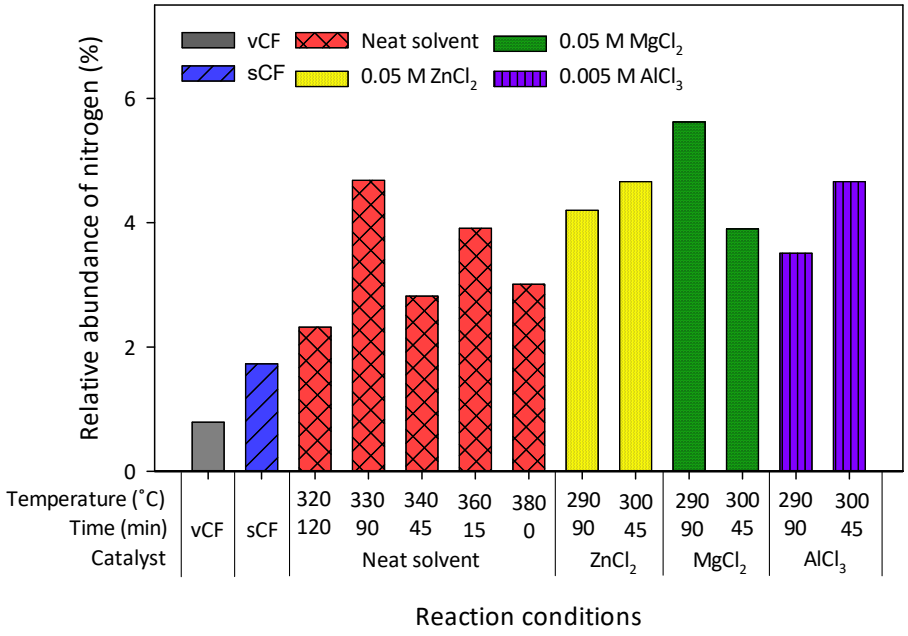

***Figure 73**. Relative abundance of nitrogen present on the surface of the Toray T700S fibres after processing at each of the conditions in Table 22.*

For all reaction conditions, there is a significant increase in nitrogen abundance compared to the as-received virgin fibre. Upon dissolving the sizing using Soxhlet extraction, the RA of nitrogen approximately doubles from 0.79% to 1.73%. Similar findings have been reported elsewhere [116], [307], [308] and is thought to be due to the exposure of the fibre surface: incomplete carbonisation of the PAN pre-cursor used in the carbon fibre manufacturing process results in the presence of nitrogen containing groups. However, the concentration of nitrogen detected is 0.6 to 3.9% higher than the sCF fibres for all fibres processed at the conditions described in Table 22, with the largest increase observed for the 0.05 M $MgCl_2$ system at 290˚C. As the epoxy resin used in the CFRP is likely to contain amines or amides, it is possible that small quantities of decomposition products chemically bond to the fibre surface and cannot be removed with a simple acetone wash at room temperature. For this reason, further investigation

is needed to determine the effect of this change in the functionality of the fibre surface by using the recovered fibres to manufacture and test a new composite material.

In addition to elemental analysis, high resolution spectra were also obtained in order to quantify changes in the functional groups C-O-C and O-C=O. The RA of each are shown in Figure 74 and Figure 75 respectively. The concentration of C-O-C is constant between the virgin material and sCF fibres, however, there is an increase in the RA of the O-C=O moiety. This suggests that the latter functional group is bonded to the fibre surface, rather than being part of the sizing and is, therefore, a more reliable indicator of any changes to the chemical structure at the surface. Previous research characterising fibres recovered from a composite material using supercritical propanol has noted a reduction in RA of C-OH and C=O bonds of 6.45 and 1.07% respectively [117]. This change is of a comparable magnitude to all of the findings presented as part of this work. The overall abundance of oxygen is reduced after processing the fibres at all conditions with the neat acetone / water solvent, and a similar effect is seen here in the change of the C-O-C group (Figure 74). Comparing across the fibres with the sizing removed, there is very little change observed in the RA of O-C=O groups with a maximum reduction of just 1.2% for the fibres processed at 340˚C. There was also an increase of 1.2% in this functional group for fibres recovered from a reaction temperature of 380˚C. It is possible that this higher temperature results in a greater degree of surface oxidation, which has been noted in earlier work, especially in the presence of water.

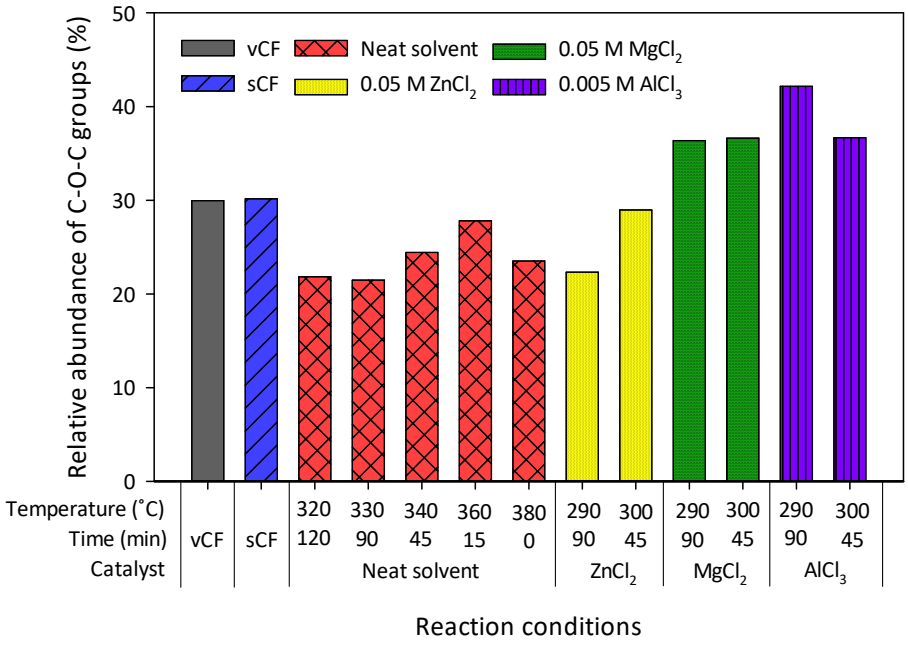

***Figure 74**. Relative abundance of C-O-C functional groups.*

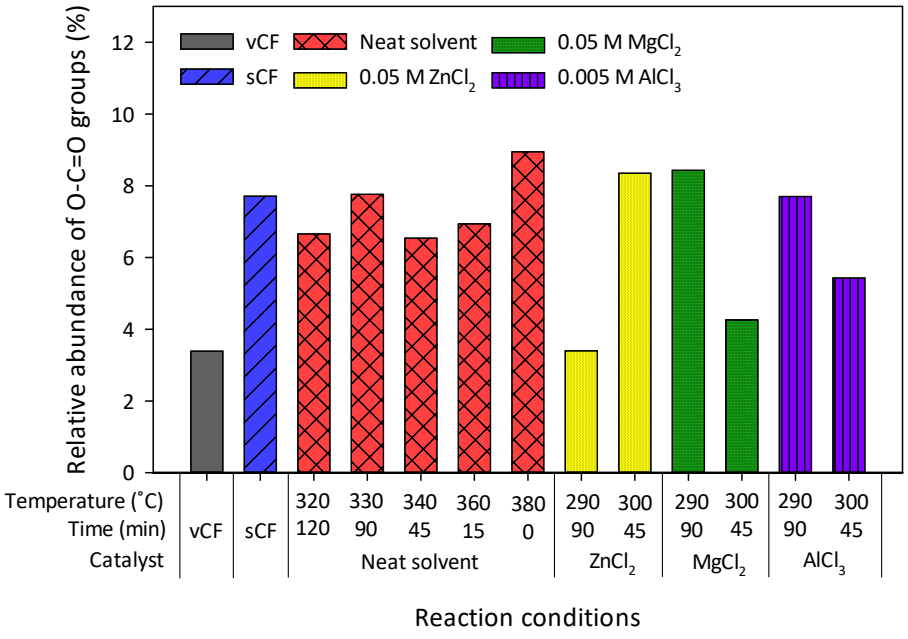

***Figure 75**. Relative abundance of O-C=O functional groups.*

Upon increasing the temperature of the $ZnCl_2$ solvent system from 290 to 300˚C, there is an increase in the abundance of both the C-O-C and O-C=O moiety of 6.6 and

5.0% respectively. Compared to the fibres with the sizing removed, the $ZnCl_2$ system more than halves the concentration of O-C=O groups at 290˚C, while the higher temperature of 300˚C effectively maintains RA at approximately 8%. This suggests that the carbon fibre surface is more sensitive to reaction time than temperature with this catalyst system. The opposite is true for the fibres processed with 0.05 M $MgCl_2$ and 0.005 M $AlCl_3$ solutions where increasing the temperature by 10˚C results in a reduction of the O-C=O functional group by 4.2 and 2.3% respectively. For both of these catalysts, the RA of O-C=O was similar to that of the unsized fibres after processing at 290˚C. There was, however, an increase in C-O-C by between 6 and 12% depending on the conditions studied. In view of both of these functional groups, the solvent systems which result in the least change to the surface chemistry, when compared to the unsized fibres, appears to be the neat solvent mixture at 360˚C, 0.05 M $ZnCl_2$ at 300˚C and 0.05 M $MgCl_2$ at 290˚C. These findings suggest that both of these metal chlorides are suitable catalysts when considering the impact of the recycling process on the surface properties of the recovered carbon fibre. If an increase in the RA of C-O-C of 12% can be tolerated, the 0.005 M $AlCl_3$ system may also be suitable when supplied at 290˚C as the abundance of O-C=O groups are similar to that of the sCF fibres. As a result of this XPS analysis, four sets of conditions have been identified which do not result in significant changes to the surface properties of the fibres. It is, therefore, likely that material recovered from these recycling conditions will adhere well to a new layer of sizing.

5.5 Single Fibre Tensile Testing (SFTT)

Single fibre tensile tests were conducted according to ISO 11566 (1996) [114] in order to determine the influence of the recycling process on the tensile strength and modulus of the Toray T700S carbon fibres. The fibre diameter was determined using optical microscopy. Figure 76 demonstrates that the software was sufficiently calibrated whilst Figure 77 shows a fibre diameter measurement being taken. Typical force-displacement curves are also provided in Figure 78 for a range of conditions and the maximum load supported was used to calculate the strength of each individual fibre using Equation (31). These force-displacement curves are characteristic of brittle materials and in each case, there is a linear elastic deformation region before the failure point is reached. No plastic behaviour, which is indicative of more ductile materials, was observed.

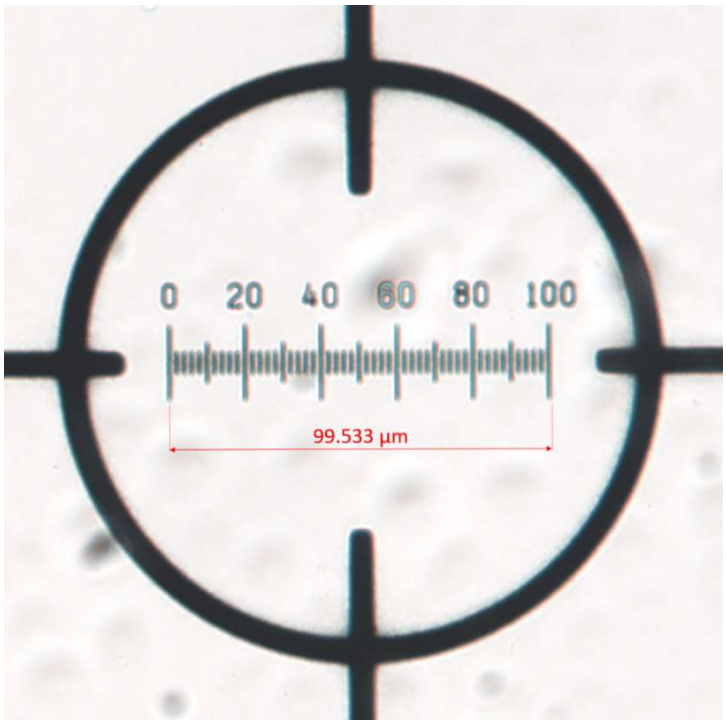

***Figure 76**. Optical microscopy image of calibration slide (magnification = x40).*

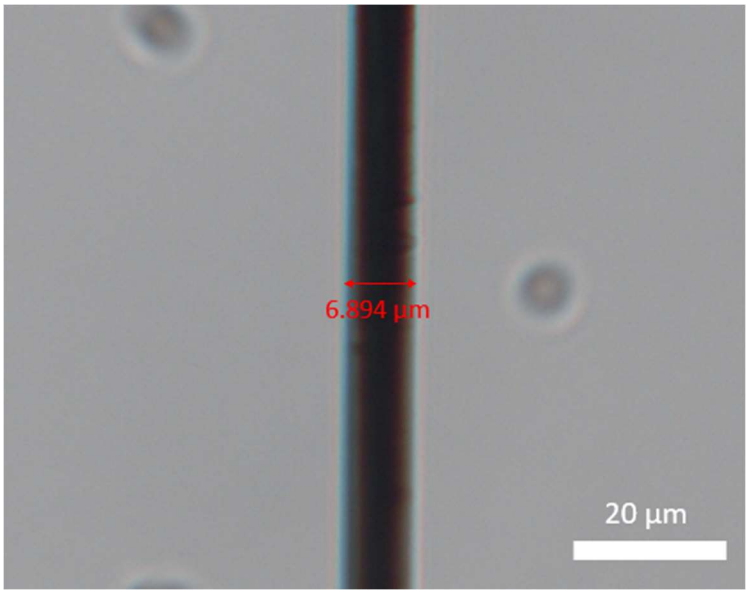

***Figure 77**. Optical microscopy image of carbon fibre showing diameter = 6.984 µm (magnification = x40).*

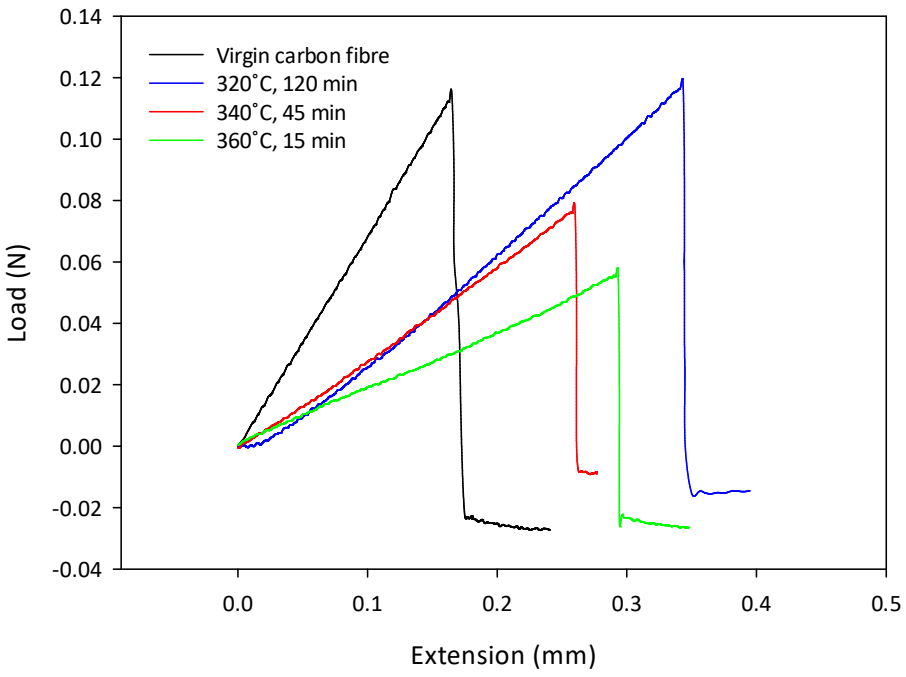

***Figure 78**. Typical force displacement curves for Toray T700S carbon fibres processed with the neat acetone / water solvent mixture at a range of conditions.*

Using 2-parameter unimodal Weibull analysis (Equations (32) and (33)), it is possible to calculate a scale factor which is a more useful indicator of the strength of the

whole population than the mean. The tensile strength of each fibre was used to draw Weibull plots for fibres processed with each of the conditions investigated; the scale factor (σ_0, GPa) was taken as the intercept of the linear regression line with the x-axis (i.e. at $\ln\left(-\ln\left(1-P(\sigma)\right)\right)=0$). The distributions obtained for virgin fibres and those processed at 360˚C (t_R = 15 min) are shown in Figure 79 and the Weibull plots for all fibres tested are provided in Appendix 4. For all populations, there is good agreement between the data set and the corresponding Weibull fit: R^2 values are in the range of 0.934 to 0.988 which confirms the result of the Anderson-Darling statistic described in Section 5.2.6 that these data can be described by this particular distribution.

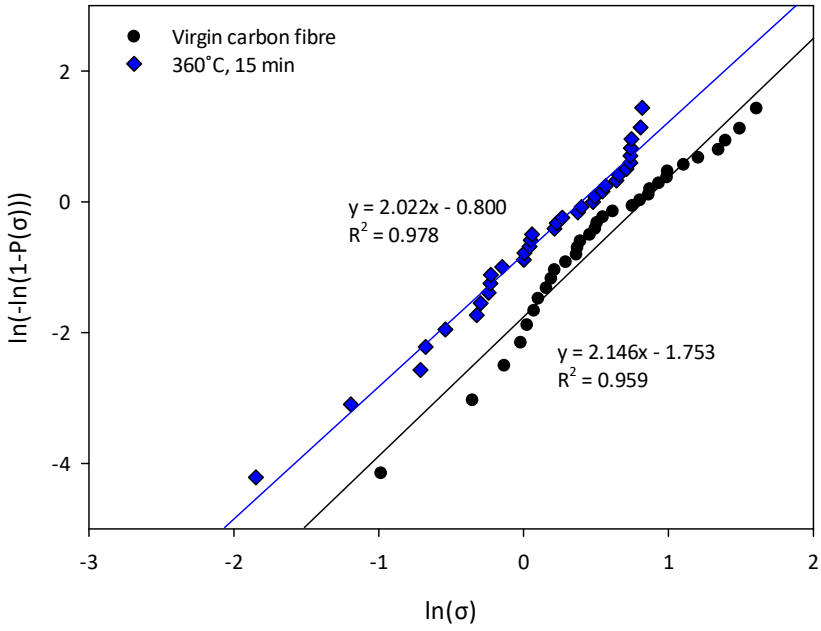

***Figure 79**. Linearised Weibull plots obtained for virgin Toray T700S carbon fibre and fibres processed with a neat acetone / water solvent at 360˚C for 15 min.*

In addition to the Weibull plots, the scale and shape factor for each data set was also estimated in MINITAB™ (2018). The values for σ_0 calculated using both approaches

are shown in Figure 80 and there is generally very close agreement between the two different methods. Across all populations, the average difference in σ_0 is 1.19% with the largest of 4.17% occurring for fibres processed at 330˚C (t_R = 90 min). The spread of each data set is also shown by the error bars in Figure 80. This is discussed in detail below, but initial analysis shows that, within each data set, there is generally a large range in fibre strength with the maximum observed up to 40% larger than σ_0. This is not unexpected due to the random distribution of surface defects which act as failure initiation points. Similar ranges in single fibre tensile strength have also been previously reported [116], [117], [309].

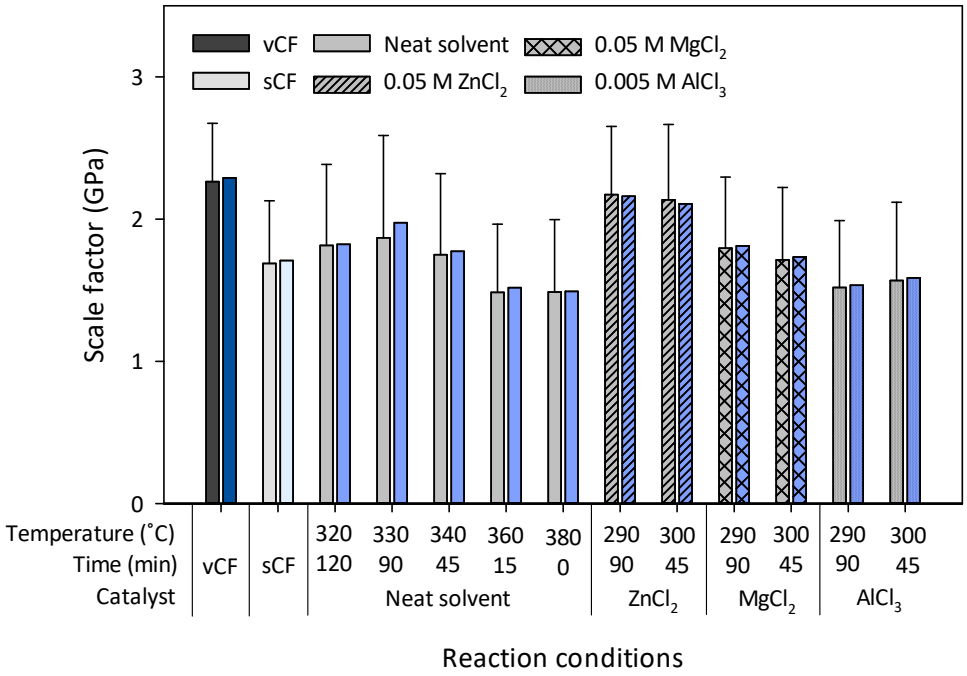

***Figure 80**. Scale factor for Toray T700S carbon fibres processed at each of the conditions investigated (grayscale = calculated from Weibull plot, blue = estimated in Minitab 18.0).*

As expected, the virgin carbon fibres were the strongest tested with a scale factor of 2.26 GPa, however, this differs from the manufacturer's data by a factor of 2

[299]. This is not thought to be due to error in the experimental technique as the Toray T700S fibres recovered from the CFRP demonstrated a strength in the range of 3.8 to 4.7 GPa (see Appendix 3) and is, therefore, similar to that quoted by the manufacturer. Furthermore, the T700S fibres characterised in this chapter were investigated as part of previous research and the average tensile strength was shown to be 2.0 ± 0.3 GPa [111]. It is thus possible that the batch of the as-received carbon fibres investigated did not conform to the required specification.

Upon removing the sizing via the Soxhlet extraction process (sCF fibres), the tensile strength was reduced by 25.3% despite only being subjected to relatively mild temperatures of 60˚C. As the solvents are unlikely to damage the fibres under these conditions, it is possible that the sizing on virgin fibres could cover some surface defects thereby limiting the number of failure points within the gauge length. Compared to these fibres, processing at temperatures between 320 and 340˚C with the neat acetone / water solvent demonstrates a slight increase in strength to between 1.75 and 1.89 GPa. A small decrease in fibre diameter was also observed of between 0.03 and 0.21 µm, which is similar to that recorded by Burn [116]. As this is an order of magnitude larger than the typical thickness of the sizing [305], it is possible that the outer layer of each fibre is also removed during the recycling process. This layer consists of highly orientated graphitic planes which are up to 1.5 µm thick [310], yet remain relatively weak [311]. Removal of some, or all, of this layer can also reduce the number of surface defects and subsequently leads to an increase in the tensile strength [272].

Despite shorter processing times, there is a clear temperature effect on the tensile properties of the fibre. Fibres processed at 320 and 330˚C exhibited a strength 7.1 and 9.6% more than that of the sCF fibres, yet increasing the reactor temperature to 360 and 380˚C resulted in a reduction in fibre strength of up to 12.4%. Previous work has suggested that higher temperatures increase the risk of fibre damage [242], [248], [249], although differences in solvent system, fibre type and process conditions make it difficult to directly compare these findings to earlier research. To ensure recovered material can be reused in high-value applications, lower reaction temperatures of between 320 and 330˚C are recommended for the recycling of CFRPs when using a neat acetone / water solvent mixture.

The choice of catalyst supplied in the reaction has a strong influence on the tensile properties of the carbon fibre recovered. The scale factor for M-290 and M-300 fibres was 1.80 and 1.71 GPa respectively and is, therefore, similar to that of the N-320 and N-330 fibres. The use of 0.005 M $AlCl_3$, however, resulted in a reduction in strength of up to 10% compared to the sCF fibres. Although the concentration of this catalyst was supplied at an order of magnitude lower than the $ZnCl_2$ and $MgCl_2$ systems, it appears that the Al^{3+} ions also attack the carbon fibre as well as resin. Unless this reduction in strength is tolerable when considering a new composite material, it is suggested that alternative weak-Lewis acids are used to lower the necessary reaction temperature of this recycling process. Of all the solvent systems considered, the presence of $ZnCl_2$ appeared to be the most beneficial in terms of fibre strength. Fibres processed at both 290 and 300˚C displayed a similar scale factor in the range of 2.11 to 2.17 GPa and are,

therefore, the strongest of all fibres recovered and up to 22% stronger than the sCF fibres. This does correlate to a slight reduction in fibre diameter, but this alone does not account for the increase in strength. It is thus hypothesised that the Zn^{2+} ions are particularly effective at removing the weaker graphitic planes on the carbon fibre surface which may correlate to the reduction in the RA of oxygen observed with XPS. However, further research is required to confirm the mechanism behind this strengthening effect.

In addition to considering the scale factor, the distribution of each data set can be characterised through the Weibull shape factor which was taken as the gradient of each Weibull plot and estimated in MINITAB™. The magnitude of *w* calculated from both methods is illustrated by Figure 81. Compared to σ_0, there is a larger deviation in the values obtained from the two techniques of between 2.44 and 15.79%, with the Weibull plot more likely to give the higher value. Despite these differences, similar trends are observed across the different process conditions employed: the shape factor of the virgin fibres is very similar to those with the sizing removed via Soxhlet extraction and those processed with the neat solvent mixture at all temperatures considered. For all catalyst systems, an increase in the temperature from 290 to 300˚C results in a reduction in *w* thus suggesting that this higher temperature results in a greater spread of data. Fibres processed with 0.005 M $AlCl_3$ had a similar shape factor to the virgin material, although there is a significant decrease in the spread of the distribution when using the $ZnCl_2$ and $MgCl_2$ catalysts. The 0.05 M $ZnCl_2$ system resulted in the strongest fibres and the greatest value of *w*. Compared to the sCF fibres, the shape factor of the

Z-290 fibres increased by 66 to 94% when determined from the Weibull plot and in Minitab respectively. This suggests that $ZnCl_2$ also acts to homogenise the strength of the fibres. However, as fibres are used in tows, it would be beneficial to manufacture and characterise a new CFRP with fibres recovered with this solvent system in order to ensure the recovered material can be used in high performance applications.

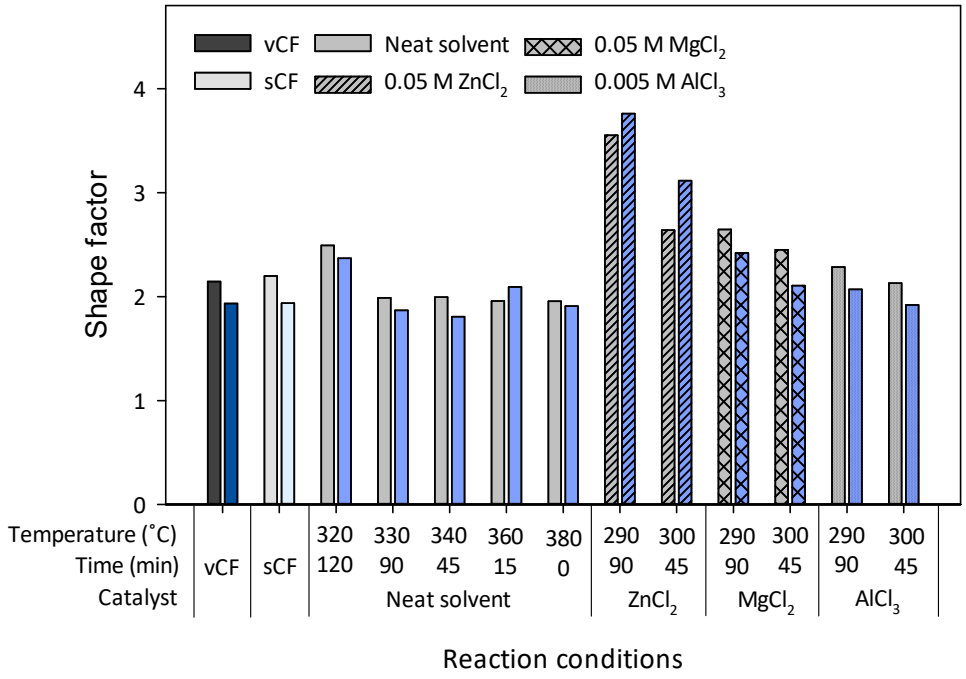

***Figure 81**. Shape factor for Toray T700S carbon fibres processed at each of the conditions investigated (grayscale = calculated from Weibull plot, blue = estimated in Minitab 18.0).*

The tensile modulus is a measure of the stiffness of a material and was calculated using Equation (35). All fibres demonstrated brittle behaviour and a high level of stiffness which was largely unchanged from the virgin fibres as demonstrated by Figure 82. The modulus of the unsized (sCF) carbon fibre was measured to be 133 ± 38 GPa and, after processing at 330˚C for 90 min and 380˚C for 0 min, this was reduced by 2.2 and 15% respectively. This is similar to the trend observed in the change of tensile strength

of the fibres shown in Figure 80: there is a decrease in the mechanical properties of the fibres with an increase in process temperature when using a neat acetone / water solvent. Also similar to Figure 80, is the influence of the chloride catalysts with the 0.005 $AlCl_3$ solution causing the greatest degradation of the fibre properties: the reduction in the modulus compared to the sCF fibres was 23 and 26% after processing at 290 and 300˚C respectively.

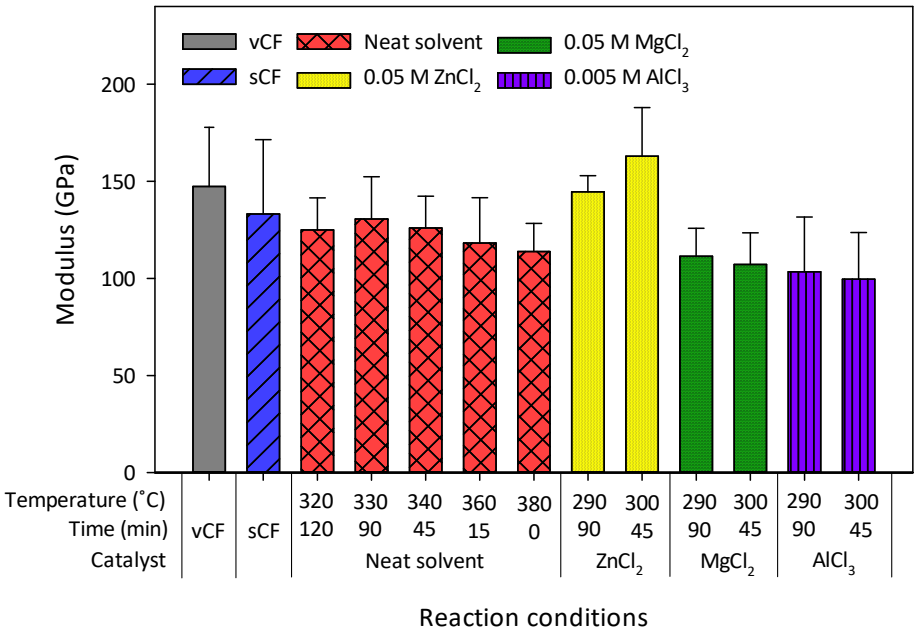

***Figure 82**. Tensile modulus for Toray T700S carbon fibres processed at each of the conditions investigated (calculated using Equation (35)).*

For both temperatures investigated, the $MgCl_2$ system gave values similar to that of the neat acetone / water mixture under a reaction temperature of 340˚C. This in turn suggests that this Lewis acid also influences the modulus as more severe process conditions (320 and 330˚C) resulted in the recovery of fibres with greater stiffness. Of all conditions studied, the use of the $ZnCl_2$ solution enabled the recovery of fibres with

the highest modulus with an increase of 8.3% (T_R = 290˚C) and 22% (T_R = 300˚C) when compared to the sCF fibres. As this catalyst and acetone / water solvent system facilitates the recovery of clean fibres and may improve the mechanical properties, a 0.05 M $ZnCl_2$ acetone / water solvent mixture is recommended for the recycling of this CFRP and may also be suitable for the recovery of carbon fibres from alternative polymer matrices.

5.6 Concluding Remarks

Fibres processed at 11 different recycling conditions have been characterised in order to assess their suitability for reuse in a new composite material. To directly compare the influence of the recycling processes on the fibre quality, virgin Toray T700S carbon fibres and fibres with the sizing removed using Soxhlet extraction were also analysed. The characterisation techniques employed include SEM to visually confirm the removal of all resin and XPS to study the change in functional groups on the fibre surface. The mechanical properties were also investigated through single fibre tensile tests which allowed both the changes in tensile strength and modulus to be determined.

SEM micrographs demonstrated that with the neat acetone / water solvent, it was possible to obtain fibres completely free of resin at temperatures above 330˚C and a process time of 90 min. However, upon increasing the temperature to 340˚C, small fissures were visible on the surface of fibres which may act as failure points and, therefore, reduce the tensile strength of the material. Although relatively low concentrations of $ZnCl_2$, $MgCl_2$ and $AlCl_3$ were used, there was evidence of the catalyst

depositing on to the surface of the fibres. Elemental analysis using EDX confirmed the presence of zinc, magnesium, aluminium and chlorine in the stoichiometric proportions expected. As these salts may influence the properties of a new composite material, it is desirable to remove them from the fibre surface. This was easily achieved by rinsing the fibres with water at ambient conditions due to their high solubility in this medium and confirmed using EDX. The findings in this chapter therefore confirms the results presented in Chapters 3 and 4: the metal chlorides investigated do facilitate the recovery of clean fibres at lower operating temperatures and in shorter process times than those necessary for a neat acetone / water solvent mixture.

XPS identified significant changes in the functionality of the fibre surface when compared to both virgin fibres and fibres with the sizing removed via Soxhlet extraction. All process conditions increased the RA of nitrogen detected at the fibre surface, possibly due to the removal of the sizing and / or outer graphitic planes of the fibre thus exposing the nitrile groups present within the PAN based fibres. Compared to the neat acetone / water solvent, the catalyst systems considered generally resulted in a greater increase in the abundance of nitrogen and may, therefore, improve the interfacial properties of the fibres. There was, however, no obvious correlation between the relative abundance of oxygen and process conditions. With the exception of the $AlCl_3$ system at 290˚C, all processes resulted in a reduction in the surface concentration of oxygen: the largest and smallest changes of 9.0 and 2.8% were observed for the $ZnCl_2$ solution at 290˚C and the neat solvent mixture at 340˚C respectively. When also considering changes in the C-O-C and O-C=O moiety, it appears that the conditions

which are most similar to the SCF fibres (and, therefore, most likely to adhere to a new sizing material) are those processed with the neat solvent mixture at 360˚C, the 0.05 M $ZnCl_2$ solution at 300˚C and the 0.05 M $MgCl_2$ system at 290˚C.

The mechanical properties of the fibres were quantified through single fibre tensile tests and the resulting data sets were fitted to a Weibull distribution in order to calculate the scale and shape parameters. The values of these parameters determined from a linear regression line showed good agreement with the estimates found from MINITAB™ and thus suggests that both approaches are suitable. At 320 and 330˚C, the neat acetone / water solvent is able to maintain a similar tensile strength to that of the virgin fibre with the sizing removed, although higher process temperatures result in a reduction of strength by up to 12.4%. A similar decrease is observed in the presence of $AlCl_3$, while $MgCl_2$ appears to have little influence on the quality of the recovered fibres under the conditions investigated. The inclusion of $ZnCl_2$ at a concentration of 0.05 M has a positive effect on the strength and modulus with both properties increasing by up to 22%. By considering the RA of the surface functional groups, it is apparent that a 0.05 M $ZnCl_2$ solution heated to 300˚C for 45 min is able to obtain the highest quality fibres of all the recycling conditions investigated.

The research presented thus far has identified novel solvent / catalyst systems and the conditions necessary for the recovery of carbon fibres. This chapter has also quantified the changes in the surface and mechanical properties of the fibre as a result of the recycling processes, however, the action of the solvent and the catalysts is not yet

well understood. In order to address this, chapter 6 describes the analysis of the organic liquid products (OLPs) with the aim of identifying the compounds and chemical bonds present.

CHAPTER 6.
ORGANIC PRODUCT ANALYSIS

6.1 Introduction

One of the key advantages of solvolytic recycling techniques over pyrolytic processes is the retention of a potentially useful mixture of valuable organic compounds. Depending on the polymer matrix used in the composite material, these organic products are likely to differ when processing different CFRPs and thus need to be identified before a suitable separation process can be designed. This chapter aims to analyse the organic liquid products (OLPs) which were recovered from the reactor after processing the CFRP investigated at each of the minimum conditions necessary to fully degrade the epoxy resin. These conditions are listed in Table 22, Chapter 5. As the initial formulation of this resin is held in commercial confidence, it is not possible to use the resulting data to confirm the action of the solvent and catalysts. For this reason, this chapter also describes the synthesis of a typical thermoset epoxy resin and identifies the key products obtained following its decomposition, also using the conditions listed in Table 22, Chapter 5.

This chapter is structured using a similar approach to Chapters 3 and 5 where the methodology used to manufacture and characterise a typical epoxy is first described, followed by the analytical techniques employed to analyse the OLP recovered from both the model resin and the CFRP. Although two different materials are considered in this chapter, the methods used for the analysis are the same and are described in Section

6.2. Section 6.3 considers the key products that were obtained from the CFRP while Sections 6.4 and 6.5 relate to the characterisation of the model epoxy and its decomposition products.

6.2 Experimental Methodology

6.2.1 Materials

The epoxy prepolymer selected to synthesise a model resin was a high purity diglycidyl ether of bisphenol A (DGEBA), Dow D.E.R 332 (Dow Chemical Company, USA) with an epoxy equivalent weight of 171 to 175 g eq^{-1}. This means that in every 171 to 175 g of DGEBA, there is 1 mol of reactive epoxy groups. The stoichiometry of the curing reaction with diamine 4,4'-diamonodiphenyl sulphone (DDS) is 1:1. To ensure that there is no excess or surplus of either component which leads to a reduction in mechanical properties as described in section 2.3.2, it is desirable to mix the two compounds together in the ratio 0.58 : 0.42 w/w DGEBA : DDS. The molecular structure of each compound is shown in Figure 2, Chapter 2 and is repeated overleaf. Both materials were supplied by Sigma Aldrich (UK) and used as delivered. These precursors were chosen to manufacture the model epoxy resin as they are commonly used to manufacture thermoset composite materials as well as the relative simplicity of their bonding network. A resin based on this formulation has also been investigated in previous work [252] thus allowing for direct comparison with this research. In addition to the polymer precursors, a PVA Mould Release Agent was supplied by Easy Composites (UK) to facilitate easy removal of the resin from the mould.

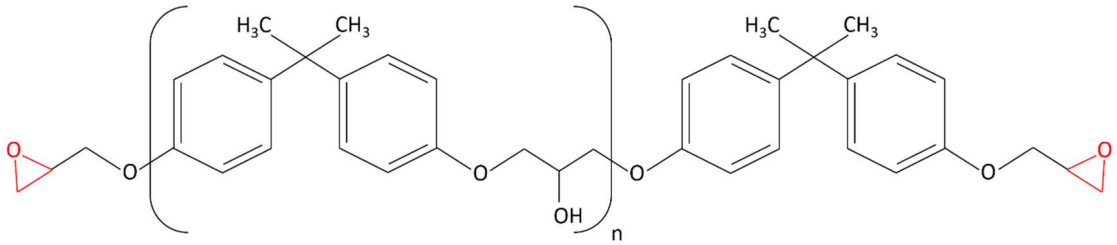

a)

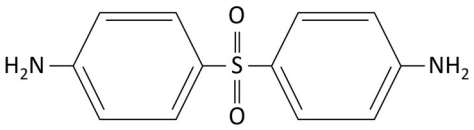

b)

Figure 2*. Molecular structure of a) DGEBA; and b) DDS* [252].

The solvent systems used in the degradation experiments comprised of the same acetone / water solvent mixture described in detail in Chapter 3. This was supplied neat and in the presence of 0.20 M KOH and NaOH, 0.05 M $ZnCl_2$ and $MgCl_2$ and 0.005 $AlCl_3$.

6.2.2 Model Resin Synthesis

DGEBA is a highly viscous liquid at ambient conditions and was, therefore, gently warmed in an oven to 70˚C before pouring 79.25 g into a glass beaker. This was heated to 115 ± 5˚C on a magnetic hot-plate (Fisher Scientific, UK) and stirred at 340 rpm. While stirring, 61.64 g of DDS was added, giving a proportion of DGEBA : DDS of 0.56 : 0.44 w/w resulting in a slight excess of DDS. The temperature and mixing speed were maintained for 60 min, after which a colourless solution was obtained. This mixture was poured into an aluminium tray which had been coated beforehand with the PVA Mould Release agent. The tray was placed in a Lenton WF120 oven (Lenton, UK) to thermally

cure the resin by heating from 30 to 250˚C at a rate of 1˚C min^{-1} and holding at the maximum temperature for 70 min. The mixture was allowed to cool inside the oven overnight and, when the temperature had returned to approximately 25˚C, the tray was removed. The molecular structure of the cured resin was provided in Figure 2, Chapter 2 and is also shown below. In preparation for experimentation, samples measuring (18 ± 2) x (13 ± 2) x (5 ± 1) mm were cut using a diamond-edge rotary saw.

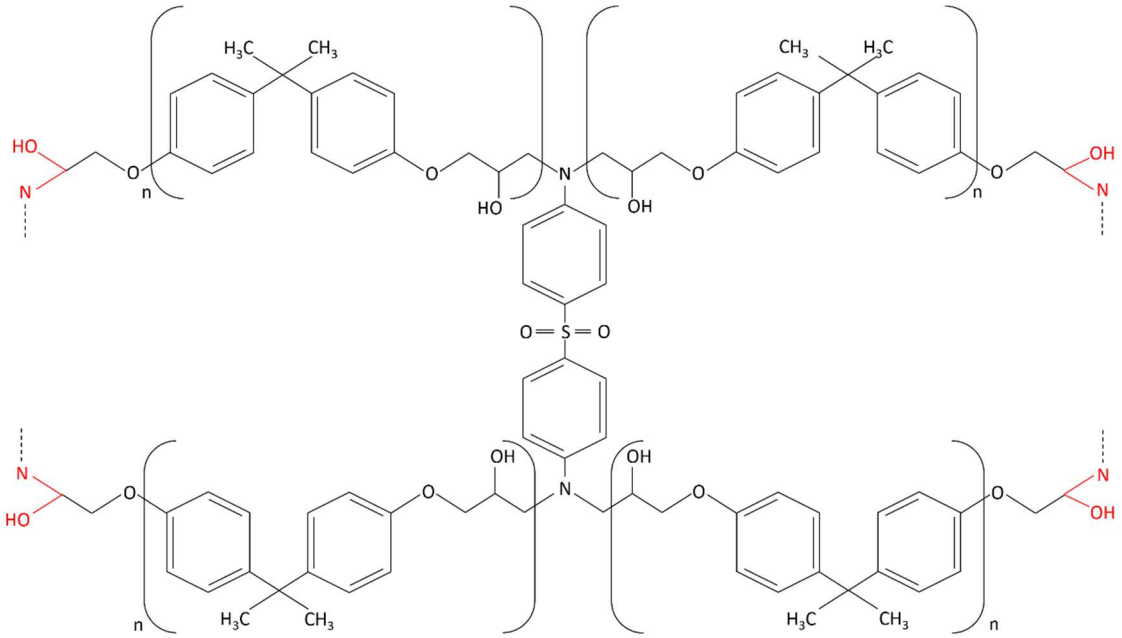

***Figure 2**. c) Molecular structure of cured DGEBA-DDS resin* [252].

6.2.3 Model Resin Characterisation

The model resin was thermally analysed using TGA Method 1 and DSC Method 1, both of which are described in detail in Chapter 3, Section 3.2.2. For both techniques, 3 samples in the mass range 10 to 15 mg were investigated and used to determine the peak degradation and glass transition temperatures. DGEBA, DDS and the cured resin

were also analysed using Fourier-Transform Infrared Spectrometry (FTIR) as described in Section 6.2.6.

6.2.4 Resin Decomposition

A single piece of the model resin was placed into a stainless steel basket before being loaded into the reactor system described in Section 3.2.3. The methodology followed for the decomposition of this model resin is the same as that used for the investigation of the CFRP as detailed in Chapter 3. The conditions investigated for the degradation of the CFRP and the model epoxy resin are listed in Table 26. These are the minimum necessary reaction time and temperature which gave an *RD* of > 92% for the CFRP when using the neat acetone / water solvent, 0.05 M $ZnCl_2$, 0.05 M $MgCl_2$ and 0.005 M $AlCl_3$ solvent systems. In addition, samples of the OLP obtained following the partial decomposition of the CFRP using 0.20 M KOH and NaOH solutions were also analysed. These conditions were selected for investigation as they resulted in the highest *RD* for the basic additives.

***Table 26**. Reaction conditions used to process the CFRP and model epoxy resin to generate an OLP mixture for GC-MS and FTIR analysis.*

Additive	Sample Reference	Temperature, T_R (˚C)	Pressure, p (MPa)	Reaction time, t_R (min)
None	N-320	320	19.7	120
	N-330	330	22.0	90
	N-340	340	23.5	45
	N-360	360	27.0	15
	N-380	380	30.0	0
0.20 M KOH	K-300	300	16.0	60
0.20 M NaOH	Na-300	300	16.0	60
0.05 M $ZnCl_2$	Z-290	290	14.5	90
	Z-300	300	16.0	45
0.05 M $MgCl_2$	M-290	290	14.5	90
	M-300	300	16.0	45
0.005 M $AlCl_3$	A-290	290	14.5	90
	A-300	300	16.0	45

6.2.5 Gas Chromatography – Mass Spectrometry (GCMS)

Gas chromatography coupled with time-of-flight mass spectrometry (GC-TOF MS) is a common analytical technique used to separate, and subsequently identify, a wide range of compounds. The OLP was recovered from the reactor after processing both the CFRP and the model epoxy resin at the conditions specified in Section 6.2.4. Prior to analysis, the OLP was diluted at a ratio of 1:30 v/v using the same acetone / water solvent mixture used in the reaction (ratio of 80:20 v/v). Assuming complete

decomposition of the resin, this gave a solution with a concentration of the OLP of approximately 1 mg mL^{-1}.

GCMS analysis was conducted using a Waters Micromass GCT Premier (Waters Corporation, USA) in conjunction with a ZB-WAX column (Phenomenex, USA). The heating rate was set to 10˚C min^{-1} up to a maximum temperature of 300˚C and the system was held at this temperature for 30 min; this heating profile is referred to as GCMS Method 1 and is illustrated by Figure 83. Each peak in the chromatogram obtained represented a different compound, the identity of which was confirmed by comparing the mass spectrometry fragmentation pattern with that found in MassLynx software provided by the National Institute of Standards and Technology (NIST, USA). This comparison is automated with the software providing a probability of the suggested molecule being present in the mixture, although each spectrum was also checked manually.

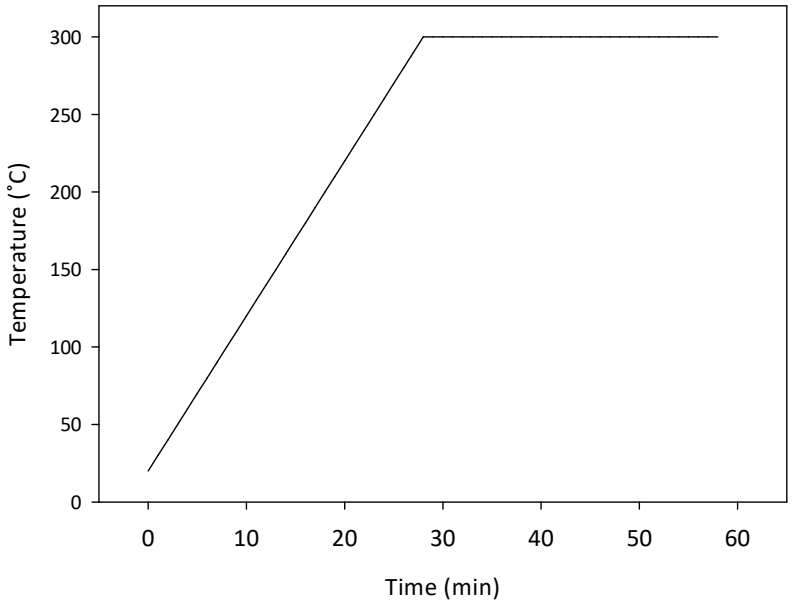

***Figure 83**. Heating profile for GCMS Method 1.*

6.2.6 Fourier-Transform Infra-red Spectrometry

To gain further insight into the reaction mechanism, the change in the chemical bonds present in the OLP was observed through Fourier-Transform Infra-red Spectrometry (FTIR). Samples of the OLP characterised with this technique were recovered from the same experiments as those analysed with GC-MS. In addition to these, samples of the DGEBA pre-polymer, DDS cross-linking agent and the cured model resin were also investigated. FTIR was carried out using a Jasco FTIR-6300 spectrometer (Jasco Corporation, USA) which was equipped with an Attenuated Total Reflectance (ATR) or "Golden Gate" accessory (Specac, UK). As the OLP contained water and there is a strong absorption band in the range of 3700 – 3100 cm^{-1} due to the presence of O-H bonds [312], samples were dried at 100˚C overnight in a Gallenkamp OVL570 vacuum oven (Sanyo Gallenkamp, UK). This ensured that any O-H groups detected will be

associated with the degradation products and not due to any residual solvent within the sample. It also means that any volatile components will be lost, however, these compounds should be identified through analysis of the OLP using GC-MS. FTIR spectroscopy data was obtained using wavenumbers over the range of 4000 to 800 cm^{-1} with a resolution of 4 cm^{-1}, 128 accumulations per sample and an aperture of 3.5 mm. The spectra obtained were processed using Spectra Analysis software provided by Jasco. Each curve was smoothed using the Savitzky-Golay method and a convolution width of 19. The peaks observed were identified and labelled within the software and analysis was carried out using Larkin, 2018 [312].

6.3 Analysis of Organic Products from the CFRP

6.3.1 Gas Chromatography – Mass Spectrometry

Analysis of the OLP recovered after processing the CFRP at the conditions listed in Table 26 identified the presence of a wide range of organic compounds, mostly comprising aryls and amine derivatives. Peaks with an intensity of less than 10% of the maximum were not considered to represent major decomposition products and are, for this reason, excluded from the analysis presented in this chapter. A complete set of the chromatograms obtained following the GC-MS of the OLP recovered after processing the CFRP at each of the conditions considered (shown in Table 26) is provided in Appendix 5.

The chromatogram for the OLP recovered following a reaction with the neat acetone / water solvent at 320˚C is shown in Figure 84 and the compounds are named

in Table 27. When using this solvent system, the product mixture obtained was similar at all conditions investigated with the most abundant compound identified in all cases as 4-methyl-3-penten-2-one (10.88 min). However, it is not thought that this compound is a result of the decomposition reaction and may be due to the self-condensation of the acetone used as part of the solvent mixture. Although this reaction, illustrated by Figure 85, normally requires the presence of a basic [313] or metal oxide [314] catalyst, it is possible the high temperatures and pressures used resulted in its formation.

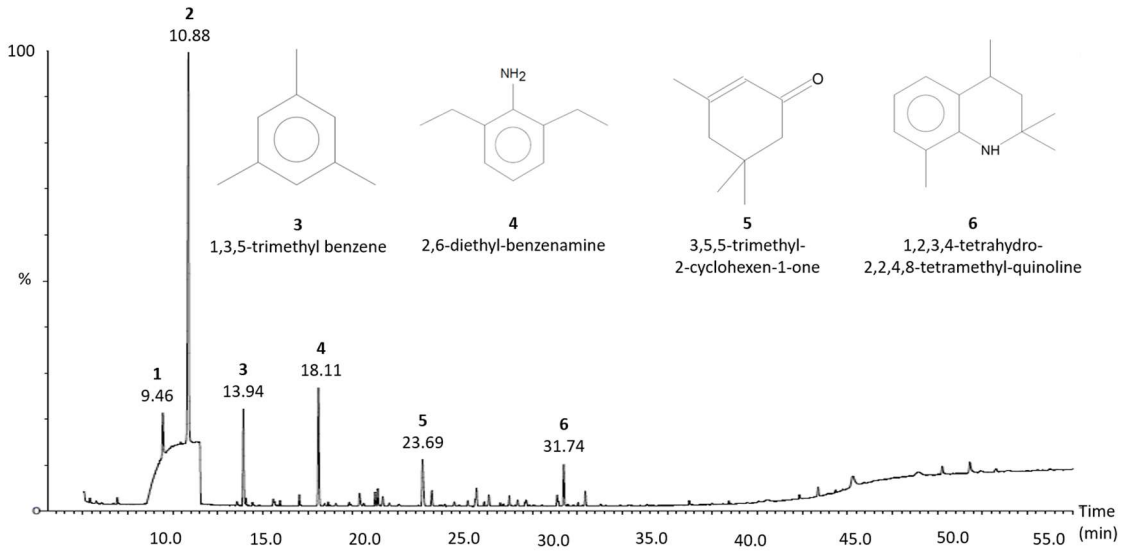

***Figure 84**. GC-MS chromatogram of the OLP recovered after processing the CFRP at 320˚C for 120 min with the neat acetone / water solvent.*

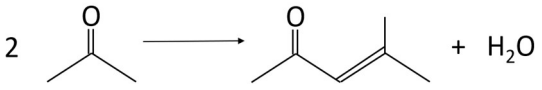

***Figure 85**. Self-condensation of acetone to form 4-methyl-3-penten-2-one and water.*

***Table 27**. Summary of organic compounds identified in the OLP recovered after processing the CFRP at 320˚C for 120 min with the neat acetone / water solvent. Probability from NIST MassLynx library software. Compounds in italics thought to originate from reaction of the solvent.*

Peak no.	Compound	Probability
1	*4-methyl-4-penten-2-one*	*63.6*
2	*4-methyl-3-penten-2-one*	*54.7*
3	Trimethyl benzene	72.7
4	2,6-diethyl-benzenamine	93.4
5	*3,5,5-trimethyl-2-cyclohexen-1-one*	*48.3*
6	1,2,3,4-tetrahydro-2,2,4,8-tetramethyl-quinoline	72.1

The major products from the decomposition of the resin have been identified as trimethyl benzene (13.94 min), 2,6-diethyl-benzenamine (18.11 min) and 1,2,3,4-tetrahydro-2,2,4,8-tetramethyl-quinoline (31.74 min). 3,5,5-trimethyl-2-cyclohexen-1-one was also identified at 23.69 min and may be due to the further reaction of 4-methyl-3-penten-2-one with acetone [315]. The structure of each molecule is also shown within Figure 84. Attention is drawn in particular to the presence of trimethyl benzene as it was not possible to determine the exact position of the methyl branches. 1,3,5- , 1,2,3- and 1,2,4- isomers all have similar mass spectrometry fragmentation patterns and the NIST Library software gave the same probability that each molecule was present in the OLP. Due to time and budget constraints, it was not possible to compare GCMS data of each of the pure compounds with Figure 84. As amines are frequently used as cross-linking agents in epoxy resins, it is unsurprising that numerous nitrogen-containing compounds have been identified.

Although all chromatograms obtained when using the neat acetone / water solvent were similar, it should be noted that additional molecules such as aniline and pyrazoles were also identified at higher reaction temperatures. For this reason, it appears that temperatures in the range of 340 to 380˚C do not act to reduce the number of different products in the organic mixture and it is, therefore, preferable to lower the reactor temperature when considering the downstream processing that is necessary to separate the mixture into high purity products.

The chromatograms of the OLP recovered from experiments using a 0.20 M KOH acetone / water solvent is shown in Figure 86 and is very similar to that obtained using a NaOH additive. A summary of the compounds identified and the associated probability of that molecule identified is listed in Table 28. 4-methyl-3-penten-2-one (Figure 86, Peak 2) was again detected in both cases, however the presence of OH- ions also resulted in the formation of 4-hydroxy-4-methyl-pentan-2-one (Figure 86, Peak 8) and, compared to the neat solvent mixture, there is a greater abundance of 3,5,5-trimethyl-2-cyclohexen-1-one (Figure 86, Peak 5). Under alkaline conditions, acetone more readily undergoes aldol condensation [289] and it is, therefore, unsurprising that both compounds were present in the OLP. Although the results presented in Chapter 3 demonstrated that alkaline catalysts do not accelerate the decomposition reaction, the carbon atom adjacent to the oxygen within the epoxy functional group can undergo nucleophilic substitution under basic conditions. This results in the cleavage of the C-O bond and liberates the local R-groups [313]. A compound unique to the alkaline systems however, was 3,5-dimethyl phenol (Figure 86, Peak 10) and it is possible that one of the

methyl groups of the trimethyl benzene detected in the neat solvent has undergone nucleophilic substitution due to the presence of OH- ions.

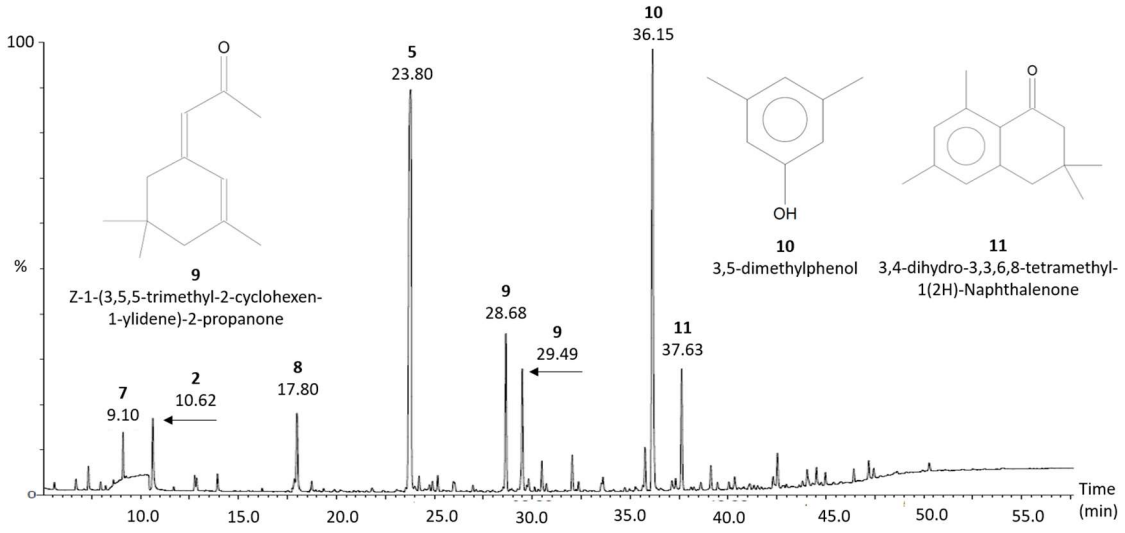

***Figure 86**. GC-MS chromatogram of the OLP recovered after processing the CFRP at 300˚C for 60 min using a 0.20 M KOH acetone / water solvent.*

***Table 28**. Summary of all organic compounds identified in the OLP recovered after processing the CFRP at 300˚C for 60 min with the 0.20 M KOH acetone / water solvent. Probability from NIST MassLynx library software. Compounds in italics thought to originate from reaction of the solvent.*

Peak no.	Compound	Probability
2	*4-methyl-3-penten-2-one*	*64.9*
5	*3,5,5-trimethyl-2-cyclohexen-1-one*	*50.3*
7	*3-Methylene-1,5,5-trimethylcyclohexene*	*68.2*
8	*4-hydroxy-4-methyl-pentan-2-one*	*93.7*
9	*Z-1-(3,5,5-trimethyl-2-cyclohexen-1-ylidene)-2-propanone*	*71.7*
10	3,5-dimethylphenol	65.1
11	3,4-dihydro-3,3,6,8-tetramethyl-1(2H)-Naphthalenone	59.6

The chromatogram obtained for the NaOH system is provided in Appendix 5 and, although this additive achieved a higher value of *RD*, the range of products obtained is significantly smaller. This suggests that KOH facilitates a number of additional side reactions which may result in more complex downstream processing if considering the use of an alkaline catalyst in an alternative solvent system.

For all conditions investigated, $ZnCl_2$, $MgCl_2$ and $AlCl_3$ all resulted in a similar product mixture. Example chromatograms for the products obtained from each solvent system after processing the CFRP at 300˚C for 45 min are shown in Figure 87 to Figure 89. A summary of all the compounds identified when using these catalysed systems is provided in Table 29.

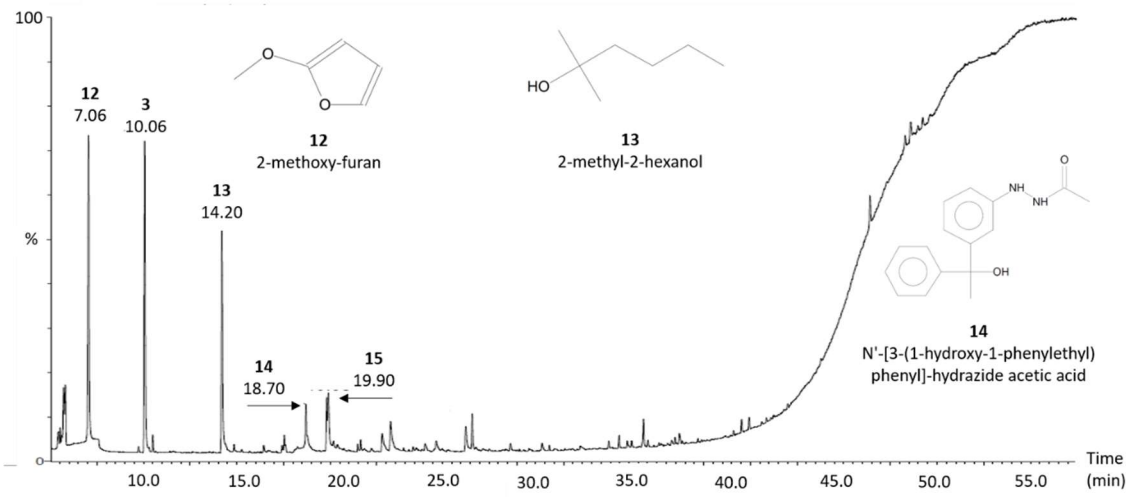

Figure 87. *GC-MS chromatogram of the OLP recovered after processing the CFRP at 300˚C for 45 min using a 0.05 M $ZnCl_2$ acetone / water solvent.*

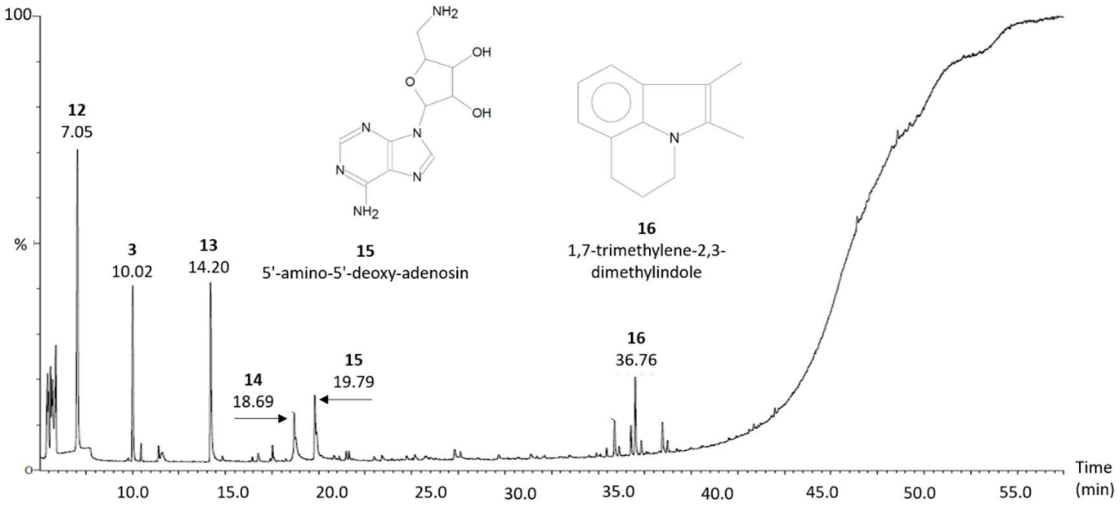

***Figure 88**. GC-MS chromatogram of the OLP recovered after processing the CFRP at 300˚C for 45 min using a 0.05 M $MgCl_2$ acetone / water solvent.*

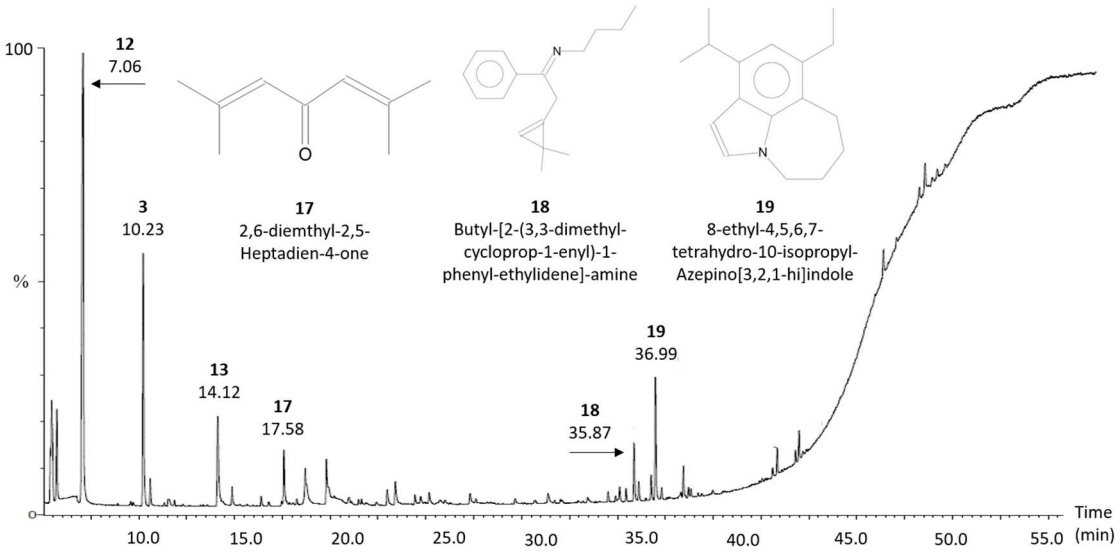

***Figure 89**. GC-MS chromatogram of the OLP recovered after processing the CFRP at 300˚C for 45 min using a 0.005 M $AlCl_3$ acetone / water solvent.*

***Table 29**. Summary of all organic compounds identified in the OLP recovered after processing the CFRP at 300˚C for 45 min with 0.05 M $ZnCl_2$, 0.05 M $MgCl_2$ and 0.005 M $AlCl_3$ acetone / water solutions. Probability from NIST MassLynx library software.*

Peak no.	Compound	Probability		
		$ZnCl_2$	$MgCl_2$	$AlCl_3$
3	Trimethyl benzene	81.6	86.7	82.5
12	2-methoxy-furan	58.4	54.5	64.2
13	2-methyl-2-hexanol	75.4	40.4	57.1
14	N'-[3-(1-hydroxy-1-phenylethyl)phenyl] hydrazide acetic acid	52.4	48.2	-
15	5'-amino-5'-deoxy-adenosin	88.6	44.2	-
16	1,7-Trimethylene-2,3-dimethylindole	-	52.9	-
17	2,6-dimethyl-2,5-Heptadien-4-one	-	-	85.5
18	Butyl-[2-(3,3-dimethyl-cycloprop-1-enyl)-1-phenyl-ethylidene]-amine	-	-	49.8
19	8-ethyl-4,5,6,7-tetrahydro-10-isopropyl-Azepino[3,2,1-hi]indole	-	-	71.9

As previously identified in Figure 84 and Figure 86, trimethyl benzene (Peak 3) was also obtained as the major degradation product. Peak 12 in Figure 87 represents 2-methoxy-furan, the presence of which may be explained by the Diels-Alder reaction. Dienes, originating from the resin, readily react to form hetero-aromatic compounds, such as furan (and its derivatives) in the presence of weak Lewis acids [316]. 2-methyl-2-hexanol is the third most abundant compound identified and was possibly formed due to the cleavage of branched groups from the cyclic structures. The smaller peaks (numbered 14 and 15 in Figure 87) are due to the much larger compounds N'-[3-(1-hydroxy-1-phenylethyl)-phenyl]-hydrazide acetic acid and 5’-amino-5’-adenosin. As

trimethyl benzene has been identified, it is apparent that these molecules are liberated due to the cleavage of bonds within the benzene skeleton, thereby leaving the amine groups from the cross-linking agent bonded to benzene. This therefore suggests that, although solvolysis can recover a mixture of potentially useful organic compounds, it is unlikely that the original monomers used to manufacture the thermoset resin can be obtained.

The use of $MgCl_2$ and $AlCl_3$ as catalysts yielded higher concentrations of molecules with much higher molecular weight. These are identified in Figure 88 as Peak 16 and in Figure 89 as Peaks 18 and 19. This suggests that 0.05 M $ZnCl_2$ more effectively cleaves the bonds within the epoxy network which, therefore, results in smaller compounds. However, it should be noted that $AlCl_3$ was supplied at a concentration an order of magnitude lower and, as shown by the results presented in Chapter 3, was able to achieve a similar *RD* to the $ZnCl_2$ system under the same reaction conditions. The presence of the hetero-aromatic compounds 1,7-trimethylene-2,3-dimethylindole (Peak 16) and 8-ethyl-4,5,6,7-tetrahydro-10-isopropyl-Azepino[3,2,1-hi]indole (Peak 19) in the product mixture is likely formed as a branched amine group bonded to the benzene ring was closed as a result of the presence of the weak Lewis acids. This also explains how the hetero nitrogen atom came to be included within the cyclic structure [316].

6.3.2 Fourier-Transform Infra-red Spectrometry

The dried OLP recovered from selected conditions were characterised through FTIR, the spectra of which are shown in Figure 90 and Figure 91. Peaks were analysed using Larkin, 2018 [312]. In all cases, there is a broad band between wavenumbers of 3650 to 3150 cm^{-1} which is indicative of the stretching of O-H bonds. Although this may be due to some residual solvent, the GCMS data demonstrated the presence of compounds containing hydroxy and amino functional groups. It is, therefore, not surprising that there is a strong infrared absorption in this region. A doublet, which would confirm the presence of the secondary amines identified by GCMS, is not observed. However, this is a relatively weak signal and may be lost in the more intense band caused by O-H bonds. Also not visible in the FTIR spectra are peaks between 3060 to 2990 and 1200 to 1245 cm^{-1} which would highlight the presence of an epoxy functional group. This suggests that the resin in the CFRP investigated was fully cured.

The doublet identified at 2960 and 2865 cm^{-1} in both Figure 90 and Figure 91 are likely due to the out-of-phase and in-phase stretching of methyl groups while the additional peaks at 1455 and 1377 cm^{-1} are representative of the bending vibrations of the C-H bonds. The FTIR spectra also confirm the presence of the cyclic compounds which were identified by GCMS: the peak at 2920 cm^{-1} is characteristic of aryl CH_2 groups while the peaks at 1620, 1500 and 1450 cm^{-1} are typical of the stretching of C-C rings. Furthermore, all spectra indicate the presence of olefins due to the peak at 1690 cm^{-1} which is indicative of the stretching of C=C double bonds [312].

One of the most significant differences between the spectra is the presence of a large peak at 1660 and 1500 cm^{-1} only when KOH or NaOH is added to the solvent system. These peaks are highlighted in Figure 90 and are due to the presence of C=N and C-NH respectively [312]. These results suggest that temperatures in excess of 320˚C or metal chlorides at a temperature of above 290˚C are capable of cleaving the C=N double bonds which are commonly present in an epoxy resin. Figure 91 does demonstrate evidence of an aryl N-H group, thus supporting the GC-MS results obtained after the decomposition reaction with all three weak Lewis acids. If these compounds are not present as part of the epoxy matrix, it is possible that they can form through the nucleophilic substitution of amines into existing cyclic compounds [317], thereby explaining the presence of C-N bonds despite the effective cleavage by the metal ions.

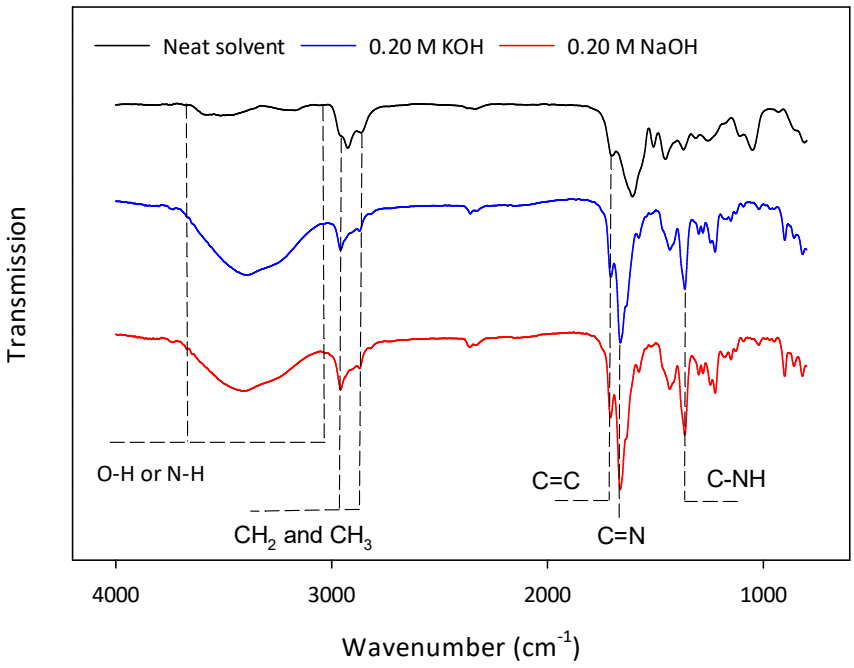

Figure 90. *FTIR spectra of the dried OLP recovered after the decomposition of the CFRP with a neat acetone / water solvent mixture (T_R = 320˚C, t_R = 120 min), a 0.20 M KOH solution ((T_R = 300˚C, t_R = 60 min) and a 0.20 M NaOH solution (T_R = 300˚C, t_R = 60 min).*

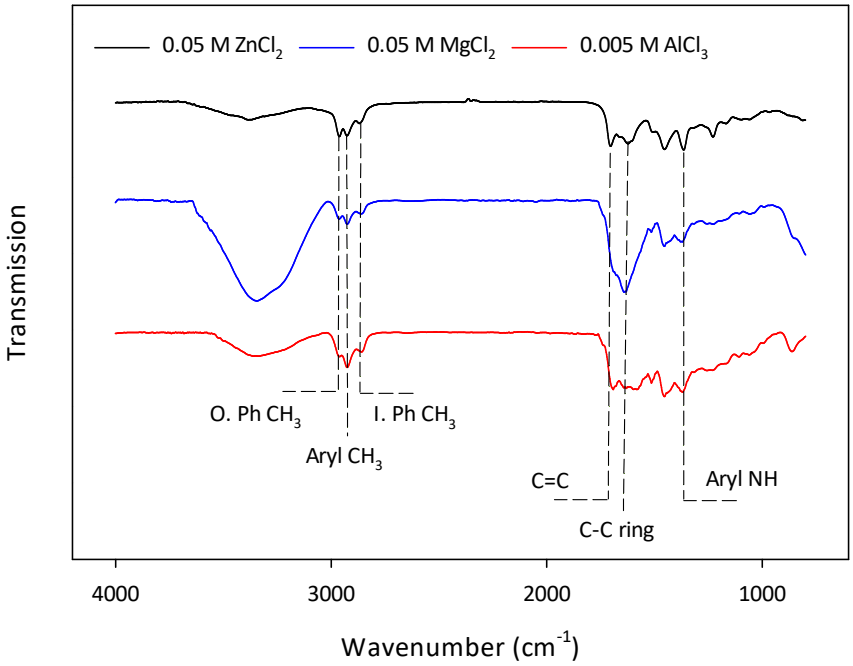

Figure 91. *FTIR spectra of the dried OLP recovered after the decomposition of the CFRP with a 0.05 M $ZnCl_2$, 0.05 $MgCl_2$ and 0.005 M $AlCl_3$ acetone / water solvent (T_R = 300˚C, t_R = 45 min). O. Ph = out-of-phase; I. Ph = In-phase.*

6.4 Characterisation of Model Resin

After curing the DGEBA-DDS mixture, the model resin was characterised using TGA, DSC and FTIR. Example TGA and DSC thermograms are shown Figure 92 and Figure 93 respectively. TGA demonstrated that this resin was very thermally stable and did not show any significant mass loss before reaching 320˚C. Peak degradation was reached at 404 ± 2˚C and, typically, there was 90% mass loss after TGA Method 1 was completed. The residual mass remaining was likely due to the formation of pyrolytic char following the thermal degradation of the resin. DSC demonstrated that the T_g of the resin is 198 ± 5˚C which is within the temperature range reported in previous work [252] and is indicative of a high degree of cross-linking of approximately 0.95 [318].

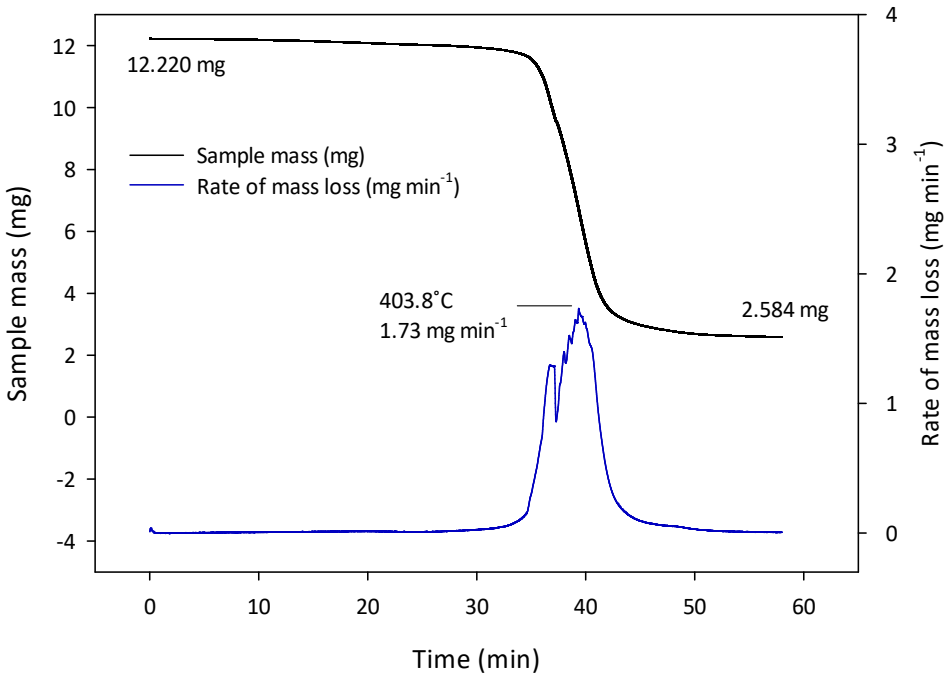

***Figure 92**. Example TGA thermogram of the model resin (sample mass = 12.220 mg).*

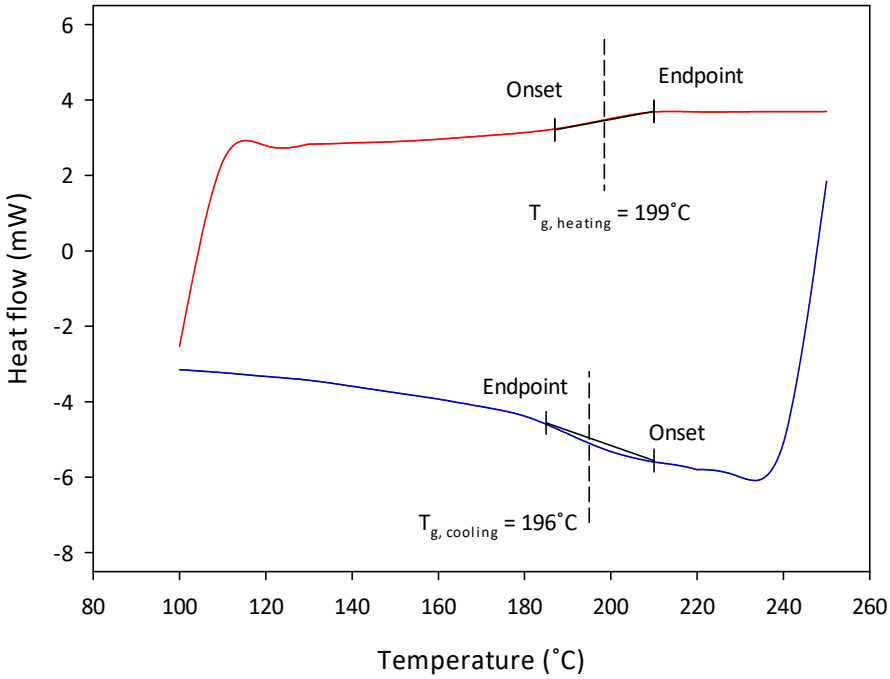

***Figure 93**. Example DSC curve for the model epoxy resin.*

FTIR was used to analyse the as-received DGEBA and DDS and the cured resin in order to identify the major functional groups present. The spectra of all three compounds are shown in Figure 94 and act as a reference when comparing the change in the chemical structure as a result of the decomposition reaction. The spectra obtained for DGEBA and DDS are very similar to those available in the open literature [319] with strong peaks at 1615 and 1500 cm^{-1} which represent stretching of the aromatic C=C and C-C bonds respectively [312]. Furthermore, there is also evidence of the expected carbonyl functional group at 1230 cm^{-1}. Somewhat surprisingly, the singlet and doublet between 2975 and 2870 cm^{-1} which indicate the presence of aromatic and aliphatic C-H bonds are only prevalent in the spectra for DGEBA. It is possible that these relatively weak signals are overshadowed by the stretching of N-H bonds in the DDS. As a primary amine, this is represented by the doublet at 3300 cm^{-1} and a second peak at 1625 cm^{-1} due to the bending vibration. Also unique to DGEBA is a small peak at 3057 cm^{-1} which is characteristic of the stretching of the C-H group within an oxirane ring. Further evidence of an epoxy functional group is shown by the small, sharp peak at 909 cm^{-1} due to the stretching of the C-O bond [319]. The sharp peak at 1060 cm^{-1} present in both DDS and the cured resin is indicative of sulphinyl (S=O) bonds. As previous work has noted a characteristic smell of hydrogen sulphide following the degradation of this epoxy resin [252] it is hypothesised that this peak will not be visible in the spectra obtained from the dried OLP recovered following the decomposition reaction.

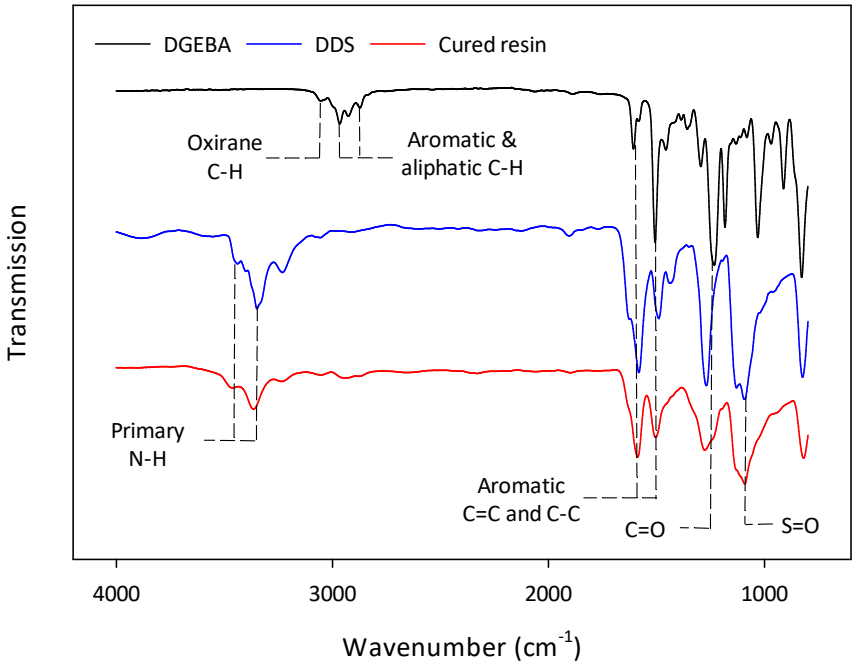

***Figure 94**. FTIR spectra of as-received DGEBA and DDS and the cured epoxy resin.*

6.5 Analysis of Organic Products from Model Resin

6.5.1 Gas Chromatography – Mass Spectrometry

A set of 11 different reaction conditions were selected for the decomposition of the DGEBA-DDS resin based on their ability to fully degrade the CFRP. Each condition considered was also able to fully solubilise this model resin as there were no solids remaining in the reactor following each of the reactions. The GC-MS chromatograms of the OLP obtained for all cases are similar and examples for each solvent system considered are provided in Figure 95 to Figure 98. Table 30 and Table 31 also provides a summary of each of the compounds present in the OLP following the decomposition of the model epoxy.

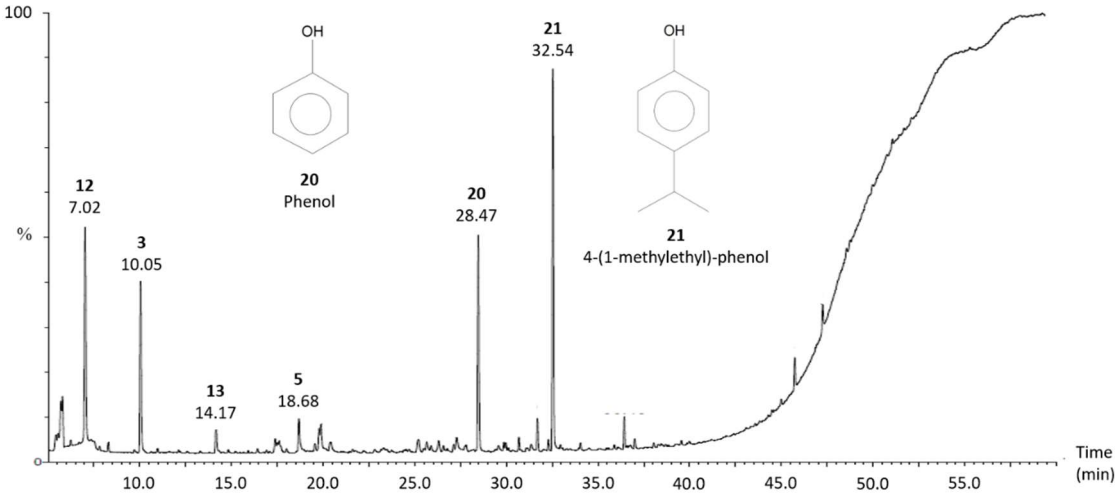

***Figure 95**. GCMS chromatogram of the OLP recovered after processing the model DGEBA-DDS resin at 320˚C for 120 min with an acetone / water solvent.*

***Table 30**. Summary of all organic compounds identified in the OLP recovered after processing the model epoxy resin at 320˚C for 120 min with the neat acetone / water solvent. Probability from NIST MassLynx library software. Compounds in italics thought to originate from reaction of the solvent.*

Peak no.	Compound	Probability
3	Trimethyl benzene	81.9
5	*3,5,5-trimethyl-2-cyclohexen-1-one*	*54.7*
12	2-methoxy-furan	57.4
13	2-methyl-2-hexanol	80.0
20	Phenol	48.4
21	4-(1-methylethyl)-phenol	53.2

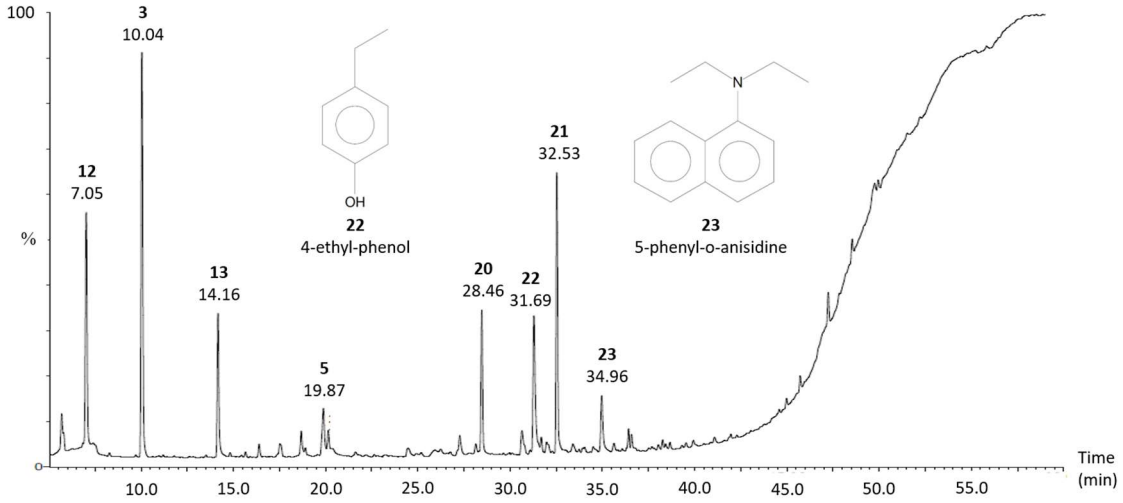

***Figure 96**. GCMS chromatogram of the OLP recovered after processing the model DGEBA-DDS resin at 300˚C for 45 min with an acetone / water solvent and 0.05 M $ZnCl_2$ catalyst.*

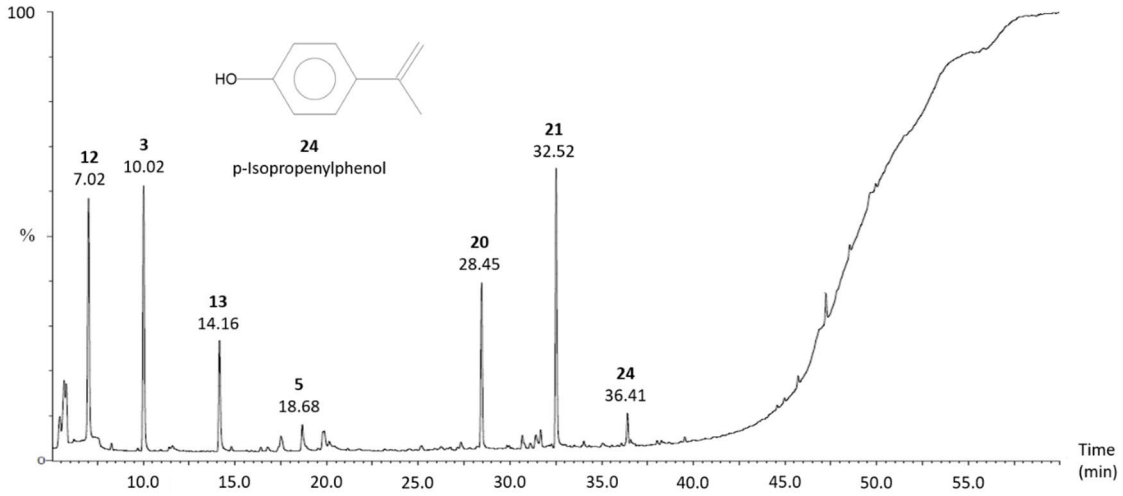

***Figure 97**. GCMS chromatogram of the OLP recovered after processing the model DGEBA-DDS resin at 300˚C for 45 min with an acetone / water solvent and 0.05 M $MgCl_2$ catalyst.*

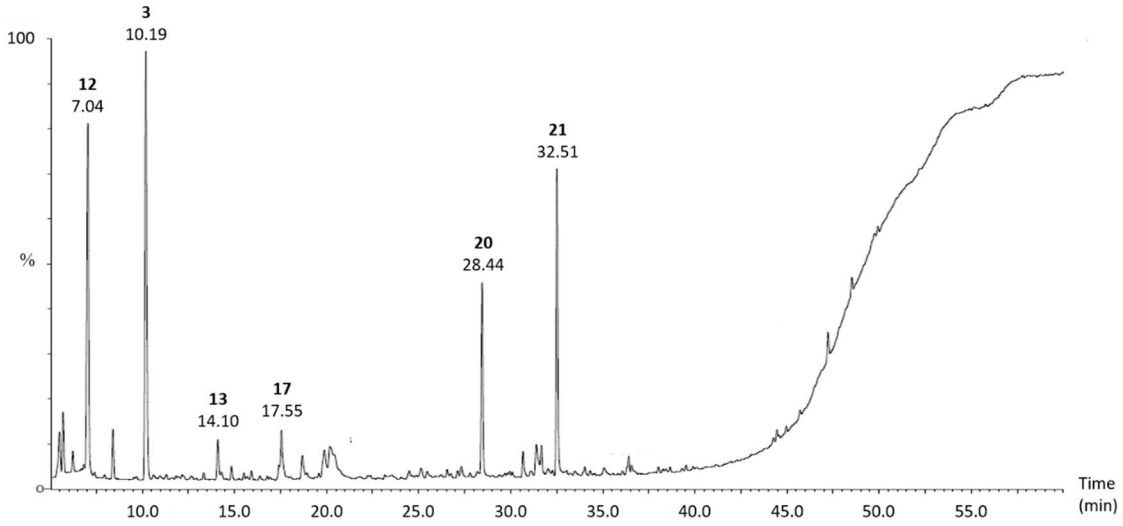

***Figure 98**. GCMS chromatogram of the OLP recovered after processing the model DGEBA-DDS resin at 300˚C for 45 min with an acetone / water solvent and 0.005 M $AlCl_3$ catalyst.*

***Table 31**. Summary of all organic compounds identified in the OLP recovered after processing the model epoxy resin at 300˚C for 45 min with 0.05 M $ZnCl_2$, 0.05 M $MgCl_2$ and 0.005 M $AlCl_3$ acetone / water solutions. Probability from NIST MassLynx library software. Compounds in italics thought to originate from reaction of the solvent.*

Peak no.	Compound	Probability		
		$ZnCl_2$	$MgCl_2$	$AlCl_3$
3	Trimethyl benzene	71.6	79.2	75.9
5	*3,5,5-trimethyl-2-cyclohexen-1-one*	*48.2*	*58.5*	-
12	2-methoxy-furan	81.4	62.4	54.1
13	2-methyl-2-hexanol	42.8	76.4	64.3
17	2,6-dimethyl-2,5-Heptadien-4-one	-	-	76.5
20	Phenol	78.3	47.6	72.7
21	4-(1-methylethyl)-phenol	76.4	62.8	65.4
22	4-ethyl-phenol	62.4	-	-
23	5-Phenyl-o-anisidine	78.8	-	-
24	p-Isopropenylphenol	-	84.5	-

Two classes of compounds were identified, the first of which are believed to be due to a reaction of the solvent. Peaks 5 and 12 which represent 3,5,5-trimethyl-2-cyclohexhen-1-one and 2-methoxy-furan respectively were identified when considering the degradation of both the model epoxy and the RTM6 resin in the CFRP. Their presence is explained in Section 6.3.1. It is, however, surprising that 2-methoxy-furan (Peak 12, Figure 95) was identified as a result of the decomposition of the model resin using the neat acetone / water solvent mixture; this compound was not present following the degradation of the CFRP using the same conditions. As the experiments with the model epoxy were carried out after all of the reactions with the CFRP, it is likely that there was some contamination by the weak Lewis acids used in the reactor. These low concentrations of metal chlorides are still able to facilitate the Diels-Alder reactions of dienes [317].

Products from the decomposition reaction predominantly consist of trimethyl benzene (Peak 3), phenol (Peak 20) and its derivatives (Peaks 21 to 24) as illustrated by Figure 95 to Figure 98. Considering the structure of the epoxy resin (Figure 2), it therefore appears that the neat solvent mixture and weak Lewis acids act in a similar way and effectively cleave both C-C and C-O bonds which liberates the local cyclic structures. Although the mixture of organics is complex, it does appear that all solvent systems considered preserve these cyclic groups well. A similar result was noted when analysing the OLP recovered following the decomposition of the CFRP. Although any gaseous products were not collected, there was also a characteristic smell of hydrogen sulphide gas upon opening the reactor. This explains the absence of sulphur-containing

compounds within the GCMS chromatograms despite the thiol moiety in the chemical structure of the matrix. Both of these findings have been previously reported following the decomposition of a resin with the same formulation and different solvents [252].

Although the chromatograms obtained from the catalysed systems (Figure 96 to Figure 98) are similar, it is apparent that the different additives favour the production of different phenol derivatives. The use of $ZnCl_2$ (Figure 96) results in a wider range of different products compared to $MgCl_2$ and $AlCl_3$. With the former catalyst, 4-ethyl-phenol (Peak 22) was produced in a similar quantity as phenol. A low concentration of 5-phenyl-o-anisidine (Peak 23) was also detected as a result of the reaction of diethyl aniline with another cyclic compound.

Both $MgCl_2$ and $AlCl_3$ appear to homogenise the OLP mixture with just five products identified which appear to have originated from the resin, rather than the solvent. Unlike the OLP obtained from the CFRP, there was no indication of higher molecular weight compounds which demonstrates that, with this resin formulation, $MgCl_2$ and $AlCl_3$ are equally effective at accelerating the decomposition reaction when compared to the 0.05 M $ZnCl_2$ catalyst. $MgCl_2$ is the only additive which yields a significant proportion of p-isopropenyl-phenol which suggests that this catalyst may favour the generation of unsaturated hydrocarbons. Although the resin formulations of the CFRP and the model epoxy are highly likely to be different, 2,6-dimethyl-2,5-Heptadien-4-one (Peak 17 in Figure 89 and Figure 98) was identified following the decomposition of both materials. It was also not observed when using any other solvent

/ catalyst system and may, therefore, be a result of the condensation of three acetone molecules which occurs more readily in the presence of Al^{3+} ions than the other weak Lewis acids investigated [289].

6.5.2 Fourier-Transform Infra-red Spectrometry

The FTIR spectra of the dried OLP obtained following the solubilisation of the model epoxy resin using the neat solvent mixture, 0.05 M $ZnCl_2$, 0.05 M $MgCl_2$ and 0.005 M $AlCl_3$ are shown in Figure 99. Each sample contains a broad peak centred around 3350 cm^{-1} due to the stretching of O-H bonds. This is expected as phenol and its derivatives were identified by GCMS as major products of the degradation reaction. Although this broad peak may mask the vibrations of N-H bonds, there is also no peak visible at 1650 cm^{-1} (due to N-H bending) or at 1340 cm^{-1} which would indicate the presence of amines. These FTIR spectra, therefore, suggest that the concentration of amines is very low and the C-N bonds present in the polymer network are effectively cleaved during the reaction. Previous work has demonstrated that metal ions do facilitate this process [277], [293], however, the data presented also suggests that the action of the acetone / water solvent is similar. It is, therefore, hypothesised that nitrogen is oxidised during the reaction and may be released as a gas upon opening the reactor.

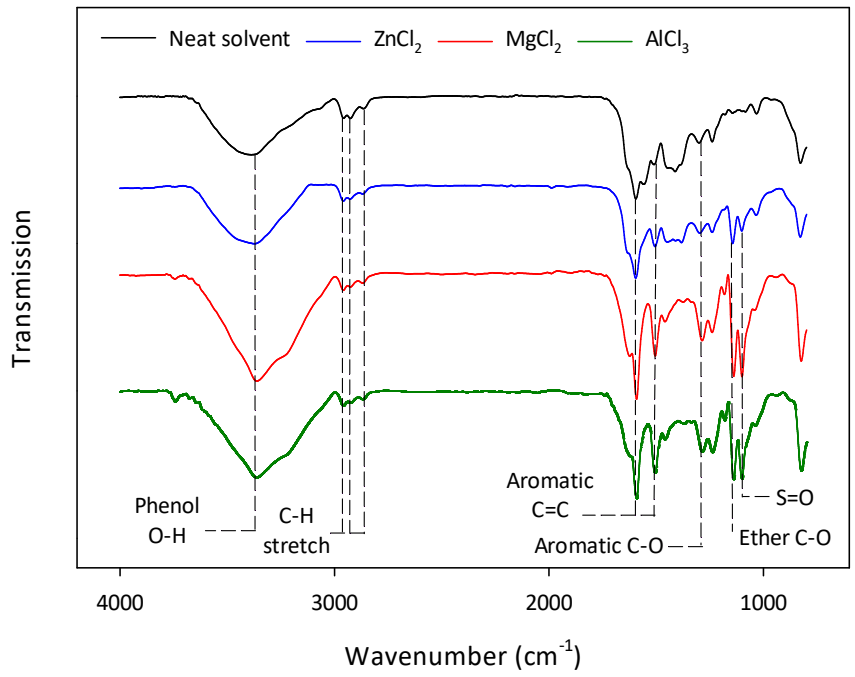

***Figure 99**. FTIR spectra of the dried OLP recovered after the decomposition of the model epoxy resin with a neat acetone / water solvent (T_R = 320˚C, t_R = 120 min) and 0.05 M $ZnCl_2$, 0.05 M $MgCl_2$ and 0.005 M $AlCl_3$ catalysts (T_R = 300˚C, t_R = 45 min).*

Similar to the spectra shown in Section 6.3.2, a triplet is also visible for each of the curves shown in Figure 99 between 2970 and 2860 cm^{-1} due to the out-of-phase and in-phase stretching of C-H bonds. As suggested by the chromatograms in Section 6.5.1, organic cyclic structures are the most abundant class of compound present in the OLP. This is also demonstrated by the sharp peaks visible at 1600 and 1500 cm^{-1} which are due to the stretching of aromatic C=C double bonds. All of the spectra analysed also indicate the presence of C-O bonds, however, there is a significant difference between the products obtained from the neat solvent mixture and when using the metal chloride catalysts. All spectra (including that of the cured resin as shown in Figure 94) display a peak at 1270 cm^{-1}. This is likely due to an aromatic carbonyl functional group as these bonds are present in both the resin network and in the phenolic degradation products.

The second peak at 1140 cm^{-1}, however, is only visible in the OLP recovered following a reaction with metal chlorides and correlates to the aliphatic ether bonds which are present in 2-methoxy-furan. This is a product of a side reaction of the solvent and, therefore, the peak at 1140 cm^{-1} is not due to changes in the chemical structure of the resin.

In the cured epoxy resin, there is a strong peak at 1060 cm^{-1} due to the stretching of the sulphinyl (S=O) bonds and it is this peak, or lack thereof, which represents the most significant difference in the OLP obtained from using the four different solvent systems. There is no evidence of a peak at this wave number from the neat acetone / water mixture and the intensity is significantly lower when $ZnCl_2$ is supplied when compared to the $MgCl_2$ and $AlCl_3$ catalysts. These spectra therefore suggest that the higher temperatures used with the neat solvent and Zn^{2+} ions facilitate the cleavage of the S=O functional group whereas the other metal ions considered do not. It should, however, be noted that upon opening the reactor following all experiments, there was a strong smell of hydrogen sulphide. Sulphur containing compounds were also not identified in any of the GCMS chromatograms presented in Section 6.5.1. For this reason, the concentration of sulphurous material in the OLP appears to be very low, despite the strong peak identified at 1060 cm^{-1} for the $MgCl_2$ and $AlCl_3$ systems in Figure 99.

6.6 Concluding Remarks

The results presented in this chapter demonstrate that the compounds present in the OLP are dependent on the resin used as the matrix material in the CFRP as well as the solvent system used for the degradation. Although the proportion of the compounds appear to differ, the process temperature and reaction time do not have a significant influence on the products generated. Analysis of the OLP recovered from the CFRP and the model epoxy revealed that trimethyl benzene is a major decomposition product for all conditions studied. In both resin systems, the metal chlorides also facilitated the production of 2-methyl-2-hexanol. While the decomposition of the model epoxy resin yielded a range of phenolic derivatives for all solvent systems, the degradation of the CFRP resulted in the generation of different compounds depending on the solvent system used. In the neat acetone / water mixture, 2-6-diethyl-benzenamine and 1,2,3,4-tetrahydro-2,2,4,8-tetramethyl-quinoline were identified, however, the use of different metal chlorides resulted in the production of much larger compounds, each unique to the catalyst system investigated. The number of different species present across the two polymers and four solvent systems considered does highlight the challenge of further processing this, at present, waste material. However, the identification of these potentially valuable compounds represents an advantage of chemical recycling methods when compared to pyrolysis. The latter technique tends to generate only a low-value gaseous mixture which is suitable for use only as a fuel in the process.

Characterisation of the OLP recovered from both polymers using FTIR confirmed some of the GCMS findings. The broad band in the range of 3650 to 3150 cm^{-1} is

indicative of O-H bonds due to the presence of phenol and its derivatives. There were also sharp peaks representing methyl groups and cyclic C-C bonds, largely due to trimethyl benzene and, again, phenolic compounds. Compared to the model epoxy resin, CFRP material appeared to contain a greater proportion of nitrogen in the polymer matrix. FTIR of the OLP recovered from the latter material using KOH and NaOH solutions revealed the presence of C=N and C-NH bonds. These were not present in the spectra obtained for reactions where *RD* > 92% due to effective scission of these bonds by the neat solvent and metal chlorides. Although there are two amine groups per molecule of DDS (used as the curing agent in the manufacture of the model epoxy resin), it was not possible to identify C-N or N-H bonds in the FTIR of the OLP recovered after the decomposition of this material. Sulphinyl functional groups were identified and it is apparent that the high temperatures used with the neat solvent mixture and $ZnCl_2$ effectively cleave the S=O bond. As this moiety is present when considering $MgCl_2$ and $AlCl_3$ systems, it is possible that these catalysts act in a slightly different way to $ZnCl_2$, despite demonstrating similar decomposition characteristics.

The results presented in this chapter also demonstrate that the solvent itself reacts at the conditions investigated. Acetone undergoes aldol condensation meaning 4-methyl-3-penten-2-one was identified in the OLP. This further reacts to form 3,5,5-trimethyl-2-cyclohexen-1-one and, especially in the presence of basic media, 4-hydroxy-4-methyl-pentan-2-one. Similarly, the presence of weak-Lewis acids resulted in ring closure and the formation of 2-methoxy-furan. As some of the solvent is eliminated from the reaction, it will need to be replaced if recovering the remainder in an industrial scale

process which may lead to increased operating costs. Additional work could aim to quantify the loss of the solvent, and the concentration of the resinous products, by developing a series of calibration curves through further GC-MS analyses.

Although dependent on the polymer matrix and solvent system, it is possible to recover a mixture of potentially valuable molecules when using this solvolytic process to recycle CFRPs. If an effective separation process can be developed, the recovery and reuse of these compounds have the potential to improve resource efficiency and generate additional revenue when compared to commercialised pyrolysis techniques. Development of this separation process or identification of methods to homogenise the reaction mixture from multiple types of polymer therefore represents an important area for future research.

CHAPTER 7.
CONCLUSIONS & FUTURE WORK

5.1 Research Outcomes

As a result of the research presented in this thesis, it has been demonstrated that a supercritical mixture of acetone and water is capable of fully decomposing a thermally stable, RTM6 epoxy resin thus liberating carbon fibres as a valuable product. A temperature of 320˚C was necessary to obtain a resin decomposition (*RD*) of more than 92 wt.% in a reasonable reaction time of 120 min. A strong temperature dependence of this reaction was highlighted by further experiments conducted at 330 and 340˚C; under these conditions, the reaction time required for near-complete decomposition of the RTM6 epoxy resin was reduced by 25.0 and 62.5% respectively.

Contrary to previous research, the inclusion of the alkaline salts NaOH and KOH does not accelerate the decomposition of the resin. It was apparent that these alkaline salts favour the aldol condensation of acetone over a reaction with the epoxy matrix and thus renders them incompatible with this solvent system.

For the same reaction time as with the neat acetone / water solvent, the inclusion of various metal chlorides facilitated the recovery of clean fibres whilst reducing the necessary process temperature by 40˚C. $AlCl_3$ was identified as the most effective catalyst: a concentration of 0.005 M had the same effect on *RD* as 0.05 M solutions of $ZnCl_2$ and $MgCl_2$. Although different concentrations of these catalysts were necessary,

all three weak-Lewis acids significantly enhanced the degradation of the matrix. Within an industrial process, the high temperatures and pressures necessary when using the neat acetone / water solvent system are likely to lead to costly processing equipment: a significant barrier to the commercialisation of this technology. The reduction in operating conditions achieved by the implementation of these metal chloride catalysts will not only reduce the capital expenditure of the process equipment, but also minimise the operating costs. It is, therefore, hoped that this research contributes to the successful development of an industrial CFRP recycling process. In order to further the understanding of the degradation reaction, the reaction kinetics of these systems were investigated alongside that of the neat solvent mixture.

Two independent approaches were taken in order to study the reaction kinetics: a conventional first order rate equation and a shrinking core model were both considered which have not, until this research, been applied to the same data set. Even when increasing the reactor loading, it was apparent that the solvent and catalyst were always in excess and the decomposition rate was, therefore, not dependent on the concentration of resin in the solvent. As the reaction rate decreased as the decomposition progressed, it was assumed that the rate was proportional to the mass fraction of the polymer remaining within the composite material. Based on this, a conventional first order rate equation was successfully fitted to the degradation data obtained for the pure acetone / water mixture and the three metal chlorides investigated in detail. A reaction-rate limited, shrinking core model (SCM) for a spherical particle could also be applied to the same data set. Analysis of these models

demonstrated that both were able to predict *RD* to within a reasonable degree of accuracy: the majority of the calculated values were within 5% of the experimental data.

Rate constants were calculated at various temperatures for both the first order rate equation and the SCM applied. Through this, it was possible to determine the Arrhenius parameters activation energy, E_A, and frequency factor, k_0, for each solvent system. Dependent on which model was fitted to the data, E_A and k_0 were 183 to 222 kJ mol^{-1} and 6.69 $x10^{13}$ to 7.64 $x10^{17}$ min^{-1} respectively for the neat acetone / water mixture. It was apparent that $ZnCl_2$ resulted in the greatest reduction of these parameters, however, it was supplied at a concentration an order of magnitude higher than $AlCl_3$. Calculation of these Arrhenius parameters may also aid in the design of an industrial scale process.

As a result of the decomposition experiments described in Chapters 3 and 4, a set of 11 conditions were identified as capable of recovering clean carbon fibres from an RTM6 epoxy matrix. In order to decouple the influences of the CFRP manufacturing process, service life and recycling process on the quality of the fibres, virgin material was placed in the reactor alongside the CFRP investigated. This also meant that the mechanical and surface properties of the virgin fibres, both with and without the layer of sizing, could be independently verified. It was demonstrated that upon processing fibres at up to 330˚C with the neat solvent mixture, the tensile strength and modulus of the fibres showed a slight increase of up to 9.6%. At higher temperatures, however, there was a continuous reduction in both of these properties of up to 12.4% when

processed at 380˚C. $AlCl_3$ effectively degraded the polymer matrix, however, it was apparent that this catalyst also attacks the fibres as the tensile strength and modulus were significantly reduced, possibly due to the loss of carbon from the surface. Although $ZnCl_2$ and $MgCl_2$ were supplied at a higher concentration, there was little change in mechanical properties when using the latter catalyst but an increase in strength and modulus of 6.8 and 11.0% respectively in the presence of $ZnCl_2$.

Characterisation of the fibre surface demonstrated a significant change in the functional groups present after processing the virgin carbon fibre. With the exception of the $AlCl_3$ system at 290˚C, all conditions investigated resulted in a reduction in the concentration of oxygen at the surface and an increase in nitrogen, possibly due to the removal of the outer fibre surface and subsequent exposure of the nitrile groups within the PAN-based fibres. Based on the mechanical and surface properties, it can be concluded that $ZnCl_2$ supplied at a concentration of 0.05 M in an acetone / water solvent mixture and heated to 300˚C was able to recover the highest quality fibres. SEM micrographs, however, did reveal the presence of a deposit on the fibre surface and EDX confirmed the presence of $ZnCl_2$. Due to its high solubility in water, this was easily removed upon rinsing the fibres, although it is worth noting that the catalysts investigated may influence adhesion to a new polymer matrix. As the fibres characterised as part of this research project often demonstrate similar, or even improved, properties compared to virgin material, it is hoped that the data presented within this thesis mitigates concerns manufacturers may have regarding the use of carbon fibre recycled from a commercial solvolysis process within secondary CFRPs.

By comparing the infrared spectra of the dried organic liquid products (OLP) recovered from each of the solvent systems, it was apparent that both the neat acetone / water mixture and metal chlorides effectively cleaved the C-N bonds within the CFRP matrix. Interestingly, the action of the neat solvent and $ZnCl_2$ on the model epoxy resin resulted in the scission of the sulphinyl functional groups, whereas $MgCl_2$ and $AlCl_3$ did not. Although all systems fully decomposed the model resin under the reaction conditions investigated, this suggests that they follow different reaction mechanisms.

Analysis of the OLP using gas chromatography with mass spectrometry (GCMS) identified trimethyl benzene as a major degradation product from both the CFRP and the model epoxy resin. This latter material also yielded phenolic derivatives for all solvent systems considered, whereas the product mixture of the decomposed CFRP was dependent on the presence and type of catalyst. The wide range of compounds present does highlight the challenge of further processing this, currently, waste material, although the identification of these organic products also represents a potential advantage over pyrolytic recycling technologies. If an effective separation process can be developed, this mixture of organic compounds may generate an additional revenue stream thereby enhancing the economic feasibility of an industrial scale process.

6.2 Future Work

Based on the key findings presented in this thesis, research within the field of recycling high performance composite materials may be directed into a number of different areas. Some suggestions for these future directions are outlined below.

1. Through the use of metal chlorides, the necessary process temperature for the recovery of clean fibres was significantly decreased. Further investigation of higher catalyst concentrations at lower temperatures than those investigated in this work may allow even greater reductions to be achieved thus minimising the environmental burden and economic cost of the recycling process developed as part of this thesis.

2. A comprehensive life cycle analysis (LCA) of this recycling technology should be conducted. However, as economies of scale would be achieved with an industrial process, analysis of the lab-scale process described in this thesis would lead to unrealistic results. It would, therefore, first be necessary to design a process capable of handling a similar quantity of material which is currently recycled commercially using pyrolytic techniques. The necessary equipment could then be specified and suitable mass and energy balances for this theoretical process may then be conducted. This would allow the environmental impact of manufacturing equipment and transport, use and disposal of materials to be quantified and compared to that of other CFRP disposal routes, namely landfilling and pyrolysis.

3. Although the results presented demonstrate that the recycling process has little influence on the properties of the fibres under certain conditions, certain characteristics, such as interfacial shear strength, have not yet been quantified. It would also be useful to manufacture a secondary CFRP from

recovered fibres in order to further prove the capability of this recycling technology.

4. As a wide and varying range of organic products are produced, further research may wish to focus on developing suitable separation techniques in order to maximise the value of this resource. Alternatively, it would be useful to investigate to what proportion the OLP can be used directly in a new composite material without any deterioration in its mechanical performance. Doing so may not only generate an additional source of revenue, but also help close the loop of the supply chain and thereby further improve resource efficiency.

5. The recycling techniques investigated in this thesis has only been conducted at lab scale and with a limited range of polymers. As a consequence, it would be useful to study the scale up of this process and evaluate its ability to handle a mixture of both thermoplastic and thermoset waste. If successful, the completion of such an investigation would be a significant step towards the commercialisation of this technology.

Through the weight reduction of vehicles, increased service life of structural components and the manufacture of high-capacity wind turbines, CFRPs have enormous potential to facilitate the drive towards a sustainable future, yet, at present, their disposal options remain severely limited. By developing and analysing a novel recycling process, together with characterisation of the fibrous and organic liquid products, it is

hoped that this research project makes a significant contribution towards the efficient recycling of these high-performance composite materials.

REFERENCES

[1] M. Sauer and M. Kuhnel, "Composites Market Report 2018," *Carbon Compos.*, no. November, pp. 27–59, 2018.

[2] S. J. Pickering and T. A. Turner, "Research and development in support of carbon fibre recycling," in *CAMX 2014 - The Composites & Advanced Materials Expo: Combined Strength. Unsurpassed Innovation.*, 2014.

[3] G. . Oliveux, L. O. Dandy, and G. A. Leeke, "Current Status of Recycling of Fibre Reinforced Polymers : review of technologies , reuse and resulting properties resulting properties," *Prog. Mater. Sci.*, vol. 72, no. July 2015, pp. 61–99, 2015.

[4] Composites UK, "End of Life Options for Composite Materials," 2019. [Online]. Available: https://compositesuk.co.uk/composite-materials/properties/end-life-options. [Accessed: 10-Dec-2019].

[5] F. L. Matthews and R. D. Rawlings, *Composite Materials: Engineering and Science*, 1st ed. Oxford: The Alden Press, 1994.

[6] M. J. John and S. Thomas, "Natural Polymers: An Overview," in *Natural Polymers: Composites*, 1st ed., M. J. John and S. Thomas, Eds. Cambridge, UK: The Royal Society of Chemistry, 2012, pp. 1–7.

[7] S. V. Hoa, *Principles of the Manufacturing of Composite Materials*, 1st ed. Pennsylvania, U.S: DEStech Publications Inc., 2009.

[8] R.-M. Wang, S.-R. Zheng, and Y.-G. Zheng, *Polymer Matrix Composites and Technology*, 1st ed. Cambridge, UK: Woodhead Publishing Ltd., 2011.

[9] E. Kohler and J. Niehus, "Aluminium-Matrix Composite Materials in Combustion Engines," in *Metal Matrix Composites: Custom-made Materials for Automotive and Aerospace Engineering2*, 1st ed., K. U. Kainer, Ed. Geesthacht, Germany: Wiley-VCH, 2006, pp. 95–110.

[10] B. Clauss, "Fibres for Ceramic Matrix Composites," in *Ceramic Matrix Composites: Fiber Reinforced Ceramics and their Applications*, 1st ed., W. Krenkel, Ed. Darmstadt, Germany: Wiley-VCH, 2008, pp. 1–20.

[11] K. K. Chawla, *Composite Materials: Science and Engineering*, 2nd ed. New York, USA: Springer, 1998.

[12] A. R. Bunsell and J. Renard, *Fundamentals of Fibre Reinforced Composite*

Materials, 1st ed. Bristol, UK: IOP Publishing Ltd, 2005.

[13] S. S. Yao, F. L. Jin, K. Y. Rhee, D. Hui, and S. J. Park, "Recent advances in carbon-fiber-reinforced thermoplastic composites: A review," *Composites Part B: Engineering*. 2018.

[14] N. Uddin, "Introduction," in *Developments in Fiber-Reinforced Polymer (FRP) Composites for Civil Engineering*, 1, Ed. Cambridge, UK: Woodhead Publishing Ltd., 2014, pp. 23–31.

[15] S. Gharde and B. Kandasubramanian, "Mechanothermal and chemical recycling methodologies for the Fibre Reinforced Plastic (FRP)," *Environ. Technol. Innov.*, vol. 14, no. 1, pp. 1–30, 2019.

[16] I. Alkorta and J. Elguero, "The carbon-carbon bond dissociation energy as a function of the chain length," *Chem. Phys. Lett.*, 2006.

[17] J. B. Huang, G. S. Zeng, and X. S. Li, "Theoretical studies on bond dissociation enthalpies for model compounds of typical plastic polymers," in *IOP Conference Series Earth and Environmental Science*, 2018, vol. 167, no. 1, pp. 3–7.

[18] L. C. Hollaway and P. R. Head, "Composite Materials and Structures in Civil Engineering," in *Comprehensive Composite Materials*, 1st ed., A. Kelly and C. Zweben, Eds. Elsevier Ltd., 2000, pp. 489–527.

[19] H. Li and K. Englund, "Recycling of carbon fiber-reinforced thermoplastic composite wastes from the aerospace industry," *J. Compos. Mater.*, vol. 51, no. 9, pp. 1265–1273, 2017.

[20] H. Shaikh *et al.*, "Progress in Carbon Fiber and Its Polypropylene- and Polyethylene-Based Composites," *Polym. - Plast. Technol. Eng.*, vol. 53, no. 17, pp. 1845–1860, 2014.

[21] C. Red, "Thermoplastics in Aerospace Composites Outlook, 2014-2023," 2014. [Online]. Available: https://www.compositesworld.com/articles/the-outlook-for-thermoplastics-in-aerospace-composites-2014-2023. [Accessed: 18-Jul-2019].

[22] S. Beland, *High Performance Thermoplastics and Their Composites*, 1st ed. New Jersey, USA: Noyes Publications, 1990.

[23] L. Ardelean, C. Bortun, A. Podariu, and L. Rusu, "Manufacture of Different Tpes of Thermoplastic," in *Thermoplastic Composite Materials*, 1st ed., A. Z. El-Sonbati, Ed. Rijeka, Croatia: IntechOpen, 2012, pp. 25–48.

[24] G. Kinvi-Dossou *et al.*, “Innovative acrylic thermoplastic composites versus conventional composites: Improving the impact performances,” *Compos. Struct.*, vol. 217, pp. 1–13, 2019.

[25] J. Barnes, “Advanced Thermoplastics,” in *Handbook of Polymer-Fiber Composites*, 1st ed., F. R. Jones, Ed. Essex, UK: Longman Scientific & Technical, 1994, pp. 69–73.

[26] A. J. Jefferson and ArumugamV., *Repair of Polymer Composites: Methodology, Techniques and Challenges*, 1st ed. Cambridge, UK: Woodhead Publishing Ltd., 2018.

[27] R. Akkerman and H. P., “Thermoplastic composites manufacturing by thermoforming,” in *Advances in Composites Manufacturing and Process Design*, 1st ed., P. Boisse, Ed. Cambridge, UK: Woodhead Publishing Ltd., 2015, pp. 111–129.

[28] J. Studer *et al.*, “Effect of fabric architecture, compaction and permeability on through thickness thermoplastic melt impregnation,” *Compos. Part A Appl. Sci. Manuf.*, vol. 122, pp. 45–53, 2019.

[29] J. H. Shin, D. Kim, T. Centea, and S. R. Nutt, “Thermoplastic prepreg with partially polymerized matrix: Material and process development for efficient part manufacturing,” *Compos. Part A Appl. Sci. Manuf.*, vol. 119, pp. 154–164, 2019.

[30] J. Misumi and T. Oyama, “Low viscosity and high toughness epoxy resin modified by in situ radical polymerization method for improving mechanical properties of carbon fiber reinforced plastics,” *Polymer (Guildf).*, 2018.

[31] M. Folkes, “Injection moulding,” in *Handbook of Polymer-Fiber Composites1*, 1st ed., F. R. Jones, Ed. Essex, UK: Longman Scientific & Technical, 1994, pp. 165–167.

[32] Grand View Research, “Carbon Fiber Reinforced Plastic Market Size, Share & Trends Analysis Report By Raw Material, By Product (Thermosetting, Thermoplastic), By Application, And Segment Forecasts, 2018 - 2025,” California, US, 2016.

[33] R.-M. Wang, S.-R. Zheng, and Y.-P. Zheng, “Forming technology of polymer matrix composites,” in *Polymer Matrix Composites and Technology*, Cambridge, UK: Woodhead Publishing Ltd., 2011, pp. 253–319.

[34] R.-M. Wang, S.-R. Zheng, and Y.-P. Zheng, “Matrix materials,” in *Polymer Matrix Composites and Technology*, 1st ed., California, US: Woodhead

Publishing Ltd., 2011, pp. 101–167.

[35] D. J. Allen and H. Ishida, “Thermosets: Phenolics, Novolacs, and Benzoxazine,” in *Encyclopedia of Materials: Science and Technology*, K. H. Jurgen Buschow, M. C. Flemings, E. J. Kramer, P. Veyssiere, R. W. Cahn, B. Ilschner, and S. Mahajan, Eds. Amsterdam, Netherlands: Elsevier Ltd., 2001, pp. 9226–9229.

[36] W. Hesse and J. Lang, “Phenolic resins,” in *Ullmann’s Encyclopedia of Industrial Chemistry*, 7th ed., G. Bellussi, Ed. Weinheim, Germany: John Wiley & Sons, Inc., 2011, pp. 583–600.

[37] A. Kandelbauer, G. Tondi, O. C. Zaske, and S. H. Goodman, “Unsaturated polyesters and vinyl esters,” in *Handbook of Thermoset Plastics*, 3rd ed., H. Dodiuk and S. H. Goodman, Eds. Oxford, Uk: Elsevier Ltd., 2013, pp. 111–172.

[38] C. Mangeon, E. Renard, F. Thevenieau, and V. Langlois, “Networks based on biodegradable polyesters: An overview of the chemical ways of crosslinking,” *Mater. Sci. Eng. C*, vol. 80, pp. 760–770, 2017.

[39] P. B. Zetterlund and A. F. Johnson, “Free volume-based modelling of free radical crosslinking polymerisation of unsaturated polyesters,” *Polymer (Guildf).*, vol. 43, pp. 2036–2048, 2002.

[40] F. R. Johannes, “Unsaturated Polyester Resins,” in *Brydson’s Plastics Materials: Eighth Edition*, 3rd ed., Amsterdam, Netherlands: Elsevier Ltd., 2018, pp. 1–69.

[41] R.-M. Wang, S.-R. Zheng, and Y.-P. Zheng, “Interface of polymer matrix composites,” in *Polymer Matrix Composites and Technology*, 1st ed., Cambridge, UK: Woodhead Publishing Ltd., 2011, pp. 169–209.

[42] H. Panda, *Epoxy Resins Technology Handbook (Manufacturing Process, Synthesis, Epoxy Resin Adhesives and Epoxy Coatings)*, 2nd ed. Delhi, India: Asia Pacific Business Press, 2019.

[43] Hexcel, “HexFlow RTM6 Product Data,” 2016. [Online]. Available: https://www.imatec.it/wp-content/uploads/2016/05/RTM6_global.pdf. [Accessed: 20-Jun-2019].

[44] A. Chatterjee and J. W. Gillespie, “Moisture Absorption Behavior of Epoxies and Their S2 Glass Composites,” *J. Appl. Polym. Sci.*, vol. 108, no. 1, pp. 3942–3951, 2008.

[45] Z. Ahmad, M. P. Ansell, and D. Smedley, “Moisture absorption characteristics of epoxy based adhesive reinforced with CTBN and ceramic particles for bonded-in timber connection: Fickian or non-Fickian behaviour,” *IOP Conf. Ser. Mater. Sci. Eng.*, vol. 17, pp. 1–15, 2011.

[46] B. Bjorkner, A. Ponten, E. Zimerson, and M. Frick, “Plastic materials,” in *Contact Dermatitis*, 4th ed., P. J. Frosch, T. Menne, and J.-P. Lepoittevin, Eds. Berlin, Germany: Springer, 2006, pp. 595–599.

[47] A. M. Amaro, L. Bernardo, D. G. Pinto, S. Lopes, and J. Rodrigues, “The influence of curing agents in the impact properties of epoxy resin nanocomposites,” *Compos. Struct.*, vol. 174, pp. 26–32, 2017.

[48] S. Alessi, G. Spadaro, E. Caponetti, A. Spinella, O. Güven, and M. Akbulut, “Study of the curing process of DGEBA epoxy resin through structural investigation,” *Macromol. Chem. Phys.*, vol. 216, no. 5, pp. 538–546, 2015.

[49] I. K. Narma, V. B. Gupta, and N. K. Sini, “Thermosetting Resin - Properties,” in *Comprehensive Composite Materials II*, 2nd ed., P. W. R. Beaumont and C. H. Zweben, Eds. Amsterdam, Netherlands: Elsevier Ltd., 2018, pp. 401–468.

[50] D. Incerti, T. Wang, D. Carolan, and A. Fergusson, “Curing rate effects on the toughness of epoxy polymers,” *Polymer (Guildf).*, 2018.

[51] A. M. Amaro, L. Bernardo, D. G. Pinto, S. Lopes, and J. Rodrigues, “The influence of curing agents in the impact properties of epoxy resin nanocomposites,” *Compos. Struct.*, vol. 174, pp. 26–32, 2017.

[52] D. Santiago, X. Fernández-Francos, X. Ramis, and M. Sangermano, “Comparative curing kinetics and thermal–mechanical properties of DGEBA thermosets cured with a hyperbranched poly(ethyleneimine) and an aliphatic triamine,” *Thermochim. Acta*, vol. 526, no. 1, pp. 9–21, 2011.

[53] A. Surnova, D. Balkaev, D. Musin, R. Amirov, and A. M. Dimiev, “Fully exfoliated graphene oxide accelerates epoxy resin curing, and results in dramatic improvement of the polymer mechanical properties,” *Compos. Part B Eng.*, vol. 162, pp. 685–691, 2019.

[54] J. S. Yoon, K. Kim, and H. S. Seo, “Computational modeling for cure process of carbon epoxy composite block,” *Compos. Part B Eng.*, vol. 164, pp. 693–702, 2019.

[55] W. Jilani *et al.*, “Effects of curing agent on conductivity, structural and dielectric properties of an epoxy polymer,” *Polymer (Guildf).*, vol. 79, pp.

73–81, 2015.

[56] F. Mustafa and I. Bicu, “Rheological and thermal behaviour of DGEBA/EA and DGEHQ/EA epoxy systems crosslinked with TETA,” *Polym. Test.*, vol. 20, no. 5, pp. 533–538, 2001.

[57] V. M. Kagathara and P. H. Parsania, “Preparation and evaluation of mechano-electrical properties and chemical resistance of epoxy laminates of halogenated bisphenol-C resins,” *Polym. Test.*, vol. 20, no. 6, pp. 713–716, 2001.

[58] A. M. Atta, N. O. Shaker, and N. E. Maysour, “Influence of the molecular structure on the chemical resistivity and thermal stability of cured Schiff base epoxy resins.,” *Prog. Org. Coatings*, vol. 56, no. 2–3, pp. 100–110, 2006.

[59] M. Jackson, M. Kaushik, S. Nazarenko, S. Ward, R. Maskell, and J. Wiggins, “Effect of free volume hole-size on fluid ingress of glassy epoxy networks,” *Polymer (Guildf).*, vol. 52, no. 204528–4535, 2011.

[60] L. Li, Y. Yu, Q. Wu, G. Zhan, and S. Li, “Effect of chemical structure on the water sorption of amine-cured epoxy resins,” *Corros. Sci.*, vol. 51, no. 12, pp. 3000–3006, 2009.

[61] K. Frank and J. Wiggins, “Effect of stoichiometry and cure prescription on fluid ingress in epoxy networks,” *J. Appl. Polym. Sci.*, vol. 130, no. 1, pp. 264–276, 2013.

[62] I. Merdas, A. Tcharkhtchi, F. Thominette, J. Verdu, K. Dean, and W. Cook, “Water absorption by uncrosslinked polymers, networks and IPNs having medium to high polarity,” *Polymer (Guildf).*, vol. 43, no. 17, pp. 4619–4625, 2002.

[63] N. Longieras, M. Sebban, P. Palmas, A. Rivaton, and J. L. Gardette, “Multiscale approach to investigate the radiochemical degradation of epoxy resins under high-energy electron-beam irradiation,” *J. Polym. Sci. Part A Polym. Chem.*, vol. 44, pp. 865–887, 2005.

[64] T. Devanne, A. Bry, L. Audouin, and J. Verdu, “Radiochemical ageing of an amine cured epoxy network. Part I: Change of physical properties,” *Polymer (Guildf).*, 2005.

[65] D. P. R. Queiroz, F. Fraïsse, B. Fayolle, M. Kuntz, and J. Verdu, “Radiochemical ageing of epoxy coating for nuclear plants,” *Radiat. Phys. Chem.*, vol. 79, no. 3, pp. 362–364, 2010.

[66] Y. Zahra, F. Djouani, B. Fayolle, M. Kuntz, and J. Verdu, “Thermo-oxidative aging of epoxy coating systems,” *Prog. Org. Coatings*, vol. 77, no. 2, pp. 380–387, 2014.

[67] E. Ernault, E. Richaud, and B. Fayolle, “Thermal-oxidation of epoxy/amine followed by glass transition temperature changes,” *Polym. Degrad. Stab.*, 2017.

[68] C. Damian, E. Espuche, and M. Escoubes, “Influence of three ageing types (thermal oxidation, radiochemical and hydrolytic ageing) on the structure and gas transport properties of epoxy-amine networks,” *Polym. Degrad. Stab.*, 2001.

[69] Y. S. Song, J. R. Youn, and T. G. Gutowski, “Life cycle energy analysis of fiber-reinforced composites,” *Compos. Part A Appl. Sci. Manuf.*, vol. 40, pp. 1257–1265, 2009.

[70] P. Bhatt and A. Goe, “Carbon Fibres: Production, Properties and Potential Use,” *Mater. Sci. Res. India*, vol. 14, no. 1, pp. 52–57, 2017.

[71] B. A. Newcomb, “Processing, structure, and properties of carbon fibers,” *Compos. Part A Appl. Sci. Manuf.*, vol. 91, pp. 262–282, 2016.

[72] A. Katunin, K. Krukiewicz, R. Turczyn, P. Sul, and M. Bilewicz, “Electrically conductive carbon fibre-reinforced composite for aircraft lightning strike protection,” in *IOP Conference Series: Materials Science and Engineering*, 2017, pp. 1–5.

[73] B. A. Newcomb and H. G. Chae, “The properties of carbon fibers,” in *Handbook of Properties of Textile and Technical Fibres*, 2nd ed., A. R. Bunsell, Ed. Cambridge, UK: Woodhead Publishing Ltd., 2018, pp. 841–871.

[74] H. Rahmani, S. H. Mahmoudi, A. Ashori, and M. Golriz, “Elastic Properties of Carbon Fibre-Reinforced Epoxy Composites,” *Polym. Polym. Compos.*, vol. 23, no. 7, pp. 475–482, 2015.

[75] M. H. El-Newehy, A. Alamri, and S. S. Al-Deyab, “Optimization of amine-terminated polyacrylonitrile synthesis and characterization,” *Arab. J. Chem.*, vol. 7, pp. 235–241, 2014.

[76] X. H. Zhang and Q. W. Li, “Carbon fiber spinning,” in *Activated Carbon Fiber and Textiles*, 1st ed., J. Y. Chen, Ed. Cambridge, UK: Woodhead Publishing Ltd., 2017, pp. 39–60.

[77] J. H. Lee *et al.*, “Melt processable polyacrylonitrile copolymer precursors for

carbon fibers: Rheological, thermal, and mechanical properties," *J. Ind. Eng. Chem.*, vol. 71, pp. 112–118, 2019.

[78] H. Khayyam *et al.*, "PAN Precursor Fabrication, Applications and Thermal Stabilization Process in Carbon Fiber Production: Experimental and Mathematical Modelling," *Prog. Mater. Sci.*, vol. In Press, 2019.

[79] N. Yusof and A. F. Ismail, "Post spinning and pyrolysis processes of polyacrylonitrile (PAN)-based carbon fiber and activated carbon fiber: A review," *J. Anal. Appl. Pyrolysis*, vol. 93, pp. 1–13, 2012.

[80] H. G. Chae *et al.*, "High strength and high modulus carbon fibers," *Carbon N. Y.*, 2015.

[81] K. A. Banaie, M. Mirjalili, and R. Eslami-Farsani, "The study of the correlation between ascending and descending rates of the imposed specific stress and transposition of chemical reactionsduring PAN precursorfibers stabilization," *Polym. Degrad. Stab.*, vol. 156, pp. 234–244, 2018.

[82] S. Park, H. S. Kil, D. Choi, S. K. Song, and S. Lee, "Rapid stabilization of polyacrylonitrile fibers achieved by plasma-assisted thermal treatment on electron-beam irradiated fibers," *J. Ind. Eng. Chem.*, vol. 69, pp. 449–454, 2019.

[83] W. Zhang *et al.*, "Significantly reduced pre-oxidation period of PAN fibers by continuous electron beam irradiation: Optimization by monitoring radical variation," *Polym. Degrad. Stab.*, vol. 158, pp. 72–82, 2018.

[84] S. Y. Son, A. Y. Jo, G. Y. Jung, Y. S. Chung, and S. Lee, "Accelerating the stabilization of polyacrylonitrile fibers by UV irradiation," *J. Ind. Eng. Chem.*, no. 73, pp. 47–51, 2019.

[85] M. Al Aiti, D. Jehnichen, D. Fischer, H. Brünig, and G. Heinrich, "On the morphology and structure formation of carbon fibers from polymer precursor systems," *Prog. Mater. Sci.*, vol. 98, pp. 477–551, 2018.

[86] J. Goma and M. Oberlin, "Graphitization of thin carbon films," *Thin Solid Films*, vol. 65, pp. 221–232, 1980.

[87] M. Minus and S. Kumar, "The processing, properties, and structure of carbon fibers," *J. Miner. Met. Mater. Soc.*, vol. 57, no. 2, pp. 52–58, 2005.

[88] M. S. A. Rahaman, A. F. Ismail, and A. Mustafa, "A review of heat treatment on polyacrylonitrile fiber," *Polym. Degrad. Stab.*, vol. 92, pp. 1421–1432, 2007.

[89] F. Liu, H. Wang, L. Xue, L. Fan, and ZhuZ., “Effect of microstructure on the mechanical properties of PAN-based carbon fibers during high-temperature graphitization,” *J. Mater. Sci.*, vol. 43, no. 12, pp. 4316–4322, 2008.

[90] W. Kowbel, E. Hippo, and N. Murdie, “Influence of graphitization environment of pan based carbon fibers on microstructure,” *Carbon N. Y.*, vol. 27, no. 2, pp. 219–226, 1989.

[91] F. R. Barnet and M. K. Norr, “Carbon fiber etching in an oxygen plasma,” *Carbon N. Y.*, vol. 11, no. 4, pp. 281–288, 1973.

[92] L. Y. Yuan, C. S. Chen, S. S. Shyu, and J. Y. Lai, “Plasma surface treatment on carbon fibers. Part 1: Morphology and surface analysis of plasma etched fibers,” *Compos. Sci. Technol.*, vol. 45, pp. 1–7, 1992.

[93] Z. Li, J. Wang, Y. Tong, and L. Xu, “Anodic Oxidation on Structural Evolution and Tensile Properties of Polyacrylonitrile Based Carbon Fibers with Different Surface Morphology,” *J. Mater. Sci. Technol.*, vol. 28, no. 12, pp. 1123–1129, 2012.

[94] Y. Sun, Y. Lu, and C. Yang, “Stripping mechanism of PAN-based carbon fiber during anodic oxidation in NaOH electrolyte,” *Appl. Surf. Sci.*, vol. 486, pp. 128–136, 2019.

[95] M. Sharma, S. Gao, E. Mäder, H. Sharma, L. Y. Wei, and J. Bijwe, “Carbon fiber surfaces and composite interphases,” *Compos. Sci. Technol.*, vol. 102, pp. 35–50, 2014.

[96] L. Yao *et al.*, “Comparison of sizing effect of T700 grade carbon fiber on interfacial properties of fiber/BMI and fiber/epoxy,” *Appl. Surf. Sci.*, vol. 263, pp. 326–333, 2012.

[97] Z. Dai, B. Zhang, F. Shi, M. Li, Z. Zhang, and Y. Gu, “Effect of sizing on carbon fiber surface properties and fibers/epoxy interfacial adhesion,” *Appl. Surf. Sci.*, vol. 257, pp. 6980–6985, 2011.

[98] C. Ozkan, N. Gamze Karsli, A. Aytac, and V. Deniz, “Short carbon fiber reinforced polycarbonate composites: Effects of different sizing materials,” *Compos. Part B Eng.*, vol. 62, pp. 230–235, 2014.

[99] R. L. Zhang, Y. D. Huang, L. Liu, Y. R. Tang, D. Su, and L. W. Xu, “Effect of emulsifier content of sizing agent on the surface of carbon fibres and interface of its composites,” *Appl. Surf. Sci.*, vol. 257, pp. 3519–3523, 2011.

[100] R. L. Zhang, Y. D. Huang, L. Liu, Y. R. Tang, D. Su, and L. W. Xu, “Effect of the

molecular weight of sizing agent on the surface of carbon fibres and interface of its composites," *Appl. Surf. Sci.*, vol. 257, pp. 1840–1844, 2011.

[101] R. Zhang, Y. Huang, L. Liu, Y. Tang, D. Su, and L. Xu, "Influence of sizing emulsifier content on the properties of carbon fibers and its composites," *Mater. Des.*, vol. 33, pp. 367–371, 2012.

[102] I. Giraud, S. Franceschi-Messant, E. Perez, C. Lacabanne, and E. Dantras, "Preparation of aqueous dispersion of thermoplastic sizing agent for carbon fiber by emulsion/solvent evaporation," *Appl. Surf. Sci.*, vol. 266, pp. 94–99, 2013.

[103] J. Chen, K. Wang, and Y. Zhao, "Enhanced interfacial interactions of carbon fiber reinforced PEEK composites by regulating PEI and graphene oxide complex sizing at the interface," *Compos. Sci. Technol.*, vol. 154, pp. 175–186, 2018.

[104] A. Vedrtnam and S. P. Sharma, "Study on the performance of different nano-species used for surface modification of carbon fiber for interface strengthening," *Compos. Part A Appl. Sci. Manuf.*, vol. 125, pp. 1–18, 2019.

[105] H. Okuda, R. J. Young, F. Tanaka, J. Watanabe, and T. Okabe, "Tensile failure phenomena in carbon fibres," *Carbon N. Y.*, vol. 107, pp. 474–481, 2016.

[106] E. S. Penev, V. I. Artyukhov, and B. I. Yakobson, "Basic structural units in carbon fibers: Atomistic models and tensile behavior," *Carbon N. Y.*, vol. 85, pp. 72–78, 2015.

[107] X. Qin, Y. Lu, H. Xiao, Y. Wen, and T. Yu, "A comparison of the effect of graphitization on microstructures and properties of polyacrylonitrile and mesophase pitch-based carbon fibers," *Carbon N. Y.*, vol. 50, pp. 4459–4469, 2012.

[108] F. Vautard, J. Dentzer, M. Nardin, J. Schultz, and B. Defoort, "Influence of surface defects on the tensile strength of carbon fibers," *Appl. Surf. Sci.*, vol. 322, pp. 185–193, 2014.

[109] S. K. Jeon, O. H. Kwon, H. S. Jang, K. S. Ryu, and S. H. Nahm, "Effect of high pressure hydrogen on the mechanical characteristics of single carbon fiber," *Appl. Surf. Sci.*, vol. 432, pp. 176–182, 2018.

[110] B. Dong, L. Tian, and B. Pan, "Tensile testing of carbon fiber multifilament using an advanced video extensometer assisted by dual-reflector imaging," *Meas. J. Int. Meas. Confed.*, vol. 138, pp. 325–331, 2019.

[111] L. O. Dandy, “Supercritical fluids and their application to the recycling of high-performance carbon fibre reinforced composite materials,” University of Birmingham, 2015.

[112] L. O. Dandy, G. Oliveux, J. Wood, M. J. Jenkins, and G. A. Leeke, “Counting carbon fibres by electrical resistance measurement,” *Compos. Part A Appl. Sci. Manuf.*, vol. 68, pp. 276–281, 2015.

[113] W. N. Reynolds and J. V. Sharp, “Crystal shear limit to carbon fibre strength,” *Carbon N. Y.*, vol. 12, pp. 103–110, 1974.

[114] International Organisation for Standardisation, “ISO 11566:1996: Carbon fibre - Determination of the tensile properties of single-filament specimens,” Geneva, Switzerland, 2011.

[115] J. L. Thomason, “On the application of Weibull analysis to experimentally determined single fibre strength distributions.,” *Compos. Sci. Technol.*, vol. 77, pp. 74–80, 2013.

[116] D. T. Burn *et al.*, “The usability of recycled carbon fibres in short fibre thermoplastics: interfacial properties.,” *J. Mater. Sci.*, vol. 51, no. 16, pp. 7699–7715, 2016.

[117] G. Jiang, S. J. Pickering, E. H. Lester, T. A. Turner, K. H. Wong, and N. A. Warrior, “Characterisation of carbon fibres recycled from carbon fibre / epoxy resin composites using supercritical n -propanol,” *Compos. Sci. Technol.*, vol. 69, no. 2, pp. 192–198, 2009.

[118] E. D. McCarthy and C. Soutis, “Determination of interfacial shear strength in continuous fibre composites by multi-fibre fragmentation: A review,” *Compos. Part A Appl. Sci. Manuf.*, vol. 118, pp. 281–292, 2019.

[119] J. Liu, H. Ge, J. Chen, D. Wang, and H. Liu, “The preparation of emulsion type sizing agent for carbon fiber and the properties of carbon fiber/vinyl ester resin composites,” *J. Appl. Polym. Sci.*, vol. 124, pp. 864–872, 2011.

[120] J. Chen, J. Liu, and D. Wang, “Effect of Emulsion Type Sizing Agents on the Properties of Carbon Fiber and Carbon Fiber Reinforced Polymer Matrix Composite,” *Adv. Mater. Res.*, vol. 236–238, pp. 2295–2298, 2011.

[121] J. W. Shim, S. J. Park, and S. K. Ryu, “Effect of modification with HNO3 and NaOH on metal adsorption by pitch-based activated carbon fibers,” *Carbon N. Y.*, vol. 39, pp. 1635–1642, 2001.

[122] S. Tiwari, J. Bijwe, and S. Panier, “Tribological studies on polyetherimide

composites based on carbon fabric with optimized oxidation treatment," *Wear*, vol. 271, pp. 2252–2260, 2011.

[123] S. Tiwari, J. Bijwe, and S. Panier, "Influence of plasma treatment on carbon fabric for enhancing abrasive wear properties of polyetherimide composites," *Tribol. Lett.*, vol. 41, pp. 153–162, 2011.

[124] J. Q. Li, Y. D. Huang, S. Y. Fu, L. H. Yang, H. tao Qu, and G. shun Wu, "Study on the surface performance of carbon fibres irradiated by γ-ray under different irradiation dose," *Appl. Surf. Sci.*, vol. 256, pp. 2000–2004, 2010.

[125] J. Wang, C. A. Fuentes, D. Zhang, X. Wang, A. W. Van Vuure, and D. Seveno, "Wettability of carbon fibres at micro- and mesoscales," *Carbon N. Y.*, vol. 120, pp. 438–446, 2017.

[126] F. Liu, Z. Shi, and Y. Dong, "Improved wettability and interfacial adhesion in carbon fibre/epoxy composites via an aqueous epoxy sizing agent," *Compos. Part A Appl. Sci. Manuf.*, vol. 112, pp. 337–345, 2018.

[127] F. Stojcevski, T. B. Hilditch, T. R. Gengenbach, and L. C. Henderson, "Effect of carbon fiber oxidization parameters and sizing deposition levels on the fiber-matrix interfacial shear strength," *Compos. Part A Appl. Sci. Manuf.*, vol. 114, pp. 212–224, 2018.

[128] F. Stojcevski, T. B. Hilditch, and L. C. Henderson, "A comparison of interfacial testing methods and sensitivities to carbon fiber surface treatment conditions," *Compos. Part A Appl. Sci. Manuf.*, vol. 118, pp. 293–301, 2019.

[129] C. Wang *et al.*, "Enhancing the interfacial strength of carbon fiber reinforced epoxy composites by green grafting of poly(oxypropylene) diamines," *Compos. Part A Appl. Sci. Manuf.*, vol. 99, pp. 58–64, 2017.

[130] X. Yuan, B. Zhu, X. Cai, J. Liu, K. Qiao, and J. Yu, "Optimization of interfacial properties of carbon fiber/epoxy composites via a modified polyacrylate emulsion sizing," *Appl. Surf. Sci.*, 2017.

[131] S. J. Park, M. K. Seo, and Y. S. Lee, "Surface characteristics of fluorine-modified PAN-based carbon fibers," *Carbon N. Y.*, vol. 41, pp. 723–730, 2003.

[132] D. Semitekolos, P. Kainourgios, C. Jones, A. Rana, E. P. Koumoulos, and C. A. Charitidis, "Advanced carbon fibre composites via poly methacrylic acid surface treatment; surface analysis and mechanical properties investigation," *Compos. Part B Eng.*, vol. 155, pp. 237–243, 2018.

[133] N. Koutroumanis *et al.*, "A novel mild method for surface treatment of carbon fibres in epoxy-matrix composites," *Compos. Sci. Technol.*, vol. 157, pp. 178–184, 2018.

[134] A. P. Hinterreiter *et al.*, "Determination of the surface chemistry of ozone-treated carbon fibers by highly consistent evaluation of X-ray photoelectron spectra," *Carbon N. Y.*, vol. 146, pp. 97–105, 2019.

[135] L. Liu *et al.*, "Interfacial characterization, control and modification of carbon fiber reinforced polymer composites," *Compos. Sci. Technol.*, vol. 121, pp. 56–72, 2015.

[136] N. van de Werken, M. S. Reese, M. R. Taha, and M. Tehrani, "Investigating the effects of fiber surface treatment and alignment on mechanical properties of recycled carbon fiber composites," *Compos. Part A Appl. Sci. Manuf.*, vol. 119, pp. 38–47, 2019.

[137] M. J. Emerson, V. A. Dahl, K. Conradsen, L. P. Mikkelsen, and A. B. Dahl, "Statistical validation of individual fibre segmentation from tomograms and microscopy," *Compos. Sci. Technol.*, vol. 160, pp. 208–215, 2018.

[138] Y. C. Chiou, H. Y. Chou, and M. Y. Shen, "Effects of adding graphene nanoplatelets and nanocarbon aerogels to epoxy resins and their carbon fiber composites," *Mater. Des.*, vol. 178, pp. 1–11, 2019.

[139] N. A. Krans, N. Ahmad, D. Alloyeau, K. P. de Jong, and J. Zečević, "Attachment of iron oxide nanoparticles to carbon nanofibers studied by in-situ liquid phase transmission electron microscopy," *Micron*, vol. 117, pp. 40–46, 2019.

[140] M. Seyring, A. Simon, I. Voigt, U. Ritter, and M. Rettenmayr, "Quantitative crystallographic analysis of individual carbon nanofibers using high resolution transmission electron microscopy and electron diffraction," *Carbon N. Y.*, vol. 116, pp. 347–355, 2017.

[141] Q. Wu, M. Li, Y. Gu, S. Wang, and Z. Zhang, "Imaging the interphase of carbon fiber composites using transmission electron microscopy: Preparations by focused ion beam, ion beam etching, and ultramicrotomy," *Chinese J. Aeronaut.*, vol. 28, no. 5, pp. 1529–1538, 2015.

[142] E. Klinklin and M. Guigon, "Characterization of the interface in carbon-fibre reinforced composites by transmission electron microscopy," *Colloids Surfaces A Physicochem. Eng. Asp.*, vol. 74, pp. 243–250, 1993.

[143] B. Bruck, T. Guglhoer, S. Haug, and W. M. Mueller, "Surface Characterization

of Carbon Fibers by Atomic Force Microscopy: Roughness Quantification by Power Spectral Density," in *21st Symposium on Composites*, 2017, pp. 447–456.

[144] B. N. Zaitsev, N. I. Baklanova, and T. M. Zima, "Atomic force microscopy study of surface-modified carbon fibers," *Inorg. Mater.*, vol. 44, no. 6, pp. 592–597, 2008.

[145] A. Schneller, L. Henry, J. Doerfler, W. M. Mueller, C. Aymonier, and S. Horn, "Recycling of carbon fibers from carbon fiber reinforced thermoset polymers by use of sub- and supercritical fluids," *ECCM 2016 - Proceeding 17th Eur. Conf. Compos. Mater.*, no. June, 2016.

[146] L. Yuyan, S. Guohua, and M. Linghui, "Recycling of carbon fibre reinforced composites using water in subcritical conditions," *Mater. Sci. Eng. A*, vol. 520, no. 1–2, pp. 179–183, 2009.

[147] F. Léonard, J. Stein, C. Soutis, and P. J. Withers, "The quantification of impact damage distribution in composite laminates by analysis of X-ray computed tomograms," *Compos. Sci. Technol.*, vol. 152, pp. 139–148, 2017.

[148] S. C. Garcea, I. Sinclair, S. M. Spearing, and P. J. Withers, "Mapping fibre failure in situ in carbon fibre reinforced polymers by fast synchrotron X-ray computed tomography," *Compos. Sci. Technol.*, vol. 149, pp. 81–89, 2017.

[149] S. C. Garcea, Y. Wang, and P. J. Withers, "X-ray computed tomography of polymer composites," *Compos. Sci. Technol.*, vol. 156, pp. 305–319, 2018.

[150] N. Forintos and T. Czigany, "Multifunctional application of carbon fiber reinforced polymer composites: Electrical properties of the reinforcing carbon fibers – A short review," *Compos. Part B Eng.*, vol. 162, pp. 331–343, 2019.

[151] Y. J. Kim *et al.*, "Simultaneous enhancement of mechanical and electrical properties of carbon nanotube fiber by infiltration and subsequent carbonization of resorcinol-formaldehyde resin," *Compos. Part B Eng.*, 2019.

[152] X. Qian *et al.*, "Evolution of microstructure and electrical property in the conversion of high strength carbon fiber to high modulus and ultrahigh modulus carbon fiber," *Compos. Part A Appl. Sci. Manuf.*, vol. 112, pp. 111–118, 2018.

[153] L. Bhanuprakash, S. Parasuram, and S. Varghese, "Experimental investigation on graphene oxides coated carbon fibre/epoxy hybrid

composites: Mechanical and electrical properties," *Compos. Sci. Technol.*, vol. 179, pp. 134–144, 2019.

[154] G. Faneca, I. Segura, J. M. Torrents, and A. Aguado, "Development of conductive cementitious materials using recycled carbon fibres," *Cem. Concr. Compos.*, vol. 92, pp. 135–144, 2018.

[155] A. B. Strong, *Fundamentals of Composites Manufacturing: Materials, Methods and Applications*, 2nd ed. Michigan, USA: Society of Manufacturing Engineers, 2008.

[156] D. M. Corbridge, L. T. Harper, D. S. A. De Focatiis, and N. A. Warrior, "Compression moulding of composites with hybrid fibre architectures," *Compos. Part A Appl. Sci. Manuf.*, vol. 95, pp. 87–99, 2017.

[157] S. J. Park and B. J. Kim, "Carbon fibers and their composites," *Springer Ser. Mater. Sci.*, vol. 210, 2015.

[158] E. M. Sozer, P. Simacek, and S. G. Advani, "Resin transfer molding (RTM) in polymer matrix composites," in *Manufacturing Techniques for Polymer Matrix Composites (PMCs)*, S. G. Advani and L.-T. Hsiao, Eds. Cambridge, UK: Woodhead Publishing Ltd., 2012, pp. 245–309.

[159] V. Achim and E. Ruiz, "Guiding selection for reduced process development time in RTM," *Int. J. Mater. Form.*, vol. 3, no. SUPPL. 2, pp. 1277–1286, 2010.

[160] E. Poodts, G. Minak, L. Mazzocchetti, and L. Giorgini, "Fabrication, process simulation and testing of a thick CFRP component using the RTM process," *Compos. Part B Eng.*, vol. 56, pp. 673–680, 2014.

[161] K.-T. Hsiao and D. Heider, "Vacuum assisted resin transfer molding (VARTM) in polymer matrix composites," in *Manufacturing Techniques for Polymer Matrix Composites (PMCs)*, S. G. Advani and K.-T. Hsiao, Eds. Cambridge, UK: Woodhead Publishing Ltd., 2012, pp. 310–347.

[162] G. Eckold, "Manufacture," in *Design and Manufacture of Composite Structures*, Cambridge, UK: Woodhead Publishing Ltd., 1994, pp. 251–304.

[163] A. T. Marques, "Fibrous materials reinforced composites production techniques," in *Fibrous and Composite Materials for Civil Engineering Applications*, R. Fanguiero, Ed. Cambridge, UK: Woodhead Publishing Ltd., 2011, pp. 191–215.

[164] C. Atas, Y. Akgun, O. Dagdelen, B. M. Icten, and M. Sarikanat, "An experimental investigation on the low velocity impact response of

composite plates repaired by VARIM and hand lay-up processes," *Compos. Struct.*, vol. 93, pp. 1178–86, 2011.

[165] K. Zhang, Y. Gu, M. Li, and Z. Zhang, "Effect of rapid curing process on the properties of carbon fiber/epoxy composite fabricated using vacuum assisted resin infusion molding," *Mater. Des.*, vol. 54, pp. 624–631, 2014.

[166] S. Bickerton, Q. Govignon, and P. Kelly, "Resin infusion/liquid composite moulding (LCM) of advanced fibre-reinforced polymer (FRP)," in *Advanced Fibre-Reinforced Polymer (FRP) Composites for Structural Applications*, J. Bai, Ed. Cambridge, UK: Woodhead Publishing Ltd., 2013, pp. 155–186.

[167] A. Khennane, "Filament winding processes in the manufacture of advanced fibre-reinforced polymer (FRP) composites," in *Advanced Fibre-Reinforced Polymer (FRP) Composites for Structural Applications*, J. Bai, Ed. Cambridge, UK: Woodhead Publishing Ltd., 2012, pp. 187–206.

[168] E. Vargas Rojas, D. Chapelle, D. Perreux, B. Delobelle, and F. Thiebaud, "Unified approach of filament winding applied to complex shape mandrels," *Compos. Struct.*, 2014.

[169] L. Zu, H. Xu, B. Zhang, D. Li, and B. Zi, "Design of filament-wound composite structures with arch-shaped cross sections considering fiber tension simulation," *Compos. Struct.*, vol. 194, pp. 119–125, 2018.

[170] M. Sayem Uddin, E. V. Morozov, and K. Shankar, "The effect of filament winding mosaic pattern on the stress state of filament wound composite flywheel disk," *Compos. Struct.*, vol. 107, pp. 260–275, 2014.

[171] Z. Qureshi, T. Swait, R. Scaife, and H. M. El-Dessouky, "In situ consolidation of thermoplastic prepreg tape using automated tape placement technology: Potential and possibilities," *Compos. Part B Eng.*, vol. 66, pp. 255–267, 2014.

[172] P. Maung, B. G. Prusty, J. M. White, M. David, A. W. Phillips, and N. A. St John, "Structural performance of a shape-adaptive composite hydrofoil using automated fibre placement," *Eng. Struct.*, vol. 183, pp. 351–365, 2019.

[173] C. Schmidt, P. Weber, T. Hocke, and B. Denkena, "Influence of Prepreg Material Quality on Carbon Fiber Reinforced Plastic Laminates Processed by Automated Fiber Placement," in *Procedia CIRP*, 2018.

[174] L. S. Lee and R. Jain, "The role of FRP composites in a sustainable world," *Clean Technol. Environ. Policy*, vol. 11, no. 3, pp. 247–249, 2009.

[175] F. Meng, S. J. . Pickering, and J. . McKechnie, “An environmental comparison of carbon fibre composite waste end-of-life options,” in *SAMPE Europe Conference 2018*, 2018, no. September.

[176] F. Meng, J. McKechnie, T. Turner, K. H. Wong, and S. J. Pickering, “Environmental Aspects of Use of Recycled Carbon Fiber Composites in Automotive Applications,” *Environ. Sci. Technol.*, vol. 51, no. 21, pp. 12727–12736, Nov. 2017.

[177] Y. Ma and S. Nutt, “Chemical treatment for recycling of amine/epoxy composites at atmospheric pressure,” *Polym. Degrad. Stab.*, vol. 153, pp. 307–317, 2018.

[178] I. Okajima, K. Watanabe, and T. Sako, “Chemical Recycling of Carbon Fiber Reinforced Plastic with Supercritical Alcohol,” *J. Adv. Res.*, vol. 3, no. 2, pp. 1–4, 2012.

[179] A. Jacob, “Composites can be recycled.,” *Reinf. Plast.*, vol. 55, pp. 45–46, 2011.

[180] S. J. Pickering, Z. Liu, T. A. Turner, and K. H. Wong, “Applications for carbon fibre recovered from composites,” in *IOP Conference Series: Materials Science and Engineering*, 2016, vol. 139, pp. 1–18.

[181] K. Wood, “Carbon fiber reclamation: going commercial,” *High Perform. Compos.*, vol. 3, pp. 1–2, 2010.

[182] S. Job, G. Leeke, P. T. Mativenga, G. Oliveux, S. Pickering, and N. A. Shuaib, “Composites recycling: Where are we now?,” 2016.

[183] ELG Carbon Fibre Ltd., “Carbon fibre non-woven mats,” 2017. [Online]. Available: http://www.elgcf.com/products/100-recycled-carbon-fibre-nonwoven-mat. [Accessed: 04-Aug-2019].

[184] K. Zhang, J. Lim, S. Nassiri, K. Englund, and H. Li, “Reuse of carbon fiber composite materials in porous hot mix asphalt to enhance strength and durability,” *Case Stud. Constr. Mater.*, vol. 11, pp. 1–13, 2019.

[185] J. Rybicka, A. Tiwari, and G. A. Leeke, “Technology readiness level assessment of composites recycling technologies,” *J. Clean. Prod.*, vol. 112, pp. 1001–1012, 2016.

[186] S. Verma, B. Balasubramaniam, and R. K. Gupta, “Recycling, reclamation and re-manufacturing of carbon fibres,” *Curr. Opin. Green Sustain. Chem.*, vol. 13, pp. 86–90, 2018.

[187] J. Maris, S. Bourdon, J. M. Brossard, L. Cauret, L. Fontaine, and V. Montembault, “Mechanical recycling: Compatibilization of mixed thermoplastic wastes,” *Polym. Degrad. Stab.*, vol. 147, pp. 245–266, 2018.

[188] J. Palmer, L. Savage, O. R. Ghita, and K. E. Evans, “Sheet moulding compound (SMC) from carbon fibre recyclate,” *Compos. Part A Appl. Sci. Manuf.*, vol. 41, pp. 1232–1237, 2010.

[189] C. E. Kouparitsas, C. N. Kartalis, P. C. Varelidis, C. J. Tsenoglou, and C. D. Papaspyrides, “Recycling of the fibrous fraction of reinforced thermoset composites,” *Polym. Compos.*, vol. 23, no. 4, pp. 682–689, 2002.

[190] E. Uhlmann and P. Meier, “Carbon Fibre Recycling from Milling Dust for the Application in Short Fibre Reinforced Thermoplastics,” *Procedia CIRP*, vol. 66, pp. 277–282, 2017.

[191] K. Ogi, T. Nishikawa, Y. Okano, and I. Taketa, “Mechanical properties of ABS resin reinforced with recycled CFRP,” *Adv. Compos. Mater. Off. J. Japan Soc. Compos. Mater.*, vol. 16, no. 2, pp. 181–194, 2007.

[192] C. Thomas, P. H. R. Borges, T. H. Panzera, A. Cimentada, and I. Lombillo, “Epoxy composites containing CFRP powder wastes,” *Compos. Part B Eng.*, vol. 59, pp. 260–268, 2014.

[193] N. A. Shuaib, P. T. Mativenga, J. Kazie, and S. Job, “Resource efficiency and composite waste in UK supply chain,” *Procedia CIRP*, vol. 29, pp. 662–667, 2015.

[194] X. Li, R. Bai, and J. McKechnie, “Environmental and financial performance of mechanical recycling of carbon fibre reinforced polymers and comparison with conventional disposal routes,” *J. Clean. Prod.*, 2016.

[195] J. Howarth, S. S. R. Mareddy, and P. T. Mativenga, “Energy intensity and environmental analysis of mechanical recycling of carbon fibre composite,” *J. Clean. Prod.*, vol. 81, pp. 46–50, 2014.

[196] H. Bluhm, W. Frey, H. Giese, P. Hoppe, C. Schulteiss, and R. Strassner, “Application of pulsed HV discharges to material fragmentation and recycling,” *IEEE Trans. Dielectr. Electr. Insul.*, vol. 7, no. 5, pp. 625–636, 2000.

[197] P. T. Mativenga, N. A. Shuaib, J. Howarth, F. Pestalozzi, and J. Woidasky, “High voltage fragmentation and mechanical recycling of glass fibre thermoset composite,” *CIRP Ann. - Manuf. Technol.*, vol. 65, pp. 45–48, 2016.

[198] M. Roux, C. Dransfeld, N. Eguémann, and L. Giger, “Processing and recycling of a thermoplastic composite fibre/peek aerospace part,” *16th Eur. Conf. Compos. Mater. ECCM 2014*, no. June, pp. 22–26, 2014.

[199] K. Oshima, S. Matsuda, M. Hosaka, and S. Satokawa, “Rapid removal of resin from a unidirectional carbon fiber reinforced plastic laminate by a high-voltage electrical treatment,” *Sep. Purif. Technol.*, vol. In Press, 2019.

[200] C. L. Duan, Z. J. Diao, Y. M. Zhao, and W. Huang, “Liberation of valuable materials in waste printed circuit boards by high-voltage electrical pulses,” *Miner. Eng.*, vol. 70, pp. 170–177, 2015.

[201] T. Leißner, D. Hamann, L. Wuschke, H. G. Jäckel, and U. A. Peuker, “High voltage fragmentation of composites from secondary raw materials – Potential and limitations,” *Waste Manag.*, vol. 74, pp. 123–134, 2018.

[202] M. K. Hagnell and M. Åkermo, “The economic and mechanical potential of closed loop material usage and recycling of fibre-reinforced composite materials,” *J. Clean. Prod.*, vol. 223, pp. 957–968, 2019.

[203] S. Pimenta and S. T. Pinho, “Recycling of Carbon Fibers,” in *Handbook of Recycling: State-of-the-art for Practitioners, Analysts, and Scientists*, E. Worrell and M. A. Reuter, Eds. London, UK: Elsevier Ltd, 2014, pp. 269–283.

[204] G. G. Matielli Rodrigues, J. M. Faulstich De Paiva, J. Braga Do Carmo, and V. R. Botaro, “Recycling of carbon fibers inserted in composite of DGEBA epoxy matrix by thermal degradation,” *Polym. Degrad. Stab.*, vol. 109, pp. 50–58, 2014.

[205] A. M. Cunliffe and P. T. Williams, “Characterisation of products from the recycling of glass fibre reinforced polyester waste by pyrolysis,” *Fuel*, vol. 82, pp. 2223–2230, 2003.

[206] S. R. Naqvi, H. M. Prabhakara, E. A. Bramer, W. Dierkes, R. Akkerman, and G. Brem, “A critical review on recycling of end-of-life carbon fibre/glass fibre reinforced composites waste using pyrolysis towards a circular economy,” *Resour. Conserv. Recycl.*, vol. 136, pp. 118–129, 2018.

[207] L. Mazzocchetti, T. Benelli, E. D’Angelo, C. Leonardi, G. Zattini, and L. Giorgini, “Validation of carbon fibers recycling by pyro-gasification: The influence of oxidation conditions to obtain clean fibers and promote fiber/matrix adhesion in epoxy composites,” *Compos. Part A Appl. Sci. Manuf.*, vol. 112, pp. 504–514, 2018.

[208] M. A. Nahil and P. T. Williams, “Recycling of carbon fibre reinforced

polymeric waste for the production of activated carbon fibres," *J. Anal. Appl. Pyrolysis*, vol. 91, pp. 67–75, 2011.

[209] L. J. Brown, F. X. Collard, and J. Görgens, "Fast pyrolysis of fibre waste contaminated with plastic for use as fuel products," *J. Anal. Appl. Pyrolysis*, vol. 138, pp. 261–269, 2019.

[210] J. S. Jeong, K. W. Kim, K. H. An, and B. J. Kim, "Fast recovery process of carbon fibers from waste carbon fibers-reinforced thermoset plastics," *J. Environ. Manage.*, vol. 247, pp. 816–821, 2019.

[211] K. W. Kim, H. M. Lee, J. H. An, D. C. Chung, K. H. An, and B. J. Kim, "Recycling and characterization of carbon fibers from carbon fiber reinforced epoxy matrix composites by a novel super-heated-steam method," *J. Environ. Manage.*, 2017.

[212] J. Yang, J. Liu, W. Liu, J. Wang, and T. Tang, "Recycling of carbon fibre reinforced epoxy resin composites under various oxygen concentrations in nitrogen-oxygen atmosphere," *J. Anal. Appl. Pyrolysis*, 2015.

[213] L. O. Meyer, K. Schulte, and E. Grove-Nielsen, "CFRP-recycling following a pyrolysis route: Process optimization and potentials," *J. Compos. Mater.*, vol. 43, no. 9, pp. 1121–1132, 2009.

[214] F. Meng, J. McKechnie, T. A. Turner, and S. J. Pickering, "Energy and environmental assessment and reuse of fluidised bed recycled carbon fibres," *Compos. Part A Appl. Sci. Manuf.*, vol. 100, pp. 206–214, 2017.

[215] S. J. Pickering, R. M. Kelly, J. R. Kennerley, C. D. Rudd, and N. J. Fenwick, "A fluidised-bed process for the recovery of glass fibres from scrap thermoset composites," *Compos. Sci. Technol.*, vol. 60, pp. 509–523, 2000.

[216] H. L. H. Yip, S. J. Pickering, and C. D. Rudd, "Characterisation of carbon fibres recycled from scrap composites using fluidised bed process," *Plast. Rubber Compos.*, vol. 31, no. 6, pp. 278–282, 2002.

[217] S. J. Pickering, "Recycling technologies for thermoset composite materials—current status," *Compos. Part A Appl. Sci. Manuf.*, vol. 37, no. 8, pp. 1206–1215, 2006.

[218] F. Meng, J. McKechnie, and S. J. Pickering, "An assessment of financial viability of recycled carbon fibre in automotive applications," *Compos. Part A Appl. Sci. Manuf.*, vol. 109, pp. 207–220, 2018.

[219] F. Meng, J. Mckechnie, and S. J. Pickering, "Towards a circular economy for

end-of-lifecarbonfibre composite materials viafluidised bed process," in *21st International Conference on Composite Materials (ICCM21)*, 2017, pp. 1–8.

[220] E. Witten and V. Mathes, "Composites Market Report2018," 2018.

[221] E. Lester, S. Kingman, K. H. Wong, C. Rudd, S. Pickering, and N. Hilal, "Microwave heating as a means for carbon fibre recovery from polymer composites: A technical feasibility study," *Mater. Res. Bull.*, vol. 39, pp. 1549–1556, 2004.

[222] Eltron Research & Development Inc., "Catalytic Microwave Assisted Gasification for Recycling Polymer Matrix Composites," 2009. [Online]. Available: http://www.eltronresearch.com/docs/Catalytic_Microwave_Gasification_Polymer_Matrix_Composites.pdf. [Accessed: 01-Aug-2019].

[223] W. Nie, J. Liu, W. Liu, J. Wang, and T. Tang, "Decomposition of waste carbon fiber reinforced epoxy resin composites in molten potassium hydroxide," *Polym. Degrad. Stab.*, vol. 111, pp. 247–256, 2015.

[224] T. Wu, W. Zhang, X. Jin, X. Liang, G. Sui, and X. Yang, "Efficient reclamation of carbon fibers from epoxy composite waste through catalytic pyrolysis in molten ZnCl 2," *RSC Adv.*, vol. 9, no. 1, pp. 377–388, 2019.

[225] United Nations Framework on Climate Change, "Paris Agreement - Status of Ratification," 2020. [Online]. Available: https://unfccc.int/process/the-paris-agreement/status-of-ratification. [Accessed: 07-Jan-2020].

[226] M. J. Keith, L. Roman-Ramires, G. A. Leeke, and A. Ingram, "Recycling a carbon fibre reinforced polymer with a supercritical acetone/water solvent mixture: Comprehensive analysis of reaction kinetics," *Polym. Degrad. Stab.*, vol. 161, pp. 225–234, 2019.

[227] J. Gosau, T. F. Wesley, and R. E. Allred, "Integrated Composite Recycling Process," in *Proceedings of the 38th SAMPE Technical Conference*, 2006.

[228] J. Gosau, T.-F. Wesley, and R. Allred, "Carbon fiber reclamation from state-of-the-art 2nd generation aircraft composites.," 2009.

[229] W. Dang, M. Kubouchi, S. Yamamoto, H. Sembokuya, and K. Tsuda, "An approach to chemical recycling of epoxy resin cured with amine using nitric acid," *Polymer (Guildf).*, vol. 43, pp. 2953–2958, 2002.

[230] W. Dang, M. Kubouchi, H. Sembokuya, and K. Tsuda, "Chemical recycling of

glass fiber reinforced epoxy resin cured with amine using nitric acid," *Polymer (Guildf).*, vol. 46, pp. 1905–1912, 2005.

[231] J. Jiang *et al.*, "On the successful chemical recycling of carbon fiber/epoxy resin composites under the mild condition," *Compos. Sci. Technol.*, vol. 151, pp. 243–251, 2017.

[232] P. Feraboli, H. Kawakami, B. Wade, F. Gasco, L. Deoto, and A. Masini, "Recyclability and reutilization of carbon fiber fabric / epoxy composites," *J. Compos. Mater.*, vol. 46, no. 12, pp. 1459–1473, 2012.

[233] M. L. Longana, H. Yu, I. Hamerton, and K. D. Potter, "Development and application of a quality control and property assurance methodology for reclaimed carbon fibers based on the HiPerDiF (High Performance Discontinuous Fibre) method and interlaminated hybrid specimens," *Adv. Manuf. Polym. Compos. Sci.*, vol. 4, no. 2, pp. 48–55, 2018.

[234] G. Oliveux, J. Bailleul, A. Gillet, O. Mantaux, and G. A. Leeke, "Recovery and reuse of discontinuous carbon fibres by solvolysis: Realignment and properties of remanufactured materials," *Compos. Sci. Technol.*, vol. 139, pp. 99–108, 2016.

[235] P. Xu, J. Li, and J. Ding, "Chemical recycling of carbon fibre / epoxy composites in a mixed solution of peroxide hydrogen and N , N-dimethylformamide," *Compos. Sci. Technol.*, vol. 82, pp. 54–59, 2013.

[236] Y. Ma, D. Kim, and S. R. Nutt, "Chemical treatment for dissolution of amine-cured epoxies at atmospheric pressure," *Polym. Degrad. Stab.*, vol. 146, pp. 240–249, 2017.

[237] J. Li, P. L. Xu, Y. K. Zhu, J. P. Ding, L. X. Xue, and Y. Z. Wang, "A promising strategy for chemical recycling of carbon fiber/thermoset composites: Self-accelerating decomposition in a mild oxidative system," *Green Chem.*, vol. 14, no. 12, pp. 3260–3263, 2012.

[238] M. Sakuma, M. Koyama, and H. Fukuda, "Establishment of CFRP recycling method processable under atmospheric pressure," in *18th International Conference on Composite Materials (ICCM18)*, 2011, pp. 1–4.

[239] T. Liu, M. Zhang, X. Guo, C. Liu, T. Liu, and J. Xin, "Mild chemical recycling of aerospace fi ber / epoxy composite wastes and utilization of the decomposed resin," *Polym. Degrad. Stab.*, vol. 139, pp. 20–27, 2017.

[240] J. R. Hyde, E. Lester, S. Kingman, S. Pickering, and K. H. Wong, "Supercritical propanol, a possible route to composite carbon fibre recovery: A viability

study," *Compos. Part A Appl. Sci. Manuf.*, vol. 37, no. 11, pp. 2171–2175, 2006.

[241] G. Simenou, E. Le Gal La Salle, J.-L. Bailleul, and J. Bellettre, "Kinetic of the hydrolysis of three different carbon fibre reinforced epoxy (CFRE) in high temperature and high pressure water," *ECCM 2016 - Proceeding 17th Eur. Conf. Compos. Mater.*, no. June, 2016.

[242] R. Pinero-Hernanz *et al.*, "Chemical recycling of carbon fibre composites using alcohols under subcritical and supercritical conditions," *J. Supercrit. Fluids*, vol. 46, no. 1, pp. 83–92, 2013.

[243] Y. N. Kim *et al.*, "Application of supercritical water for green recycling of epoxy-based carbon fiber reinforced plastic," *Compos. Sci. Technol.*, vol. 173, no. January, pp. 66–72, 2019.

[244] C. C. Knight, C. Zeng, C. Zhang, and B. Wang, "Recycling of woven carbon-fibre-reinforced polymer composites using supercritical water," *Environ. Technol.*, vol. 33, no. 6, pp. 639–644, 2012.

[245] R. Pinero-Hernanz *et al.*, "Chemical recycling of carbon fibre reinforced composites in nearcritical and supercritical water," *Compos. Part A Appl. Sci. Manuf.*, vol. 39, no. 3, pp. 454–461, 2008.

[246] G. Oliveux, J. L. Bailleul, and E. L. G. La Salle, "Chemical recycling of glass fibre reinforced composites using subcritical water," *Compos. Part A Appl. Sci. Manuf.*, vol. 43, pp. 1809–1818, 2012.

[247] H. Sato *et al.*, "Sixteen thousand evaluated experimental thermodynamic property data for water and steam," *J. Phys. Chem. Ref. Data*, vol. 20, p. 1023, 1991.

[248] L. Henry, A. Schneller, J. Doer, W. M. Mueller, C. Aymonier, and S. Horn, "Semi-continuous flow recycling method for carbon fibre reinforced thermoset polymers by near- and supercritical solvolysis," *Polym. Degrad. Stab.*, vol. 133, pp. 264–274, 2016.

[249] I. Okajima, M. Hiramatsu, Y. Shimamura, T. Awaya, and T. Sako, "Chemical recycling of carbon fiber reinforced plastic using supercritical methanol," *J. Supercrit. Fluids*, vol. 91, pp. 68–76, 2014.

[250] H. Yan, C. Lu, D. Jing, C. Chang, N. Liu, and X. Hou, "Recycling of carbon fibers in epoxy resin composites using supercritical 1-propanol," *New Carbon Mater.*, vol. 31, no. 1, pp. 46–54, 2016.

[251] I. Okajima, K. Watanabe, S. Haramiishi, M. Nakamura, Y. Shimamura, and T. Sako, “Recycling of carbon fiber reinforced plastic containing amine-cured epoxy resin using supercritical and subcritical fluids,” *J. Supercrit. Fluids*, vol. 119, pp. 44–51, 2017.

[252] G. Oliveux, L. O. Dandy, and G. A. Leeke, “Degradation of a model epoxy resin by solvolysis routes,” *Polym. Degrad. Stab.*, vol. 118, pp. 96–103, 2015.

[253] E. Yildirir, J. A. Onwudili, and P. T. Williams, “Recovery of carbon fibres and production of high quality fuel gas from the chemical recycling of carbon fibre reinforced plastic wastes,” *J. Supercrit. Fluids*, vol. 92, pp. 107–114, 2014.

[254] R. Piñero-Hernanz *et al.*, “Chemical recycling of carbon fibre composites using alcohols under subcritical and supercritical conditions,” *J. Supercrit. Fluids*, vol. 46, pp. 83–92, 2008.

[255] C. C. Knight, C. Zeng, C. Zhang, and R. Liang, “Fabrication and properties of composites utilizing reclaimed woven carbon fiber by sub-critical and supercritical water recycling,” *Mater. Chem. Phys.*, vol. 149, pp. 317–323, 2015.

[256] Y. Liu, J. Liu, Z. Jiang, and T. Tang, “Chemical recycling of carbon fibre reinforced epoxy resin composites in subcritical water: Synergistic effect of phenol and KOH on the decomposition ef fi ciency,” *Polym. Degrad. Stab.*, vol. 97, no. 3, pp. 214–220, 2012.

[257] P. Yang, Q. Zhou, X. Yuan, J. M. N. Van Kasteren, and Y. Wang, “Highly efficient solvolysis of epoxy resin using poly (ethylene glycol) / NaOH systems,” *Polym. Degrad. Stab.*, vol. 97, no. 7, pp. 1101–1106, 2012.

[258] M. Gagliardi, P. Lenarda, and M. Paggi, “A reaction-diffusion formulation to simulate EVA polymer degradation in environmental and accelerated ageing conditions,” *Sol. Energy Mater. Sol. Cells*, vol. 164, pp. 93–106, 2017.

[259] M. N. Siddiqui, E. V. Antonakou, H. H. Redhwi, and D. S. Achilias, “Kinetic analysis of thermal and catalytic degradation of polymers found in waste electric and electronic equipment,” *Thermochim. Acta*, vol. 675, pp. 69–76, 2019.

[260] M. Celina, E. Linde, D. Brunson, A. Quintana, and N. Giron, “Overview of accelerated aging and polymer degradation kinetics for combined radiation-thermal environments,” *Polym. Degrad. Stab.*, vol. 166, pp. 353–378, 2019.

[261] G. Oliveux, J. Bailleul, E. Le, G. La, N. Lefèvre, and G. Biotteau, “Recycling of glass fibre reinforced composites using subcritical hydrolysis: Reaction mechanisms and kinetics , influence of the chemical structure of the resin,” *Polym. Degrad. Stab.*, vol. 98, no. 3, pp. 785–800, 2013.

[262] S. M. Al-Salem, “Kinetic studies relating to polymer degradation and stability,” in *Plastics to Energy: Fuel, Chemicals, and Sustainability Implications*, S. M. Al-Salem, Ed. Kuwait, 2019, pp. 233–268.

[263] O. Levenspiel, *Chemical Reaction Engineering*. New Jersey: John Wiley & Sons, Inc., 1999.

[264] I. Okajima, K. Watanabe, S. Haramiishi, M. Nakamura, Y. Shimamura, and T. Sako, “Recycling of carbon fiber reinforced plastic containing amine-cured epoxy resin using supercritical and subcritical fluids.,” *J. Supercrit. Fluids*, vol. 119, pp. 44–51, 2016.

[265] L. O. Dandy, G. Oliveux, J. Wood, M. J. Jenkins, and G. A. Leeke, “Accelerated degradation of Polyetheretherketone (PEEK) composite materials for recycling applications,” *Polym. Degrad. Stab.*, vol. 112, pp. 52–62, 2015.

[266] H. Tagaya, Y. Shibasaki, C. Kato, J. Kadokawa, and B. Hatano, “Decomposition reactions of epoxy resin and polyetheretherketone resin in sub- and supercritical water,” *J. Mater. Cycles Waste Manag.*, vol. 6, no. 1, pp. 1–5, 2004.

[267] M. H. Akonda, C. A. Lawrence, and B. M. Weager, “Recycled carbon fibre-reinforced polypropylene thermoplastic composites,” *Compos. Part A Appl. Sci. Manuf.*, vol. 43, pp. 79–86, 2012.

[268] S. Pimenta and S. T. Pinho, “The effect of recycling on the mechanical response of carbon fibres and their composites,” *Compos. Struct.*, vol. 94, pp. 3669–3684, 2012.

[269] A. Greco, A. Maffezzoli, G. Buccoliero, F. Caretto, and G. Cornacchia, “Thermal and chemical treatments of recycled carbon fibres for improved adhesion to polymeric matrix,” *J. Compos. Mater.*, vol. 47, no. 3, pp. 369–377, 2013.

[270] F. Knappich, M. Klotz, M. Schlummer, J. Wölling, and A. Mäurer, “Recycling process for carbon fiber reinforced plastics with polyamide 6, polyurethane and epoxy matrix by gentle solvent treatment,” *Waste Manag.*, vol. 85, pp. 73–81, 2019.

[271] Y. Bai, Z. Wang, and L. Feng, “Chemical recycling of carbon fibers reinforced

epoxy resin composites in oxygen in supercritical water," *Mater. Des.*, vol. 31, no. 2, pp. 999–1002, 2010.

[272] T. A. Langston and R. D. Granata, "Influence of nitric acid treatment time on the mechanical and surface properties of high-strength carbon fibers," *J. Compos. Mater.*, vol. 48, no. 3, pp. 259–276, 2014.

[273] S. H. Lee, H. O. Choi, J. S. Kim, C. K. Lee, Y. K. Kim, and C. S. Ju, "Circulating flow reactor for recycling of carbon fiber from carbon fiber reinforced epoxy composite," *Korean J. Chem. Eng.*, vol. 28, no. 2, pp. 449–454, 2011.

[274] J. Li, P. Xu, Y. Zhu, J. Ding, L. Xue, and Y. Wang, "A promising strategy for chemical recycling of carbon fiber/thermoset composites: self-accelerating decomposition in a mild oxidative system," *Green Chem.*, vol. 14, no. 12, pp. 3260–3263, 2012.

[275] M. Das, R. Chacko, and S. Varughese, "An Efficient Method of Recycling of CFRP Waste Using Peracetic Acid," *ACS Sustain. Chem. Eng.*, vol. 6, no. 2, pp. 1564–1571, 2018.

[276] P. Yang, Q. Zhou, X. Li, K. Yang, and Y. Wang, "Chemical recycling of fiber-reinforced epoxy resin using a polyethylene glycol / NaOH system," *J. Reinf. Plast. Compos.*, vol. 33, no. 22, pp. 2106–2114, 2014.

[277] Y. Wang *et al.*, "Chemical Recycling of Carbon Fiber Reinforced Epoxy Resin Composites via Selective Cleavage of the Carbon − Nitrogen Bond," *Sustain. Chem. Eng.*, vol. 3, no. 12, pp. 3332–3337, 2015.

[278] M. J. Keith, A. Ingram, and G. A. Leeke, "Catalytic degradation of a carbon fibre reinforced epoxy resin with an acetone / water solvent," in *Proceedings of the 18th European Conference on Composite Materials (ECCM18)*, 2018, no. June, pp. 24–28.

[279] M. Sauer and M. Kühnel, "Composites Market Report 2017: The global CF and CC Market," Augsberg, Germany, 2017.

[280] . Severn Trent Water, "Check My Water Quality." Severn Trent Water Inc., 2018.

[281] Toray, "T700S Carbon Fibre Data Sheet." pp. 1–2, 2015.

[282] EasyComposites, "Technical Data Sheet: Epoxy Infusion Resin." Easy Composites Ltd., Stoke-on-Trent, pp. 4–5, 2010.

[283] D. Ambrose, B. E. Broderick, and R. Townsend, "The Critical Temperatures and Pressures of Thirty Organic Compounds," *J. Chem. Technol. Biotechnol.*,

vol. 24, p. 359, 1974.

[284] J. Gross and G. Sadowski, “Perturbed-Chain SAFT: An Equation of State Based on a Perturbation Theory for Chain Molecules,” *Ind. Eng. Chem. Res.*, vol. 40, no. 4, p. 1244, 2001.

[285] J. Gross and G. Sadowski, “Application of the Perturbed-Chain SAFT Equation of State to Associating Systems,” *Ind. Eng. Chem. Res.*, vol. 41, no. 22, p. 5510, 2002.

[286] L. A. Román-Ramírez, F. García-Sánchez, R. C. D. Santos, and G. A. Leeke, “Vapour–Liquid Equilibrium of Propanoic Acid + Water at 423.2, 453.2 and 483.2 K from 1.87 to 19.38 bar. Experimental and Modelling with PR, CPA, PC-SAFT and PCP-SAFT,” *Fluid Phase Equilib.*, vol. 388, p. 151, 2015.

[287] D. F. Othmer, M. M. Chudgar, and S. L. Levy, “Binary and Ternary Systems of Acetone, Methyl Ethyl Ketone, and Water.,” *Ind. Eng. Chem.*, vol. 44, no. 8, p. 1872, 1952.

[288] J. Moosburger-will, M. Greisel, M. G. R. Sause, R. Horny, and S. Horn, “Influence of Partial Cross-Linking Degree on Basic Physical Properties of RTM6 Epoxy Resin,” *J. Appl. Polym. Sci.*, vol. 130, no. 6, pp. 4338–4346, 2013.

[289] D. Pauwels, J. Hereijgers, K. Verhulst, K. De Wael, and T. Breugelmans, “Investigation of the electrosynthetic pathway of the aldol condensation of acetone,” *Chem. Eng. J.*, vol. 289, pp. 554–561, 2016.

[290] U.S. National library of Medicine, “HSDB: 4-Hydroxy-4-Methyl-2-Pentanone,” 2014. .

[291] E. Peek, “Chloride Metallurgy - Process Technology Development,” in *EPD Congress*, 2011, pp. 469–485.

[292] M. Li, D. Constantinescu, and L. Wang, “Mixed Solvents and Correlation Using the LIQUAC Model,” *Ind. Eng. Chem. Res.*, vol. 49, no. 10, pp. 4981–4988, 2010.

[293] T. Deng *et al.*, “Cleavage of C-N Bonds in carbon fibre/epoxy resin composites,” *Green Chem.*, vol. 17, no. 4, pp. 2141–2145, 2015.

[294] I. M. Smallword, *Handbook of Organic Solvent Properties*. London, UK: Gray Publishing, 1996.

[295] O. Söhnel and P. Novotny, *Densities of Aqueous Solutions of Inorganic Substances*. Amsterdam: Elsevier Ltd., 1985.

[296] M. J. Keith, G. A. Leeke, P. Khan, and A. Ingram, “Catalytic degradation of a carbon fibre reinforced polymer for recycling applications,” *Polym. Degrad. Stab.*, vol. 166, pp. 188–201, 2019.

[297] M. J. Keith, G. Oliveux, and G. A. Leeke, “Optimisation of solvolysis for recycling carbon fibre reinforced composites,” in *ECCM 2016 - Proceeding of the 17th European Conference on Composite Materials*, 2016.

[298] E. Wiberg, A. F. Holleman, and N. Wiberg, *Inorganic Chemistry*. London, UK: Academic Press, 2013.

[299] . Toray Carbon Fibres America Inc, “T700S Data Sheet.” Toray Carbon Fibres America, Inc., California, pp. 1–2, 2015.

[300] G. C. Smith, *Handbook of Surface and Interface Analysis: Methods for Problem-Solving*. New York: Marcel Dekker, Inc, 1998.

[301] K. H. Wong, D. S. Mohammed, S. J. Pickering, and R. Brooks, “Effect of coupling agents on reinforcing potential of recycled carbon fibre for polypropylene composite,” *Compos. Sci. Technol.*, vol. 72, no. 7, pp. 835–844, 2012.

[302] P. H. Kvam and B. Vidakovic, *Nonparametric Statistics with Applications to Science and Engineering*. Atlanta, USA: John Wiley & Sons, Inc., 2011.

[303] W. Weibull, “A statistical distribution function of wide applicability.,” *J. Appl. Mech.*, vol. 18, no. 1, pp. 293–297, 1951.

[304] Instron Corporation, “Instron Series 5500 Load Frames Including Series 5540, 5560, 5580 Reference Manual - M10-14190-EN Revision A,” Massachusetts, 2005.

[305] H. Yuan, S. Zhang, C. Lu, S. He, and F. An, “Improved interfacial adhesion in carbon fiber/polyether sulfone composites through an organic solvent-free polyamic acid sizing,” *Appl. Surf. Sci.*, vol. 279, pp. 279–284, 2013.

[306] A. Grozdanov and G. Bogoeva-Gaceva, “Carbon Fibers/Polyamide 6 Composites Based on Hybrid Yarns,” *J. Thermoplast. Compos. Mater.*, vol. 23, pp. 99–110, 2010.

[307] G. Jiang, S. J. Pickering, G. S. Walker, K. H. Wong, and C. D. Rudd, “Surface characterisation of carbon fibre recycled using fluidised bed.,” *2Applied Surf. Sci.*, vol. 254, no. 9, pp. 2588–2593, 2008.

[308] W. B. Liu *et al.*, “Properties of carbon fiber sized with poly (phthalazinone ether ketone) resin,” *J. Appl. Polym. Sci.*, vol. 128, pp. 3702–3709, 2013.

[309] M. J. Keith, A. Ingram, and G. A. Leeke, “Recycling carbon fibre with an acetone / water solvent and zinc chloride catalyst: Resin degradation and fibre characterisation.,” in *Society for the Advancement of Materials and Process Engineering*, 2018, pp. 1–8.

[310] S. M. Lee, *Handbook of composite reinforcements*. California: Wiley, 1992.

[311] H. Zhang, Z. ZHang, and C. Breidt, “Comparison of short carbon fibre surface treatments on epoxy composites: Enhancement of the mechanical properties,” *Compos. Sci. Technol.*, vol. 64, no. 13, pp. 2021–2029, 2004.

[312] P. J. Larkin, *Infrared and Raman Spectroscopy.*, 1st ed. Elsevier Ltd, 2018.

[313] K. Kosswig, “Surfactants,” in *Ullmann’s Encyclopedia of Industrial Chemistry*, 1st ed., Weinheim, Germany: Wiley, 2002.

[314] I. Krivtsov *et al.*, “A new peroxo-route for the synthesis of Mg–Zr mixed oxides catalysts: Application in the gas phase acetone self-condensation,” *Appl. Catal. A Gen.*, vol. 477, pp. 26–33, 2014.

[315] G. S. Salvapati, K. V. Ramanamurty, and M. Janardanarao, “Selective catalytic self-condensation of acetone,” *J. Mol. Catal.*, vol. 54, no. 1, pp. 9–30, 1989.

[316] F. A. Carey and R. J. Sundberg, *Advanced Organic Chemistry: Part B: Reactions and Synthesis*, 5th ed. New York: Springer, 2007.

[317] J. M. Neri, N. Cavalcanti, Livia, R. M. Araujo, and F. G. Menezes, “2,3-Dichloroquinoxaline as a versatile building block for heteroaromatic nucleophilic substitution: A review of the last decade,” *Arab. J. Chem.*, vol. In press., 2017.

[318] S. R. White, P. T. Mather, and M. J. Smith, “Characterization of the cure state of DGEBA-DDS epoxy using ulstrasonic, dynamic mechanical and thermal probes,” *Polym. Eng. Sci.*, vol. 42, no. 1, pp. 51–67, 2004.

[319] M. Gonzalez, J. C. Cabanelas, and J. Baselga, “Applications of FTIR on Epoxy Resins – Identification, Monitoring the Curing Process, Phase Separation and Water Uptake.,” in *Infrared Spectroscopy - Materials Science, Engineering and Technology*, no. April, Madrid: IntechOpen, 2012, pp. 261–284.

APPENDIX

A.1 Measurement of Real Reactor Volume

The batch reactor used for all decomposition experiments had a nominal volume of 100 mL, however, this does not take into consideration the pipework and fittings mounted to the reactor lid which would increase the volume, nor the space taken up inside the vessel by the thermocouple. The actual volume of the reactor may be determined using the pressure – temperature (p-T) relationship of a particular substance. Water was selected as the working fluid due to the abundance of thermodynamic data widely available. Deionised (DI) water was degassed by heating to 60˚C in a water bath and sonicating for 30 min. This was subsequently sealed in a jar, the lid of which had been modified to include a steel dip pipe and valve connected to rubber tubing. A high vacuum pump was connected to the reactor lid and the vessel and associated pipework was evacuated. The pump was isolated and a small quantity of water allowed to be drawn into the vessel through the rubber tubing. The water storage jar was then similarly isolated and any water in the rubber tubing was allowed to drain back. The quantity of water in the vessel, determined by a difference in mass, was found to be 6.24 g. The system was then heated from room temperature to 390˚C and the pressure measured. The pressure – density relationship for water over a range of temperatures was taken from the NIST website. This data is shown in Figure A1 and the experimentally recorded pressure is overlaid on to the curves.

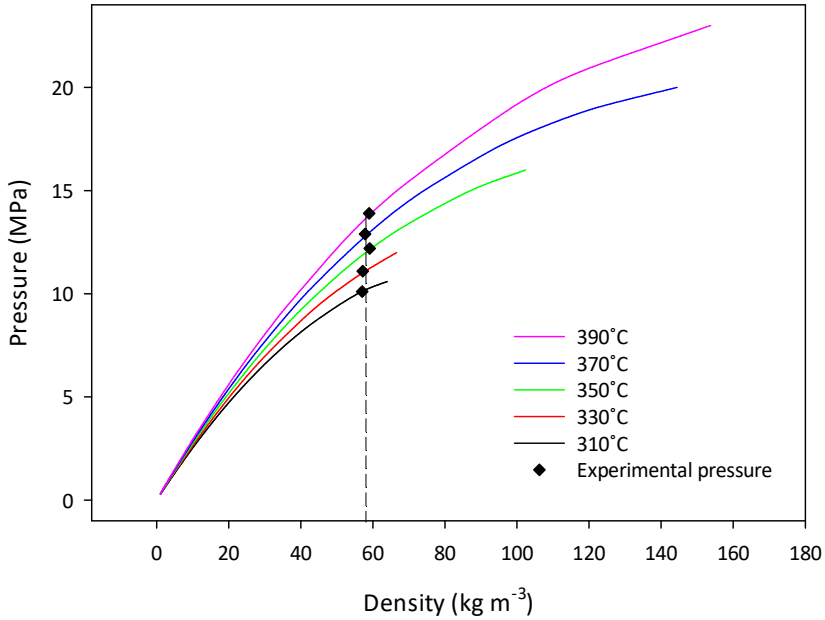

***Figure A1**. Pressure density relationship for water at a range of temperatures. Data taken from NIST, 2019.*

Extrapolating a line of best fit through to the x-axis of Figure A1 gives a density of the system of 58.08 kg m^{-3}. Dividing the mass of water in the vessel (6.24 $x10^{-3}$ kg) by this density gives a volume of 1.074 $x10^{-4}$ m^3, which is equivalent to 107.4 mL. It is worth noting, therefore, that under normal operation, there will be some solvent in the pipework outside the reactor. This will be cooler than the temperature measured in the vessel but, as it was not in contact with the CFRP, is not thought to significantly alter the reaction. The volume of the reactor was also verified by sealing it and pumping water through the reactor lid. When the pressure started to increase, the pump was stopped and isolated. A relief valve mounted to the reactor lid was then opened and water under pressure was removed. The remaining water was then collected and the volume measured to give a value of 104 mL.

A.2 Sizing Removal of Carbon Fibre

The thermogram shown in Figure A2 demonstrates that the as-received virgin carbon fibre contained approximately 1 wt.% of sizing. The mass loss of the fibre which had been processed using the Soxhlet extraction method was less than 0.1% thus demonstrating that more than 90% of the sizing had been removed.

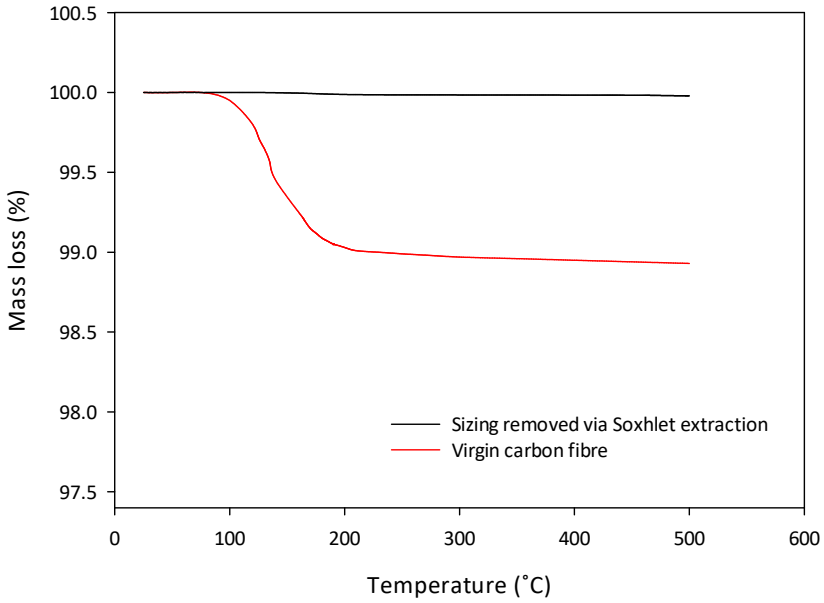

***Figure A2**. TGA thermogram of the as-received virgin carbon fibre and carbon fibre with the sizing removed via Soxhlet extraction.*

A.3 Supplementary Tensile Test Data

Weibull plots for each of the virgin Toray T700 fibres processed with the neat solvent and weak-Lewis acid systems are shown in Figure A3 to Figure A7. Tensile test data for the fibres recovered from the RTM6 epoxy resin at various conditions is provided in Figure A8.

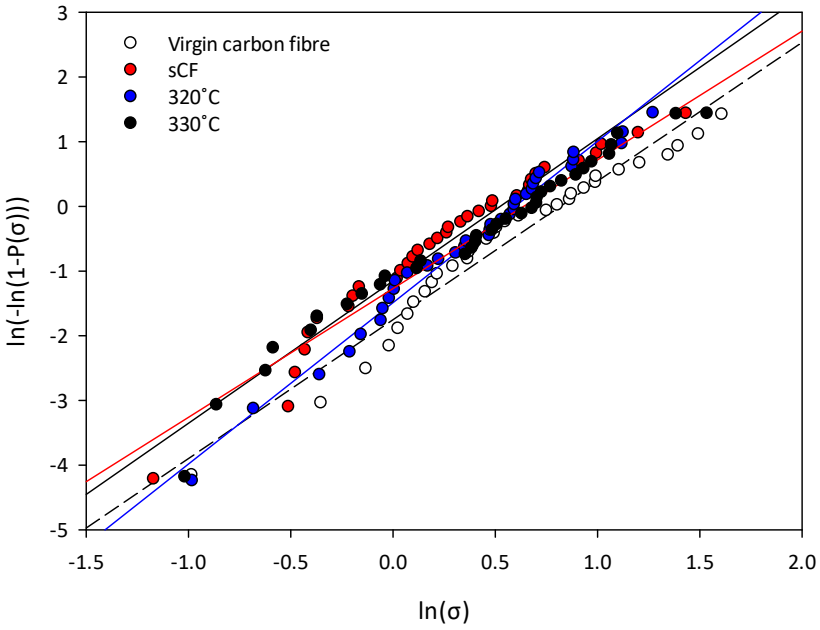

***Figure A3**. Weibull plots for virgin carbon fibres with the sizing removed via Soxhlet extraction and after processing with the neat acetone / water solvent at 320 and 330˚C.*

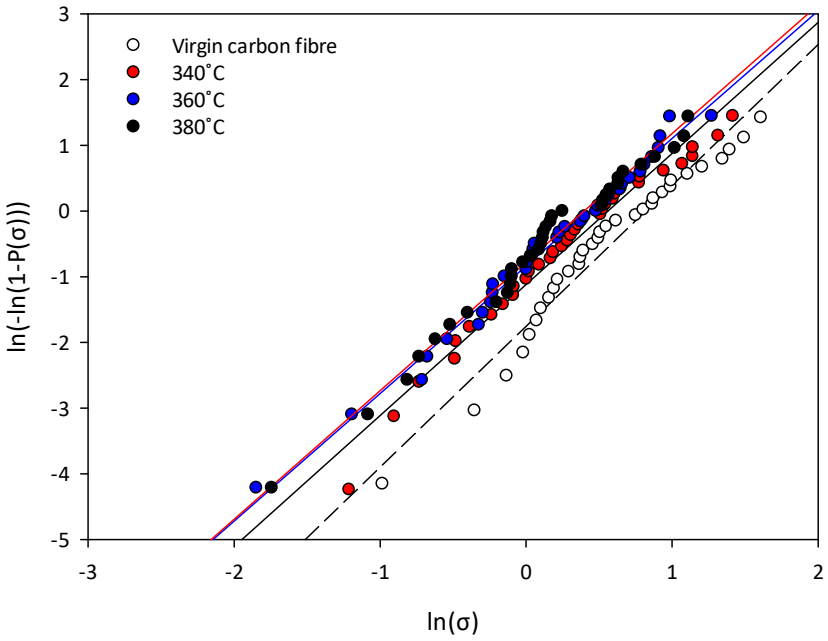

***Figure A4**. Weibull plots for virgin carbon fibres after processing with the neat acetone / water solvent at 340, 360 and 380˚C.*

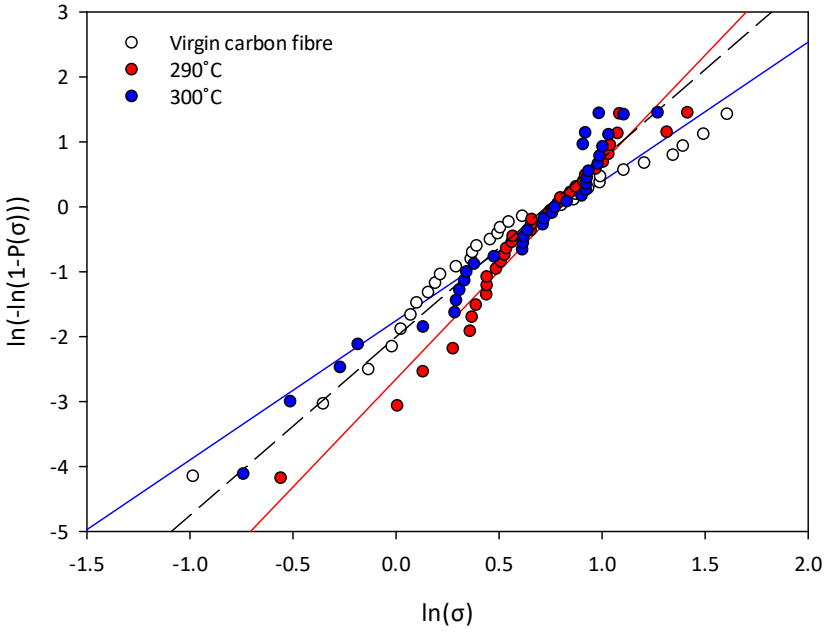

***Figure A5**. Weibull plots for virgin carbon fibres after processing with the 0.05 M $ZnCl_2$ solvent system at 290 and 300˚C.*

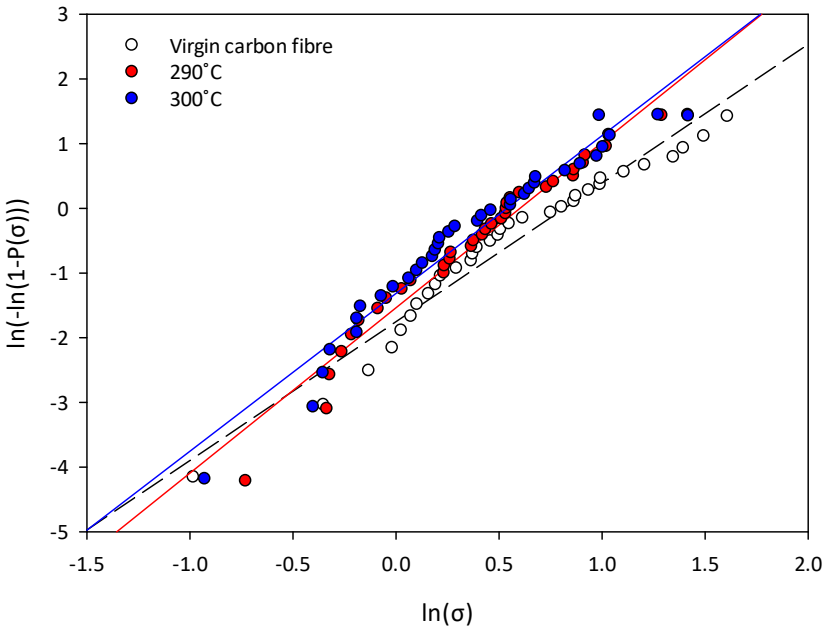

***Figure A6**. Weibull plots for virgin carbon fibres after processing with the 0.05 M $MgCl_2$ solvent system at 290 and 300˚C.*

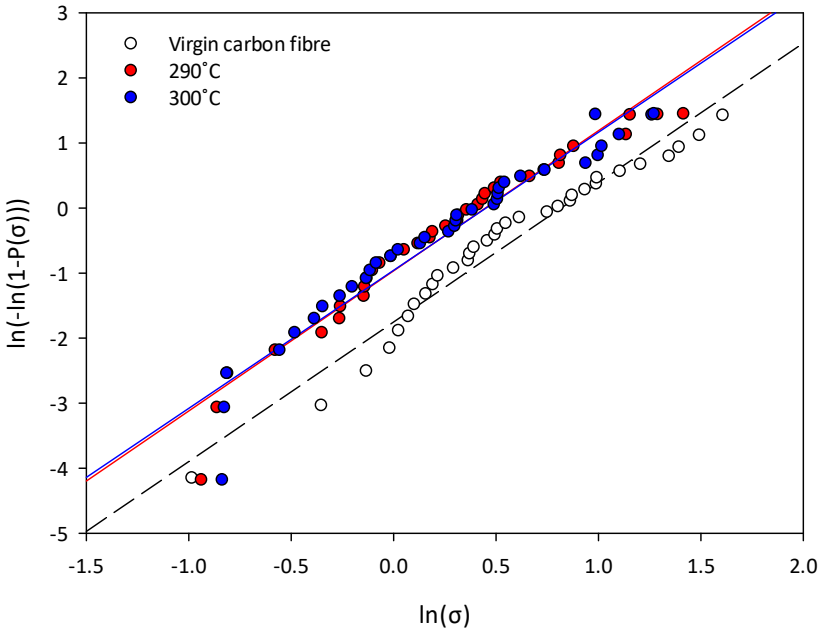

***Figure A7**. Weibull plots for virgin carbon fibres after processing with the 0.05 M $AlCl_3$ solvent system at 290 and 300˚C.*

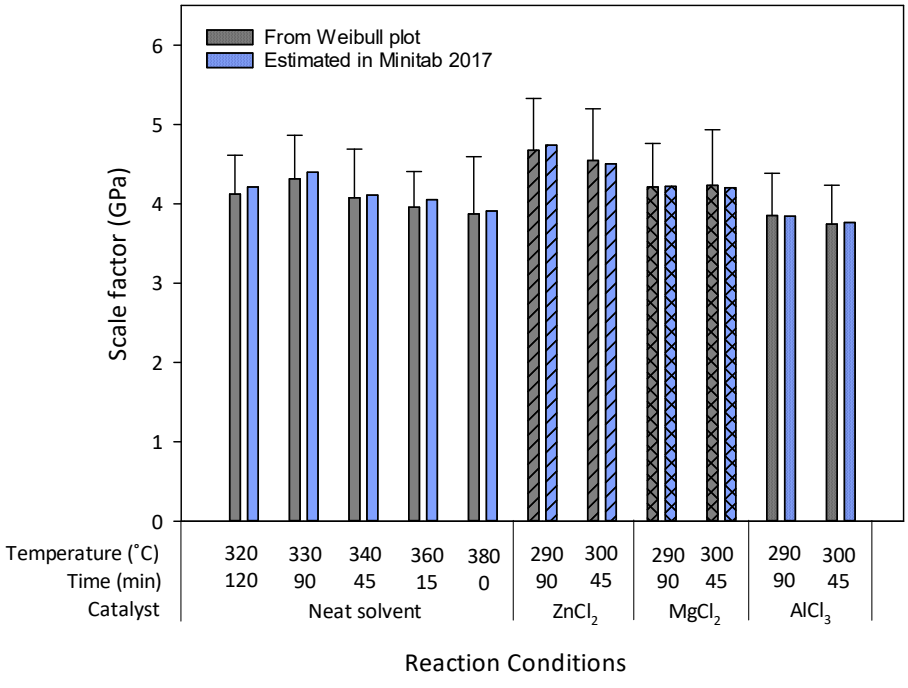

***Figure A8**. Scale factor for the tensile tests conducted with Toray T700S carbon fibres recovered the RTM6 epoxy resin using a range of conditions (grey = Weibull plot, blue = estimated in Minitab 2017).*

A.4 Supplementary Scanning Electron Microscopy (SEM) Micrographs

SEM micrographs for fibres recovered using the catalyst systems (0.05 M ZnCl2, 0.05 M MgCl2 and 0.005 M AlCl3) are provided in Figure A9 to Figure A11. For fibres recovered from each set of conditions, two images are shown: one without rinsing with water and one after rinsing with water.

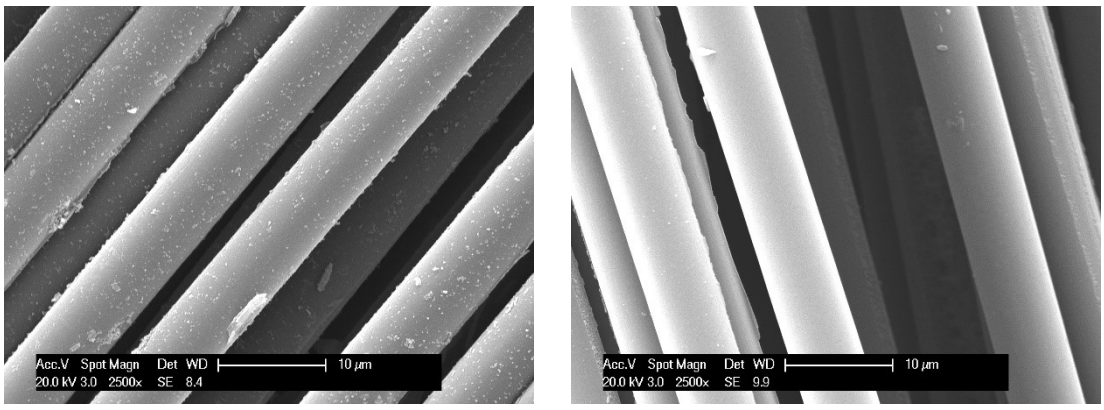

a) **b)**

***Figure A9**. SEM micrographs of carbon fibre recovered from an RTM6 epoxy resin using a 0.05 M $ZnCl_2$ acetone / water solvent at 300˚C a) before rinsing with water and; b) after rinsing with water.*

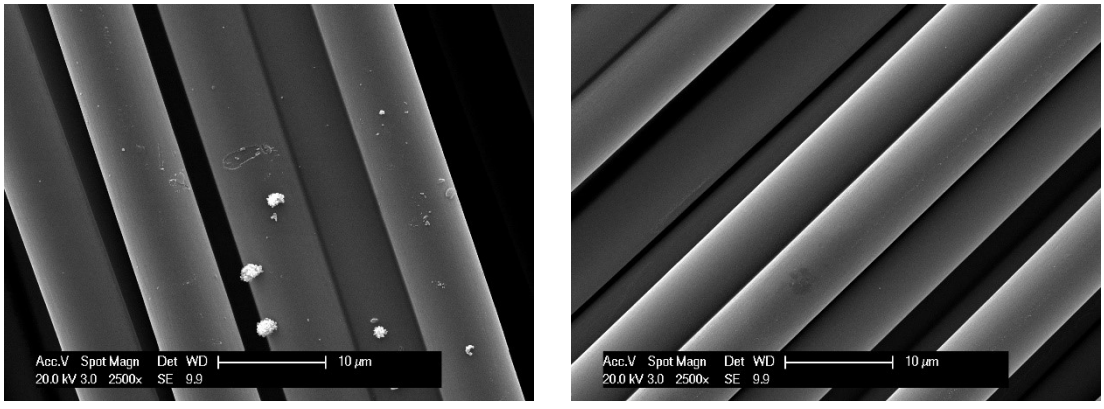

a) **b)**

***Figure A10**. SEM micrographs of carbon fibre recovered from an RTM6 epoxy resin using a 0.05 M $MgCl_2$ acetone / water solvent at 300˚C a) before rinsing with water and; b) after rinsing with water.*

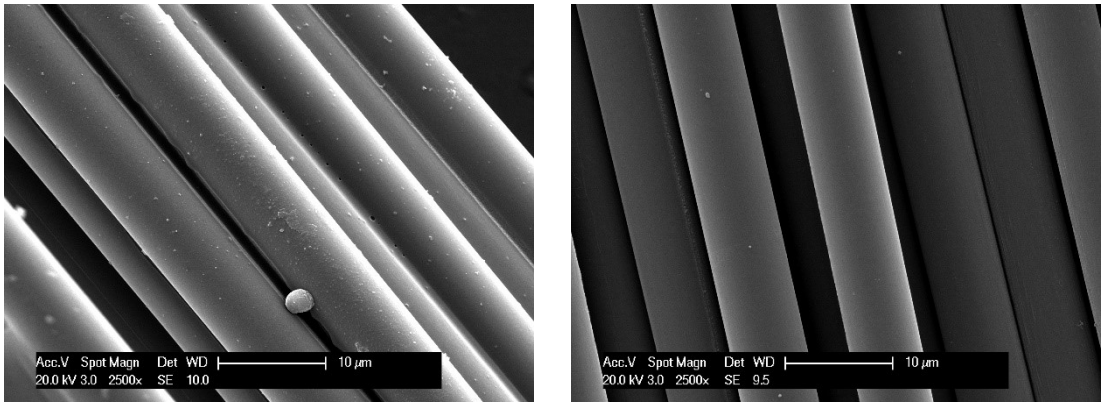

a) **b)**

Figure A11. *SEM micrographs of carbon fibre recovered from an RTM6 epoxy resin using a 0.005 M $AlCl_3$ acetone / water solvent at 300˚C a) before rinsing with water and; b) after rinsing with water.*

A.5 Supplementary Gas Chromatography-Mass Spectrometry (GC-MS) Chromatograms

All additional gas chromatography-mass spectrometry (GCMS) chromatograms for the organic liquid products recovered after processing the CFRP and model epoxy resin are supplied in Figure A12 to Figure A26 below. Table A Lists all compounds identified.

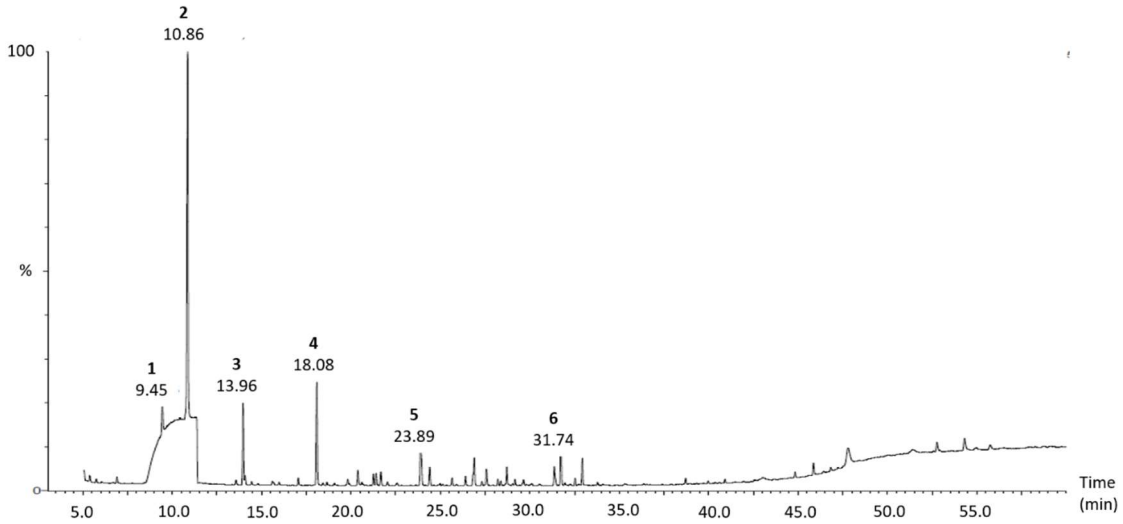

Figure A12. *GC-MS chromatogram for the organic liquid products recovered after processing the CFRP with the neat acetone / water solvent at 330˚C for 90 min.*

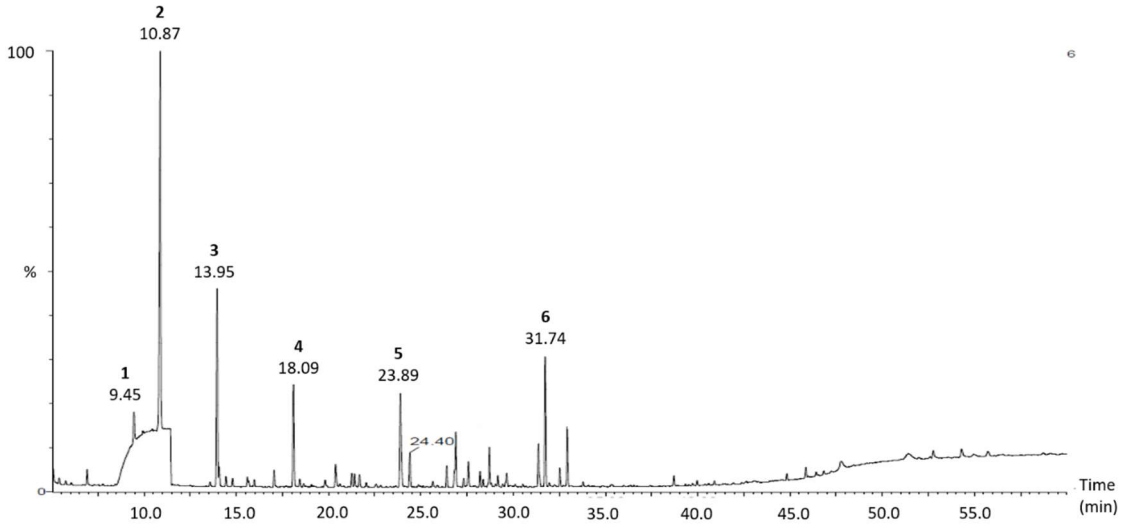

***Figure A13**. GC-MS chromatogram for the organic liquid products recovered after processing the CFRP with the neat acetone / water solvent at 340˚C for 45 min.*

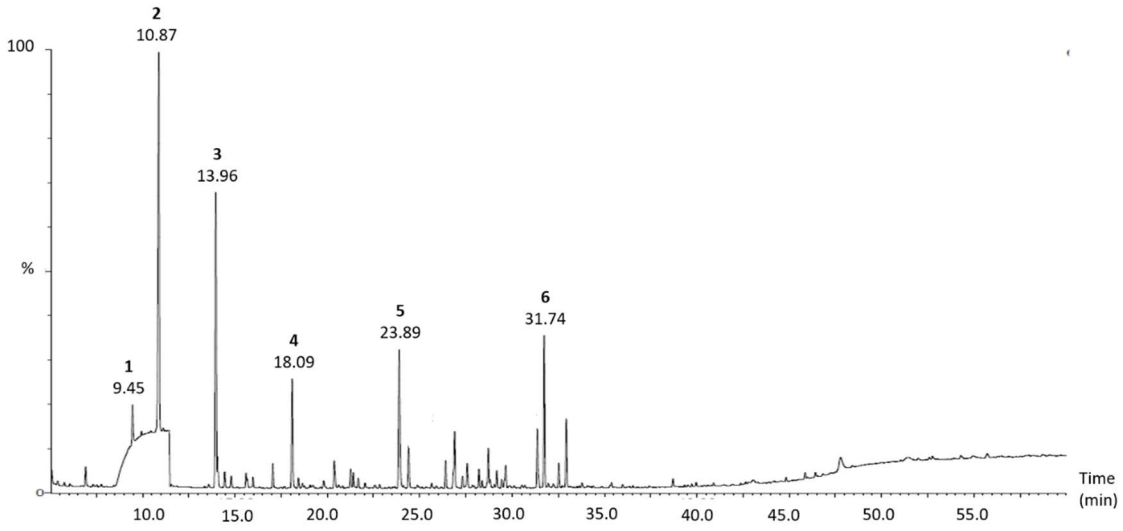

***Figure A14**. GC-MS chromatogram for the organic liquid products recovered after processing the CFRP with the neat acetone / water solvent at 360˚C for 15 min.*

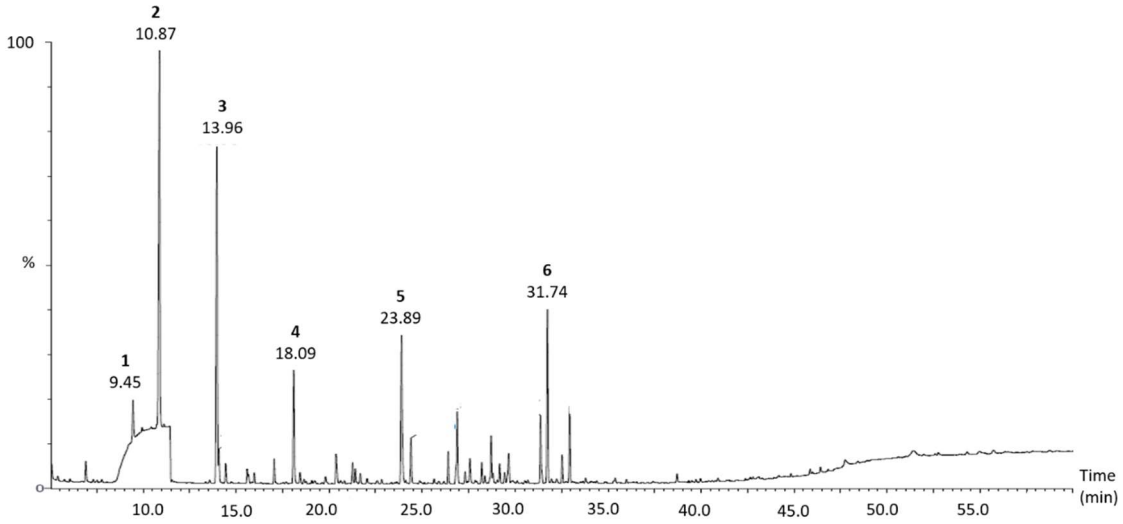

***Figure A15**. GC-MS chromatogram for the organic liquid products recovered after processing the CFRP with the neat acetone / water solvent at 380˚C for 0 min.*

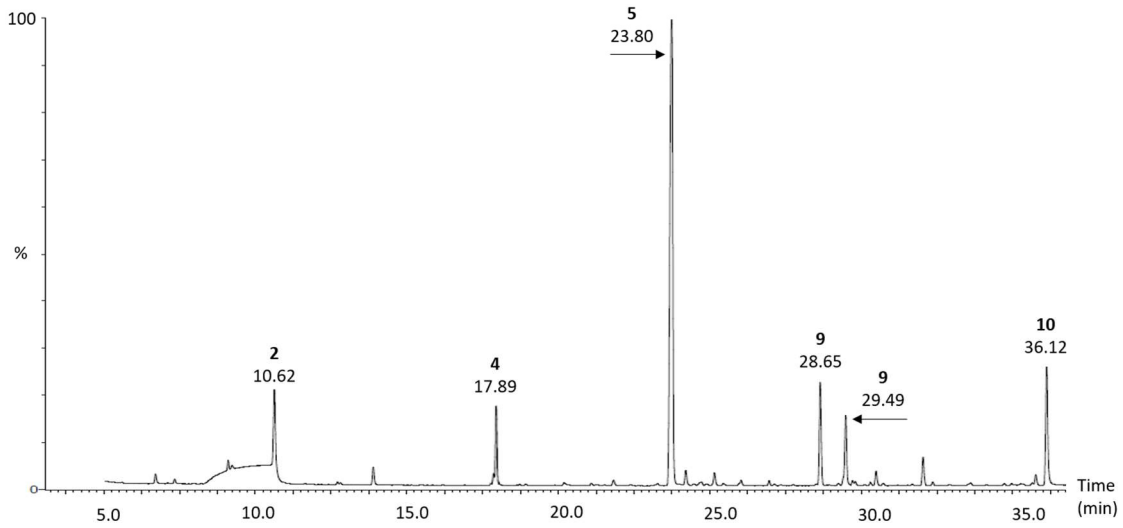

***Figure A16**. GC-MS chromatogram for the organic liquid products recovered after processing the CFRP with the 0.20 M NaOH, acetone / water solvent at 300˚C for 0 min.*

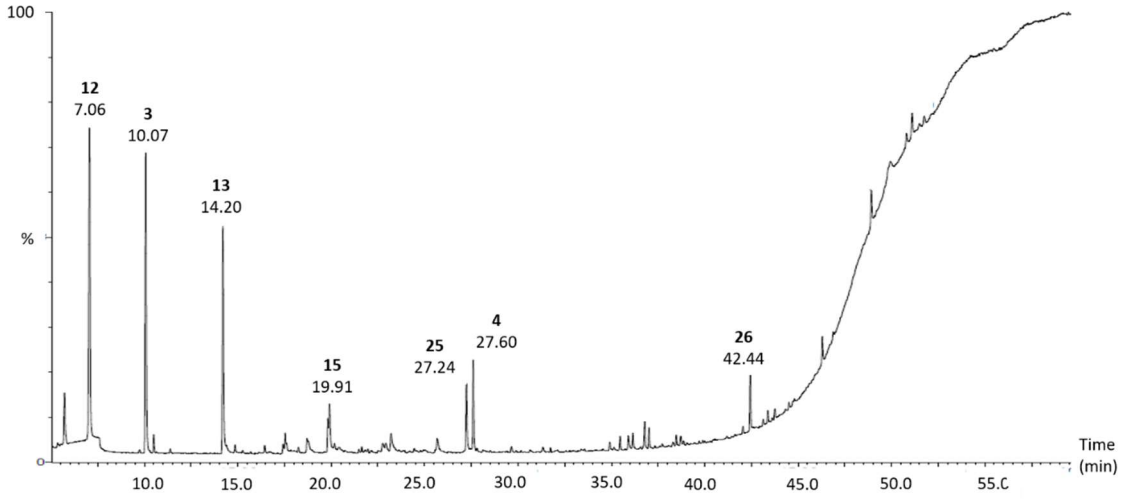

***Figure A17**. GC-MS chromatogram for the organic liquid products recovered after processing the CFRP with the 0.05 M $ZnCl_2$ acetone / water solvent at 290˚C for 90 min.*

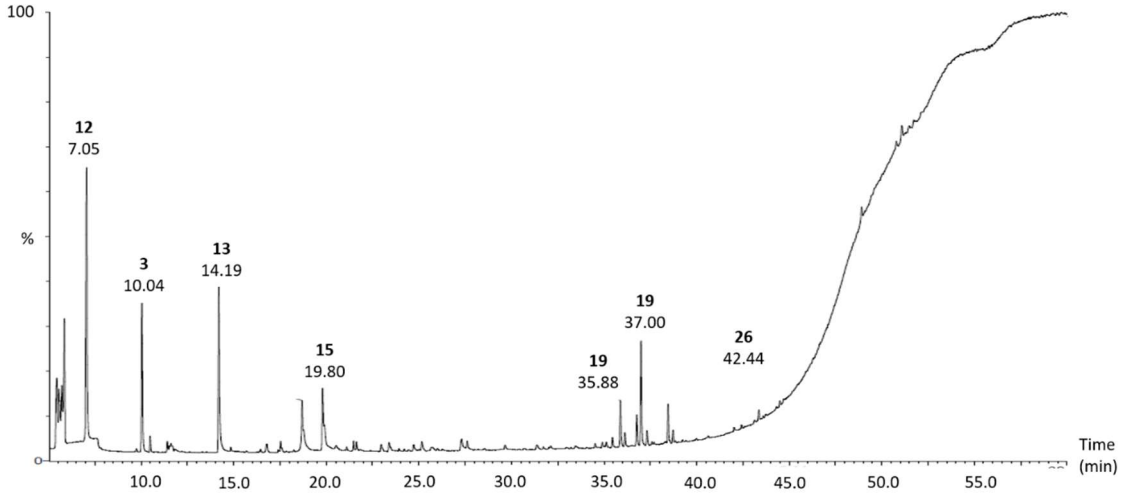

***Figure A18**. GC-MS chromatogram for the organic liquid products recovered after processing the CFRP with the 0.05 M $MgCl_2$ acetone / water solvent at 290˚C for 90 min.*

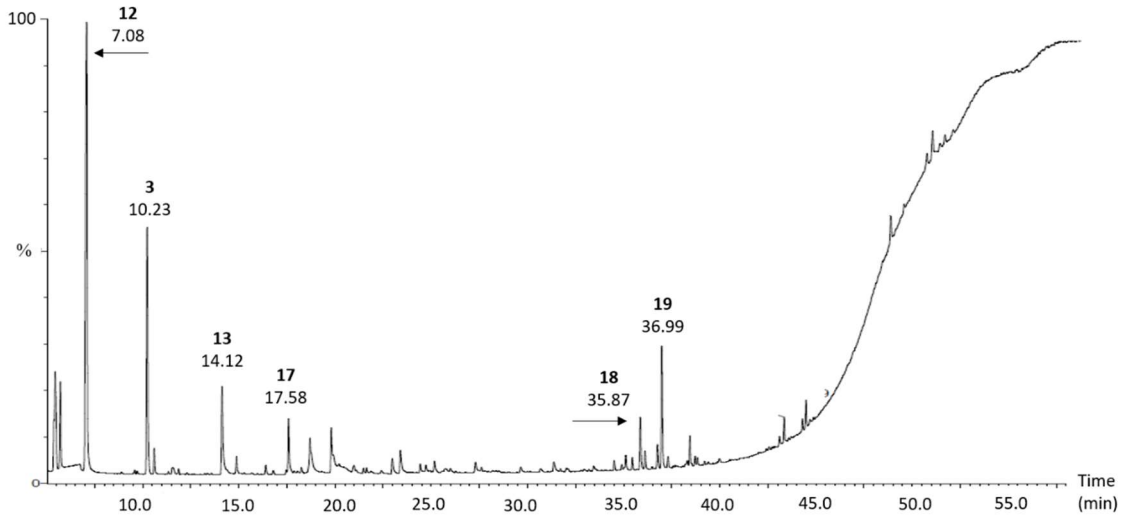

***Figure A19**. GC-MS chromatogram for the organic liquid products recovered after processing the CFRP with the 0.005 M $AlCl_3$ acetone / water solvent at 290˚C for 90 min.*

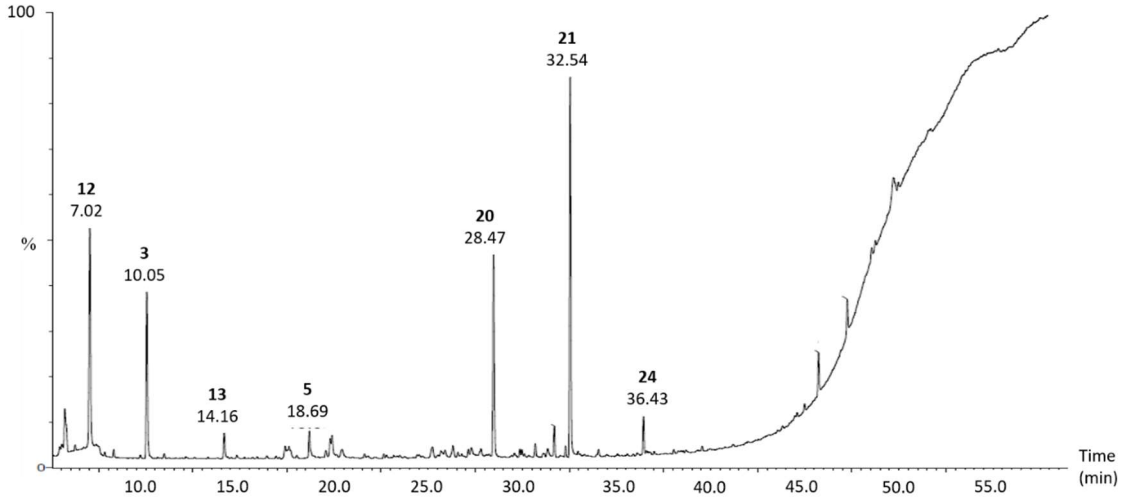

***Figure A20**. GC-MS chromatogram for the organic liquid products recovered after processing the model epoxy resin with the neat acetone / water solvent at 330˚C for 90 min.*

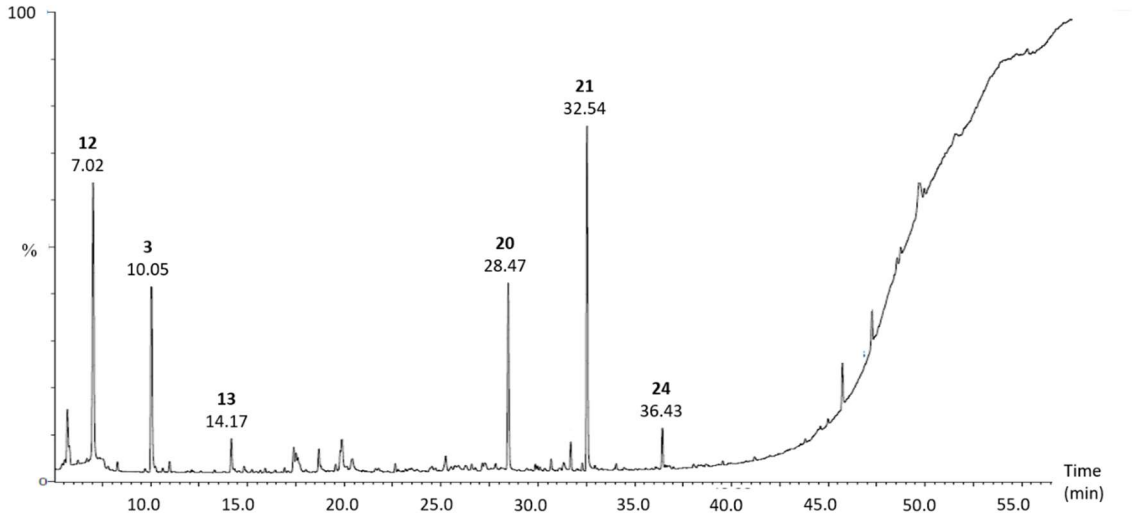

***Figure A21**. GC-MS chromatogram for the organic liquid products recovered after processing the model epoxy resin with the neat acetone / water solvent at 340˚C for 45 min.*

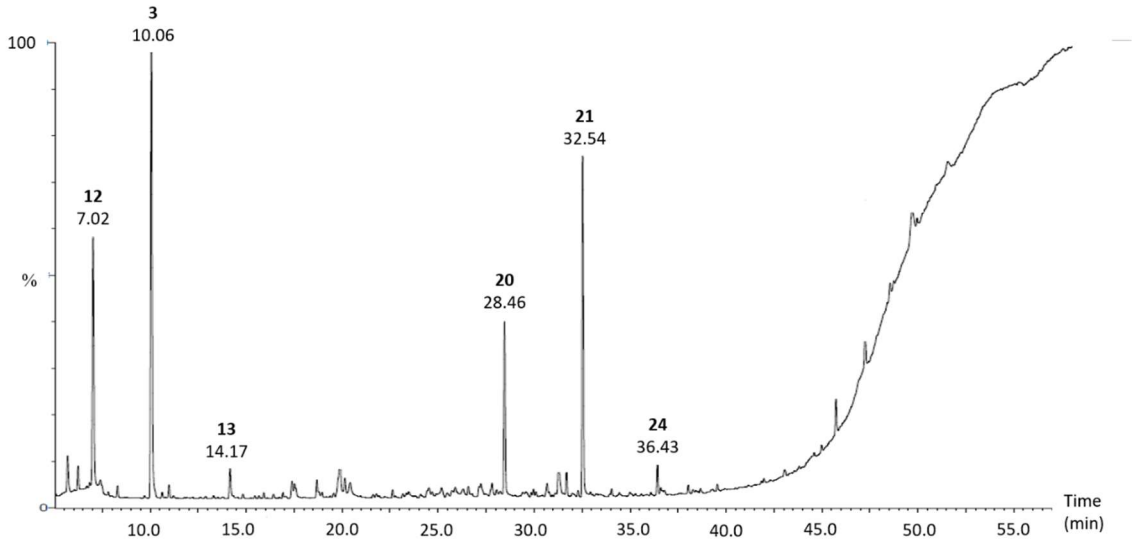

***Figure A22**. GC-MS chromatogram for the organic liquid products recovered after processing the model epoxy resin with the neat acetone / water solvent at 360˚C for 15 min.*

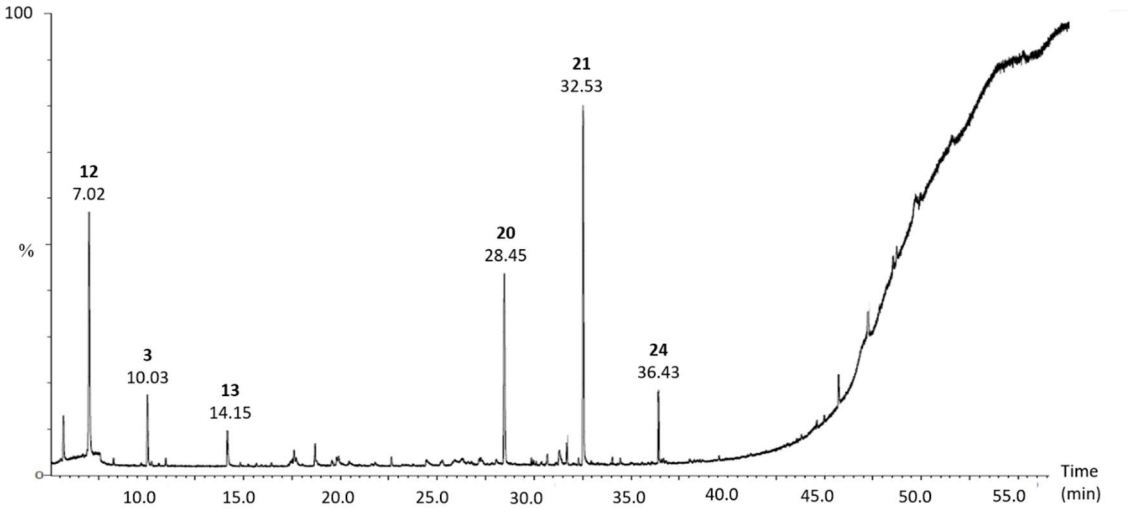

***Figure A23**. GC-MS chromatogram for the organic liquid products recovered after processing the model epoxy resin with the neat acetone / water solvent at 380˚C for 0 min.*

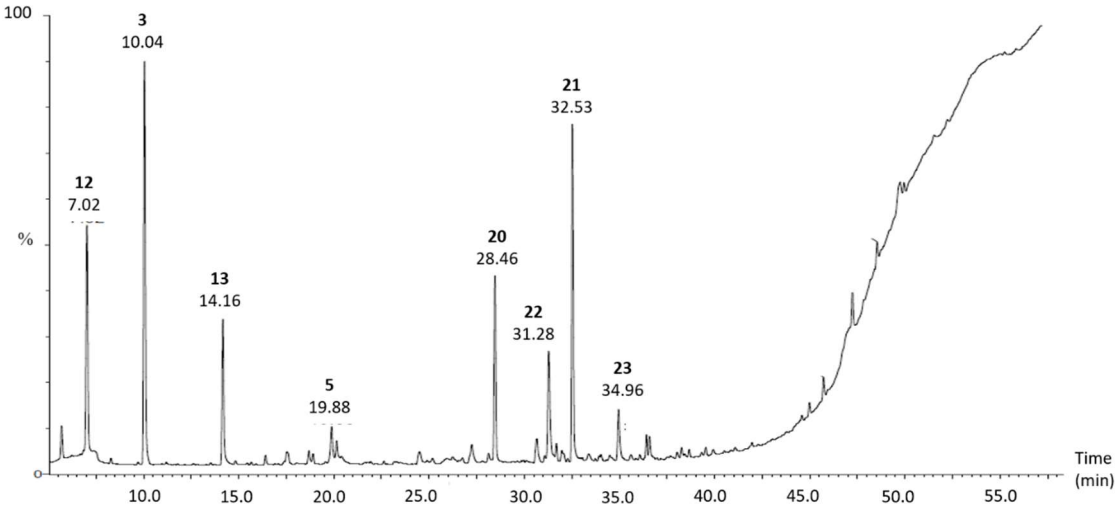

***Figure A24**. GC-MS chromatogram for the organic liquid products recovered after processing the model epoxy resin with the 0.05 M $ZnCl_2$ acetone / water solvent at 290˚C for 90 min.*

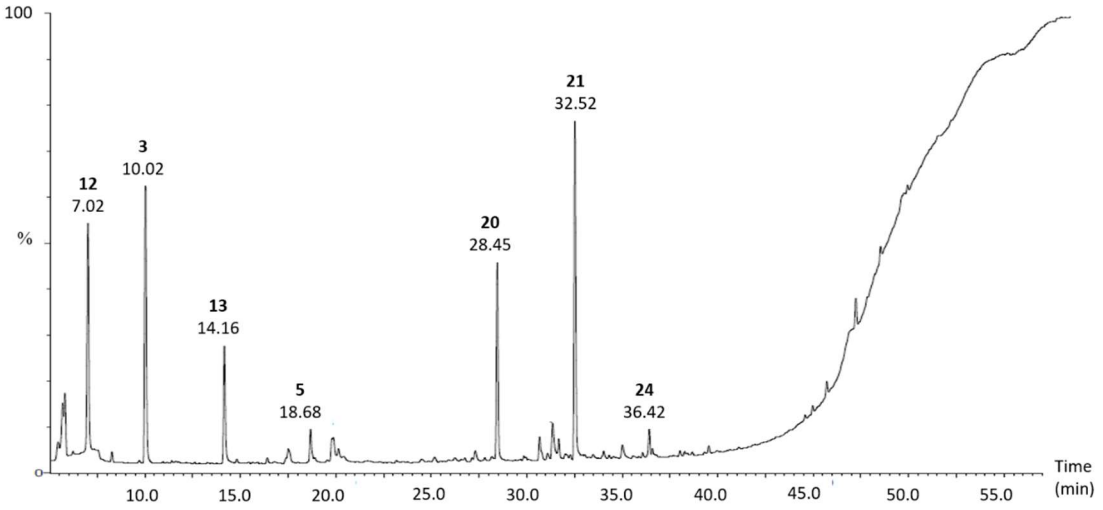

***Figure A25**. GC-MS chromatogram for the organic liquid products recovered after processing the model epoxy resin with the 0.05 M $MgCl_2$ acetone / water solvent at 290˚C for 90 min.*

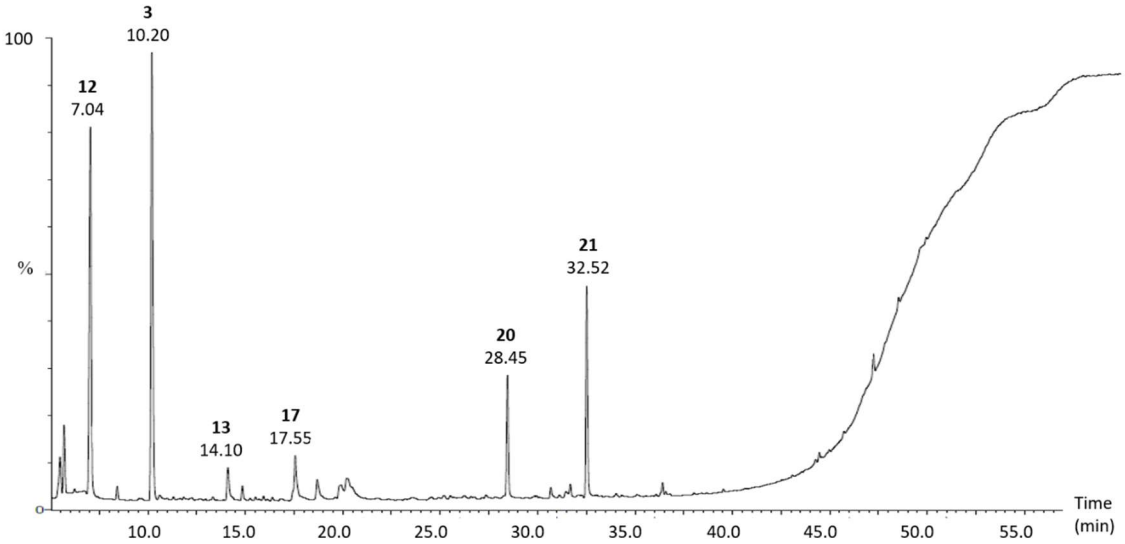

***Figure A26**. GC-MS chromatogram for the organic liquid products recovered after processing the model epoxy resin with the 0.005 M $AlCl_3$ acetone / water solvent at 290˚C for 90 min.*

***Table A1**. Summary of all compounds identified in the organic liquid product recovered after processing the CFRP and model epoxy resin.*

Peak no.	Compound
1	4-methyl-4-penten-2-one
2	4-methyl-3-penten-2-one
3	Trimethyl benzene
4	2,6-diethyl-benzenamine
5	3,5,5-trimethyl-2-cyclohexen-1-one
6	1,2,3,4-tetrahydro-2,2,4,8-tetramethyl-quinoline
7	3-Methylene-1,5,5-trimethylcyclohexene
8	4-hydroxy-4-methyl-pentan-2-one
9	Z-1-(3,5,5-trimethyl-2-cyclohexen-1-ylidene)-2-propanone
10	3,4-dimethylphenol
11	3,4-dihydro-3,3,6,8-tetramethyl-1(2H)-Naphthalenone
12	2-methoxy-furan
13	2-methyl-2-hexanol
14	N'-[3-(1-hydroxy-1-phenylethyl)phenyl] hydrazide acetic acid
15	5'-amino-5'-deoxy-adenosin
16	1,7-Trimethylene-2,3-dimethylindole
17	2,6-dimethyl-2,5-Heptadien-4-one
18	Butyl-[2-(3,3-dimethyl-cycloprop-1-enyl)-1-phenyl-ethylidene]-amine
19	8-ethyl-4,5,6,7-tetrahydro-10-isopropyl-Azepino[3,2,1-hi]indole
20	Phenol
21	4-(1-methylethyl)-phenol
22	4-ethyl-phenol
23	5-Phenyl-o-anisidine
24	p-Isopropenylphenol
25	2-isopropyl-6-methylaniline
26	1,1-dioxide-2-methyl-thianaphthene